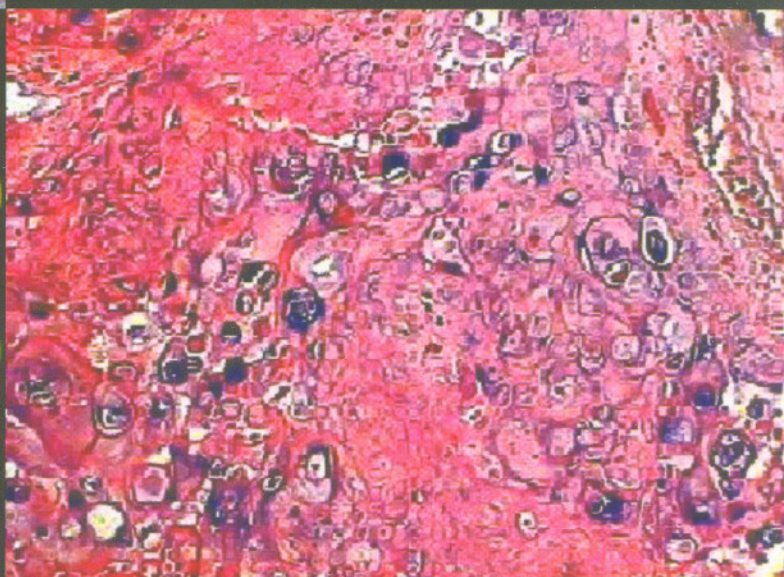
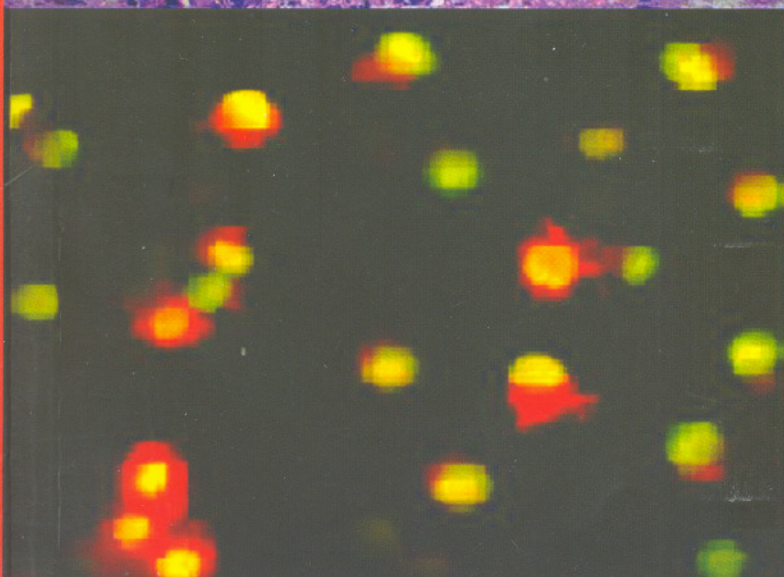
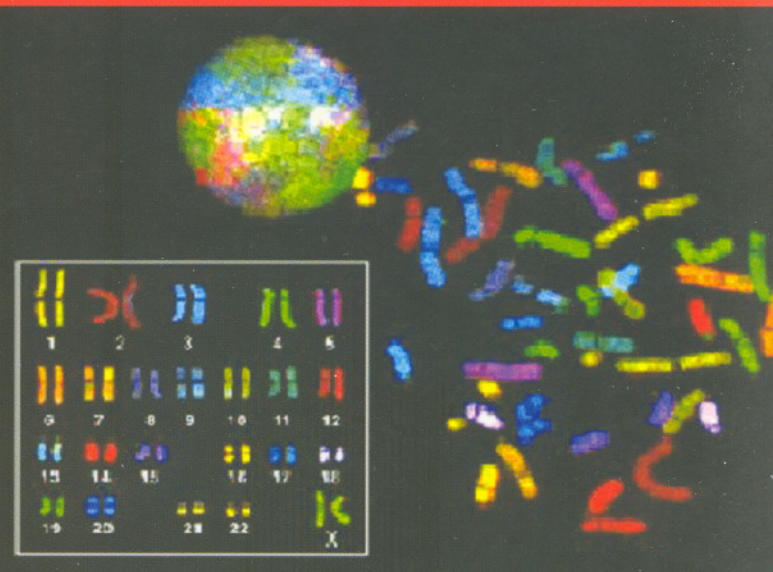
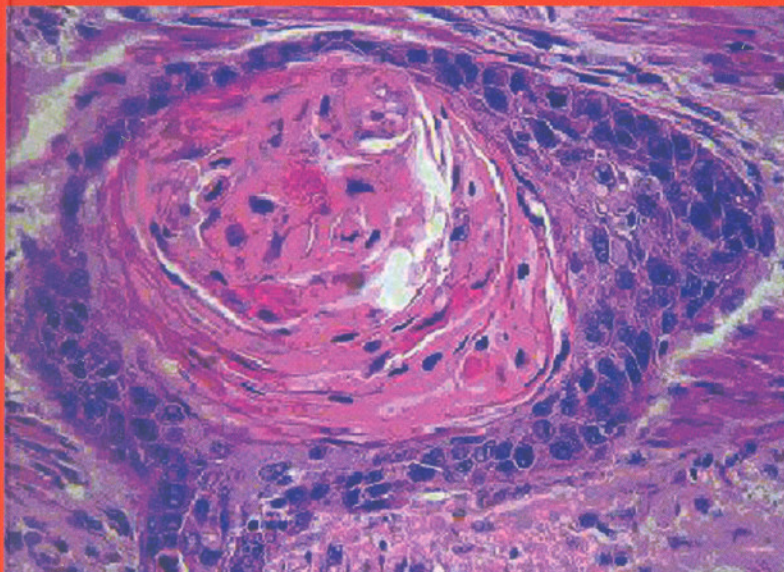


ISSN 1097-8135

Life Science Journal

Acta Zhengzhou University Overseas Edition



Life Science Journal

Acta Zhengzhou University Overseas Edition
Published by Zhengzhou University and Marsland Press

EDITORIAL COMMITTEE

Editor in Chief: Shen Changyu, Ph.D., Zhengzhou University, China

Associate Editors: Ma Hongbao, Ph.D., Michigan State University, UAS

Xin Shijun, Prof., Zhengzhou University, China

Li Qingshan, Ph.D., Zhengzhou University, China

Cherng Shen, Ph.D., M.D., Chengshiu University, China

Executive Editors: Wang Haoyi, Zhengzhou University, China

Yang Hongmei, Zhengzhou University, China

Editorial Consultants: (in alphabetical order)

An Xiuli, Ph.D., New York Blood Center, USA

Chen George, Ph.D., Michigan State University, UAS

Dong Ziming, M.D., Zhengzhou University, China

Duan Guangcai, Ph.D., M.D., Zhengzhou University, China

Edmondson Jingjing Z., Ph.D., Zhejiang University, China

Li Xinhua, M.D., Zhengzhou University, China

Li Yuhua, Ph.D., Emory University, USA

Lindley Mark, Ph.D., Columbia University, USA

Liu Hongmin, Ph.D., Zhengzhou University, China

Liu Zhanju, Ph.D., M.D., Zhengzhou University, China

Lu Longdou, Ph.D., Henan Normal University, China

Qi Yuanming, Ph.D., M.D., Zhengzhou University, China

Shan Zhiying, Ph.D., University of Florida, USA

Shang Fude, Ph.D., Henan University, China

Song Chunpeng, Ph.D., Henan University, China

Sun Yingpu, Ph.D., Zhengzhou University, China

Wang Lexin, Ph.D., M.D., Charles Sturt University, Australia

Wang Lidong, Ph.D., M.D., Zhengzhou University, China

Wen Jianguo, Ph.D., M.D., Zhengzhou University, China

Xu Cunshuan, Ph.D., Henan Normal University, China

Xue Changgui, M.D., Zhengzhou University, China

Zhang Jianying, Ph.D., University of Texas, USA

Zhang Kehao, Ph.D., M.D., Zhengzhou University, China

Zhang Shengjun, Ph.D., M.D., Johns Hopkins University, USA

Zhang Xueguo, Ph.D., Henry Ford Hospital, USA

Zhang Zhan, Ph.D., Zhengzhou University, China

Zhang Zhao, Ph.D., M.D., Zhengzhou University, China

Zhu Huaijie, Ph.D., Columbia University, USA

Life Science Journal, Acta Zhengzhou University Overseas Edition, is an international journal with the purpose to enhance our natural and scientific knowledge dissemination in the world under the free publication principle. The journal is calling for papers from all who are associated with Zhengzhou University – home and abroad. Any valuable papers or reports that are related to life science are welcome. Other academic articles that are less relevant but are of high quality will also be considered and published. Papers submitted could be reviews, objective descriptions, research reports, opinions/debates, news, letters, and other types of writings. All publications of Life Science Journal are under vigorous peer-review. Let's work together to disseminate our research results and our opinions.

CONTENTS

1. Alteration of protein profiles in human esophageal multistage carcinogenesis: highlight on promising biomarker and challenges for high-risk subject screening and early diagnosis	1 - 5
Lidong Wang, Aiqun Wu, Yupei Qin, Xiaoshan Feng, Mei Zhang, Baochi Liu, Guolan Xing	
2. Isolation and characterization of rbcL gene from <i>Dunaliella salina</i>	6 - 12
Yurong Chai, Yun Sun, Weidong Pan, Yanlong Jia, Lexun Xue	
3. Establishment and characterization of lung adenocarcinoma cell lines with multidrug resistance	13 - 16
Zhiju Wang, Min Li, Wenchao Zhao, Guoqiang Zhao, Ziming Dong	
4. Thymidine phosphorylase induced by IFN-alpha2b enhances 5-fluorouracil antitumor activity <i>in vitro</i> and <i>in vivo</i>	17 - 20
Qi Li, Baoping Qiao, Jiaxiang Wang, Jinxing Wei, Weixing Zhang	
5. Changes of Z-line at gastroesophageal junction in symptom-free subjects from high-incidence area for esophageal cancer in Henan	21 - 23
Lidong Wang, Baochi Liu, Xin Song, Shanshan Gao, Zongmin Fan, Bin Liu, Changwei Feng, Xin He, Yanrui Zhang, Jilin Li, Xinying Jiao, Xiaoshan Feng, Guolan Xin, Mei Zhang, Aiqun Wu	
6. Expression of vascular endothelial growth factor C in human esophageal squamous cell carcinoma	24 - 28
Hongxin Zhang, Lan Zhang, Kuisheng Chen, Dongling Gao, Fucheng He, Yunhan Zhang	
7. Expression of P53 and Bcl-2 in laryngeal squamous cell carcinoma	29 - 31
Shanting Liu, Weihua Lou, Jianzhong Sang, Ming Zhao, Zhaozhong Meng	
8. Inhibitory effect of SB203580 on neuropathic pain behaviors induced by lumbar 5 ventral rhizotomy in rats	32 - 36
Jitian Xu, Huiyin Tu, Wenjun Xin, Xianguo Liu	
9. Slowing of atrioventricular conduction in mice lacking SK2 channel	37 - 39
Qian Zhang, Ziming Dong, Valeriy Timofeyev	
10. Determination of organochlorine pesticide residues in herbs by capillary gas chromatography	40 - 42
Bin Du, Xinchao Li, Hong Liu	

11. Expression patterns and action analysis of genes associated with the responses to drugs, toxins, oxidation and unfolded proteins during rat liver regeneration	43 - 51
Hongpeng Han, Cunshuan Xu, Cuifang Chang, Gaiping Wang, Lijuan Su, Panfeng Liu, Xiaoguang Chen	
12. Expression patterns and action analysis of genes associated with the responses to physical stimuli during rat liver regeneration	52 - 60
Panfeng Liu, Lifeng Zhao, Weimin Zhang, Xiaoguang Chen, Cunshuan Xu	
13. Expression patterns and action analysis of genes associated with the responses to fear, wound and pain during rat liver regeneration	61 - 70
Hongpeng Han, Cuifang Chang, Gaiping Wang, Lijuan Su, Panfeng Liu, Xiaoguang Chen, Cunshuan Xu	
14. Conditional genetic analysis on quantitative trait loci for yield and its components in rice	71 - 76
Gangqiang Cao, Jun Zhu	
15. Application of a transformation method via the pollen-tube pathway in agriculture molecular breeding	77 - 79
Xiaoming Song, Yunhong Gu, Guangyong Qin	
16. Monitoring phytoplankton diversity in the hill stream Chandrabhaga of Garhwal Himalaya	80 - 84
Archana Sharma, Ramesh C. Sharma, Ashish Anthwal	
17. Extraction method of soil microbial DNA for molecular ecology research	85 - 88
Jinyong Huang, Wei Zhou, Linhai Chen	
18. Kinetics of methylene blue biosorption by phoenix tree's leaves powder	89 - 93
Weihua Zou, Lu Zhu, Shujian Cheng, Runping Han	
19. Author Index and Subject Index	94

On the cover : Four modern molecular biology technologies are showed. The left top is hematoxylin and eosin (HE) staining; the left bottom is the acridine orange (AO) fluorescence staining; the right top is the fluorescence *in situ* hybridization (FISH); the right bottom is *in situ* hybridization. These figures were from Henan Key Laboratory of Tumor Pathology, kindly presented by Professor Yunhan, Zhang.

Alteration of protein profiles in human esophageal multistage carcinogenesis: highlight on promising biomarker and challenges for high-risk subject screening and early diagnosis[☆]

Lidong Wang*, Aiqun Wu, Yupei Qin, Xiaoshan Feng, Mei Zhang, Baochi Liu, Guolan Xing

Henan Key Laboratory for Esophageal Cancer; Basic Medical College, Zhengzhou University, Zhengzhou, Henan 450052, China

Received December 13, 2006

Abstract

Human esophageal carcinogenesis has been well-recognized as a multistage progressive process. The early indicator for the subject predisposed to esophageal cancer (EC) is the esophageal epithelial cell hyperproliferation, morphologically manifested as basal cell hyperplasia (BCH) dysphasia (DYS) and carcinoma *in situ* (CIS), which could be considered as esophageal precancerous lesions. Follow-up studies on the subjects at high incidence area for EC have demonstrated that these precancerous lesions are unstable, i.e. these lesions could develop to cancer, or remain at the same stage for long time, and even return to normal. The molecular mechanism underlying is largely unknown. It has been demonstrated that multiple proteins with aberrant expression are involved in esophageal carcinogenesis. In this review, evidences for protein profiles in human esophageal precancerous and cancerous lesions were summarized to highlight the promising biomarkers and challenges for high-risk subject screening and early diagnosis for EC. [Life Science Journal. 2007;4(1):1–5] (ISSN: 1097–8135).

Keywords: esophageal carcinoma; carcinogenesis; protein profile; biomarker

1 Introduction

Esophageal carcinoma (EC) is one of the sixth most common malignant tumors worldwide. Linzhou (formerly Linxian) and nearby counties have been well-documented as the highest incidence area for EC, and EC remains the leading cause of cancer related death in these areas. Moreover, EC in late stage has a very poor prognosis, with a five year survival rate of less than 10%. However, the 5-year survival rate for EC in the early stage could be as high as 90%. Obviously, early diagnosis is the crucial factor in reducing mortality. But, more than 80% of the EC patients are diagnosed at the advanced stage clinically for the first time at present. One leading cause for this poor diagnosis is lack of specific biomarkers for the early EC patients who have not obvious special symptom in early stage and for large-scale high-risk subject screening. So far, endoscopic biopsy and histopathological examination in mass survey and follow-up at high incidence area remain the most effective method to identify early cancer and precancerous lesions. It is rather difficult to apply these methods for high-risk subject screening and early diagnosis in large-

scale mass survey for symptom-free subjects from high incidence area. Thus, it becomes critically important to identify promising biomarker for high-risk subject screening and early diagnosis through characterizing the morphological and molecular changes in multistage carcinogenesis of EC^[1].

Esophageal carcinogenesis has been well-recognized as a multistage and progressive process. The early indicator for the subject predisposed at EC is the aberrant hyper-proliferation of epithelial cells, morphologically manifested as basal cell hyperplasia (BCH), dysphasia (DYS) and carcinoma *in situ* (CIS), which could be regarded as esophageal precancerous lesions. High risk subject screening and follow-up studies in high-incidence area for EC have indicated that about the natural history for esophageal carcinogenesis from these precancerous lesions to cancer could be 5–10 years^[1–4]. But, the molecular mechanism underlying is still largely unknown. In this review, the progress for aberrant protein expression in human esophageal multistage carcinogenesis and the challenges in this area were summarized to highlight the promising biomarker for high-risk subject screening and early diagnosis.

2 Challenges in Studying the Mechanisms of Human Esophageal Multistage Carcinogenesis

The obvious clinical characteristic of human esophageal precancerous lesions is its instability, i.e., it

*Supported in part by Henan Education Committee Foundation and National Natural Science Foundation of China (No. 30670956).

[†]Corresponding author. Tel and Fax: 86-371-6665-8335; Email: ldwang@zzu.edu.cn

could constantly develop to the direction of cancer or remain at the same stage for many years, or even return to normal. It is difficult to interpret the phenomenon only based on morphological changes. The underlying molecular changes may be of importance in elucidating the mechanism of human esophageal multistage carcinogenesis and establishing the promising biomarkers for high-risk subject screening and early diagnosis. The challenges in these areas include: (1) To establish a large scale follow-up design on symptom-free subjects from high-risk area with repeated esophageal biopsies. This case-control study is crucial in identifying the promising biomarkers for high-risk subject screening and early diagnosis; (2) Through large scale mass survey with the promising biomarkers and esophageal biopsies to confirm the consistence in diagnosis of precancerous and cancerous lesions; (3) To establish "one drop of blood test" method for large scale high-risk subject screening and early diagnosis. Recent studies have indicated that through one drop of blood to test the autoantibodies against tumor suppressor and monogenic proteins could predict the subjects with esophageal precancerous and cancerous lesions in a small group^[5]. Obviously, this "one drop of blood test" would be more easier, economic and acceptable for the large scale mass survey. It could narrow down the number of subjects for endoscopic examination. The key scientific questions to be addressed in the mechanisms of human esophageal multistage carcinogenesis include: What are the key molecular events occurred in multistage carcinogenesis? Which of these molecular events are key factor to drive the mild esophageal precancerous lesions to severe or cancer? Would the subjects with these molecular changes during the follow-up develop to esophageal cancer earlier or more quickly than those without these molecular changes? Based on these studies, could the promising biomarkers be identified for high-risk subject screening and early diagnosis? Apparently, to answer these questions, it is very important to establish the follow-up subjects in high-risk area with repeated esophageal biopsies.

3 Nomenclature and Protein Profiles for Human Esophageal Multistage Carcinogenesis

3.1 Nomenclature of human esophageal multistage carcinogenesis

The concept of esophageal precancerous lesions comes from the histopathological observation and follow-up studies on the large-scale mass survey in high-risk area, on surgical specimen adjacent to carcinoma and on animal experiment model. Morphologically, the precancerous lesions of the esophageal epithelium are quite similar in symptom-free subjects, tissues adjacent to EC and the rat EC models induced by nitrosamine^[6,7]. It is

noteworthy that the patterns of molecular changes are not the same in morphologically similar precancerous lesions. The typical sample is that, the positive p53 immunostaining rate in human esophageal precancerous lesions is much higher than in rat model induced by nitroamine. In contrast, ras mutations are frequently observed in rat model induced by nitrosamine, not in human esophageal precancerous and cancerous lesions^[8]. Even in the same subject with similar morphological type of precancerous lesions at the different parts of the esophagus, p53 mutation pattern is different^[9]. These results indicate the discordance of "tissue phenotype" and "genetic phenotype" in esophageal multistage carcinogenesis. Thus, it becomes important to nominate these morphological changes based on molecular events, which may predict the development of these lesions either to cancer or not.

3.2 Histogenesis model of human esophageal multistage carcinogenesis^[10]

Based on the literature and recent works of our lab, the histogenesis model for the human esophageal multistage carcinogenesis is summarized as in Figure 1.

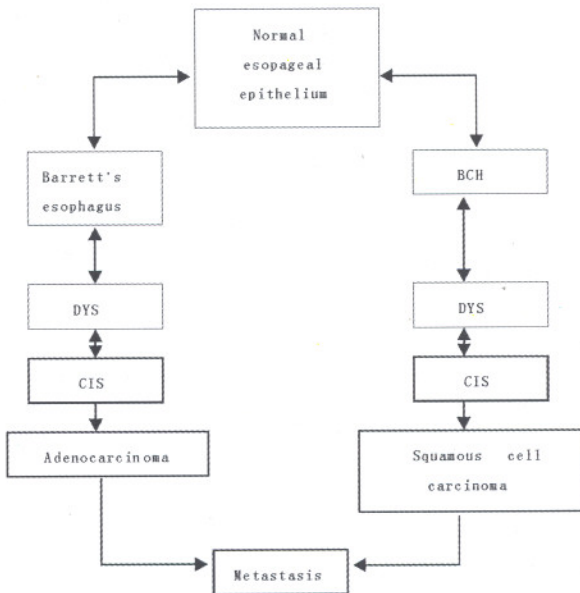


Figure 1. Histogenesis model for human esophageal multistage carcinogenesis

What needs to be emphasized is that the histological pattern of EC is quite different in western countries and in China. Primary esophageal adenocarcinoma almost takes up 50% in western countries. The histogenesis model from reflux esophagitis (gastroesophageal reflux disease, GERD) to Barrett's esophagus to DYS to CIS to esophageal adenocarcinoma is the most common type of esophageal carcinogenesis in the western countries.

However, squamous cell carcinoma almost takes up 95% in China, the incidence for primary esophageal adenocarcinoma is very low. The incidence of the reflux esophagitis in high-risk area in China is about 6% (14%-16% in the western countries). Barrett's esophagus occurrence is also very low in China (0.5% - 2%). The mechanisms for these differences are not clear. The histogenesis model from normal to BCH to DYS to CIS is the most common type of esophageal carcinogenesis in China.

3.3 Protein profiles for human esophageal multistage carcinogenesis

Figure 2 and Table 1 summarized the alterations of 57 proteins aberrant expression in human esophageal normal, precancerous and cancerous lesions^[11-58]. All these subjects were from Linzhou, Henan province, the highest incidence area for EC. Most of the precancerous and normal tissues were from high-risk subject screening in this area with endoscopic examination. These primary results demonstrated that multiple proteins changed in the multistage carcinogenesis of EC with a different degree of severities. It is noteworthy that with the lesions progressed from normal to mild and severe stage, most of proteins from p53-Rb pathway (including p53, Rb, p16, p15, p14, CyclinD1, waf1-p21, PCNA, etc.), shows apparent aberrant expression, especially the p53, and PCNA proteins. These data suggest that these molecular changes will be one of mechanisms to drive the mild lesions to severe and cancer. Further characterization is needed to verify the significance of these biomarkers in high-risk subject screening and early diagnosis.

4 Perspectives

4.1 Establish the sample and information bank for human esophageal multistage carcinogenesis and identification of the key genetic biomarkers for high-risk subject screening and early diagnosis.

4.2 Identification of the key genetic biomarkers for high-risk subject screening and early diagnosis.

Although the accumulated data have indicated that esophageal carcinogenesis is a multistage and progressive process involved by multiple genetic changes, the key genetic changes to drive the mild lesions to severe and cancer in EC is largely unknown. To establish the informative sample bank is crucial in illustrating the mechanism of human esophageal multistage carcinogenesis and identifying the biomarkers for high-risk subject screening and early diagnosis. Actually, these genetic changes at the same time could provide important clues in designing new target for treatment and prevention. It could not be overemphasized to perform systemic studies on pedigree of EC to identify the key genetic changes.

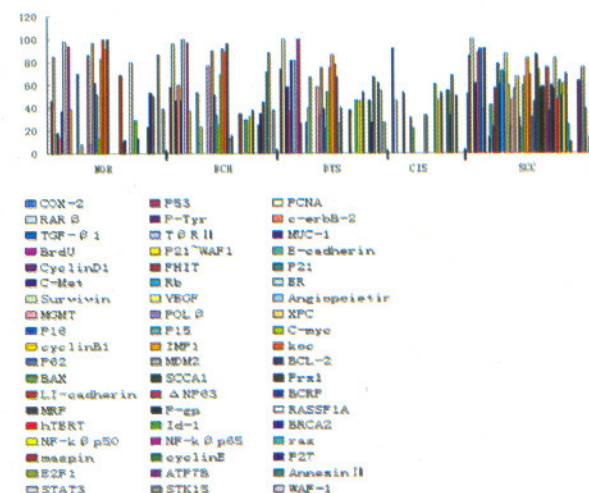


Figure 2. Alterations of 57 proteins in human esophageal multistage carcinogenesis

Table 1. Frequency of 57 proteins expression in human esophageal multistage carcinogenesis

Histological types	Positive immunostaining rate (%)		
	<50%	50% - 80%	>80%
Normal	TGF-β2, ER, POL-β, Id-1, P53, NF-κBp50, MUC1, IMP1	PCNA, COX-2, LI-cadherin	TGF-β1, E-cadherin, MGMT, cyclin-B1, P21-WAF1
BCH	POL-β, Id-1, TGF-β2, ER, MUC1, IMP1, NF-κBp65	MGMT, P53, NF-κBp50, PCNA, COX-2	TGF-β1, E-cadherin, cyclin-B1, P21-WAF1
DYS	ER, POL-β, Id-1, MUC1, LI-cadherin	E-cadherin, MGMT, P53, NF-κBp50, PCNA, NF-κBp65	TGF-β2, TGF-β1, COX-2, P21-WAF1, P21-WAF1
CIS	E-cadherin	ER, Id-1, PCNA, NF-κBp65	TGF-β2, P53
SCC	TGF-β2, ER, P16, MGMT, LI-cadherin, P21-WAF1, Annexin II, cyclin-D1, P62, MET, GSTM1, FHIT	E-cadherin, BRCA2, POL-β, Id-1, NF-κBp50, COX-2, P21-WAF1, NF-κBp65, VEGF, MDM2, NF-κBp49, BAX, KOC, ΔNp63, RARβ, Rb, c-myc, SCCA1, c-erb-2, c-met	TGF-β1, P53, MUC1, PCNA, IMP1, Bcl-2, Prx1, Survivin

4.2 Basic-clinic translation

"One drop of blood test" for high-risk subject screening and early diagnosis has been dreamed by generations of esophageal cancer researchers. Although the key molecular events involved in esophageal multistage carcinogenesis is not clear, the present accumulated data have showed that multiple autoantibody assay could predict the high-risk subjects and even identify the early EC patient. Basic-clinic translation should be emphasized to narrow down the scale for high-risk subject screening with endoscopic examination.

References

- Wang LD, Zhou Q, Feng CW, et al. Intervention and follow-up on human esophageal precancerous lesions in Henan, northern China, a high-incidence area for esophageal cancer. *Gan To Kagaku Ryoho* 2002; 29 Suppl 1: 159–72.
- Tao DM. Research evolution of epidemiology for the relationship between epithelium hyperplasia and carcinogenesis. *Chin J Cancer Prev Treat* 2001; 8(2): 206.
- Wang LD, Guo HQ, Zhou Q. The lapse of esophageal epithelium hyperplasia, 6 years follow-up for 66 cases of epithelium hyperplasia. *J Henan Med Univ (Med Sci)* 1991; 26: 328–30.
- Tao MD, Xu YZ, Gu YK, et al. Research for 46161 cases of carcinogenesis time and ratio of the esophageal normal and hyperplasia epidermis. *Cancer Res on Prev Treat* 1997; 24: 155–6.
- Wang LD, Du F, Zhang JY, et al. Multiple serum autoantibodies min-array analysis on the subjects with esophageal precancerous and cancerous lesions from Linzhou, the highest incidence area for esophageal cancer in Henan, northern China. *Proc Am Assoc Cancer Res* 2007.
- Wang LD, Hong JY, Qiu SL, et al. Accumulation of p53 protein in human esophageal precancerous lesions: a possible early biomarker for carcinogenesis. *Cancer Res* 1993; 53: 1783–7.
- Wang ZY, Wang LD, Lee MJ, et al. Inhibition of N-nitroso-methylbenzylamine-induced esophageal tumorigenesis in rats by green and black tea. *Carcinogenesis* 1995; 16: 2143–8.
- Wang LD, Yang WC, Zhou Q, et al. Alterations of WAF-1 and p53 in human esophageal cancerous and precancerous lesions. *J Zhengzhou Univ (Med Sci)* 1997; 32: 11–4.
- Wang LD, Zhou Q, Hong JY, et al. p53 protein accumulation and gene mutations in multifocal esophageal precancerous lesions from symptom free subjects in a high incidence area for esophageal carcinoma in Henan, China. *Cancer* 1996; 77: 1244–9.
- Wang LD. Studies on mechanism and prevention and cure of esophageal canceration. *Chin J New Gastroenterol* 1996; 4: 9–10.
- Wang LD, Zhou Q, Yang WC. Immunohistochemical studies on p53 tumor suppressor gene esophageal procarcinogenesis. *J Xinxiang Med Coll* 1993; 10: 4–6.
- Gao HK, Wang LD, Zhou Q, et al. p53 tumor suppressor gene mutation in early esophageal precancerous lesions and carcinomas among high risk population in Henan, China. *Cancer Res* 1994; 54: 342–45.
- Wang LD, Zhou Q, Chen YL, et al. Studies on expression of epithelial-specific protein of p40 precancerous and cancerous lesions of esophageal and gastric cardia. *J Henan Med Univ* 1995; 30: 101–3.
- Wang LD, Zhou Q, Xing Y, et al. Comparative studies of relationship between the changes of p53 tumor suppressor gene and cell proliferations in esophageal epithelia among subjects from China and the United State. *J Henan Med Univ* 1995; 30: 121–3.
- Wang LD, Zhou Q, Wang YH, et al. Comparative studies of expression of glutathione S-transferase in esophageal and gastric cardial epithelium among subjects from China and the United State. *J Henan Med Univ* 1995; 30(2): 124–7.
- Wang LD, Zhou Q, Wang YH, et al. Studies on expression of procarcinogenesis genes EGFR, C-Jun and Ras of esophagus in population in high-incidence area in Henan. *J Henan Med Univ* 1995; 30: 143–5.
- Wang LD, Zhou Q, Li YX, et al. Expression of c-erb B2, c-myc cyclin D1 in human esophageal and gastric cardial precancerous lesions. *J Henan Med Univ* 1995; 30: 146–9.
- Wang LD, Zhou Q, Gao SS, et al. Preliminary studies of Ras protein expression in human gastric cardial carcinoma. *J Henan Med Univ* 1995; 30: 149–52.
- Wang LD, Yang WC, Zhou Q, et al. Changes of tumor suppressor gene p53 and WAF-1 P21 and cell proliferation in esophageal carcinogenesis in a high-risk population in northern China. *Chin J New Gastroenterology* 1997; 3: 87–9.
- Wang LD, Zhou Q, Yang WC, et al. Expression of tumor suppressor gene Maspin in esophageal squamous cell carcinoma. *J Henan Med Univ* 1997; 32: 48–9.
- Wang LD, Li J, Li J, et al. Expression of tumor suppressor gene Rb and P16 in esophageal precancerous lesions. *J Henan Med Univ* 1997; 32: 30–3.
- Wang LD, Yu GQ, Gao SS, et al. Changes of tumor suppressor gene p16 and p53 in esophageal cancer and its adjacent cancer tissue. *J Henan Med Univ* 1997; 32: 34–6.
- Wang LD, Zhou Q, Zhang YC, et al. p53 alteration and cell proliferation in esophageal epithelia among subjects from high and low incidence areas of esophageal cancer. *Chin J New Gastroenterol* 1997; 5: 221–2.
- Wang LD, Zhou Q, Wei JP, et al. Apoptosis and its relationship with cell proliferation, p53, Waf1, p21, bcl-2 and c-myc in esophageal carcinogenesis studied with a high-risk population in northern China. *World J Gastroenterol* 1998; 4: 287–93.
- Wang LD, Yang WC, Zhou Q, et al. Relationship between the expression of p53, c-myc, bcl-2 and the apoptosis in esophageal carcinogenesis. *J Clin Exp Pathol* 1998; 14: 106–8.
- Shi ST, Yang GY, Wang LD, et al. Role of p53 gene mutations in human esophageal carcinogenesis: results from immunohistochemical and mutation analyses of carcinomas and nearby non-cancerous lesions. *Carcinogenesis* 1999; 20: 591–7.
- Xing EP, Nie Y, Song Y, et al. Mechanisms of inactivation of p14ARF, p15INK4b and p16INK4a genes in human esophageal squamous cell carcinoma. *Clin Cancer Res* 1999; 5: 2704–13.
- Li J, Feng CW, Zhao ZG, et al. A preliminary study on ras protein expression in human esophageal cancer and precancerous lesions. *World J Gastroenterol* 2000; 6: 278–80.
- Li J, Zhao ZG, Zhou Q, et al. Expression of ras protein in human esophageal cancerous and precancerous lesions. *Chin J Clin Oncol Rehabili* 1999; 6: 11–2.
- Li J, Zhou Q, Wang LD, et al. Expression of tumor suppres-

- sor gene maspin in esophageal and gastric cardia cancer. *Cancer Res Prev Treat* 1999; 26: 1–2.
31. Li J, Feng CW, Li SY, et al. Expression of nm23-H1 protein in human esophageal squamous cell carcinoma in high incidence area of esophageal cancer in China. *J Surg Henan* 1999; 5: 9–11.
32. Li J, Feng CW, Zhao ZG, et al. A preliminary study on ras protein expression in human esophageal cancer and precancerous lesions. *World J Gastroenterol* 2000; 6: 278–80.
33. Li J, Yang WC, Feng CW, et al. Preliminary study on tumor suppressor gene maspin in esophageal squamous cell carcinomas. *Chin J Cancer Prev Treat* 2000; 7: 13–5.
34. Zhou Q, Wang LD, Du F, et al. Changes of TGF- β 1 and T β RII expression in the esophageal precancerous and cancerous lesions: a study of a high-risk population in Henan, northern China. *Dis Esophagus* 2002; 15: 74–9.
35. Song ZB, Gao SS, Wang LD, et al. Correlation between p53, PCNA and the prognosis of esophageal carcinoma from the subjects in high-incidence area. *Henan Med Res* 2002; 11: 97–100.
36. An JY, Wang LD, He XW, et al. Expression of PTEN protein in esophageal squamous cell carcinomas and gastric cardia adenocarcinoma tissues from high-incidence area for esophageal cancer in Henan. *J Zhengzhou Univ (Med Sci)* 2002; 37: 750–2.
37. Zhuang ZH, Wang LD, Wang QM, et al. Expression of cyclooxygenase-2 protein in human esophageal carcinoma tissues on the subjects at high-incidence area for esophageal cancer in Henan. *J Zhengzhou Univ (Med Sci)* 2002; 37: 753–5.
38. Zhuang ZH, Wang LD, Gao SS, et al. Expression of MUC1 in esophageal and gastric cardiac carcinoma tissues from high-incidence area for esophageal cancer in Henan. *J Zhengzhou Univ (Med Sci)* 2002; 37: 774–7.
39. Feng CW, Qi YJ, Guo RF, et al. Preliminary analysis on phosphotyrosine protein in esophageal cancer and adjacent non-cancer tissues from the patients at high-incidence area for esophageal cancer in Henan. *J Zhengzhou Univ (Med Sci)* 2002; 37: 769–71.
40. Sun C, Liu B, Wang LD, et al. Expression of p53 and Rb protein in esophageal squamous cell carcinomas from the young and old patient s at high-incidence area for esophageal cancer in Henan. *J Zhengzhou Univ (Med Sci)* 2002; 37: 748–50.
41. Wang LD, Liu B, Guo RF, et al. Changes of C-erbB2 and c-myc expression in esophageal and gastriccardia carcinogenesis from the subjects at high-incidence area for esophageal cancer in Henan. *J Zhengzhou Univ (Med Sci)* 2002; 37: 739–42.
42. Qin YR, Liu Z, Guo HQ, et al. Expression of p27 gene and cyclinE in esophageal precancerous lesions from the subjects at high-incidence area for esophageal cancer in Henan. *J Zhengzhou Univ (Med Sci)* 2002; 37: 763–5.
43. Zhou Q, Zheng ZY, Wang LD, et al. P53 protein accumulation and p53 gene mutation in esophageal and gastric cardia cancer from the patients at Linzhou, Henan. *J Zhengzhou Univ (Med Sci)* 2003; 38: 313–6.
44. Zhou Q, Bai YM, Wang LD, et al. Alterations of C-erbB2 in gastrocardia precancerous and cancerous lesions: a comparative study between the high- and low-risk populations. *J Zhengzhou Univ (Med Sci)* 2003; 38: 335–7.
45. Sun C, Liu B, Wang LD, et al. Changes of p53 and Rb proteins expression in esophageal squamous cell carcinoma of the elderly and the young patients at high-risk area for the cancer in Henan Province. *Chin J Geriatr* 2003; 22: 274–6.
46. Li JX, He X, Wang LD, et al. Expression of cyclin D1 protein and mRNA in cancer and adjacent tissues in the same patient in Linzhou, a high- incidence area for esophageal cancer in northern China. *Henan Med Res* 2003; 12: 197–200.
47. Xie DL, Wang LD, Li JX, et al. Studies of relationship between gastric cardia adenocarcinoma and p15 gene methylation in patients at high-incidence area. *Chin J Tradit Chin West Med* 2004; 5: 693–5.
48. Sun C, Wang LD, Wang QM, et al. Expression of p53 and Rb protein in esophageal precancerosis and carcinoma tissue of patients and relation to their ages. *World J Gastroenterol* 2004; 12: 2222–5.
49. Yi XN, Wang LD, Song ZB, et al. Survivin expression in esophageal squamous cell carcinoma of patients from Linzhou city, a high-incidence area for esophageal cancer in northern China. *J Zhengzhou Univ (Med Sci)* 2004; 39(6): 953–6.
50. Li JX, Li YJ, Qin YR, et al. FHIT mRNA and protein expression in esophageal carcinoma and matched adjacent normal esophageal tissues at high-incidence area in Henan Province. *World Chin J Dig* 2005; 13: 1417–20.
51. Sun C, Wang LD, Wang QM, et al. Expression of RAR β and MUC1 protein in esophageal carcinoma tissue in the young and elderly patients. *Chin J Dig* 2005; 25: 620–1.
52. Lv XD, Wang LD, Qi YJ, et al. Expression of mdm2, bcl-2, bax and p53 protein in the cancer tissues of concurrent carcinomas of the esophagus and gastric cardia. *Chin J Cancer Prev treat* 2006; 13: 5–8.
53. Li J, Jiao XY, Du F, et al. Expressive changes of NF- κ B protein in the esophageal carcinoma and precancerosis tissue of the subjects at high-incidence area in Henan. *J Zhengzhou Univ (Med Sci)* 2006; 41: 22–4.
54. Wang NB, Gao SS, He X, et al. Expression of Rb in esophagus and gastric cardia concurrent carcinomas tissue from high incidence area of esophageal cancer in Henan. *J Zhengzhou Univ (Med Sci)* 2006; 41: 24–6.
55. Chang ZW, Wang LD, Gao SS, et al. Expression of FHIT and p53 in patients with familial esophageal cancer. *J Zhengzhou Univ (Med Sci)* 2006; 41: 24–6.
56. Lv XD, He X, Li JL, et al. Expression of mdm2, CyclinD1 and p16 in concurrent cancers of esophagus and gastric cardia. *J Zhengzhou Univ (Med Sci)* 2006; 41: 22–4.
57. Qin YR, Li YX, Wang LD, et al. Expression of c-myc, hTERT and c-MET in esophageal squamous cell carcinoma and lymph node metastatic tissue. *J Zhengzhou Univ (Med Sci)* 2006; 41: 34–6.
58. Li JL, Li YF, Qin YR, et al. Expression of C-erbB-2 protein and mRNA in esophageal cancer tissue. *J Zhengzhou Univ (Med Sci)* 2006; 41: 117–9.

Isolation and characterization of rbcL gene from *Dunaliella salina* [☆]

Yurong Chai¹, Yun Sun¹, Weidong Pan², Yanlong Jia², Lexun Xue^{2,*}

¹Department of Histology and Embryology, Basic Medical College, Zhengzhou University, Zhengzhou, Henan 450052, China;

²Laboratory for Cell Biology, Zhengzhou University, Zhengzhou, Henan 450052, China

Received September 12, 2006

Abstract

Ribulose-1,5-bisphosphate carboxylase/oxygenase (Rubisco) is a key enzyme in photosynthesis, and its large subunit gene, from the chloroplast genome, encodes the enzyme's catalytic site. The present study was aimed to determine the nucleotide sequence of the large subunit of Rubisco (rbcL) from *Dunaliella salina* (*D. salina*). A pair of degenerate primer was designed according to the highly conserved amino acids of the known rbcL and was used to amplify the rbcL gene from *D. salina* by touch-down PCR (TD-PCR) and rapid amplification of cDNA ends (RACE). The resulting TD-PCR product was 1,347 bp in size, encoding a polypeptide of 449 amino acids. According to this result, 5' RACE and 3' RACE were performed to obtain the 5'-end and 3'-end of the rbcL gene. The complete open reading frame of *D. salina* rbcL was long 1,416 bp encoding a polypeptide of 472 amino acids, which shared high similarity of amino acid sequences with those of other species. It can be concluded that the full-length rbcL gene is potential isolated from the chloroplast genomic DNA of *D. salina*. [Life Science Journal. 2007;4(1):6–12] (ISSN: 1097–8135).

Keywords: *Dunaliella salina*; Rubisco; rbcL; degenerate primer; RACE

1 Introduction

Genetic engineering of microalgae has been greatly developed, including prokaryotic microalgae *Cyanobacterium*, and eukaryotic microalgae *Chlamydomonas reinhardtii*, *chlorella*, etc. *Dunaliella salina*, a unicellular green alga, which was one of the most halotolerant eukaryotes, originally described by Dunal in 1938^[1], has a thin cellular membrane, and a single, large cup-shaped chloroplast with its photosynthetic thylakoid membranes, pyrenoid, and abundance β-carotene globules, but without rigid cell wall. Studies on the genetics of *Dunaliella* have been conducted for decades at a few laboratories^[2,3].

Ribulose-1, 5-bisphosphate carboxylase/oxygenase (Rubisco) is a bi-functional enzyme that catalyzes the initial step of photosynthetic carbonic reduction and photo-respiratory carbon oxidation cycles by combining CO₂ and O₂ respectively^[4]. Rubisco occurs as a hecadecamer containing of eight large subunits (rbcL) and eight small subunits (rbcS) that assemble into a L8S8 holoenzyme

in many eubacteria, cyanobacteria, algae, and higher plants. The rbcL gene encodes the enzyme's catalytic site, and it is conserved in evolution of photosynthetic plants^[5]. The nucleotide sequence analysis of the rbcL can promote the studies of the function and structure, expression and regulation of the Rubisco as well as the phylogenetic relationship of *D. salina*. In the present report the gene coding for the large subunit of Rubisco was cloned from the chloroplast DNA (cpDNA) of *D. salina* and compared with other species.

2 Materials and Methods

2.1 Materials

Dunaliella salina strain: UTEX-LB-1644 was purchased from Marine Plant Collection, Texas University (Texas, USA). It was grown in batch cultures of liquid PKS medium at 25 °C under continuous irradiance of 150 μmol potons/m²/s^[6].

E. coli JM109 was from our laboratory. Plasmid pMD18-T vector, PCR purification kit, DNA gel extraction kit, Taq polymerase and restriction enzymes were purchased from the TaKaRa Co. Ltd (Dalian, China). Trizol was from Invitrogen (California, USA). AMV First strand cDNA synthesis kit was from Shanghai Sangon Co. Ltd (Shanghai, China), and FirstChoice RLM-RACE kit was from Ambion (Texas, USA).

[☆]Supported by National Natural Science Foundation of China (No. 30540067 and 30270031). The work was finished in Henan Key Laboratory for Molecular Medicine, Zhengzhou, China.

*Corresponding author. Tel: 86-371-6665-8332; Email: lxxue@public.zz.ha.cn

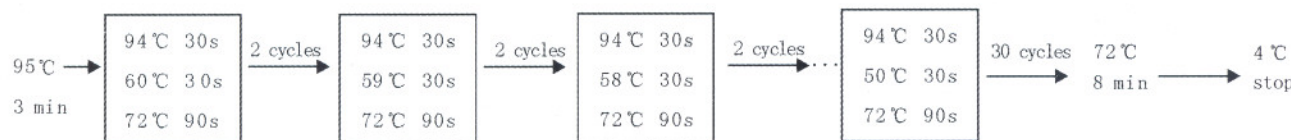
2.2 Methods

2.2.1 Primers. A pair of degenerate primers described below was synthesized based on the conservative regions: GFKAGV and ACEVWK of the *rbcL* amino acids sequence according to the GenBank data. The forward primer was 5'-GGN TTY AAR GCN GGN GT-3' and the reverse primer was 5'-YTT CCA NAC YTC RCA NGC -3' (where N was random base, Y stood for T or C and R was A or G).

2.2.2 Chloroplast DNA extraction and touch-down PCR (TD-PCR) amplification. The chloroplast DNA was isolated from *D. salina* according to Pan^[7]. The cells of about 1×10^8 were harvested by centrifugation for 5 minutes at 4 °C, 5,000 r/min, suspended by 350 μ l NET solution (0.1 M NaCl, 50 mM EDTA, 20 mM Tris-HCl, pH 8.0), added 25 μ l proteinase K (10 mg/ml) and 25 μ l SDS (20 mg/ml), and incubated at 55 °C

for 2 hours, cooled on ice. Then added 200 μ l of 5 M KAc, on ice incubation for 30 minutes, centrifuged for 5 minutes at 4 °C, 12,000 r/min. The aqueous was extracted three times with phenol and chloroform (1/1 volume), precipitated with ethanol, washed the pellet two times with 70% ethanol, and finally the pellet was resuspended in 30 μ l of TE buffer (10 mM Tris-HCl, 1 mM EDTA, pH 8.0).

To get better amplification, a modified TD-PCR was performed using about 500 ng cpDNA of *D. salina* as template^[8]. PCR amplification was performed using a Pekin Elmer DNA Thermal Cycler 480 (Pekin Elmer Biosystems, California, USA). PCR reaction system contained: template 2 μ l, dNTP (each 2.5 mM) 2.5 μ l, primers (20 μ M) 1 μ l, 10× buffer 5 μ l, Taq polymerase (5 u/ μ l) 0.5 μ l, ddH₂O 39 μ l, with a final volume of 50 μ l. PCR program was carried out as following:



2.2.3 Cloning and analyzing of TD-PCR product. The PCR product was fractionated in 1% agarose gel electrophoresis and then the investigated band was purified according to manufacturer's instruction of the DNA gel extraction kit and ligated to the pMD18-T vector. Competent *E. coli* JM109 cells were transformed with the ligation product, then grown on LB-agar plates containing 100 μ g/ml ampicillin, 80 μ g/ml X-gal and 80 μ g/ml IPTG. White colonies were cultured in a 3 ml LB liquid medium containing 100 μ g/ml ampicillin. Plasmid DNA mini-extraction, purification and enzyme digestion were referred to Sambrook^[9].

The positive recombinant plasmid DNA was sequenced by the Shanghai Sangon Co. Ltd (Shanghai, China). The amino acid sequence was deduced from the above DNA data with DNACLUB program. Sequence analysis was performed using GENTYX (Genetic Information Processing Software, Version5.0) program.

2.2.4 Amplification of *rbcL* 5'- and 3'-ends. To obtain the *rbcL* 5'- and 3'-ends of *D. salina*, the total RNA of *D. salina* was extracted with Trizol reagent and rapid amplification of cDNA ends (RACE) was performed by FirstChoice RLM-RACE kit as the protocol described. According to the sequencing result of TD-PCR, gene specific primers (GSP) were designed for 5' RACE and 3' RACE. The 5' end of *rbcL* was amplified with GSP1 (5'-CTGGTGGTACACCAGGTTGTGG-3') and the 3' end of *rbcL* was amplified with GSP2 (5'-GCACCAGGTGCCGTAGCTAAC-3'). The RACE products were separated by electrophoresis; the target

bands were purified by PCR purification kit and ligated to the pMD18-T vector for sequence analysis.

3 Results

3.1 PCR and cloning of the *rbcL* gene

The agarose gel electrophoresis result of the TD-PCR from cpDNA of *D. salina* was shown in Figure 1. The fragment size of the resulting product was about 1,300 bp, then the PCR product was purified and subcloned into the pMD18-T vector. The recombinant plasmids were identified by *Eco*RI and *Hind* III, which included in the multiple cloning sites (MCS) of pMD18-T vector and the correct one was shown in Figure 2. The candidate plasmid was sequenced and named pDS-*rbcL*.

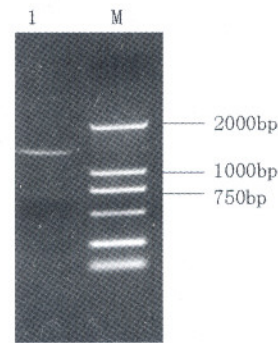


Figure 1. Agarose gel electrophoresis analysis of the PCR product
Lane M: marker, TaKaRa DL2000bp; Lane 1: 1.3 kb PCR product

To obtain the full length DNA sequence of rbcL, RACE was performed to isolate it's 5' end and 3' end. A 350 bp fragment corresponding to the 5' end of the gene was obtained using GSP1 and 5'RACE primer. A fragment about 400 bp was obtained by 3'RACE. The two fragments were then subcloned into the pMD18-T vector, respectively (Figure 3), named pDS-rbcL5, pDS-rbcL3, and sequenced.

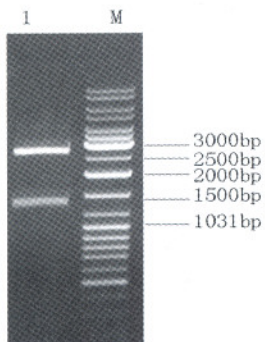


Figure 2. Identification of the recombinant plasmid containing the rbcL fragment

Lane M: marker, Sangon GeneRulerTM DNA Ladder mix; Lane 1: pDS-rbcL/EcoRI + Hind III

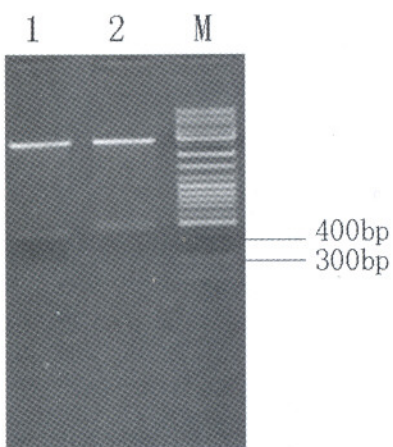


Figure 3. Identification of the recombinant plasmid containing the 5' end and 3' end of rbcL

Lane M: marker, Sangon GeneRulerTM DNA Ladder mix; Lane 1: pDS-rbcL5/EcoRI + Hind III; Lane 2: pDS-rbcL3/EcoRI + Hind III.

3.2 The nucleotide sequences and the deduced amino acid sequences of rbcL

Sequencing result showed that the TD-PCR product from cpDNA of *D. salina* was 1,347 bp long, encoding 449 amino acids residues. Putting the TD-PCR product and 5' end and 3' end fragments together, it was indicated that a complete open reading frame (ORF) of 1,416 bp was obtained. The full length of rbcL has an ORF encoding a putative polypeptide of 472 amino acids

residues (Figure 4). The multiple alignments and BLAST analysis revealed that it shared high identities with rbcL gene of other species in nucleotide sequences, and the highest degree of identification was found with *Dunaliella parva* of 97%.

3.3 Comparison of the amino acid sequences

The amino acid sequences of the rbcL from *D. salina* were aligned in Figure 5. A high degree of similarity to other rbcL was obtained, 99% to *Dunaliella parva*, 93% to *Chlamydomonas reinhardtii*, 85% to *Spinacia oleracea* and 82% to *Zea mays*, respectively. In rbcL of *D. salina*, there are three amino acids deletion mutation between K-Lys and Y-Tyr. Besides, the amino acid sequences of rbcL from *D. salina* are totally identified with the published data of rbcL from *D. parva*, which contained 376 amino acids. Other amino acids like D, M, L, S, Q, I, C, etc., Marked by gray boxes in Figure 5 were identical with those in a green alga *Chlamydomonas reinhardtii* but not in higher plants such as spinach and maize, which was consistent to the phylogenetic relationship of the organisms. Sequences I, II, III, IV were completely identical with those in *Chlamydomonas reinhardtii*, in which I-A1 (12 amino acids), III-A2 (20 amino acids), IV-A3 (13 amino acids), determined the sequences of the catalytic sites and II-C (17 amino acids) determined the sequences of the CO₂ activator peptide in rbcL of *Chlamydomonas reinhardtii*^[10].

Table 1 showed the codon usage in the rbcL gene of *D. salina*. It can be seen that T and A were used more frequently in codons ending than C and G. The preference for T and A as a third base had also been found previously in the rbcL genes of *Chlamydomonas reinhardtii* and *Euglena Gracilis*^[10,11] and other chloroplast rbcL gene.

Based on the rbcL alignment from different species, a pair of degenerate PCR primers was designed to clone the gene of rbcL from *D. salina*. Because of the shorter degenerate primers of only 18 base pairs and the expected PCR product of about 1.3 kb in length, it is difficult to clone so long gene fragment of rbcL from the complex chloroplast genomic DNA, just as what we did in previous experiments. However, TD-PCR can avoid mispriming of the shorter primers and improve the specificity of the PCR^[12]. In this study, the annealing temperature of first cycle was designed at 60 °C to increase the specificity of PCR reaction.

4 Conclusion

In the present study we determined the full length nucleotide sequences of rbcL using TD-PCR and RACE technique from the chloroplast DNA of *D. salina*, a unicellular green alga which can live under the environments with salinity ranging from 0.05 M to 5 M of NaCl. For its unique character,

D. salina would be a promising host of bioreactor and will potentially be a novel system to produce biologically active materials, for example oral vaccine, at lower cost. However, as a stress-tolerance living organism, relative slowly growth rate of *D. salina* made it non-convenient to be genetic modified and

there is less known about the mechanism involved in the lower growth rate of it. One possible reason may lie in the photosynthesis. So it is critical to study the genes associated with the mechanism of photosynthesis of *D. salina* and improve the photosynthetic rate.

```

GCTGATGGCGATGAATGAAACACTGCGTTGCTGGCTTGATGAAAAACTCCACCGACTACT
GCATTGAGGAGCTCTGTGGCTACTAGTAGTAGTAAGAACCTTGGACTTCCTTGAATACC
TAGGCATGCCAGCAACTCTGCTGAGGAAGTCATCTCTTCGTCTGTTCTCCTGCATGCTC
AACCATGAGAGTTGTCAACAACAAG
[ATG] G T A C C A C A A A C T G A A A C T A A A G C T G G T A C T G G A T T T A A G G C T G G T G T A A A A G A T
M V P Q T E T K A G T G F K A G V K D
T A C C G T T T A A C A T A T T A C T C C A G A C T A C G T A G T T A G C G A A A C T G A T A T T T T A G C A
Y R L T Y Y T P D Y V V S E T D I L A
G C T T T C C G T A T G A C T C C A C A A C C T G G T G T A C C A C C A G A A G A G T G C A G C C G T A
A F R M T P Q P G V P P E E C G A A V
G C A G C T G A G T C A T C A A C A G G T A C A T G G A C T A C A G T A T G G A C T G A C G G T C T A A C A A G T
A A E S S T G T W T T V W T D G L T S
T T A G A C C G T T A C A A A G G T C G T T G T A C T G A T T T A G A A C C T G T A C C A G G G G A A G A A A T
L D R Y K G R C Y D L E P V P G E E N
C A G T A C A T C G C T T A C G T G C G T A C C A A T C G A C C T T T T G A A G A A G G T T C A G T A A C A
Q Y I A Y V A Y P I D L F E E G S V T
A A C T T A T T C A C T T C A A T T G T A G G T A A C G T A T T C G G T T T C A A A G C G T T A C G T G C A T T A
N L F T S I V G N V F G F K A L R A L
C G T T T A G A A G A C C T T C G T A T T T C A C C A G C T T A C G T T A A A A C A T T C G T G G A C C A C C T
R L E D L R I S P A Y V K T F V G P P
C A C G G T A T C C A A G T T G A A C G T G A C A A A T A T G G T C G T G G T T T A T T A G G T T G T A C A A T T
H G I Q V E R D K Y G R G L L G C T I
A A A C C A A A A T T A G G T T T A T C A G C T A A A A A C T A C G G T C G T G C T G T T A C G A A T G T T A
K P K L G L S A K N Y G R A V Y E C L
C G T G G T G G T T T A G A C T T A C G A A G G A T G A C G A A A A C G T A A A C T C T C A A C C A T T C A T G
R G G L D F T K D D E N V N S Q P F M
C G T T G G A G A C C G T T T C T T A T T C G A G C T G A A G C T A T T A C A A A G C A C A A A C A G A A
R W R D R F L F V A E A I Y K A Q T E
A C A G G T G A A A T T A A A G G T C A C T A C T T A A A C T G T A C A G C T G G T A C G T T C T G A A G G T A T G
T G E I K G H Y L N C T A G T S E G M
C T T C A A C G T G C A C A A T G T G C T A A A G A A T T A G G T G T A C C A A T T G T A A T G C A T G A C T A C
L Q R A Q C A K E L G V P I V M H D Y
C T A A C T G G T G G T T T C A C A G C A A A C T C A T T A G C A C A T T T C T G T C G T G A C C A C G G T
L T G G F T A N T S L A H F C R D H G
C T T T T A T T A C A C A T T C A C G C T G C G A T G C A C G C T G T A A T T G A C C G T C A A C G T A A C C A C
L L L H I H R A M H A V I D R Q R N H
G G T A T T C A C A T T C C G T G T T A G C T A A A A C T T A C G T A T G C A G G T G G T G C A C C A C C T T
G I H F R V L A K T L R M S G G D H L
C A C T C A G G T A C T G T A G T A G G T A A A C T A G A A G G T G A A C G T G A A G T A A C T T T A G G T T T C

```

H S G T V V G K L E G E R E V T L G F
 GTA GAC TTA ATG CGT GAT AAC TTC GTA GAA AAA GAC CGT AGC CGT GGT ATC TAC TTC
 V D L M R D N F V E K D R S R G I Y F
 ACT CAA GAC TGG TGT TCA ATG CCA GGT GTA ATG CCA GTA GCT TCT GGT GGT ATT CAC
 T Q D W C S M P G V M P V A S G G I H
 GTA TGG CAC ATG CCA GCT CTA GTT GAA ATT GTC GGT GAT GAC GCT TGT TTA CAA TTC
 V W H M P A L V E I V G D D A C L Q F
 GGT GGT GGT ACT TTA GGT CAC CCT TGG GGT AAC GCA CCA GGT GCC GTA GCT AAC CGT
 G G G T L G H P W G N A P G A V A N R
 GTT GCT TTA GAA GCT TGT ACA CAA GCT CGT AAC GAA GGA CGT GAC CTT GCT CGT GAA
 V A L E A C T Q A R N E G R D L A R E
 GGT GGT AAC GTA ATT CGT TCA GCT TGT AAA TGG TCT CCT GAA TTA GCA GCT GCA TGC
 G G N V I R S A C K W S P E L A A A C
GAA GTC TGG AAG GAA ATT AAA TTC GAA TTC GAT ACA GTT GAC AAA TTA [TAA]
 E V W K E I K F E F D T V D K L stop
 TATTTCTTTTCGTCGGAAAAAACATTATCAAAGAAAATCTGGGATTTCTTGAGAAA
 TCTCGAAGATTCGAATATCCTTAAGGATATCGAAACTCGACATTAGTTTTCCCAA
 GGGTCCCCTCAGAGGCCCGGTATTAGAATTCTTTCTAATAGGTTAATCCCTACCT
AAAAAAAAAAACCTATAGT GAGTCGTATTAATCGGATCCGCG

Figure 4. Nucleotide sequences and the deduced amino acids of rb₂L from *D. salina* (GenBank Accession No: AY531529). The primers of TD-PCR were wave-lined. Primers of GSP1 and GSP2 were double-lined. The primers of 5'RACE and 3'RACE in the kit were underlined. Start codon and termination codon were boxed.

D.salina	MVPQTETKAGTGFKAGVKDYRLTYTTPDYYVSETDILAFRMTQPGVPPEECGAAVAAEESSTGTWTTVWT
D.parva	GFKAGVKDYRLTYTTPDYYVSETDILAFRMTQPGVPPEECGAAVAAEESSTGTWTTVWT
C.reinhardtii	MVPQTETKAGAGFKAGVKDYRLTYTTPDYYVVRDTDILAFRMTQLGVPPPEECGAAVAAEESSTGTWTTVWT
S.olerealea	MSPQTETKASVGFKAGVKDYKLTYYTPEYETLTDILAFRVSQPGVPPEEEAGAAVAAEESSTGTWTTVWT
Z.mays	MSPQTETKASVGFKAGVKDYKLTYYTPEYETKDTDILAFRVTQPLGVPPPEEEAGAAVAAEESSTGTWTTVWT
D.s	DGLTSLDRYKGRCYDLEPVPGEEENQYIAYVAPIDLFEEGSVTNFTSIVGNVFGFKALRALRLEDLRISP
D.p	DGLTSLDRYKGRCYDLEPVPGEEENQYIAYVAPIDLFEEGSVNLFTSIVGNVFGFKALRALRLEDLRISP
C.r	DGLTSLDRYKGRCYDIEPVPGEDNQYIAYVAPIDLFEEGSVNMFTSIVGNVFGFKALRALRLEDLRISC
S.o	DGLTNLDRYKGRCYHIEPVAGEENQYICVAYPLDLFEEGSVNMFTSIVGNVFGFKALRALRLEDLRIPV
Z.m	DGLTSLDRYKGRCYHIEPVPGDPDQYICVAYPLDLFEEGSVNMFTSIVGNVFGFKALRALRLEDLRIPP

I -A1

II -C

D.s	AYVKTIVGPPPHGIQVERDK---...YGR <u>G</u> LLGCTIKPKLGLSAKNYGRAVYECLRGGLDFTKDDENVNSQPFMR
D.p	AYVKTIVGPPPHGIQVERDKLNKYGRGLLGCTIKPKLGLSAKNYGRAVYECLRGGLDFTKDDENVNSQPFMR
C.r	AYVKTIVGPPPHGIQVERDK <u>L</u> NKYGR <u>G</u> LLGCTIKPKLGLSAKNYGRAVYECLRGGLDFTKDDENVNSQPFMR
S.o	AYVKTIVGPPPHGIQVERDKLNKYGRPLLGCTIKPKLGLSAKNYGRAVYECLRGGLDFTKDDENVNSQPFMR
Z.m	AYS <u>K</u> TIVGPPPHGIQVERDKLNKYGRPLLGCTIKPKLGLSAKNYGRACYECLRGGLDFTKDDENVNSQPFMR
D.s	WRDRFLFVAEAIYKAQTETGEIKGHYLNCTAGTSEGMLQRAQCAKELGPIVMHDYLGGFTANT\$LAHFC
D.p	WRDRFLFVAEAIYKAQTETGEIKGHYLNCTAGTSEGMLQRAQCAKELGPIVMHDYLGGFTANTSLAHFC
C.r	WRDRFLFVAEAIYKAQAETGEVKGHYLNATAGTCCEMMKRAVCAKELGPIVMHDYLGGFTANTS LAIYC
S.o	WRDRFLFCAEALYKAQAETGEIKGHYLNATAGTCEDMMKRAVFARELGVPIVMHDYLGGFTANTTL SHYC
Z.m	WRDRFVFCAEAIYKAQAETGEIKGHYLNATAGTCCEMIKRAVFARELGVPIVMHDYLGGFTANTTL SHYC
<hr/> III -A2 <hr/>	
D.s	RDHG <u>LLL</u> H I H R AMHAVIDRQRNH <u>G</u> IHFRLAKTLRMSGGDH <u>L</u> HSGTVVGKLEGEREVTGFVDLMRDNFVE
D.p	RDHG <u>LLL</u> H I H R AMHAVIDRQRNH <u>G</u> IHFRLAKTLRMSGGDH <u>L</u> HSGTVVGKLEGEREVTGFVDLMRDNFVE
C.r	RDNG <u>LLL</u> H I H R AMHAVIDRQRNH <u>G</u> IHFRLAKALRMSGGDH <u>L</u> HSGTVVGKLEGEREVTGFVDLMRDDYVE
S.o	RDNG <u>LLL</u> H I H R AMHAVIDRQKNHGMHFRVLAKALRLSGGDHIHSGTVVGKLEGERDITLGFVDLLRDDYTE
Z.m	RDNG <u>LLL</u> H I H R AMHAVIDRQKNHGMHFRVLAKALRMSGGDH <u>I</u> HSGTVVGKLEGEREITLGFVDLLRDDFIE
<hr/> <hr/>	
D.s	KDRSRGIYFTQDW <u>C</u> SMPGV <u>M</u> PVASGGIHVVWHMPALVEIVGDDA <u>C</u> LQFGGGTLGHPWGNAPGAANRVALEA
D.p	KDRSRGIYFTQDWCSMPGVMPVASGGIHVVWH
C.r	KDRSRGIYFTQDWCSMPGVMPVASGGIHVVWHMPALVEIFGDDACLQFGGGTLGHPWGNAPGAANRVALEA
S.o	KDRSRGIYFTQSWVSTPGVLVASGGIHVVWHMPALTEIFGDDSVLQFGGGTLGHPWGNAPGAANRVALEA
Z.m	KDRSRGIFFTQDWVSMPGVIPVASGGIHVVWHMPALTEIFGDDSVLQFGGGTLGHPWGNAPGAANRVALEA
<hr/> IV -A3 <hr/>	
D.s	CT <u>Q</u> ARNEGRDLAREGGNVIR <u>SACK</u> WSPELAAACEVW <u>K</u> EIKFEFDVDKL
D.p	
C.r	CTQARNEGRDLAREGGDVIR <u>SACK</u> WSPELAAACEVW <u>K</u> EIKFEFDTIDKL
S.o	CVQARNEGRDLAREGNTIIREATKWSPELAAACEVW <u>K</u> EIKFEFPAMDTV
Z.m	CVQARNEGRDLAREGNEIIKAACKWSAELAAACEIW <u>K</u> EIKFDGFKAMDTI

Figure 5. Comparison of the *rbcL* amino acid sequences from *D. salina* with that from other species.

D.s: *D. salina*; D.p: *D. parva* with 376 amino acids; C.r: *Chlamydomonas reinhardtii* with 475 amino acids; S.o: *Spinaci oleracea* with 475 amino acids; Z.m: *Zea mays* with 476 amino acids. The active sites A1, A2, A3, and the CO₂ activation region were underlined. The nucleotides in gray boxes were fully identified with those from *Chlamydomonas reinhardtii*. The deletion mutation between K (Lys) and Y (Tyr) were boxed.

Table 1. Codon usage in the rbcL gene of *Dunaliella salina*

TTT-Phe	3 (0.6)	TCT-Ser	4 (0.8)	TAT-Tyr	2 (0.4)	TGT-Cys	11 (2.3)
TTC-Phe	15 (3.2)	TCC-Ser		TAC-Tyr	15 (3.2)	TGC-Cys	1 (0.2)
TTA-Leu	27 (5.7)	TCA-Ser	11 (2.3)	TAA		TGA	
TTG-Leu		TCG-Ser		TAG		TGG-Trp	8 (1.7)
CTT-Leu	7 (1.5)	CCT-Pro	5 (1.1)	CAT-His	2 (0.4)	CGT-Arg	29 (6.1)
CTC-Leu		CCC-Pro		CAC-His	13 (2.8)	CGC-Arg	
CTA-Leu	4 (0.8)	CCA-Pro	16 (3.4)	CAA-Gln	11(2.3)	CGA-Arg	
CTG-Leu		CCG-Pro		CAG-Gln	1(0.2)	CGG-Arg	
ATT-Ile	13 (2.8)	ACT-Thr	16 (3.4)	AAT-Asn	1 (0.2)	AGT-Ser	1 (0.2)
ATC-Ile	4 (0.8)	ACC-Thr		ACA-Thr	13 (2.8)	ACG-Thr	2 (0.4)
ATA-Ile		AAC-Asn	13 (2.8)	AAA-Lys	16 (3.4)	AGA-Arg	1 (0.2)
ATG-Met	10 (2.1)	AGC-Ser	2 (0.4)	AAG-Lys	3 (0.6)	AGG-Arg	
GTT-Val	9(1.9)	GCT-Ala	24(5.1)	GAT-Asp	6(1.3)	GGT-Gly	47(10.0)
GTC-Val	2(0.4)	GCC-Ala	2(0.4)	GAC-Asp	18(3.8)	GGC-Gly	
GTA-Val	25 (5.3)	GCA-Ala	11(2.3)	GAA-Glu	26(5.5)	GCG-Ala	3(0.6)
GTG-Val		GGA-Gly	3 (0.6)	GAG-Glu	2(0.4)	GGG-Gly	1 (0.2)

Numbers in parenthesis indicated per cent of polypeptide (472 amino acids) having this codon.

References

- Avron M, Ben-Amotz A. *Dunaliella*: Physiology, Biochemistry and Biotechnogy. Florida, CRV Press, 1992.
- Geng DG, Wang YQ, Wang P, Li WB, Sun YR. Stable expression of hepatitis B surface antigen gene in *Dunaliella salina* (Chlorophyta). J of Applied phycology 2003; 15(6): 451–6.
- Li J, Ren HW, Huang JH, Yu MM, Ru BG. Transient expression of reporter gene EGFP in transformed *Dunaliella salina*. Chinese J of Biochem Mol Biol 2003; 19(3):338–42.
- Andersson I, Taylor TC. Structural framework for catalysis and regulation in ribulose-1, 5-bisphosphate carboxylase/oxygenase. Arch Biochem Biophys 2003; 414(2):130–40.
- McIvor L, Maggs CA, Stanhope MJ. RbcL sequences indicate a single evolutionary origin of multinucleate cells in the red algal tribe Callithamnieae. Mol Phylogenetic Evol 2002; 23(3): 433–46.
- Fisher M, Pick U, Zamir A. A salt-induced 60-kilodalton plasma membrane protein plays a potential role in the extreme halotolerance of the alga *Dunaliella*. Plant physiol 1994; 106: 1359 – 65.
- Pan WD, Zhang GX, Yuan BM, Li J, Wang JM, Xue LX. Cloning of 16S RNA sequence of the *Dunaliella salina* chloroplast. Journal of Zhengzhou University (Medical Sciences) 2004; 39(1):9 – 12.
- Zhang GX, Yuan BM, Xu PR, Wang JM, Xue LX. Modified touch down PCR efficiently improves specificity of PCR. Life Science Research 2002;6(4):314 – 7.
- Sambrook J, Fritsch EF, Maniatis T. Molecular Cloning: A Laboratory Manual (2nd). New York: Cold Spring Harbor Laboratory Press, Cold Spring Harbor. 1989.
- Dron M, Rahire M, Rochaix JD. Sequence of the chloroplast DNA region of *Chlamydomonas reinhardtii* containing the gene of the large subunit of ribulose bisphosphate carboxylase and parts of its flanking genes. J Mol Biol 1982; 162: 775 – 93.
- Gingrich JC, Hallick R. The *Euglena gracilis* chloroplast ribulose-1, 5-bisphosphate carboxylase gene. J of Biol Chem 1985; 260(30): 16162 – 8.
- Fietto JL, DeMarco R, Verjovski-Almeida S. Use of degenerate primers and touch-down PCR for construction of cDNA libraries. Biotechniques 2002; 32:1404 – 8.

Establishment and characterization of lung adenocarcinoma cell lines with multidrug resistance[☆]

Zhiju Wang¹, Min Li², Wenchao Zhao¹, Guoqiang Zhao², Ziming Dong^{3,*}

¹Department of Physiology, Basic Medical College, Zhengzhou University, Zhengzhou, Henan 450052, China; ²Department of Microbiology and Immunology, Basic Medical College, Zhengzhou University, Zhengzhou, Henan 450052, China; ³Department of Pathophysiology, Basic Medical College, Zhengzhou University, Zhengzhou, Henan 450052, China

Received October 15, 2006

Abstract

Objective. Many discoveries of multidrug resistance (MDR) have resulted from studies with drug-resistant tumor cell lines as their models. Till now, there has been no report on the detailed characterization of such a cell line from lung adenocarcinoma (LA). By long-term exposure of an established LA cell (A549 cell) to increase concentrations of paclitaxel, we established a series of subcultures that were considerably more resistant to this drug. **Methods.** Paclitaxel-resistant sublines (A549/TXL) were established *in vitro* by exposing to stepwise increased concentrations of the drug in a cell culture medium. Biological morphology was analyzed by morphometry and flow cytometry. The chemoresistance indexes of cells were measured by methyl tetrazolium assay. Evaluation of growth, *in vitro* drug sensitivity, and a pharmacokinetic study were performed. **Results.** Compared with parent cells, the resistant sublines were smaller and mixed with giant cells in different sizes and with different numbers of nuclei. The resistant cells, A549/TXL20 were 19.3 times more resistant to paclitaxel and 67.4 times more resistant to cisplatin than the parent cells. The resistant cells also demonstrated cross-resistance to mitomycin, vinblastine, hydroxycamptothecine, and 5-flourouracil (5-FU). Compared with the A549 cell line, an unreasonably higher level of drug-resistance and lower drug concentration was detected in A549/TXL20 cells after exposure to the drug in the culture medium. **Conclusion.** The paclitaxel-induced MDR sublines may be used as an experimental system for the search of a means to overcome drug resistance and elucidate possible mechanisms of acquired MDR involved in human lung adenocarcinoma. [Life Science Journal. 2007;4(1):13–16] (ISSN: 1097–8135).

Keywords: lung adenocarcinoma; multidrug resistance; paclitaxel

1 Introduction

Chemotherapy has proven effective in the therapy or palliation of many human tumors such as testicular cancer and leukemia; however, drug resistance remains a major obstacle in the treatment of other carcinomas. Human lung adenocarcinoma (LA) displays a characteristically high degree of chemoresistance toward a broad spectrum of natural cytotoxic compounds that do not possess obvious functional or structural similarities^[1,2]. This phenomenon is termed multidrug resistance (MDR)^[3]. Since reliable therapeutic alternatives to chemotherapy are still lack, this resistance contributes considerably to the poor prognosis of patients with disseminated LAs.

Paclitaxel, an anti-microtubule agent isolated from

Taxus brevifolia, has been shown to demonstrate clinical efficacy in LA^[4]. This agent binds to and stabilizes microtubules, and consequently, induces mitotic arrest and apoptotic cell death^[5,6]. Paclitaxel-based chemotherapy produced high response rates and satisfied prognosis, and is considered to be the international standard regimen against LA^[7]. However, acquired-resistance to paclitaxel has become a serious clinical issue with the increasing prescription^[8]. With the recent demand to analyze the biological behavior of paclitaxel-resistant tumors and uncover the paclitaxel-resistance mechanism to improve the therapeutic efficacy against recurrent LA, it has become necessary to establish and analyze paclitaxel-resistant LA cell lines which properly and faithfully simulate the clinical situation.

The aim of this study is to establish MDR cell lines of human LA against the clinically important chemotherapeutic compound paclitaxel, to trace the underlying resistance mechanisms of acquired MDR.

[☆]Supported by the National Natural Science Foundation of China (No. 30471952).

*Corresponding author. Email: ziming-dong@163.com

2 Materials and Methods

2.1 Establishment of LA MDR cell lines

Culture medium RPMI-1640 containing 300 mg/L glutamine, fetal calf serum (FCS), and antibiotics were purchased from Gibco (Gaithersburg). A human LA cell line, A549, was used in this study. It was maintained in a RPMI-1640 culture medium supplemented with 10% heat-inactivated FCS, 100 U/mL penicillin, 100 mg/mL streptomycin at 37 °C in an atmosphere of 5% CO₂ and 100% humidity. A549 cells were first incubated in 0.5 nM paclitaxel for 4 weeks. These cells were then periodically treated with 1.0 nM paclitaxel for 2 hours followed by incubation in 0.5 nM paclitaxel until the cells were again almost 100% confluent. This cyclic treatment was repeated five times over a period of 18 weeks. The cells were then cultured in 5 nM paclitaxel, thus generating the paclitaxel-resistant subline A549/TXL5. On stable growth, the paclitaxel concentration was increased every 6 weeks. Stable sublines were acquired from 5 nM to 20 nM paclitaxel and named as A549/TXL5, A549/TXL10 and A549/TXL20. Before experimental use, A549/TXL cells were maintained in a paclitaxel-free culture medium and subcultured at least three times.

2.2 Growth morphometry

The growth rate, saturation density, size, and nucleus to cytoplasm (N/C) ratio were analyzed individually. HE stained, and measured for size and N/C ratio under image analyzer (L2 system, Yen-Hau, Taiwan).

2.3 MTT cytotoxicity assay

Cell number was counted on a hemocytometer and 2,000 cells were pipetted into each well of a 96-well microtiter plate in 100 μ L RPMI-1640 medium. The cells were left to adhere overnight and paclitaxel was then added at increasing concentrations in a volume of 100 μ L medium. After a 10-day incubation period, 20 μ L of MTT stock solution (0.05 mg/100 mL) were added to each well. 4 hours later, the liquid was removed, the formazan crystals released and then solubilized by the addition of 150 μ L DMSO (Merck). The extinction of the purple color, which is directly proportional to the number of viable cells, was measured at a wave-length of 540 nm in the ELISA photometer (Titertek Multiscan Plus MK III). The percentage of viable cells was calculated by the following formula: living cells = (sample ext. - blank ext.) / (control ext. - blank ext.) \times 100%. The IC₅₀ value is defined as the dosage of drugs in which 50% of cellular death (50% reduction of absorbance at 540 nm) occurred after 48-hour treatment.

2.4 Evaluation of drug sensitivity by a colonyforming assay

Cells were suspended in 6-well culture plates at various cell concentrations (10^3 , 5×10^2 , 10^2 , and 50

cells/well for untreated controls; 5×10^3 , 10^3 , 5×10^2 , and 10^2 cells/well for the 5 nM paclitaxel-treated group; 10^4 , 5×10^3 , 10^3 , and 5×10^2 cells/well for the 50 nM drug-treated group; and 5×10^4 , 10^4 , 5×10^3 , and 10^3 cells/well for the 500 nM drug-treated group). After overnight incubation, cultures were exposed to various concentrations of paclitaxel (0 nM, 10 nM, 100 nM, and 1000 nM) for 24 hours at 37 °C, and thereafter the drug was removed and each well was washed with cold PBS and re-incubated by a complete medium. 10 days later, the plates were fixed with Carnoy's fixative (ethanol: chloroform: glacial acetic acid = 6:3:1) and stained with crystal violet. The numbers of visible colonies, consisting approximately of more than 50 cells, were counted and the plating efficiency (P.E.) was calculated as (number of the colonies) / (number of the seeded cells). The surviving fraction was calculated as (P.E. in treated well) / (P.E. in untreated well). The mean value \pm SE was calculated in triplicate.

2.5 Intracellular drug concentration

The subconfluently cultured cells of A549 and A549/TXL20 were exposed to 100 nM paclitaxel for 2 hours. After rinsing twice with cold PBS, cells were harvested into tubes and cell pellets were collected after centrifugation (2,700 rpm, 5 minutes), and were analyzed by solid-phase extraction high performance liquid chromatography (SBS, Sagamihara, Japan). Intracellular paclitaxel concentration of cultured cells was indicated as the total amount of paclitaxel per 10^6 cultured cells. The detection wavelength was 227 nm, and the limit of detection for paclitaxel was 5.0 ng. The intra-day and inter-day coefficients of variation of paclitaxel were 3.5% and 4.1% over the concentration range from 70 ng to 5.0 ng.

2.6 Statistical analysis

The data were collected and analyzed by origin 7.0 software. The results were expressed as mean \pm SE. Comparisons between groups of data were carried out using Student's paired or unpaired *t*-test. Comparisons in one group of data were carried out using One-way ANOVA. *P*-value less than 0.05 was considered statistically significant. IC₅₀ values were determined by non-linear regression by GraphPad Prism software.

3 Results

3.1 Changes of cellular morphology and kinetics

A series of MDR sublines, from A549/TXL5 to A549/TXL20, were established after culturing for more than 1 year, with paclitaxel concentration in the medium increased from 5 nM to 20 nM. Cells adapted to clonal growth, smaller in size and with a lobulated giant nuclei after the drug challenge. They showed increased N/C ratio (Table 1). However, they didn't show any significant changes in growth, saturation density, cell

area and cell perimeter (Table 1 and Figure 1).

3.2 Drug-resistant strength of MDR sublines

The drug resistance of MDR subline A549/TXL20 to paclitaxel was 19.3-fold stronger than the native line at the IC₅₀ level (Table 2). The resistance against cisplatin was increased 67.4 fold. The resistance index remained stable for several weeks even after paclitaxel was withdrawn from the culture medium. Cross-resistance to mitomycin, vinblastine, hydroxycamptothecine, and 5-fluouracil (5-FU) was also observed in LA MDR sublines (Table 3).

Table 1. The biological characteristics of the A549 cell line and paclitaxel-induced multidrug resistance sublines.

Cell line	A549	A549/TXL5	A549/TXL10	A549/TXL20
Doubling time (h)	72.4	74.7	75.5	77.3
Saturation density ($\times 10^5$ cell/cm ²)	4.36	4.28	4.15	4.03
Cell area(μm ²)	352	261	242	214
N/C ratio	0.48 ± 0.1	0.76 ± 0.12	0.75 ± 0.16	0.69 ± 0.17*
Cell perimeter(μm)	76	75	72	68

*P < 0.05, compared with native cell line.

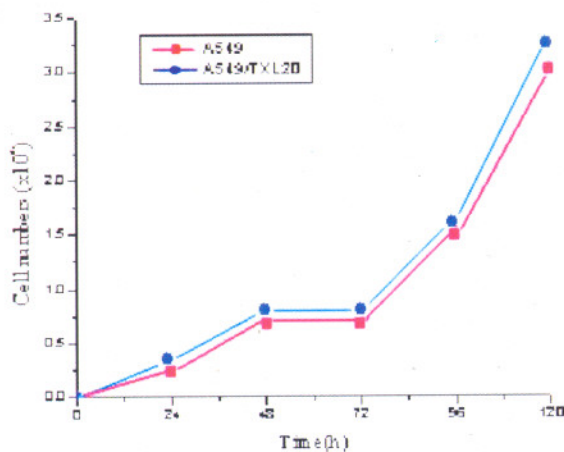


Figure 1. Growth curve of A549 cell line and A549/TXL20 cell line

3.3 Drug sensitivity evaluated by a colony-forming assay

Using the colony-forming assay, the *in vitro* drug sensitivity was evaluated by the surviving fraction of colony formation, after 24-hour exposure to paclitaxel (Figure 2). A549 cell line curves showed the colony forming ability was impaired after exposure to 0 – 1000 nM paclitaxel. On the other hand, the A549/TXL20 subline showed higher drug resistance, characterized by a much shallower slope in the curve of the surviving fraction versus drug dose, and its colony-forming ability was not impaired, even against 100 nM paclitaxel. Compared with the surviving fractions of A549, the resistance of A549/TXL20 was approximately 6,300 fold higher than the resistance of against 1,000 nM paclitaxel.

Table 2. IC₅₀ and resistance index of cell lines to paclitaxel and cisplatin.

Cell line	Paclitaxel		Cisplatin	
	IC ₅₀ (nM)	Resistance index	IC ₅₀ (μg/ml)	Resistance index
A549	81		0.065	
A549/TXL5	308	3.8	0.494	7.6
A549/TXL10	102	12.6	0.637	9.8
A549/TXL20	1560	19.3	4.381	67.4

Table 3. IC₅₀ and resistance index of A549/TXL20 and A549 to nonrelated anticancer drugs

Anticancer drugs	IC ₅₀ (μg/ml)		Resistance index
	A549	A549/TXL20	
Mitomycin	0.039	0.298	7.64
Vinblastine	0.091	0.692	7.06
Hydroxy-camptothecine	0.072	0.096	1.33
5-FU	0.194	2.896	14.93

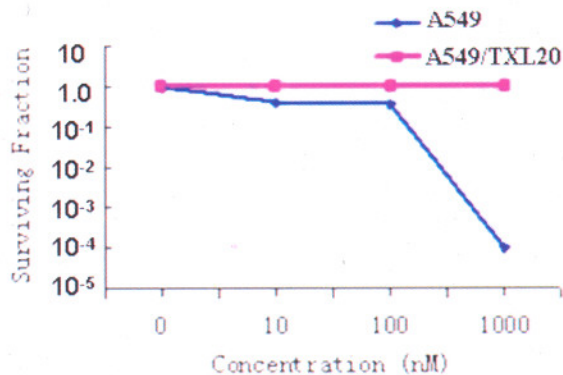


Figure 2. *In vitro* drug sensitivity of A549 and A549/TXL20 evaluated by a colony-forming assay. 10 days after 24-hour exposure to different concentrations of paclitaxel, the plating efficiency was determined by counting the colony number.

3.4 Intracellular drug concentration

Figure 3 showed intracellular paclitaxel concentrations in the cultured cells of A549 and A549/TXL20. At the 2nd hour and the 4th hour of paclitaxel exposure, A549/TXL20 cells contained about 5.6 ng, 0.91 ng paclitaxel respectively, which were much lower than that of A549 cells (64.1 ng and 63.8 ng respectively, P < 0.05).

4 Discussion

Clinical multidrug resistance to chemotherapeutic agents is a major obstacle to potentially curative treatment for LA^[1]. Therefore, one approach to improve treatment is to study the biologic character of the multidrug resistance (MDR) to find ways to reverse it. MDR is characterized by cross-resistance to structurally and functionally unrelated drugs^[9,10]. Although it has been reported that there are different kinds of mechanisms

which are responsible for MDR^[11-13], the mechanism for MDR of LA is not fully elucidated^[14,15]. In this study, we established the paclitaxel - resistant human lung adenocarcinoma cell lines (A549/TXL) by exposing the stepwise increased concentration of paclitaxel in cell media to trace the underlying resistance mechanisms of acquired MDR.

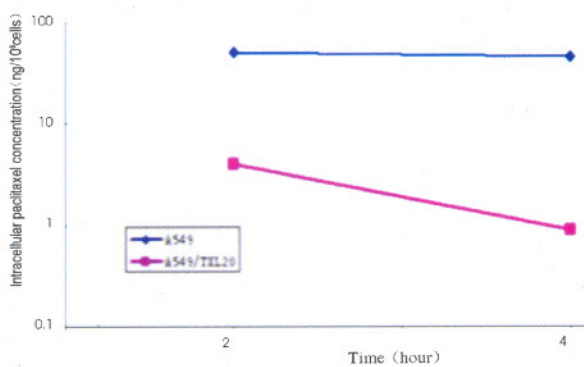


Figure 3. Intracellular paclitaxel concentration of cultured tumor cells. Paclitaxel concentration was measured by solid-phase extraction high performance liquid chromatography. Intracellular concentration of paclitaxel after 2-hour exposure of 100 nM paclitaxel.

As shown by tumor growth curves (Figure 1) and Table 1, the growth property of A549/TXL20 didn't change significantly compared with A549. In addition, compared with A549, decreased cellular size, and increased N/C ratio were shown in the A549/TXL20 (Table 1).

The paclitaxel-induced LA MDR sublines, A549/TXL20, demonstrated cross-resistance to various anti-cancer drugs, including mitomycin, vinblastine, hydroxycamptothecine and 5-FU, in addition to paclitaxel and cisplatin which are in the same family. The resistance of A549/TXL20 to cisplatin is much higher than to the original MDR-inducing drug, paclitaxel. The underlying mechanisms are not yet defined. These anti-cancer drugs have difference in structure and anticancer mechanisms. That means some common pathways may participate in the antidiug function of acquired MDR LA cells at the same time.

A549/TXL20 showed a higher level of paclitaxel-resistance which could be evaluated by drug sensitivity assays (Figure 2). Meanwhile, there was a significant difference in pharmacokinetics between A549 and A549/TXL20 after paclitaxel administration. The intracellular paclitaxel concentration in A549/TXL20 was significantly lower than in A549. These results suggested that the decreased influx and/or the increased efflux of the drug was into the A549/TXL20 cells.

In conclusion, morphological adaptation and intracellular changes could be evoked by drug challenge on LA cancer cells with acquired high drug resistance. The well-characterized MDR sublines may be used as an experimental system for the search of a means to overcome drug resistance and elucidate possible mechanisms of acquired MDR involved in human lung adenocarcinoma.

References

- Struski S, Doco-Fenzy M, Trussardi A, Masson L, Gruson N, Ulrich E, Prout M, Jardillier JC, Potron G, Cornillet-Lefebvre P. Identification of chromosomal loci associated with non-P-glycoprotein-mediated multidrug resistance to topoisomerase II inhibitor in lung adenocarcinoma cell line by comparative genomic hybridization. *Genes Chromosomes Cancer* 2001; 30(2): 136-42.
- Sugawara I, Yamada H, Nakamura H, Sumizawa T, Akiyama S, Masunaga A, Itohama S. Preferential expression of the multidrug-resistance-associated protein (MRP) in adenocarcinoma of the lung. *Int J Cancer* 1995; 64(5):322-5.
- Luqmani YA. Mechanisms of drug resistance in cancer chemotherapy. *Med Princ Pract* 2005; 14 Suppl 1: 35-48.
- Einzig AI, Wiervik PH, Saslo J, Runowicz CD, Goldberg GL. Phase II study and long-term follow-up of patients treated with paclitaxel for advanced ovarian adenocarcinoma. *J Clin Oncol* 1992; 10:1748-1753.
- Mekhail TM, Markman M. Paclitaxel in cancer therapy. *Expert Opin Pharmacother* 2002; 3(6): 755-66.
- Manfredi JJ, Parness J, Horwitz SB. Taxol binds to cellular microtubules. *J Cell Biol* 1982; 94: 688-96.
- McGuire WP, Hoskins WJ, Brady MF, Kucera PR, Partridge EE, Look KY, Clarke-Pearson DL, Davidson M. Cyclophosphamide and cisplatin compared with paclitaxel and cisplatin in patients with stage III and IV ovarian cancer. *N Engl J Med* 1996; 334:1-6.
- Rosell R, Felip E. Predicting response to paclitaxel/carbo-platin-based therapy in non-small cell lung cancer. *Semin Oncol* 2001; 28(4 Suppl 14): 37-44.
- Hendrikse NH, Vaalburg W. Dynamics of multidrug-resistance: P-glycoprotein analyses with positron emission tomography. *Methods* 2002; 27(3): 228-33.
- Pallares-Trujillo J, Lopez-Soriano FJ, Argiles JM. Lipids: A key role in multidrug resistance? *Int J Oncol* 2000; 16(4): 783-98.
- Pradines B, Pages JM, Barbe J. Chemosensitizers in drug transport mechanisms involved in protozoan resistance. *Curr Drug Targets Infect Disord* 2005; 5(4): 411-31.
- Hooijberg JH, de Vries NA, Kaspers GJ, Pieters R, Jansen G, Peters GJ. Multidrug resistance proteins and folate supplementation: therapeutic implications for antifolates and other classes of drugs in cancer treatment. *Cancer Chemother Pharmacol* 2006; 58(1): 1-12.
- Ozben T. Mechanisms and strategies to overcome multiple drug resistance in cancer. *FEBS Lett* 2006; 580(12): 2903-9.
- Paredes-Lario A, Blanco-Garcia C, Echenique-Elizondo M. Expression of multiple-drug resistant proteins in lung cancer. *Cir Esp* 2006; 79(1): 46-56.
- Wilkoff LJ, Dulmadge EA, Vasanthakumar G, Donahue JP. Etoposide-resistant human colon and lung adenocarcinoma cell lines exhibit sensitivity to homoharringtonine. *Cancer Chemother Pharmacol* 1993; 33(2): 149-53.

Thymidine phosphorylase induced by IFN-alpha2b enhances 5-fluorouracil antitumor activity *in vitro* and *in vivo*

Qi Li, Baoping Qiao*, Jiaxiang Wang, Jinxing Wei, Weixing Zhang

Department of Urology, The First Affiliated Hospital of Zhengzhou University, Zhengzhou, Henan 450052, China

Received December 11, 2006

Abstract

Objective. To explore the effect of thymidine phosphorylase expression induced by interferon-alpha on chemosensitivity of 5-fluorouracil(5-FU) in renal clear cell carcinoma. **Methods.** Renal clear cell carcinoma cell line 786-0 was treated by various concentration of interferon (IFN)-alpha2b *in vitro*, and semi-quantitative RT-PCR was used to determine TP mRNA expression. Western blot was used to determine TP protein expression. 50% inhibitory concentration of growth (IC_{50}) of 5-FU in different groups of treated 786-0 cell line was evaluated by MTT assay. The athymic mouse model of xenograft renal clear cell carcinoma were established, and effect of chemotherapy of IFN-alpha2b combined with 5-FU was examined on the growth of xenograft tumor. **Results.** IFN-alpha2b has promoted TP mRNA expression in a dose dependent manner and increased TP protein expression ($P < 0.01$). IC_{50} of 5-FU to 786-0 cell line was obviously decreased with IFN-alpha2b ($P < 0.01$). Effect of chemotherapy of 5-FU was obviously enhanced *in vivo* after IFN-alpha2b combined with 5-FU ($P < 0.05$). **Conclusion.** Up-regulating expression of TP induced by IFN-alpha2b has involved in enhanced cytotoxicity of chemotherapy. [Life Science Journal. 2007;4(1):17–20] (ISSN: 1097–8135).

Keywords: thymidine phosphorylase; interferon; renal clear cell carcinoma; 5-fluorouracil

1 Introduction

Most renal carcinoma patients are insensitive to chemotherapy. Several clinical studies proved certain cytokines combined with chemotherapy can greatly increase chemosensitivity to renal carcinoma cells^[1]. At present 5-fluorouracil (5-FU) and interferon-alpha (IFN-alpha) have applied in clinical treatment. In some cases combination of 5-FU and IFN-alpha have synergized but the underlying mechanism is still unclear. Thymidine phosphorylase (TP) is a nucleoside metabolism enzyme. Compared with adjacent non-neoplastic tissues, higher TP expression is observed in a wide variety of solid tumors including renal cell carcinoma. It is the rate-limiting enzyme of 5-FU activation in tumor and associated with catabolism of 5-FU *in vivo*^[2]. In present study, renal clear cell line 786-0 was treated by various concentrations of IFN-alpha2b to explore the mechanism of synergistic effect its through detecting TP expression and its sensitivity to 5-FU.

2 Materials and Methods

2.1 Materials

IFN-alpha2b (1.8×10^7 IU/1.5 ml) were provided

by Schering-Plough (China) Ltd. 5-FU were purchased from Sunrise(Shanghai, China). 786-0 cells, human renal clear carcinoma cell line, were obtained from the cell Bank of Chinese Academy of Science (Shanghai, China) and the culture medium was RPMI1640 supplemented with fetal serum (10%) and antibiotics. Female BALB/c Mice 4–6 weeks old weighting approximate 20 g (Institute of laboratory Animal Science, Chinese Academy of Science, China) were housed in laminar flow cabinets under specific pathogen-free conditions.

2.2 Detection of TP mRNA by RT-PCR

786-0 cells were plated on six-well plates with 1×10^6 in each well and cultured overnight before treated with IFN-alpha2b. Cells were divided into five groups numbered 1 to 5 and treated with 0, 1000, 3000, 6000 and 12000 IU/ml of IFN-alpha2b respectively for 72 hours. Total RNA of each group was extracted using the Trizol according to the manufacturer's instructions (Invitrogen Corp, England). Complementary DNA (cDNA) was synthesized using AMV RT system (Sangon, China) with 2 μ g of total RNA from each of group with the final volume of 20 μ l. The expression of TP mRNA was semi-quantitatively evaluated by PCR amplification using primer: TP: forward 5'-CATCCAGAGCCCA-GAGCAGA-3', reverse 5'-CCGAACCTAACGTC-CACCACC-3'. glyceraldehyde-3-phosphate dehydrogenase (GAPDH) was as an internal standard. GAPDH: forward: 5'-GCACCGTCAAGGCTGAGAA-3', reverse:

*Corresponding author. Email: baopingqiao@163.com

5'-AGGTCCACCACTGACACGTTG-3'. PCR reactions for two genes were carried out together by TaKaRa TaqTM(Takara, China). Each cycle consisted of denaturation at 94 °C for 40 seconds, annealing at 54 °C for 45 seconds, and extension at 72 °C for 50 seconds. Negative-control PCR was conducted using an aliquot from control RT reaction (in the absence of reverse transcriptase) as a template, and showed no PCR product. PCR products were separated by electrophoresis on 1.5% agarose gels and stained with ethidium bromide. Band intensity was determined with SYN GENE Image picture analyzing software. Expression of TP mRNA was normalized to that of GAPDH.

2.3 Detection of TP protein expression by Western blot

Treated cells were harvested and lysed in lysis buffer. Protein concentrations were measured using the Bradford method. 50 µg protein was loaded per lane and separated by 10% SDS-PAGE gel and electroblotted onto nitrocellulose membranes. The membranes were blocked in 5% skimmed milk powder diluted in TBST. The membrane was then incubated with anti-TP antibody (Santa Cruz, American.) at 1 : 500 dilution overnight. Subsequently, membranes were incubated with a secondary horseradish peroxidase (HRP)-conjugated antibody in wash buffer (0.2% skimmed milk powder diluted in TBST) at 1: 5000 dilution for 2 hours. Finally immunolabeled proteins were visualized using DAB according to the manufacturer's instructions (Zsbio, China). As a loading control, the blot was incubated and reprobed with anti-β-actin antibody (Santa Cruz, American).

2.4 Drug sensitivity *in vitro*

Rapidly growing cells were seeded in 96-well plates with density of 5×10^4 cells/well. After 24 hours, cells were divided into 5-FU group, combination group and control group. In 5-FU group and combination group, a RPMI 1640 medium containing 5-FU from 1 to 10^5 µmol/L was added to appropriate wells. Simultaneously IFN-alpha2b was added into each well in combination group at 6000 IU/ml concentration. 8 wells that were added RPMI 1640 medium without any drugs were taken as control group. The plates were incubated at 37 °C in a 5% CO₂ incubator for 72 hours. 50 µl MTT (5 mg/L) were added into each well and after incubation for another 4 hours, supernatant medium were replaced by 150 µl DMSO. The plates shaken for 10 minutes before absorbance at 492 nm were measured with a microplate reader. The inhibition rate was calculated with the formula: % inhibition = [1 - (absorbance of experimental wells/average absorbance of control wells)] × 100%. Dose-response curves were plotted, and the 50% inhibitory concentration (IC₅₀) was determined graphically.

2.5 Antitumor effect *in vivo*

The antitumor effect of 5-FU alone or combined with IFN-alpha2b was investigated in 15 xenograft-bearing BALB/c mice. Each animal was subcutaneously transplanted with 2×10^6 786-0 cells suspended in 200 µl PBS. 15 days after tumor graft, animals in 5-FU group were received 5-FU (25 mg/kg, *q. o. d*, *i. p.*). Animals in combination group were received the same dosage of 5-FU and IFN-alpha2b (3×10^5 IU/mouse, daily, *i. m.*). Animals in control group were received saline (*i. p.*). Injections were performed for 4 weeks and all animal were executed and tumor weights were scaled with a digital balance.

2.6 Statistical analysis

The results were expressed as the mean ± SD. Differences between groups were analyzed using either one-way ANOVA or one-way ANOVA on ranks with the least significant difference(LSD) tests. *P* value of 0.05 was regarded as significant. All analysis were performed using SPSS10.0 software.

3 Results

3.1 Effect of IFN-alpha2b on the expression of TP mRNA

The results of RT-PCR were shown in Figure 1. Expression quantification of group 1 to 5 were 0.5133 ± 0.0152 , 0.5667 ± 0.0115 , 0.5733 ± 0.0231 , 0.8233 ± 0.0404 , 0.8366 ± 0.0451 , respectively. There were significantly statistical differences between these groups (*F* = 78.493, *P* < 0.01). LSD analysis showed TP mRNA expression increased significantly when treated concentration of IFN-alpha2b is more than 6000 IU/ml. The expression of TP mRNA was significantly increased in a dose-dependent manner with the IFN-alpha2b concentration (*r* = 0.901, *P* < 0.05).

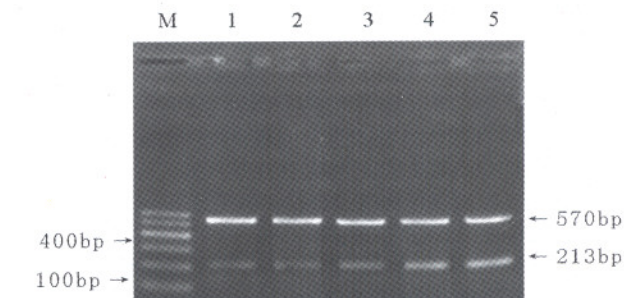


Figure 1. Results of IFN-alpha2b on the expression of TP mRNA Concentration of IFN-alpha2b (IU/ml): Lane 1: 0; Lane 2: 1,000; Lane 3: 3,000; Lane 4: 6,000; Lane 5: 12,000; Lane M: Marker

3.2 Effect of IFN-alpha2b on the expression of TP protein

Expression levels of TP protein were shown in Fig-

ure 2 by Western blot. A band at approximate 45 kDa was detected on the immunoblots, which corresponds to TP protein. Compared with control group, group 2 with 3,000 IU/ml IFN-alpha2b and group 3 with 6,000 UI/ml IFN-alpha2b were indicated stronger expression of TP protein. Quantification were 0.6167 ± 0.0611 , 0.6347 ± 0.0719 , 0.8735 ± 0.0640 in 1, 2 and 3 group respectively with software TotalLab 2.0. Increase of TP protein expression in group 3 was significant compared with control group ($F = 14.232$, $P < 0.01$).

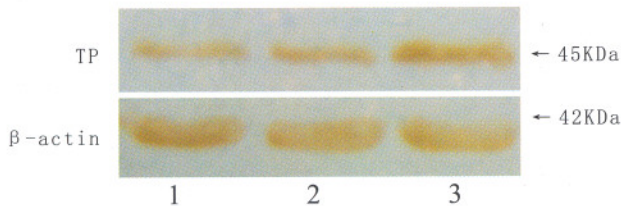


Figure 2. Results of IFN-alpha2b on the expression of TP protein Concentration of IFN-alpha2b (IU/ml). Lane 1: 0; Lane 2: 3,000; Lane 3: 6,000

3.3 IC₅₀ of 5-FU in different treated group

In both 5-FU group and combination group, inhibition rate of treated 786-0 was calculated and is directly related with the concentration of 5-FU (Table 1). IC₅₀ in 5-FU group is remarkably higher than that in combination group. The sensitivity of 786-0 cells to 5-FU was significantly enhanced in combination group ($P < 0.05$).

Table 1. Inhibition rate and IC₅₀ in 5-FU and combination group

5-FU ($\mu\text{mol/L}$)	5-FU		IFN + 5-FU	
	OD Value	IC ₅₀ (μM)	OD Value	IC ₅₀ (μM)
1×10^5	0.1748 ± 0.0056		0.1580 ± 0.0014	
1×10^4	0.2523 ± 0.0182		0.1898 ± 0.0046	
1×10^3	0.3203 ± 0.0221	13.9467 ± 3.7140	0.2283 ± 0.2165	5.3200 ± 0.1039
1×10^2	0.5000 ± 0.0248		0.3708 ± 0.0118	
10	1.1158 ± 0.0400		0.9930 ± 0.4429	
1	1.2623 ± 0.0405		1.1878 ± 0.4461	

3.4 Antitumor effect of different group *in vivo*

The weight of tumor were 1.1820 ± 0.4874 g in control group, 0.6900 ± 0.1517 g in 5-FU group and 0.2500 ± 0.1490 g in combination group. Treatment with 5-FU or 5-FU combined with IFN-alpha2b induced significant shrinkage of tumors compared with control group ($F = 11.533$, $P < 0.01$). Furthermore, combination treatment showed more effective than mere 5-FU treatment ($P < 0.05$). These results indicated that combination with IFN-alpha2b enhanced the sensitivity

to 5-FU *in vivo*.

4 Discussion

5-FU is widely used in the treatment of cancers. However the response rate is only 5% – 20% in the treatment of renal cell carcinoma. Strategies have been explored to modulate the anticancer activity of 5-FU.

5-FU can be metabolized by two ways. One is DNA pathway, and the other is RNA pathway. Compared with RNA pathway, DNA pathway is more efficient in synthesizing fluorodeoxyuridine monophosphate (FdUMP) which is one of active metabolites. FdUMP, a critical metabolite of 5-FU, binds to the nucleotide-binding site of thymidylate synthase (TS). The combination inhibits TS, subsequently blocks forming thymine which tumors need to build their nucleic acids and leads to tumor cells apoptosis. TP proved to be the rate-limiting step of the straight activation of 5-FU to FdUMP. Increasing TP expression appeared to be the appropriate way to trigger the DNA pathway^[3]. In our research it was observed that chemosensitivity of 786-0 cells to 5-FU was dramatically increased by combination IFN-alpha2b. The value of IC₅₀ of 5-FU is $13.9467 \mu\text{mol/L}$ in sole use, while in combination the value decreased to $5.3200 \mu\text{mol/L}$. In xenograft models better antitumor results were shown in combination group. Weight of tumor was merely 0.25 g in average under the treatment of combination, and under sole 5-FU treatment weight of tumor had reached 0.69 g. Those results proved combination can achieve better therapy effect. To clarify this result, our research detected the expression of TP and found expression of both TP mRNA and TP protein were up-regulated in 786-0 cells treated by IFN-alpha2b, which showed a dose-dependent manner with the IFN-alpha2b concentration. This finding indicated TP involved in enhanced chemosensitivity which was caused by combination use of 5-FU and IFN-alpha2b.

Although some pathological studies indicate TP had involved in angiogenic and antiapoptotic activities and correlated with unfavorable prognosis^[4,5], it was highlighted that those studies had not accompanied with fluoropyrimidine drugs. In our study, no matter *in vitro* or *in vivo*, enhanced sensitivity to 5-FU was observed in 786-0 cells by upregulating TP which induced through combination therapy. Several studies discovered that other cytokines such as TNF- alpha or interleukin-1 increased TP expression in tumor cells and increased sensitivity to 5-FU. In xenograft models fluoropyrimidine drugs can be more efficient in inhibiting tumor growth by transfecting tumor cells with TP gene. Those experiments suggested fluoropyrimidine drugs can be particularly activated by TP and TP is an important molecular marker for reference when chemotherapy was adopted with fluoropyrimidine drugs^[1,6]. In renal carci-

noma therapy, TP could be a candidate index to chemotherapy with fluoropyrimidine.

References

1. Gez E, Rubinov R, Gaitini D, et al. Interleukin-2, interferon-alpha, 5-fluorouracil, and vinblastine in the treatment of metastatic renal cell carcinoma: a prospective phase II study: the experience of Rambam and Lin Medical Centers 1996 – 2000. *Cancer* 2002; 95(8):1644 – 9.
2. Hirano Y, Takayama T, Kageyama S, et al. Thymidine phosphorylase and dihydropyrimidine dehydrogenase in renal cell carcinoma: relationship between histological parameters and chemosensitivity to 5-fluorouracil. *Eur Urol* 2003; 43(1):45 – 51.
3. Ciccolini J, Evrard A, Cuq P. Thymidine phosphorylase and fluoropyrimidines efficacy: a Jekyll and Hyde story. *Curr Med Chem Anticancer Agents* 2004; 4(2):71 – 81.
4. Ikeda R, Furukawa T, Mitsuo R, et al. Thymidine phosphorylase inhibits apoptosis induced by cisplatin. *Biochem Biophys Res Commun* 2003; 301(2):358 – 63.
5. Igawa H, Fujieda S, Kimura Y, et al. Influence of platelet-derived endothelial cell growth factor/thymidine phosphorylase on the cell cycle in head and neck squamous cell carcinoma *in vitro*. *Oncol Rep* 2003; 10(4):967 – 71.
6. Morita T, Matsuzaki A, Tokue A. Enhancement of sensitivity to capecitabine in human renal carcinoma cells transfected with thymidine phosphorylase cDNA. *Int J Cancer* 2001; 92(3): 451 – 6.

Changes of Z-line at gastroesophageal junction in symptom-free subjects from high-incidence area for esophageal cancer in Henan[☆]

Lidong Wang^{1*}, Baochi Liu¹, Xin Song¹, Shanshan Gao¹, Zongmin Fan¹, Bin Liu², Changwei Feng³,
Xin He¹, Yanrui Zhang⁴, Jilin Li⁵, Xinying Jiao⁵, Xiaoshan Feng¹, Guolan Xin¹, Mei Zhang¹, Aiqun Wu¹

¹Henan Key Laboratory for Esophageal Cancer, Basic Medical College, Zhengzhou University, Zhengzhou, Henan 450052, China;

²Department of Gastroenterology, Tongren Hospital, Capital Medical University, Beijing 100013, China; ³Department of Gastroenterology, The Second Affiliated Hospital of Zhengzhou University, Zhengzhou, Henan 450003, China; ⁴Department of Gastroenterology, Henan Province People's Hospital, Zhengzhou, Henan 450014, China; ⁵Department of Pathology, Yaocun Esophageal Cancer Hospital, Linzhou, Henan 456500, China

Received December 11, 2006

Abstract

Z-Line is the boundary at esophageal and gastric cardia junction. Upgrowth of Z-line has been regarded as a manifestation of reflux esophagitis, which may induce Barrett's esophagus in western countries. The present study was undertaken to characterize the appearance changes of Z-line and its correlation with esophageal and gastric cardia precancerous lesions on symptom-free subjects from the high-incidence area for esophageal cancer in Henan. Endoscopy and mucosal biopsy histopathological examination were performed on 1, 217 symptom-free subjects (≥ 30 years old) from the high-incidence area for esophageal cancer in Linzhou, Henan. Z-line appearance was recorded as upgrowth, irregular, and indistinct. All the biopsies were fixed with 85% alcohol and processed for routine HE staining and histopathology. The endoscopic observation was correlated with histopathological results. The detection rates for the upgrowth (≥ 3 cm), irregular and indistinct Z-line were 12%, 10% and 1%, respectively. The incidence for Z-line upgrowth and irregular in male at different age groups was apparently higher than that in female ($P < 0.05$). The incidence for irregular Z-line in young female was higher than in other age groups ($P < 0.05$). With the age increasing, a decreasing tendency for Z-line upgrowth was observed both in male and female. The subjects with Z-line upgrowth had a higher incidence for esophageal basal cell hyperplasia and dysplasia in lower esophageal segment than in those without Z-line upgrowth ($P < 0.05$). The incidence for chronic superficial gastritis, atrophic gastritis with intestinal metaplasia was higher in the subjects with Z-line upgrowth than in those without Z-line upgrowth. The present results demonstrate that there is an apparent change of Z-line upgrowth in symptom-free subjects from the high-incidence area for esophageal cancer in Henan. Z-line upgrowth is related with both esophageal and gastric cardia lesions, suggesting that Z-line upgrowth may be one of the early indicators for esophageal and gastric cardia carcinogenesis. The present observations provide new insight for understanding of esophageal and gastric cardia carcinogenesis. [Life Science Journal. 2007;4(1):21–23] (ISSN: 1097–8135).

Keywords: esophageal neoplasm; high-incidence area; precancerous lesion; Z-line; esophagus; gastric cardia

1 Introduction

The boundary of the transitional zone from esophageal squamous epithelium to gastric cardia columnar epithelium, which is collapsed by mucosa of the junction between esophagus and cardia, has been nomi-

nated as "Z-line". The description of normal conformation of Z-line is not unanimous. Abnormal appearance of Z-line, especially upgrowth, has been known as one of manifestation of reflux esophagitis, which may induce Barrett's esophagus in western countries^[1,2]. Barrett's esophagus has been regarded as one of precancerous lesions for esophageal adenocarcinoma^[3]. However, both reflux esophagitis and Barrett's esophagus are uncommon in Chinese population at high risk for esophageal cancer^[4]. In China, squamous cell carcinoma(SCC) is the predominant histological type of esophageal cancer (95%)^[5]. In contrast, in western countries, more than

[☆]Supported in part by National Outstanding Young Scientist Award of China (No. 30025016) and National Natural Science Foundation of China (No. 30670956).

*Corresponding author. Lidong Wang, M. D., Ph. D., Tel and Fax: 86-371-6665-8335; Email: ldwang@zzu.edu.cn

half of the esophageal cancer is adenocarcinoma^[6]. We have found the different abnormal appearance changes of Z-line under endoscopic examination on the symptom-free subjects from the high-incidence area for esophageal cancer in Henan, China. These changes become clear after esophageal mucosa stained with iodine, including upgrowth, irregular, and indistinct. Biological significance of the conformation changes is not clear. We hypothesized that Z-line upgrowth, resulted in prolongation of gastric columnar epithelium into the lower esophagus, might be one of the important early indicators in carcinogenesis of adenocarcinoma at the gastroesophageal junction. The present study was thus undertaken to characterize the appearance changes of Z-line in symptom-free subjects from the high incidence area for esophageal cancer in Linzhou, northern China and to correlate these changes with occurrence of esophageal and gastric cardia precancerous lesions.

2 Materials and Methods

2.1 Subjects

1,217 symptom-free subjects (26–65 years old) from Linzhou, the high-incidence area for esophageal cancer in Henan Province were enrolled for the screening of early esophageal and gastric cardia cancers. All the subjects were examined by endoscopy, mucosal biopsy and histopathological examinations, and the appearance changes of Z-line were recorded under endoscopy.

2.2 Endoscopic biopsy and classification of Z-line appearance changes

Biopsies were taken from each subject at middle esophagus (30–32 cm to Z-line), lower esophagus (3 cm above gastroesophageal junction) and gastric cardia. All the biopsies were immediately fixed with 85% alcohol. The appearance of Z-line changes were classified into four different types, i.e., normal: Z-line was regular and clear; upgrowth: Z-line presents finger or ligulate-like prolongation into lower esophagus ($\geq 3\text{cm}$); irregular: Z-line presents clear, irregular boundary, without apparent prolongation; indistinct: the boundary of esophageal and gastric cardia transitional zone is not clear.

2.3 Histopathological examination

Histopathological diagnosis for esophageal epithelia was made based on the changes in cell morphology and tissue architecture using previously established criteria^[6]. In brief, the normal esophageal epithelium contained one to three proliferating basal cell layers; the papillae were confined to the lower half of the whole epithelium thickness. In basal cell hyperplasia (BCH), the proliferating basal cells surpassed 15% of the total epithelial thickness. Dysplasia was characterized by nuclear atypia (enlargement, pleomorphism, and hyperchromasia), loss of normal cell polarity, and abnormal tissue maturation. SCC was characterized by confluent and in-

vasive sheets of cohesive, polymorphous cells with hyperchromatic nuclei. The following histopathological classification was used for the gastric cardia epithelia: chronic superficial gastritis (CSG), inflammation manifested by mild lymphocyte and plasma cell infiltration; chronic atrophic gastritis (CAG), glandular morphology disappeared partially or completely absent in the mucosa and replaced by connective tissue, interglandular space infiltrated mainly by plasma cells and lymphocytes; gastric cardia dysplasia (GDYS), neoplastic features including nuclear atypia and/or architectural abnormalities confined to the gastric cardia epithelium, without invasion; gastric cardia adenocarcinoma (GCA), invasion of neoplastic gastric cells through the basement membrane^[6].

2.4 Statistical analysis

The χ^2 test was used for the percentage of lesions with different types of Z-line appearance changes. Spearman correlation test and linear tendency test were used for the correlation between different Z-line types and epithelial lesions ($P < 0.05$) was considered significant.

3 Results

Of the 1,217 symptom-free subjects examined the detection rates for the Z-line appearance of upgrowth, irregular, indistinct and normal types were 12% (141/1,217), 10% (122/1,217), 1% (14/1,217) and 77% (940/1,217), respectively.

The distribution of appearance changes of Z-line by age and gender was summarized in Table 1. The incidence for Z-line upgrowth and irregular in male at different age groups was apparently higher than that in female ($P < 0.05$). With the age increasing, a decreasing tendency for Z-line upgrowth was observed both in male and female. The incidence for irregular Z-line in young female (40–49) was higher than in other age groups ($P < 0.05$). The incidence for indistinct type of Z-line in male and female at different age groups was apparently lower than that for upgrowth and irregular types of Z-line.

Table 1. Distribution of Z-line appearance changes by age and gender

Cases examined (n)	Appearance changes of Z-line		
	Upgrowth n (%)	Irregular n (%)	Indistinct n (%)
Male			
30–	53	31 (22.0)*	21 (15.0)*
40–	57	28 (20.0)	26 (18.0)
50–	56	23 (16.0)	32 (23.0)
60–	22	12 (8.5)	9 (6.0)
Female			
30–	19	14 (10.0)	5 (4.0)
40–	36	18 (13.0)	15 (10.0)**
50–	26	13 (11.0)	10 (7.0)
60–	7	2 (1.0)	4 (3.0)

*Male vs. female, $P < 0.05$ (χ^2 test). **40-age group vs. other age group in female, $P < 0.05$ (χ^2 test).

Table 2 showed the correlation between Z-line appearance changes and gastric cardia pathological lesions on the symptom-free subjects. Cardia pathological changes progressed from normal appearance to upgrowth Z-line ($P < 0.05$). However, the cardia pathological lesions were similar in irregular and indistinct Z-line groups ($P > 0.05$).

Table 2. Correlation between Z-line appearance changes and gastric cardia epithelial lesions

Z-line's appearance changes	Cases examined (n)	Gastric cardia epithelial lesions			
		Normal n (%)	CSG n (%)	CAG + IM n (%)	GDYS n (%)
Upgrowth	106	45 (42)	39 (37)*	19 (18)*	3 (3)
Irregular	76	37 (49)	29 (38)	8 (11)	2 (3)
Indistinct	6	4 (67)	1 (17)	1 (17)	0 (0)
Normal	586	303 (52)	182 (31)	13 (12)	28 (5)

*Upgrowth vs. normal, $P < 0.05$ (χ^2 test).

Table 3 showed the correlation between Z-line appearance changes and lower esophageal lesions on the symptom-free subjects. The subjects with Z-line upgrowth had a higher incidence for esophageal basal cell hyperplasia and esophageal dysplasia (EDYS) in lower esophageal segment than in those without Z-line upgrowth ($P < 0.05$). However, the detection rate for lower esophageal lesions was similar in the irregular and indistinct types of Z-line appearance changes ($P > 0.05$).

Table 3. Correlation between Z-line appearance changes and esophageal epithelial lesions at lower esophagus

Z-line appearance changes	Cases examined (n)	Lower esophageal epithelial lesions		
		Normal n (%)	BCH n (%)	EDYS n (%)
Upgrowth	98	35 (36)	58 (59)*	5 (5)*
Irregular	85	56 (66)	29 (34)	0 (0)
Indistinct	7	6 (86)	1 (14)	0 (0)
Normal	707	425 (60)	263 (37)	19 (3)

*Upgrowth vs. normal, $P < 0.05$ (χ^2 test).

Table 4 showed the correlation between Z-line appearance changes and the middle esophageal lesions on the symptom-free subjects. The subjects with Z-line upgrowth had a higher incidence for esophageal basal cell hyperplasia and EDYS in middle esophageal segment than in those without Z-line upgrowth ($P < 0.05$). The similar results were observed in the middle esophageal lesions and the Z-line appearance changes of irregular and indistinct types as in the lower esophagus ($P > 0.05$).

4 Discussion

The present studies demonstrate that there is an apparent change (23%) of Z-line in symptom-free subjects from the high-incidence area for esophageal cancer in Henan, including upgrowth (12%), irregular (10%),

indistinct (1%). The incidence of esophageal and gastric cardia epithelial lesions, especially in the lower segment from the subjects with Z-line upgrowth was higher than in those without Z-line upgrowth. These results indicate that upgrowth of Z-line may be an early indicator for both esophageal and gastric cardia carcinogenesis in high-risk area. Z-line upgrowth might alternate both lower esophageal and gastric cardia epithelial environment and make these people prone to occurrence of pre-cancerous lesions. Our hypothesis is that the primary esophageal and gastric cardia adenocarcinoma, adenocarcinoma at the junction of esophagus and cardia and Barrett's esophagus related esophageal adenocarcinoma might be a group of related diseases.

Table 4. Correlation between Z-line appearance changes and esophageal epithelial lesions at middle esophagus

Z-line appearance changes	Cases examined (n)	Middle esophageal epithelial lesions		
		Normal n (%)	BCH n (%)	EDYS n (%)
Upgrowth	115	63 (55)	41 (36)*	11 (10)*
Irregular	84	61 (73)	21 (25)	2 (2)
Indistinct	7	5 (71)	2 (29)	0 (0)
Normal	749	444 (59)	267 (36)	38 (5)

*Upgrowth vs. normal, $P < 0.05$ (χ^2 test).

The mechanism of Z-line upgrowth is not clear. Reflux esophagitis may be one of the key factors in Z-line upgrowth development in western countries. Barrett's esophagus may develop after reflux esophagitis. However, the incidence of both reflux esophagitis and Barrett's esophagus in Chinese population, especially in high-risk area for esophageal and gastric cardia cancers, is much lower than in western countries. Z-line upgrowth in Chinese people may not be a result of reflux esophagitis. Further studies are needed to illustrate the mechanism and significance of Z-line upgrowth in Chinese people.

References

- Wallner B, Sylvan A, Janunger KG, et al. Immunohistochemical markers for Barrett's esophagus and associations to esophageal Z-line appearance. *Scand J Gastroenterol* 2001; 36: 910-5.
- Wallner B, Sylvan A, Janunger KG. Endoscopic assessment of the "Z-line" (squamocolumnar junction) appearance: reproducibility of the ZAP classification among endoscopists. *Gastointest Endosc* 2002; 55: 65-9.
- Liu B, Wang LD. About Barrett's esophagus. *World Chin J Dig* 1999; 7: 921-5.
- Zhang YR, Zhou Y, Qin YR, et al. Prevalence and significance of reflux esophagitis: comparative study on the subjects at high-and low-incidence areas for esophageal cancer in Henan. *Journal of Zhengzhou University(Medical Sciences)* 2002; 37: 761-3.
- Wang LD, Zhou Q. Mechanism and clinical research of esophageal carcinogenesis. *World Chin J Dig* 1998; 6: 12-4.
- Wang LD, Zhou Q, Yang CS. Esophageal and gastric cardia epithelial cell proliferation in northern Chinese subjects living in a high-incidence area. *J Cell Biochem Suppl* 1997; 28-29: 159-65.

Expression of vascular endothelial growth factor C in human esophageal squamous cell carcinoma

Hongxin Zhang¹, Lan Zhang¹, Kuisheng Chen¹, Dongling Gao¹, Fucheng He², Yunhan Zhang^{1,*}

¹Department of Pathology, The First Affiliated Hospital, Zhengzhou University; Henan Key Laboratory of Tumor Pathology, Zhengzhou, Henan 450052, China; ²Department of Clinical Laboratory, The First Affiliated Hospital, Zhengzhou University, Zhengzhou, Henan 450052, China

Received August 20, 2006

Abstract

To examine the expression of vascular endothelial growth factor C (VEGF-C) in human esophageal squamous cell carcinoma (ESCC) and to clarify its role in lymphatic metastasis in ESCC. Esophageal carcinoma EC9706 cells and samples of 49 patients with primary ESCC were investigated by using S-P immunohistochemistry (IHC), semi-quantitative RT-PCR *in situ* and hybridization (ISH) technology for VEGF-C expression, respectively. VEGF-C positive expressions were found in EC9706 cells through ICH, ISH and RT-PCR, respectively. Positive IHC for VEGF-C was observed in 36 of 49 cases of ESCC. The brown staining granules for VEGF-C were identified in the cytoplasm of carcinoma cells. There was significantly difference between the expression of VEGF-C in the group with lymph node metastasis and the group without lymph node metastasis ($\chi^2 = 4.7, P < 0.05$). Positive ISH for VEGF-C was observed in 23 of 49 cases of ESCC. The blue-purple staining granules for VEGF-C were identified in the cytoplasm of carcinoma cells. There was a significant difference between the expression of VEGF-C in lymph node group and group without lymph node metastasis ($\chi^2 = 31.3, P < 0.01$). The expression of VEGF-C protein level was significantly higher in group with lymph node metastasis than in group without lymph node metastasis. Of 49 ESCC, VEGF-C gene expression was observed by RT-PCR in 29 cases. There was a significant difference between the expression of VEGF-C in group with lymph node metastasis and group without lymph node metastasis ($\chi^2 = 23.3, P < 0.01$). VEGF-C mRNA expression was significantly higher in group with lymph node metastasis than in group without lymph node metastasis. The expression of VEGF-C mRNA level was not significantly associated with age, gender, or pathological grade. There was a correlation between VEGF-C mRNA expressions by RT-PCR and ISH ($\chi^2 = 18.5, P < 0.01$) in ESCC, but no significant difference between the two methods. VEGF-C expression may induce lymphangiogenesis in human ESCC. There must be a close correlation between VEGF-C expression and lymph node metastasis. VEGF-C may be serve as a useful prognostic factor in ESCC. [Life Science Journal. 2007;4(1):24–28] (ISSN: 1097–8135).

Keywords: esophageal squamous cell carcinoma; EC9706 cells; VEGF-C; lymphatic metastasis

1 Introduction

Esophageal carcinoma is a common cause of death throughout the world including China especially in the Taihang mountain range. The lymphatic system is the primary pathway of metastasis for esophageal squamous cell carcinoma (ESCC) and the extent of lymph node involvement is a key prognostic factor for the outcome of patients. However, the mechanism of lymphatic metastasis remains unclear.

Lymphangiogenesis, the development of new lymph

vessels, is a relatively new area of clinical investigations. Recent studies show that vascular endothelial growth factor C (VEGF-C) has been identified as a new member of the VEGF family, and is believed to be the only lymphangiogenesis factor in that gene family^[1]. It activates both vascular endothelial growth factor receptor 2 (VEGFR-2) and VEGFR-3^[2]. However, little investigation was on VEGF-C expression in ESCC. The purpose of this study was to detect the expression of VEGF-C and its association with lymph node metastasis in ESCC with immunohistochemistry (IHC), *in situ* hybridization (ISH) and RT-PCR technique. The relationship of VEGF-C to clinicopathological features was investigated furthermore.

*Corresponding author. Tel: 86-371-6665-8175 (Office); Email: yhzhang@zzu.edu.cn

2 Materials and Methods

2.1 Materials

2.1.1 Reagents. Trizol reagent, TaKaRa One Step RNA PCR Kit (AMV), PCR primers for VEGF-C and β -actin, probe for VEGF-C, VEGF-C rabbit anti-human polyclonal antibody, and S-P immunohistochemical staining kit (SP9001) were purchased from Invitrogen Corporation (USA); TaKaRa Biotechnology (Dalian) Co. Ltd Beijing AuGCT Biotechnology Co. Ltd (Beijing, China); Beijing Zhongshan Golden Bridge Biotechnology Co. Ltd, respectively.

2.1.2 Clinical data. The resected specimens from 49 cases of ESCC were obtained from the Anyang Tumor Hospital, Henan, China, between September to November 2004. The carcinoma tissues and normal tissues were immediately placed in liquid nitrogen and pooled at -80°C until use for RT-PCR. Of 49 cases of ESCC, 25 were male, 24 were female, with a mean age of 58.3 years old, arranging from 44 to 76 years. All had not received any radiotherapy or chemotherapy. All the specimens were clearly identified by experienced pathologists. Routine pathological diagnosis showed that grade I, II and III were 14, 23 and 12 cases respectively. Among them, 20 cases presented lymph node metastasis, and 29 cases had no lymph node metastasis.

2.1.3 Cell culture. Human esophageal carcinoma EC9706 cell line was kindly provided by the Chinese Academy of Medical Sciences. The cell line was grown in monolayer culture containing humidified 50 ml/L CO_2 and 950 ml/L air at 37°C . It was cultured in RPMI-1640 medium supplemented with 10% fetal calf serum, 100 $\mu\text{g}/\text{ml}$ streptomycin, and 100 U/ml penicillin (pH 7.2–7.4).

2.2 Methods

2.2.1 RNA isolation and RT-PCR. The total RNA was extracted from ESCC tissue samples stored at -80°C and EC9706 cell line by using Trizol reagent according to the procedures described in the kit. The quality of the isolated RNA was determined by gel electrophoresis, and the concentration and purity of RNA were determined by A₂₆₀/A₂₈₀ ratios. Amplification of VEGF-C and β -actin as an internal control in each reaction was carried out by PCR with the following primer described previously^[3]. The primers of VEGF-C that yield 229bp and the sequences are 5'-AAG GAG GCT GGC AAC ATA AC-3' (forward) and 5'-CCA CAT CTG TAG ACG GAC AC-3' (reverse). The primers of β -actin that yield a 302 bp product as follows: 5'-TCC TCC CTG GAG AAG AGC TA-3' (forward), 5'-TCA GGA GGA GCA ATG ATC TTG-3' (reverse).

2.2.2 *In situ* hybridization (ISH). Sections ($6\ \mu\text{m}$) of the tissue and the prepared cell slides for hybridization were stained according to Chen *et al*^[4]. The probe

oligonucleotide for VEGF-C sequence was 5'-GTC ATG GAA TCC ATC TGT TGA GT-3' as described previously^[5]. Biotin-labeled VEGF-C cDNA anti-sense probe was modified by sulphur.

2.2.3 Immunohistochemistry (IHC). ESCC tissues were sectioned at the thickness of $4\ \mu\text{m}$. After deparaffinization with xylene and dehydration with graded ethanol, the tissue section and cell slides were incubated in PBS containing 30 ml/L H_2O_2 to remove endogenous peroxidases and then in PBS containing 0.1 mol/L citrate to saturate the nonspecific binding sites. After incubation with VEGF-C rabbit anti-human polyclonal antibodies at 1:150 dilution, the sections were treated with instant S-P immunohistochemical reagents and then incubated in a buffer solution containing 3,3-diaminobenzidine tetrahydrochloride (DAB) and H_2O_2 for visualization, followed by dehydration and mounting procedures. Microscopic examination of the sections was then performed. Omission of primary antibodies was used as a negative control.

2.2.4 Statistical analysis. All statistical calculations were carried out using SPSS 10.0 (SPSS Inc., Chicago, USA). Each data is presented as mean \pm SD. The Chi-square test or Student's *t* test was used to analyze data. *P* value of 0.05 or less were considered statistically significant.

3 Results

3.1 Expression of VEGF-C in EC9706 cell line

EC9706 cells expressed VEGF-C by immunohistochemical staining, ISH, and RT-PCR, respectively. The brown staining granules for VEGF-C were identified in the cytoplasm of EC9706 cells by IHC. VEGF-C mRNA (blue-purple granule) was located in cytoplasm of EC9706 cells by ISH (Figure 1).

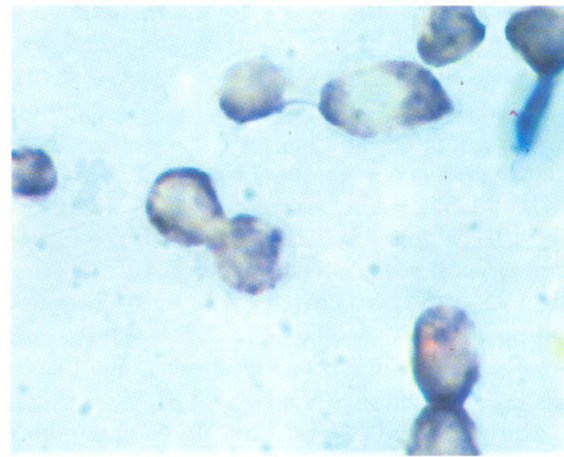


Figure 1. Expression of VEGF-C mRNA in EC9706 cells. There were blue-purple granules in cytoplasm. (ISH, $\times 1000$)

3.2 Relationship between the expression of VEGF-C and pathological features of ESCC

Positive staining was defined as the presence of VEGF-C immunoreactivity in at least 30% of tumor cells^[6]. Positive IHC for VEGF-C was observed in 36 of 49 cases of ESCC (Figure 2). Most of the metastatic lymph nodes showed positive staining for VEGF-C 18 of 20 (90.0%), compared with the cases of non-metastatic lymph node 18 of 29 (62.1%). There was a significant difference between the expression of VEGF-C in group with lymph node metastasis and group without lymph node metastasis ($\chi^2 = 4.7, P < 0.05$). The expression of VEGF-C in ESCC was significantly higher in lymph node metastasis group than in group without lymph node metastasis by IHC.

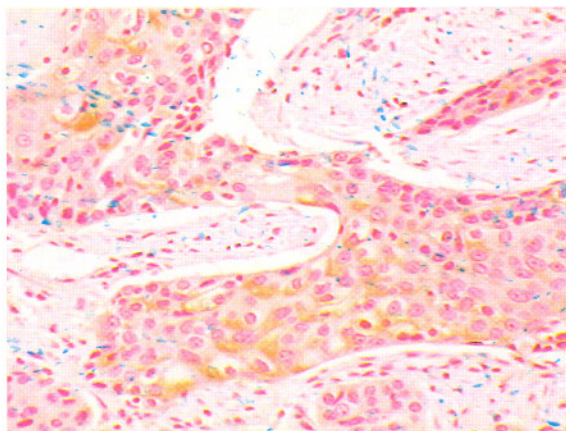


Figure 2. Expression of VEGF-C in ESCC. The brown stained granules for VEGF-C were identified in the cytoplasm of carcinoma cell (IHC, $\times 200$).

29 out of 49 cases of ESCC, VEGF-C mRNA was detected in tumor tissues by RT-PCR (Figure 3). There was a significant difference between the expression of VEGF-C in lymph node metastasis group and without lymph node metastasis group ($\chi^2 = 23.3, P < 0.01$). The expression of VEGF-C mRNA was significantly higher in lymph node metastasis group than in group without lymph node metastasis by RT-PCR.

Of 49 ESCC, 23 cases were detected VEGF-C mRNA by ISH (Figure 4). Most cases with the metastatic lymph node showed positively staining of VEGF-C by 19 of 20 (95.0%), compared with the non-metastatic lymph node group, 4 of 29 (13.8%). It was significantly higher in lymph node metastasis group than in no lymph node metastasis group ($\chi^2 = 31.3, P < 0.01$). The expression of VEGF-C mRNA was significantly higher in lymph node metastasis group than in non-metastasis lymph node group by ISH method. The expressions of VEGF-C were not significantly associated with age, gender, and pathological grade. Comparison

of VEGF-C positive expression levels in ESCC between clinicopathological features is shown in Table 1.

3.3 Correlation between the expression of VEGF-C by RT-PCR and ISH in ESCC

In present study, the detection results of VEGF-C mRNA by RT-PCR and by ISH were correlated ($\chi^2 = 18.5, P < 0.01$), but not different with each other ($\chi^2 = 2.5, P > 0.05$) (Table 2).

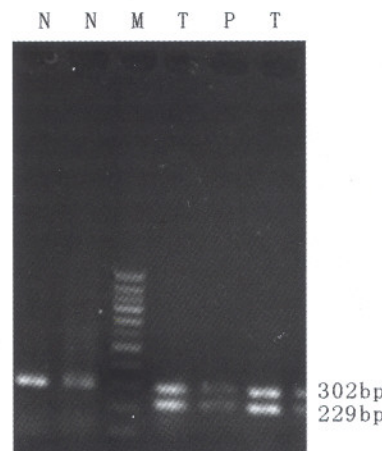


Figure 3. Expression of VEGF-C mRNA in ESCC tissues by RT-PCR. T: tumor; N: normal tissue; P: tissue adjacent to tumor; M: 100bp DNA marker.

4 Discussion

VEGF gene family is the only growth factor that is specific for vascular endothelial cells, and consists of VEGF-A, VEGF-B, VEGF-C, VEGF-D, VEGF-E and PIGF. Among them, VEGF-C is a potent stimulator of lymphangiogenesis (the growth of lymphatic vessels) both *in vitro* and *in vivo*. Recently, it has been reported that VEGF-C is expressed in several solid tumors including gastric cancer^[5], lung cancer^[6], breast cancer, thyroid carcinoma, prostate cancer, cervical cancer and colorectal carcinoma^[7]. The over-expression of VEGF-C was relevant to lymphatic spread.

VEGF-C has been implicated in the regulation of tumor lymphangiogenesis and enhancement of lymphatic invasion. It was initially identified as a ligand of VEGF receptor-3 (VEGFR-3), which at the time was an “orphan” receptor that showed sequence similarity to VEGFR-2 and VEGFR-3. Because expression of VEGFR-3 is largely restricted to lymphatic endothelium, the major function of VEGF-C appears to be the regulation of lymphatic vessel growth^[1]. It is thought that VEGF-C plays a role in the maintenance of lymphatic endothelium, and over-expression of VEGF-C has been found to induce lymphatic endothelial proliferation in the skin of transgenic mice^[8]. These results indicate that VEGF-C

is a lymphangiogenic factor. Over-expression of VEGF-C transgenes in lab revealed a direct correlation between lymphangiogenesis and lymph-node metastasis^[9]. The majority of clinical studies showed a strong positive relationship between the expression of VEGF-C and lymph node metastasis. VEGF-C could promote growth of tumor cells, which was correlated with the growth of lymphatic vessels around tumors and the intralymphatic spread of cancer. The expression of VEGF-C in tumor cell is closely associated with lymph node metastasis^[10].

In the current study, VEGF-C could be positively detected by IHC, ISH and RT-PCR. The results correlated with highly metastatic EC9706 cell line's invasive character^[11]. In addition, the result demonstrated a positive correlation of VEGF-C expression with lymph node metastasis in ESCC. A strong correlation was found between VEGF-C protein and mRNA expression and metastasis in ESCC by IHC, ISH, and RT-PCR. The result was consistent with the previous reports^[6-10]. The expressions of VEGF-C were not significantly associated with age, gender, or pathological grade, which was different from Onogawa's research^[12] in gastric carcinoma and Hanrahan's report^[7] on col-

orectal cancer. It may be that VEGF-C expresses differently in different tissues. The cases that express VEGF-C are possibly a pre-clinical status. In contrast, cases with lymph node metastasis without VEGF-C expression are likely to belong to selective expressing of VEGF-C.

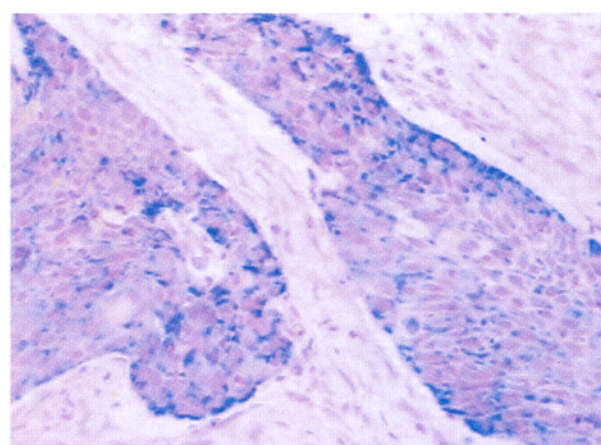


Figure 4. Expression of VEGF-C mRNA in ESCC. There were blue-purple granules in cytoplasm of carcinoma cells. (ISH, $\times 100$)

Table 1. Correlation between clinicopathological factors and the VEGF-C expression by 3 methods in ESCC

Characteristics	n	IHC			RT-PCR			ISH		
		(+)	(-)	P	(+)	(-)	P	(+)	(-)	P
Age (years)		64.5 ± 4.4	61.8 ± 4.6	>0.05 [□]	61.4 ± 3.8	60.6 ± 5.6	>0.05 [□]	60.8 ± 4.4	59.6 ± 5.7	>0.05 [□]
Gender				>0.05 [#]						>0.05 [#]
M	25	20	5		16	9		13	12	
F	24	16	8		13	11		10	14	
Histological grade				>0.05 [#]						>0.05 [#]
I	14	10	4		10	4		8	6	
II	23	17	6		12	11		10	13	
III	12	9	3		7	5		5	7	
Lymph node metastasis				<0.05 [#]						<0.01 [#]
Positive	20	18	2		20	0		19	1	
Negative	29	18	11		9	20		4	25	

[□]Student's t-test; [#]Chi-square test

Table 2. Relationship between the expression of VEGF-C by RT-PCR and ISH

Variable	ISH (+)	ISH (-)	Total
RT-PCR(+)	21	8	29
RT-PCR(-)	2	18	20
Total (n)	23	26	49

Tumor tissues consist of multiple cell types including tumor cells and host, stromal, endothelial and infiltrating cells. mRNA isolated by RT-PCR from bulk tissues represents the average amount of mRNA for all the cells in the sample and cannot determine if a specific mRNA is derived from normal or tumor cells. RNA from a few contaminating cells may be amplified during RT-PCR and obscure tumor specific alterations. RT-PCR analysis cannot reveal any site-dependent differential expression of VEGF-C. In contrast, ISH and IHC can identify the cellular source as well as reveal intratumor heterogeneity in expression. Comparison with the

trating cells. mRNA isolated by RT-PCR from bulk tissues represents the average amount of mRNA for all the cells in the sample and cannot determine if a specific mRNA is derived from normal or tumor cells. RNA from a few contaminating cells may be amplified during RT-PCR and obscure tumor specific alterations. RT-PCR analysis cannot reveal any site-dependent differential expression of VEGF-C. In contrast, ISH and IHC can identify the cellular source as well as reveal intratumor heterogeneity in expression. Comparison with the

two ways detecting VEGF-C mRNA, there was a correlation between RT-PCR and ISH, but no statistically difference between the two methods. So our finding suggests that the best way for detecting VEGF-C mRNA expression in ESCC tissue might be ISH.

In conclusion, this study has demonstrated that vascular endothelial growth factor-C may play a key role in tumor cell lymphatic metastasis. There is an association with expression of VEGF-C and lymph node metastasis in ESCC. VEGF-C may become a target for the treatment of ESCC by many methods^[15]. Furthermore the examination of VEGF-C may be useful in predicting lymph node metastasis of ESCC.

Acknowledgments

The authors wish to express their gratitude to Dr. Sanshen Zhang and his group members of Anyang Tumor Hospital for assistance in tissue collections.

References

- Jeltsch M, Kaipainen A, Joukov V, Meng X, Lakso M, Rauvala H, Swartz M, Fukumura D, Jain RK, Alitalo K. Hyperplasia of lymphatic vessels in VEGF-C transgenic mice. *Science* 1997; 276:1423–5.
- Nathanson SD. Insights into the mechanisms of lymph node metastasis. *Cancer* 2003; 98:413–23.
- Liu XE, Sun XD, Wu JM. Expression and significance of VEGF-C and FLT-4 in gastric cancer. *World J Gastroenterol* 2004; 10:352–5.
- Chen KS, Zhang L, Tang L, Zhang YH, Gao DL, Yan L, Zhang L. Expression of heparanase mRNA in anti-sense oligonucleotide-transfected human esophageal cancer EC9706 cells. *World J Gastroenterol* 2005; 11:4916–7.
- Yonemura Y, Fushido S, Bando E, Kinoshita K, Miwa K, Endo Y, Sugiyama K, Partanen T, Yamamoto H, Sasaki T. Lymphangiogenesis and the vascular endothelial growth factor receptor (VEGFR)-3 in gastric cancer. *Eur J Cancer* 2001; 37: 918–23.
- Arinaga M, Noguchi T, Takeno S, Chujo M, Miura T, Uchida Y. Clinical significance of vascular endothelial growth factor C and vascular endothelial growth factor receptor 3 in patients with nonsmall cell lung carcinoma. *Cancer* 2003; 97: 457–64.
- Hanrahan V, Currie MJ, Cunningham SP, Morrin HR, Scott PAE, Robinson BA, Fox SB. The angiogenic switch for vascular endothelial growth factor (VEGF)-A, VEGF-B, VEGF-C, and VEGF-D in the adenoma-carcinoma sequence during colorectal cancer progression. *J Pathol* 2003; 200:183–94.
- Veikkola T, Jussila L, Makinen T, Karpanen T, Jeltsch M, Petrova TV, Kubo H, Thurston G, McDonald DM, Achen MG, Stacker SA, Alitalo K. Signaling via vascular endothelial growth factor receptor-3 is sufficient for lymphangiogenesis in transgenic mice. *EMBO J* 2001; 20:1223–31.
- Karpanen T, Egeblad M, Karkkainen MJ, Kubo H, Yla-Hertuala S, Jaattela M, Jo. Vascular endothelial growth factor C promotes tumor lymphangiogenesis and intralymphatic tumor growth. *Cancer Res* 2001; 61:1786–90.
- Stacker SA, Williams RA, Achen MG. Lymphangiogenic growth factor as markers of tumor metastasis. *APMIS* 2004; 112:539–49.
- Han YL, Wei F, Xu X, Cai Y, Chen BS, Wang J, Xia SH, Hu H, Huang XP, Han YS, Wu M, Wang MR. Establishment and comparative genomic hybridization analysis of human esophageal carcinomas cell line EC9706. *Chin J Med Genet* 2002; 19:455–7.
- Onogawa S, Kitadai Y, Amioka T, Kodama M, Cho S, Kuroda T, Ochiimi T, Kimura S, Kuwai T, Tanaka S, Chayama K. Expression of vascular endothelial growth factor (VEGF)-C and VEGF-D in early gastric carcinoma: correlation with clinicopathological parameters. *Cancer Lett* 2005; 226:85–90.
- Stacker SA, Baldwin ME, Achen MG. The role of tumor lymphangiogenesis in metastatic spread. *FASEB J* 2002; 16: 922–34.
- Achen MG, McColl BK, Stacker SA. Focus on lymphangiogenesis in tumor metastasis. *Cancer Cell* 2005; 7:121–7.
- Chen ZT, Varney ML, Backora MW, Cowan K, Solheim JC, Talmadge JE, Singh RK. Down-regulation of vascular endothelial growth factor-C expression using interfering RNA vectors in mammary spontaneous metastasis and enhances survival. *Cancer Res* 2005; 65:9004–11.

Expression of P53 and Bcl-2 in laryngeal squamous cell carcinoma

Shanting Liu^{1,2,*}, Weihua Lou¹, Jianzhong Sang¹, Ming Zhao², Zhaozhong Meng²

¹Department of Laryngology, The First Affiliated Hospital, Zhengzhou University, Zhengzhou, Henan 450052, China; ²Department of Head and Neck, Henan Tumor Hospital, Zhengzhou, Henan 450008, China

Received November 27, 2006

Abstract

Objective. To investigate the expression of P53 and Bcl-2, their relationship, and their roles in the pathogenesis and development of laryngeal squamous cell carcinoma. **Methods.** Immunohistochemistry was used to study 110 cases of laryngeal carcinoma and 20 cases of normal laryngeal tissues to detect the expression of P53 and Bcl-2. **Results.** Among 110 cases of laryngeal squamous cell carcinoma, the rate of expression of P53 and Bcl-2 were 62.7% and 47.3% respectively; the expression of P53 was closely correlated with lymph node metastasis and Bcl-2 correlated with pathological grade, lymph node metastasis. P53 expression was related to Bcl-2 expression. **Conclusion.** P53 is correlated to Bcl-2. They play important roles in tumor metastasis and progression and will be the target of gene therapy in laryngeal carcinoma. [Life Science Journal. 2007;4(1):29–31] (ISSN: 1097–8135).

Keywords: laryngeal squamous cell carcinoma; p53; bcl-2; immunohistochemistry

1 Introduction

It is generally accepted that malignant tumor is caused by hyperproliferation. p53 is a type of tumor suppressor gene, whose mutation is the most common genetic aberration which has been identified as closely related to cancer so far. The apoptosis inhibition molecular of Bcl-2 family is an important component of the miscellaneous apoptosis inhibition molecules^[1]. This research is to detect the expression of P53 and Bcl-2 in laryngeal squamous carcinoma, and try to illuminate the underlying pathogenesis of laryngeal carcinoma.

2 Materials and Methods

2.1 Clinical data

Samples of 110 cases of laryngeal squamous cell carcinoma in the First Affiliated Hospital of Zhengzhou University and Henan Tumor Hospital from June 1998 to June 2001 were collected, among which 102 cases were male and 8 cases were female. The age ranges from 42 to 70, with the average age of 58.8. According to the Union International Contre Le Cancer (UICC) standard of 1997, 47 cases of them were glottic carcinoma, 58 cases were supraglottic carcinoma, and 5 cases were subglottic carcinoma. In terms of clinical stage, there were 5 cases of stage 0, 29 cases of stage I, 33 cases of stage II, 25 cases of stage III, and 18 cases were stage IV. As to the differentiation, there were 43 cases of well dif-

ferentiated squamous cell carcinoma, 51 cases of moderate differentiated squamous cell carcinoma, and 16 cases of poorly differentiated squamous cell carcinoma. In regard to the lymphatic metastasis, 48 cases were cervical lymph node metastasis and 63 cases without cervical lymph node metastasis. In addition, 20 cases of normal mucosa were collected in the operation as control.

2.2 Immunohistochemistry

All reagents were purchased from the Wuhan Boster Biology Engineering Corporation (Wuhan, China). Paraffin sections were dewaxed and dehydrated. Followed the first antibody and the second antibody core-streptavidin-peroxidases was added. After dripping by the newly confected diaminobenzidine (DAB) solution, it was observed under microscope. It was stained with hematoxylin. Grade alcohol was used for dehydration and dryness. Dimethylbenzene was used for clarity, and neutral balata was used for seal.

2.3 Results judgement

The positive signals of Bcl-2 showed as brown yellow granule or diffusing shape distribution. P53 was mainly expressed in cell nucleus, and positive cells were brown yellow. In the samples, less than 10% of positive cells were regarded as negative, and the cases of more than 10% positive cells were regarded as positive.

2.4 Statistical method

χ^2 test was operated to show the correlation between P53 and Bcl-2 expression and clinical data. Spearman correlation test conducted for the correlation between P53 and Bcl-2. The statistic software sas 9.0 was used and the significance level was set at 0.05.

*Corresponding author. Email: liushanting@163.com

3 Results

There was almost no expression of P53 and Bcl-2 in normal laryngeal mucosa. Weak positive expression in basal layer cells was in few samples. The expression rates of P53 and Bcl-2 in laryngeal carcinoma were 62.7% and 47.3% respectively. P53 was mainly expressed in cell nucleus, and positive cells were brown yellow (Figure 1). Bcl-2 signal was brown yellow granules and was mainly expressed in cytoplasm and nuclear membrane (Figure 2).

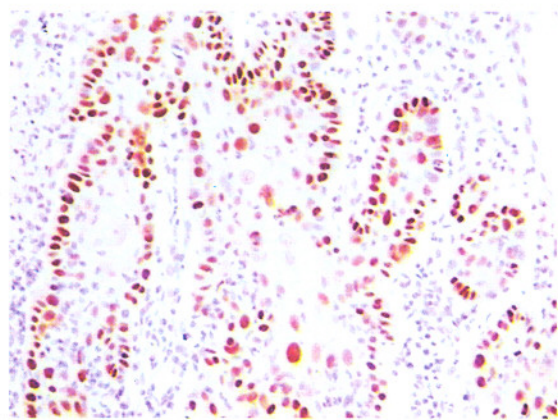


Figure 1. Expression of P53 in laryngeal squamous carcinoma by IHC. (HE \times 200)

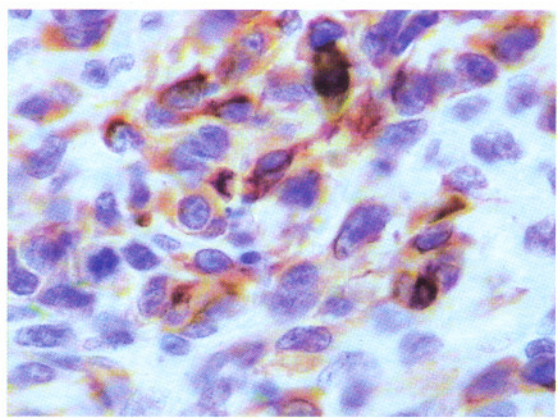


Figure 2. Expression of Bcl-2 in laryngeal squamous carcinoma by IHC. (HE \times 400)

Correlation analysis revealed: P53 was related to lymphatic metastasis but not to clinical stage, age, gender, type and differentiation (Table 1); Bcl-2 was related to differentiation and lymphatic metastasis, but not to age, gender, clinical stage and type (Table 2); P53 expression and Bcl-2 expression were positively correlated (Table 3).

4 Discussion

It is generally accepted that malignant tumor is caused by gene mutation under outside stimulation. The accumulation of this mutation will activate oncogenes and inactivate tumor suppressor genes.

p53 is an important tumor suppressor gene, located at 17P13.1, with the length of 16–20kb, comprising 11 exons, with the transcription of 2.8 kb of mRNA recorded. The encoded protein is P53. So far, p53 has been identified as a gene that is most closely related to human tumor. Its major function is to regulate cells' response to DNA damage and inhibit the growth of cells by bringing about cell cycle retardance and/or apoptosis. It plays an important role in maintaining the stability of nucleus or promoting the cell apoptosis^[2]. Mutant p53 has some new characteristics, such as prolonged half life and altered conformation, and loses the function of maintaining the stability of nucleus. The half life of wild type p53 in normal tissues is short and is easily hydrolyzed. It can not be tested in cells. In this study, no positive expression of p53 was detected in the 20 cases of normal mucosa. In the 110 cases of laryngeal carcinoma, 69 cases were positively detected. The positive rate was 62.7%, which is close to most reports. Its expression is related to cervical lymph node metastasis, but not to age, gender, clinical stage, type and differentiation, which is in accordance with the reports abroad^[3]. It can be established that p53 is closely related to the occurrence and development of laryngeal carcinoma and lymphatic metastasis. Mutant p53 not only directly inhibits apoptosis and stimulates cell proliferation, but also accumulates themselves in cells. The highly positive rate of 62.7% in this study confirmed this. In addition, the high expression rate can lead to the instability of hereditary substance subsequently and the imbalance of cancer-related genes, which will cause oncogenesis and metastasis.

Table 1. Correlation between P53 expression and clinical pathological features of the patients

Clinical pathological feature	n	P53 expression		χ^2	P value
		Negative	Positive		
Age	≤ 60 years	48	18	30	0.0019 0.9654
	> 60 years	62	23	39	
Gender	Male	102	38	64	0.0002 0.9890
	Female	8	3	5	
Clinical stage	0 + I + II	67	25	42	0.0001 0.9912
	III + IV	43	16	27	
Type	Glottic	47	17	30	
	Supraglottic	58	22	36	0.0511 0.9748
	Infraglottic	5	2	3	
Differentiation	Well	43	18	25	
	Moderate	51	19	32	1.4179 0.4922
	Poor	16	4	12	
Lymph node metastasis	Negative	62	27	33	
	Positive	48	12	36	4.6232 0.0315*

* $P < 0.05$, expression of P53 was closely correlated with lymph node metastasis.

Table 2. Correlation between Bcl-2 expression and clinicopathological features of the patients

Clinical pathological feature	n	Bcl-2 expression		χ^2	P value
		Negative	Positive		
Age	≤60 years	48	25	23	0.9035 0.0142
	>60 years	62	33	29	
Gender	Male	102	55	47	0.8026 0.3703
	Female	8	3	5	
Clinical stage	0 + I + II	67	36	31	0.0693 0.7923
	III + IV	43	22	21	
Type	Glottic	47	25	22	
	Supraglottic	58	30	28	0.1336 0.9354
	Infraglottic	5	3	2	
Differentiation	Well	43	29	14	
	Moderate	51	27	24	8.5708 0.0138*
	Poor	16	4	12	
Lymph node metastasis	Negative	62	38	24	4.1798 0.0409*
	Positive	48	20	28	

* $P<0.05$, expression of Bcl-2 was closely correlated with differentiation and lymph node metastasis.

Table 3. Correlation of Bcl-2 and P53

P53 expression	n	Bcl-2		r	P value
		Positive	Negative		
P53 (+)	69	40	29	0.2780	0.0036
P53 (-)	41	12	29		

From the aspect of cell apoptosis, the mechanism of tumor can be explained as the result of inhibiting apoptosis and hindering the decrease of tumor cells^[4]. Bcl-2 family plays an important role in controlling cell apoptosis^[1,5]. bcl-2 is a type of proto-oncogenes found in B cell lymphoma. The B cell lymphoma is often of characteristic t translocation (14:18). In most cases, bcl-2 gene on 18q21 is translocated to 14q32 which is adjacent to Ig heavy chain genes. Ig heavy chain gene has powerful promoter and enhancer, which can lead to unusually high bcl-2 expression and thus inhibits cell apoptosis and cause cancer. The data in this research suggest that there was almost no Bcl-2 expression in normal laryngeal mucosa. Bcl-2 expression rate in laryngeal carcinoma was 47.3%. A research about 176 cases of laryngeal carcinoma has found that Bcl-2 expression is related to differentiation and lymph node metastasis^[6]. The present research obtained the similar result. The data of this research also showed that Bcl-2 expression was not

correlated to age, gender, clinical stage and type. The high expression of Bcl-2 in the tissue of laryngeal carcinoma plays a vital role inhibiting cell apoptosis and oncogenesis. It is proposed that different Bcl-2 expression level may inhibit cell apoptosis differently and thus lead to different accumulation degree of damaged cells. As a result, different malignant phenotypes, such as different pathology grades, are observed.

The encoded protein of wild type p53 can be combined with the segments of 5' non-coded zone of bcl-2 genes, and inhibit the expression of bcl-2. The mutant p53 will lose the function of inhibiting bcl-2, which may lead to the increase of Bcl-2 expression. This research results showed p53 and bcl-2 were correlated, which further confirmed the hypothesis that oncogenesis is the cooperation of various factors.

To damaged normal cells, apoptosis is the ultimate event, whereas to mutant cells, apoptosis inhibition is the early event and runs through the whole process of oncogenesis. Based on this, some scholars proposed that p53 and bcl-2 be used as therapeutic targets for the treatment of malignant tumor^[7]. It is also suggested by the authors of this paper that the unique expression of p53 and bcl-2 in cancer tissues be hopefully used as an index for early treatment.

References

- Jackel MC, Sellmann L, Youssef S, et al. Prognostic significance of expression of p53, bcl-2 and bax in squamous epithelial carcinoma of the larynx – a multivariate analysis. HNO 2001; 49(3):201–9.
- Singh B, Reddy PG, Goberdhan, et al. p53 regulate cell survival by inhibiting PIK3CA in squamous cell carcinomas. Genes 2002; 16:984–93.
- Kazkavasi M, Hucumenoglu S, Siriner GI, et al. Over-expression of P53 and c-erb-2 oncoproteins in laryngeal carcinoma. Eur Arch Otorhinolaryngol 2001; 258:329–35.
- Beardsmore DM, Verbeke CS, Davies CL, et al. Apoptotic and proliferative indexes in esophageal cancer: predictors of response to neoadjuvant therapy [corrected]. Gastrointest Surg 2003; (7): 77–86.
- Georgiou A, Gomatos IP, Ferekidis E, et al. Prognostic significance of p53, bax and bcl-2 gene expression in patients with laryngeal carcinoma. Eur J Surg Oncol 2001; 27(6): 574–81.
- Yuen AP, Lam KY, Choy JT, et al. The clinicopathological significance of Bcl-2 expression in the surgical treatment of laryngeal carcinoma. Clin Otolaryngol 2001; 26(2):129–30.
- Sutter AP, Zeitz M, Scherubl H. Recent results in understanding molecular pathways in the medical treatment of esophageal and gastric cancer. Onkologie 2004; 27: 17–21.

Inhibitory effect of SB203580 on neuropathic pain behaviors induced by lumbar 5 ventral rhizotomy in rats[☆]

Jitian Xu^{1,*}, Huiyin Tu¹, Wenjun Xin², Xianguo Liu²

¹Department of Physiology, Basic Medical College, Zhengzhou University, Zhengzhou, Henan 450001, China; ²Pain Research Center, Department of Physiology, Zhongshan Medical School of Sun Yat-sen University, Guangzhou, Guangdong 510080, China

Received November 8, 2006

Abstract

Previous studies have shown that selective injury to motor fiber, but keeps primary sensory afferents intact, induced abnormal pain behaviors to a similar extent as the rat received lumbar 5 spinal nerve ligation (L5 SNL). Several lines of evidence suggest that the p38 activation in the nociceptive pathway contributes to the development of inflammatory and nerve injury induced neuropathic pain. Whereas, the role of p38 activation in the pain facilitation induced by the motor fiber injury is still unclear. In the present study, the lumbar 5 ventral rhizotomy (L5 VR) was performed in rats, and the animals were treated with SB203580, an inhibitor of activated p38, intrathecal injection started at before and after the surgery. The pain-related behaviors were tested to elucidate the effect of SB203580. The results showed that L5 VR induced a robust and long-lasting mechanical allodynia and thermal hyperalgesia in bilateral hind paws in rats started on day 1 and persisted for more than 4 weeks. Intrathecal injection of SB203580 10 minutes before L5 VR and once daily thereafter until 14th day significantly reduced the mechanical allodynia and blocked the development of thermal hyperalgesia in bilateral hind paws. Post-treatment with SB203580 performed at the first day and 8th day also clearly alleviated the established neuropathic pain following L5 VR. Taken together, the above data indicate that p38 activation might be playing an important role in the induction and maintenance of the neuropathic pain induced by the selective motor fiber injury. [Life Science Journal. 2007;4(1):32–36] (ISSN: 1097–8135).

Keywords: ventral rhizotomy; neuropathic pain; p38; mitogen-activated protein kinase; SB203580

1 Introduction

Damage to peripheral nerve very often results in neuropathic pain. Current treatments for this pain are only partially effective, and additional development is hindered by our incomplete knowledge of how neuropathic pain is induced and maintained^[1]. Increasing evidence shows that mitogen-activated protein kinases (MAPKs) play important roles in the induction and maintenance of chronic pain^[2,3]. The MAPK family has three major members, extracellular signal-regulated kinase (ERK), p38, and c-Jun N-terminal kinase (JNK), representing three different signal transduction pathways. It has been reported that p38 activation in dorsal root ganglia (DRG) and spinal cord plays an important role in the pain hypersensitivity state induced by L5 spinal nerve ligation (L5 SNL)^[4–6]. Recently, several groups show that selective lesion to motor fibers by L5 ventral rhizotomy (L5 VR), but keeps sensory neu-

rons intact, produces behavioral signs of neuropathic pain to a similar extent as in rats with L5 SNL^[7–9]. While, the underlying mechanisms of L5 VR induced neuropathic pain is still remained largely unknown. Therefore, it was hypothesized that p38 activation may be also play a role in the generation of pain-related behaviors induced by the model of selective motor fiber injury. To testify this hypothesis, in present study the L5 VR was performed in rats and the role of p38 activation in the production of mechanical allodynia and thermal hyperalgesia was evaluated by intrathecal injection of p38 inhibitor SB203580.

2 Materials and Methods

2.1 Animals

Male Sprague-Dawley rats weighing 180–250 g were used. The rats were housed in separated cages with free access to food and water. The room temperature was kept at 23 ± 2 °C under a 12:12 light-dark cycles. All animal experimental procedures were approved by the local animal care committee and were carried out in accordance with the guideline of the National Institutes of Health of America on animal care and the ethical guidelines for investigation of experimental pain in con-

[☆]Supported by the National Natural Science Foundation of China (No. 30570599).

*Corresponding author. Tel: 86-371-6136-6390; Email: jtxu@zzu.edu.cn

scious animal^[10].

2.2 Surgical procedures and drug delivery

All experimental procedures were done on rats that were deeply anesthetized with sodium pentobarbital (50 mg/kg body weight, *i. p.*). Special care was paid to prevent infection and to minimize the influence of inflammation. The L5 VR was done following the procedures described by Li *et al*^[7]. Briefly, after a midline skin incision in the L4-S1 region, the left L5 vertebra was freed of its muscular attachment. An L5 hemilaminectomy was performed, and the dura matter and arachnoid membrane were incised. The L5 ventral root was identified as it lays at the most lateral side of spinal canal and just beneath the dorsal root. The ventral root was gently pulled out and carefully transected 2–3 mm proximal to the DRG. Great care was taken to avoid any damage to the nearby L5 dorsal root and its DRG. In the sham group, all procedures of operation were identical with the experimental group except that the exposed ventral root was not transected. After surgery, the wound was washed with saline and closed in layers with 3–0 silk thread. At the end of each study, animals in L5 VR groups were deeply anesthetized with intra-peritoneal 20% urethane and were dissected to verify that the lesions were done at the correct level. Animals that had a lesion at wrong level were excluded from the study.

For intrathecal injection, a method described by Jin *et al*^[5] was followed. In brief, a polyethylene-10 (PE-10) catheter was inserted into the rat's subarachnoid space through the incision of L5 VR, and the tip of the catheter was implanted at the L5 spinal segmental level. In one group of the rats, the p38 inhibitor SB203580 (Sigma-Aldrich Co., St. Louis, MO, USA) was injected intrathecally (10 µg/10 µl) and flushed with 10 µl of saline started 10 minutes before L5 VR and once daily thereafter for 14 days. In another group of the rats, a single injection of SB203580 (10 µg/10 µl) was performed on day 1 and day 8 after surgery. The control group received same volume of vehicle (saline contained 2% DMSO) injection at same time as above. The SB203580 was dissolved in 100% DMSO and diluted by saline. The final concentration of DMSO was 2%. Behavioral test was done after the injection of SB203580 according to the experimental design.

2.3 Behavioral test

The rats were accommodated to the testing environment by exposing the rats to the testing chambers for a period of 15–20 minutes on three separate days just prior to the pre-operative testing. Mechanical sensitivity was assessed using von Frey hairs and the up-down method following the procedure as described previously^[11]. Briefly, three rats were placed under separate transparent plexiglas chambers positioned on a wire

mesh floor. Five minutes were allowed for habituation. Each stimulus consisted of applying for 2–3 seconds of the von Frey hair to the middle of the plantar surface of the foot with 5-minute interval between stimuli. Quick withdrawal or licking of the paw in response to the stimulus was considered a positive response.

Heat hypersensitivity was tested using a plantar test (7370, UgoBasil, Comerio, Italy) according to the method described by Hargreaves *et al*^[12]. Briefly, a radiant heat source beneath a glass floor was aimed at the plantar surface of the hind paw. Three measurements of latency were taken for each hind paw in each test session. The hind paw was tested alternately with greater than 5-minute intervals between consecutive tests. The three measurements of latency per side were averaged as the result per test. Two persons performed the behavioral tests and only one knew the design of the study.

2.4 Statistical analysis

Differences in changes of values over time were tested using Friedman ANOVA followed by Wilcoxon matched pairs test. The data between groups on a given testing day were analyzed with Mann-Whitney *U* test. Statistical tests were performed with SPSS 10.0 (SPSS Inc, USA). All data are expressed as mean ± SE. *P* < 0.05 was considered significant.

3 Results

3.1 L5 VR induced mechanical allodynia and thermal hyperalgesia in bilateral hind paws in rats

In consistent with a previous work^[7], we found that selective transection of L5 ventral root produced robust and prolonged bilateral mechanical allodynia and thermal hyperalgesia. Compared with sham group and pre-operative baseline, the 50% paw withdrawal threshold (Figure 1A) and paw withdrawal latency (Figure 1B) significantly decreased 1 day after L5 VR (*P* < 0.05), and persisted more than 4 weeks after surgery in bilateral hind paws.

3.2 Pre-treatment with SB203580 attenuated the abnormal pain behaviors following L5 VR

To elucidate whether the activation of p38 plays a role in the behavioral signs of neuropathic pain produced by L5 VR, a p38 inhibitor SB203580 was injected intrathecally 10 minutes before L5 VR and once daily thereafter lasting for 14 days after surgery. The results showed that the magnitude of mechanical allodynia in ipsilateral hind paw was significantly reduced and duration was shortened (Figure 2A). While mechanical allodynia in contralateral side and the thermal hyperalgesia in bilateral sides were blocked completely (Figure 2A and B). Intrathecal injection of SB203580 as above had no effect on the basal behavioral test in naive rats (data not shown).

3.3 The effect of post-treatment with SB203580 on

the established neuropathic pain induced by L5 VR

To evaluate the role of p38 activation on the established neuropathic pain, a single injection of SB203580 was designed at the first and 8th day after L5 VR, and the behavioral tests were done at 1, 3, 6 and 12 hours after the treatment. The results showed that the me-

chanical allodynia and thermal hyperalgesia were significantly reduced at both day 1 and day 8 in treatment groups. But, the effect of SB203580 only lasted for several hours (Figure 3). These results suggest that p38 activation may involve in the development and maintenance of the neuropathic pain induced by L5 VR.

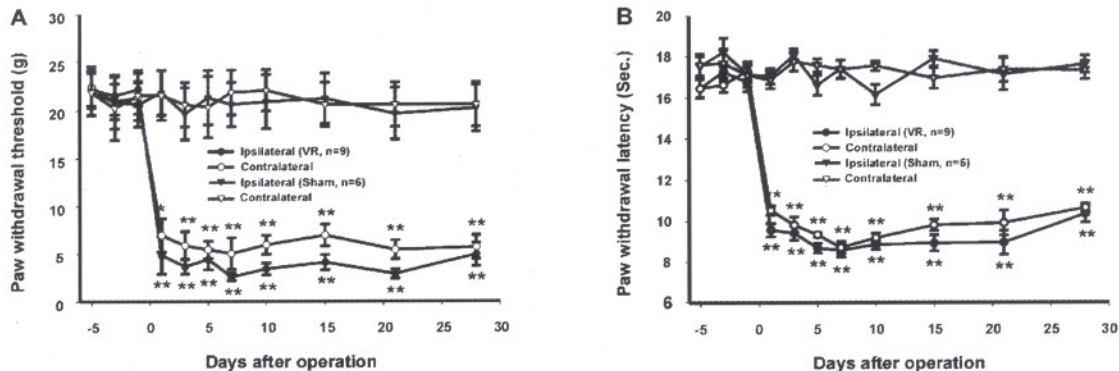


Figure 1. Lumbar 5 ventral rhizotomy (L5 VR) induced pain-related behaviors in bilateral hind paws. A: showed the changes of paw withdrawal threshold in bilateral hind paws following L5 VR. B: showed the changes of paw withdrawal latency in bilateral hind paws following L5 VR. The results revealed that both paw withdrawal threshold and paw withdrawal latency decreased significantly compared with pre-operative baseline as well as sham operation group starting on day 1 and persistent for more than 4 weeks after L5 VR. * : $P < 0.05$; ** : $P < 0.01$ compared with the sham operation group, respectively.

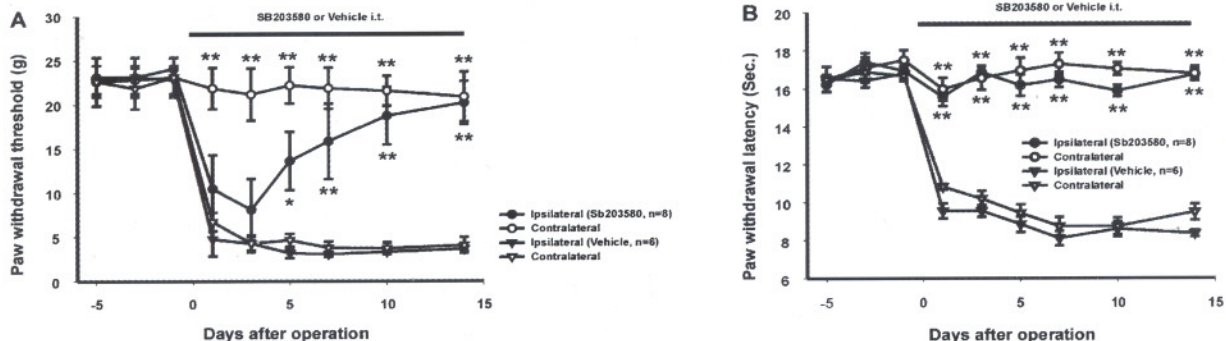


Figure 2. Intrathecal injection of p38 inhibitor SB203580 started before surgery significantly reduced the abnormal pain behaviors induced by L5 VR. A-B: Intrathecal injection of SB203580 applied 10 minutes before L5 VR and once daily thereafter until day 14 after surgery significantly attenuated mechanical allodynia (A) and thermal hyperalgesia (B). * : $P < 0.05$; ** : $P < 0.01$ versus vehicle treated group (SB203580 treated group, $n = 8$; vehicle treated group, $n = 6$).

4 Discussion

In the present study, we found that selective injury to myelinated efferent fibers by L5 VR induced abnormal pain behaviors in bilateral hind paws of rats. Intrathecal injection of SB203580, started before L5 VR, prevented the development of the mechanical allodynia and thermal hyperalgesia. Post-treatment with SB203580 also significantly reduced the pain related behaviors. It suggests that p38 activation may play an important role in the induction and maintenance of the neuropathic pain induced by L5 VR.

4.1 Neuropathic pain induced by L5 VR

As reported by several groups previously^[7,8,13,14], L5 VR, performed in the present study, created a selective injury to motor fibers in L5 spinal nerve and induced a robust and long-lasting neuropathic pain in animals. Ventral root is predominantly consisting of myelinated efferent fiber, and the unmyelinated afferent fiber is less than 4%^[15-17]. Recent study shows that selective transected L5 dorsal root failed to induce abnormal pain behaviors^[14]. Whereas, selective injury to myelinated efferent fibers after ventral rhizotomy induced an increased spontaneous activity in uninjured C-fiber nociceptive afferents and this injury also induced hyperalgesic behav-

ior^[13]. It indicates that the motor fiber injury after L5 VR is responsible for the development of neuropathic pain.

4.2 Inhibition of p38 activation reduced the thermal hyperalgesia and mechanical allodynia induced by L5 VR

The p38 inhibitor SB203580 does not inhibit the phosphorylation of p38 but binds to the ATP pocket in the enzyme, thereby inhibiting its activity^[18]. There is increasing evidence showing that neuropathic pain induced by peripheral nerve injury can be prevented by block p38 activation^[5,6]. In the present study we found that intrathecal injection of SB203580 before L5 VR, the pain related behaviors in bilateral hind paws were clearly alleviated. Post-treatment with SB203580 started on day 1 and day 8 after L5 VR also reduced the neuropathic pain. Several lines of evidence shows that Walle-

rian degeneration of injured motor fiber contributes to the development of pain hypersensitivity after L5 VR^[13,19]. TNF- α is the pioneer cytokine, which released 4 to 6 hours after nerve injury, and play a key role in the initiation of the Wallerian degeneration of injured fibers and neuropathic pain subsequently^[20,21]. Our recent works showed that L5 VR induced a significant upregulation of TNF- α and TNF receptor 1 (p55) in ipsilateral L4, L5 DRG and in bilateral L5 spinal dorsal horn^[9]. It has been reported that exogenous TNF- α activated p38 activation in cultured DRG neurons^[22]. The p38 activation in injured DRG neurons induced by L5 SNL can be blocked by intraperitoneal injection of TNF- α anti-agonist etanercept^[23]. Therefore we speculated that p38 activation in the present study might be one of results of TNF- α , which is released in sciatic nerve after L5 VR.

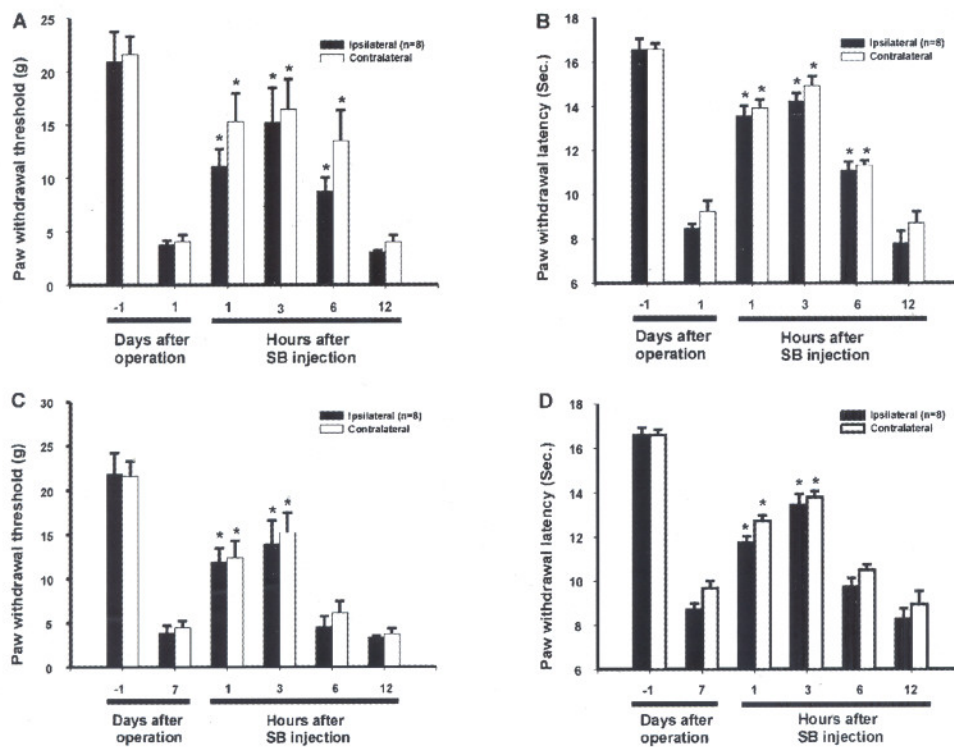


Figure 3. Effect of post-treatment with SB203580 intrathecal injection on the established neuropathic pain induced by L5 VR. A-B: SB203580 applied at 1st day after operation significantly reduced the mechanical allodynia (A) and thermal hyperalgesia (B). C-D: SB203580 applied at 8th day after operation also clearly alleviated the mechanical allodynia (C) and thermal hyperalgesia (D). $P < 0.05$; versus L5 VR base (the value of 1st day after L5 VR in Figure A and B; the value of 7th day after L5 VR in Figure C and D) ($n = 8$).

Previous study showed that acute injection of zymosan around the sciatic nerve produced bilateral mechanical allodynia^[24] and that spinal glia as well as p38 activation played important roles in the so-called sciatic inflammatory neuropathy (SIN), since both ipsilateral and mirror image allodynia can be attenuated by a glial metabolic inhibitor or by CNI-1493, a potent inhibitor

of p38^[25,26]. Recently, it had been reported that intrathecal administration of low dose carbenoxolone, a gap junction decoupler, reverses mirror image pain, while leaving ipsilateral mechanical allodynia unaffected in SIN or chronic constriction injury model^[27]. Therefore, it is likely that the communication between ipsilateral and contralateral spinal cord through glial gap junc-

tion may contribute to L5 VR induced p38 activation in contralateral spinal cord, and to mirror image pain.

References

- Zimmermann M. Pathobiology of neuropathic pain. *Eur J Pharmacol* 2001; 429: 23–37.
- Ji RR, Woolf CJ. Neuronal plasticity and signal transduction in nociceptive neurons: implications for the initiation and maintenance of pathological pain. *Neurobiol Dis* 2001; 8: 1–10.
- Obata K, Noguchi K. MAPK activation in nociceptive neurons and pain hypersensitivity. *Life Sci* 2004; 74: 2643–53.
- Ji RR, Samad TA, Jin SX, et al. p38 MAPK activation by NGF in primary sensory neurons after inflammation increases TRPV1 levels and maintains heat hyperalgesia. *Neuron* 2002; 36: 57–68.
- Jin SX, Zhuang ZY, Woolf CJ, et al. p38 mitogen-activated protein kinase is activated after a spinal nerve ligation in spinal cord microglia and dorsal root ganglion neurons and contributes to the generation of neuropathic pain. *J Neurosci* 2003; 23: 4017–22.
- Tsuda M, Mizokoshi A, Shigemoto-Mogami Y, et al. Activation of p38 mitogen-activated protein kinase in spinal hyperactive microglia contributes to pain hypersensitivity following peripheral nerve injury. *Glia* 2004; 45: 89–95.
- Li L, Xian CJ, Zhong JH, et al. Effect of lumbar 5 ventral root transection on pain behaviors: a novel rat model for neuropathic pain without axotomy of primary sensory neurons. *Exp Neurol* 2002; 175: 23–34.
- Sheth RN, Dorsi MJ, Li Y, et al. Mechanical hyperalgesia after an L5 ventral rhizotomy or an L5 ganglionectomy in the rat. *Pain* 2002; 96: 63–72.
- Xu JT, Xin WJ, Zang Y, et al. The role of tumor necrosis factor-alpha in the neuropathic pain induced by Lumbar 5 ventral root transection in rat. *Pain* 2006; 123: 306–21.
- Zimmermann M. Ethical guidelines for investigations of experimental pain in conscious animals. *Pain* 1983; 16: 109–10.
- Chaplan SR, Bach FW, Pogrel JW, et al. Quantitative assessment of tactile allodynia in the rat paw. *J Neurosci Methods* 1994; 53: 55–63.
- Hargreaves K, Dubner R, Brown F, et al. A new and sensitive method for measuring thermal nociception in cutaneous hyperalgesia. *Pain* 1988; 32: 77–88.
- Wu G, Ringkamp M, Murinson BB, et al. Degeneration of myelinated efferent fibers induces spontaneous activity in uninjured C-fiber afferents. *J Neurosci* 2002; 22: 7746–53.
- Obata K, Yamanaka H, Kobayashi K, et al. The effect of site and type of nerve injury on the expression of brain-derived neurotrophic factor in the dorsal root ganglion and on neuropathic pain behavior. *Neuroscience* 2006; 137: 961–70.
- Coggeshall RE, Emery DG, Ito H, et al. Unmyelinated and small myelinated axons in rat ventral roots. *J Comp Neurol* 1977; 173: 175–84.
- Zenker W, Stelzig M, Sulzgruber SC, et al. Fiber analysis of human ventral and dorsal roots on the basis of different acetylcholinesterase activity. *Acta Anat (Basel)* 1979; 103: 319–26.
- Nam SC, Kim KJ, Leem JW, et al. Fiber counts at multiple sites along the rat ventral root after neonatal peripheral neurectomy or dorsal rhizotomy. *J Comp Neurol* 1989; 290: 336–42.
- Koistinaho M, Koistinaho J. Role of p38 and p44/42 mitogen-activated protein kinases in microglia. *Glia* 2002; 40: 175–83.
- Obata K, Yamanaka H, Dai Y, et al. Contribution of degeneration of motor and sensory fibers to pain behavior and the changes in neurotrophic factors in rat dorsal root ganglion. *Exp Neurol* 2004; 188: 149–60.
- Shamash S, Reichert F, Rotshenker S. The cytokine network of Wallerian degeneration: tumor necrosis factor-alpha, interleukin-1alpha, and interleukin-1beta. *J Neurosci* 2002; 22: 3052–60.
- Liefner M, Siebert H, Sachse T, et al. The role of TNF-alpha during Wallerian degeneration. *J Neuroimmunol* 2000; 108: 147–52.
- Pollock J, McFarlane SM, Connell MC, et al. TNF-alpha receptors simultaneously activate Ca^{2+} mobilisation and stress kinases in cultured sensory neurons. *Neuropharmacology* 2002; 42: 93–106.
- Schafers M, Svensson CI, Sommer C, et al. Tumor necrosis factor-alpha induces mechanical allodynia after spinal nerve ligation by activation of p38 MAPK in primary sensory neurons. *J Neurosci* 2003; 23: 2517–21.
- Chacur M, Milligan ED, Gazda LS, et al. A new model of sciatic inflammatory neuritis (SIN): induction of unilateral and bilateral mechanical allodynia following acute unilateral peri-sciatic immune activation in rats. *Pain* 2001; 94: 231–44.
- Milligan ED, Twining C, Chacur M, et al. Spinal glia and proinflammatory cytokines mediate mirror-image neuropathic pain in rats. *J Neurosci* 2003; 23: 1026–40.
- Milligan ED, O'Connor KA, Armstrong CB, et al. Systemic administration of CNI-1493, a p38 mitogen-activated protein kinase inhibitor, blocks intrathecal human immunodeficiency virus-1 gp120-induced enhanced pain states in rats. *J Pain* 2001; 2: 326–33.
- Spataro LE, Sloane EM, Milligan ED, et al. Spinal gap junctions: potential involvement in pain facilitation. *J Pain* 2004; 5: 392–405.

Slowing of atrioventricular conduction in mice lacking SK2 channel

Qian Zhang¹, Ziming Dong^{2,*}, Valeriy Timofeyev³

¹Department of Physiology, Basic Medical College, Zhengzhou University, Zhengzhou, Henan 450052, China; ²Department of Pathophysiology, Basic Medical College, Zhengzhou University, Zhengzhou, Henan 450052, China; ³Division of Cardiovascular Medicine, University of California, Davis, CA95616, USA

Received December 13, 2006

Abstract

SK2 channel in the atrioventricular node (AVN) was examined by using SK2 channel-deficient (SK2 + /Δ) mice. In the present study, results showed that the PR and RR intervals were prolonged in SK2 + /Δ mice. The spontaneous action potentials(APs) recorded from the AVN exhibited a significant decrease in the beating frequency and a prolongation of AP duration in the SK2 + /Δ mice compared with the WT littermates, suggesting that the deficit causes sinus bradycardia and slower atrioventricular conduction without affecting the excitability of the sinoatrial node. Immunofluorescence confocal investigation showed further that the Ca²⁺-activated K⁺ channel is not only expressed in the working myocytes, and also in the AV conduction system. The findings demonstrate that the SK2 channel expressed in the heart contributes to AVN autorhythmicity and atrioventricular conduction. [Life Science Journal. 2007;4(1):37–39] (ISSN: 1097–8135).

Keywords: automatic activity; Ca²⁺-activated K⁺ channel; atrioventricular node; conduction; gene knockout

1 Introduction

The atrioventricular node (AVN) plays an critical role in generating the correct timing between atrial and ventricular contraction. Abnormality in atrioventricular (AV) conduction can give rise to arrhythmias^[1]. Small conductance Ca²⁺-activated K⁺ (SK) are present in most neurons and mediate the afterhyperpolarizations following action potential (AP)^[2,3]. Evidence indicated that the presence of SK2 channel, a subtype of SK channel, in cardiac myocytes plays a crucial role in cardiac AP profile and is involved in many physiological processes^[4,5]. The functional significance of different ionic channels in the generation and regulation of cardiac automaticity is currently subject of an extensive research effort.

2 Materials and Methods

2.1 Animals

All animal care and procedures were approved by the University of California, Davis Institutional Animal Care and Use Committee. Creation of SK2 knockout mice have been recently described^[6]. The transgenic line was backcrossed onto C57Bl/6J mice for greater than 7 generations before they were used. SK2-deficient

mice(SK2 + /Δ) and corresponding wild type(WT) animals from either sex were used. The age of two groups ranged from 12 – 18 weeks. Transgene presence was confirmed using PCR of tail tip and expression was assessed by immunoblotting of cardiac homogenates as described previously^[6]. All chemicals were purchased from Sigma Chemical Co.

2.2 Electrocardiographic (ECG) recordings

ECG recordings were obtained using Bioamplifier (BMA831, CWE, Incorporated, Ardmore, PA). The animals were placed on a temperature-controlled warming blanket at 37 °C. Four consecutive 2-minute epochs of ECG data were obtained from each animal. The rate-corrected QT interval (QTc) was calculated using modified Bazett's formula as previously described^[7].

2.3 AV node tissue preparation and recording

Preparations were performed according to Hancox^[8]. In Brief, the different transgenic mice were anesthetized with pentobarbital(60 mg/kg). The heart was excised rapidly and the right atrium was opened under a dissecting microscope to expose the coronary sinus, the triangle of Koch. The final preparation included the entire AV node region and surrounding atrial. The strip of the tissue was continuously superfused with Tyrode's solution contained (mmol/L) NaCl 138, KCl 4, MgCl₂ 1, CaCl₂ 2, NaH₂PO₄ 0.33, glucose 10, and HEPES 10, pH 7.4.

For electrophysiological recording, spontaneous APs were recorded from isolated AVN preparations by

*Corresponding author. Email:ziming-dong@163.com

using microelectrode techniques with 3 mol/L KCl microelectrodes at 33 °C.

2.4 Immunohistochemistry

Immunofluorescence labeling was performed on isolated single AVN cells from WT and SK2 + /Δ mice as described previously^[9]. Cells fixed with 4% formaldehyde and then permeabilized using 0.2% Triton X-100. After they were blocked with 1% BSA in PBS, the cells were incubated overnight at 4 °C with the primary antibody. The following primary antibodies were used: (1) anti-SK2 (Sigma, 1:100), a polyclonal antibody raised in rabbit; (2) anti-neurofilament 160 kD (NF 160, Chemicon, 1:100), a monoclonal antibody raised in mouse; immunofluorescence labeling for confocal microscopy was performed by treatment with FITC-conjugated goat anti-rabbit antibody (Sigma, 1:250) and Texas red-conjugated donkey anti-mouse antibody (Calbiochem, 1:250). Control experiments performed by incubation with secondary antibody only under the same experimental condition. Immunofluorescence-labeled samples were examined with a Pascal Zeiss confocal laser scanning microscope.

2.5 Statistics

Data are expressed as means ± SE. Statistical comparison was performed by Student *t* test, with a value of *P* < 0.05 considered significant.

3 Results

3.1 SK2 + / mice prolonged AV conduction

To estimate the influence of the SK2 channel on electrophysiological characteristics of the heart action, we performed surface ECG recordings from anesthetized WT and SK2 + /Δ mice. The RR interval was significantly increased from 134.97 ± 7.8 ms in the WT mice to 153.8 ± 6.1 ms in SK2 + /Δ (*P* < 0.05). The PR interval was prolonged from 35.1 ± 3.42 ms in WT mice to 42.50 ± 2.30 ms in SK2 + /Δ mice (*P* < 0.05),

pointing to a sinus bradycardia (R-R interval) with a significant prolongation of AV conduction (PR interval). The QTc interval (54.1 ± 5.95 and 58.4 ± 3.52 for WT and SK2 + /Δ mice) was not significantly modified. The other ECG parameters were not significantly modified (data not shown).

3.2 AVN preparation from SK2 + /Δ mice showed slower automaticity

The spontaneous activity of the AVN preparation was studied to test whether the slowing P-R interval observed in the ECG from the SK2 + /Δ mice was associated with dysfunction of AVN. Figure 1 showed the characteristic spontaneous APs recorded from the regions within and around the AVN at 33°C. APs recorded from the regions within the AV node can be identified by the presence of slow diastolic depolarization and a very slow upstroke of phase 0. The SK2 + /Δ mice showed a significant slow spontaneous activities of the AVN compared with WT mice (Figure 1). Analysis of the AP (Table 1) displayed a significant prolongation of the cycle length in SK2 + /Δ mice compared with WT mice (*P* < 0.05), and significant wider APD₅₀ and APD₈₀ in SK2 + /Δ mice compared with WT mice (*P* < 0.05, respectively). The DDR decreased in the AVN cells, but no significant difference between WT and SK2 + /Δ groups. The findings indicated that the present of the AV node was dysfunction and the automaticity of AVN cells decreased.

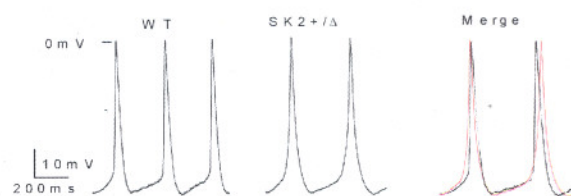


Figure 1. AVN spontaneous APs recording

Table 1. Action potential parameters measured in AVN cells from WT and SK2 + /Δ mice

	<i>n</i>	MDP (mV)	CL (ms)	APD ₅₀ (ms)	APD ₈₀ (ms)	DDR (mV/s)	V _{max} (V/s)
WT	9	49.18 ± 2.09	365.64 ± 27.62	33.82 ± 1.40	71.72 ± 2.56	26.98 ± 2.98	4.17 ± 0.53
SK2 + /Δ	9	48.11 ± 1.84	441.50 ± 25.94 *	40.00 ± 2.14 *	85.80 ± 4.17 *	19.74 ± 3.41	3.72 ± 0.75

**P* < 0.05, compared with WT. Cycle length, CL; the maximum diastolic potential, MDP; the maximum upstroke velocity, V_{max}; the rate of diastolic depolarization, DDR; AP duration at 50% and 80% repolarization, APD₅₀ and APD₈₀, respectively.

3.3 Expression of SK2 channel protein in AV node

At the mouse AV node, immunohistochemistry was used to investigate the expression of SK2 channel in the WT and SK2 + /Δ mice. To help distinguish different myocytes, NF160 was immunolabeled as marker which is expressed in the AV conduction system^[10]. Figure 2 showed SK2 (green) protein was strongly expressed in

the WT AVN cell(a). A reduced level of the SK2 labeling was detected in the SK2 + /Δ mouse(b). The control experiment eliminated the positive labeling further confirming that the labeling seen in AV nodal cell (c) was epitope-specific. In addition, the mouse atrial myocytes were more intensely labeled compared with ventricular myocytes.

4 Discussion

The present study shows for the first time the role and distribution of the SK2 channel at the AV node. The major phenotypic effects of the lack of SK2 in AVN were prolonged the PR and RR intervals. Electrophysiological study indicated a slow autorhythmicity through a prolongation of the APD and dysfunction of the AVN.

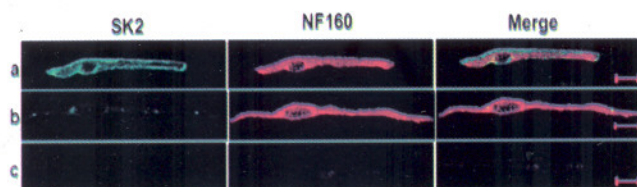


Figure 2. Confocal photomicrographs of double staining with anti-SK2 (green) and anti-NF 160 (red) antibodies in single AVN cell. The scale bar is 20 μm .

The small-conductance K_{Ca} channels are encoded by at least three genes, SK1, SK2, SK3^[11,12]. Electrophysiological studies and molecular cloning techniques have documented the expression of multiple types of voltage-gated K^+ channels in cardiac myocytes isolated from different species and from different regions of the heart^[13]. The importance of the channel is proved by the fact that the late phase of the cardiac AP is susceptible to abnormal excitation, e. g. early after depolarization and arrhythmias^[5]. In the previous, we documented that lack of SK2 channel prolonged the membrane repolarization, particularly in atria. *In vivo* electrophysiological studies showed evidence of AVN dysfunction and atrial arrhythmias (data didn't show).

In the present study, ECGs and electrophysiological recordings document both bradycardia and slowing of the atrioventricular conduction in SK2 + /Δ mice, whereas the lack of SK2 channels did not significantly modify the function of the SAN cells. The electrophysiological results indicated further that the loss of the SK2 channel slowed down the beating rate of AVN cell because of the prolonged APD through a delayed AP repolarization. The slowing of the AV conduction in the SK2 + / Δ mice is also caused by dysfunction in the excitability of the AVN. We could not completely reject the damage of

AVN cell during the surgery. The exact reasons for this finding have to be further accessed.

In this study, the expression of SK2 channel is not only detected in the mouse working myocytes, but also in the conduction system. Application of immunohistochemical imaging has shown that the expression of ion channels can provided new insights into how the AV node works at the cellular level.

References

1. De Carvalho AP, De Almeida DF. Spread of activity through the atrioventricular node. *Cir Res* 1960; 8:801–9.
2. Vergara C, Latorre R, Marrion NV, et al. Calcium-activated potassium channels. *Curr Opin Neurobiol* 1998; 8: 321–9.
3. Kohler M, Hirschberg B, Bond CT, et al. Small-conductance, calcium-activated potassium channels from mammalian brain. *Science* 1996; 273:1709 – 14.
4. Xu YF, Tuteja D, Zhang Z, et al. Molecular identification and functional roles of a Ca^{2+} -activated K^+ channel in human and mouse hearts. *J Bio Chemistry* 2003; 278:49085 – 94.
5. Lu L, Zhang Q, Timofeyev V, et al. Function coupling of SK2 to L-type Ca^{2+} channel via α -actinin2 is critical for normal cardiac functions. *Cir Res* 2007; 100: 112 – 20.
6. Chris TB, Herson PS, Strassmaier T, et al. Small conductance Ca^{2+} -activated K^+ channel knock-out mice reveal the identity of calcium-dependent afterhyperpolarization currents. *J Neuroscience* 2004; 24:5301 – 6.
7. Mitchell GF, Jeron A, Koren G. Measurement of heart rate and Q-T interval in the conscious mouse. *Am J Physiol* 1998; 274:H747 – 51.
8. Hancox JC, Levi AJ, Lee CO, et al. A method for isolating rabbit atrioventricular node myocytes which retain normal morphology and function. *Am J Physiol* 1993; 265:H755 – 66.
9. Spitzer KW, Sato N, Tanaka H, et al. Electrotonic modulation of electrical activity in rabbit atrioventricular node myocytes. *Am J Physiol* 1997; 273:H767 – 76.
10. Vitadello M, Vettore S, Lamar E, et al. Neurofilament M mRNA is expressed in conduction system myocytes of the developing and adult rabbit heart. *J Mol Cell Cardiol* 1996; 28: 1833 – 44.
11. Stocker M. Ca^{2+} -activated K^+ channels: molecular determinants and function of the SK family. *Nat Rev Neurosci* 2004; 5:758 – 70.
12. Tuteja D, Danyan XU, Timofeyev V, et al. Differential expression of small-conductance Ca^{2+} -activated K^+ channels SK1, SK2, and SK3 in mouse atrial and ventricular myocytes. *Am J Physiol Heart Circ Physiol* 2005; 289(6):H2714 – 23.
13. Pennefather P, Lancaster B, Adams PR, et al. Two distinct Ca -dependent K currents in bullfrog sympathetic ganglion cells. *Proc Natl Acad Sci USA* 1985; 2: 3040 – 4.

Determination of organochlorine pesticide residues in herbs by capillary gas chromatography

Bin Du^{1,*}, Xinchao Li², Hong Liu¹

¹School of Pharmacy, Zhengzhou University, Zhengzhou, Henan 450052, China; ²Zhongzhou University, Zhengzhou, Henan 450044, China

Received September 15, 2006

Abstract

Objective. The capillary gas chromatographic method was introduced for determining organochlorine pesticide residues (OCPs) in traditional Chinese medicines: Gastrodia Tuber, Fructus Corni and Spica Prunellae. **Methods.** The organochlorine pesticides were extracted from herbs with mixed solvents (petroleum ether), cleaned up by concentrated H₂SO₄, and separated by capillary column with electron capture detection. **Results.** The method is linear over the range 6–300 μg/L for four pesticides. Correlation coefficients varied between 0.9963 and 0.9992. Limits of detection (LODs) ranged from 3.91×10^{-8} to 9.05×10^{-8} μg/L. The average recoveries were within 77.13%–102.33% and RSD was 0.94%–2.84%. **Conclusion.** This method is accurate and reliable for OCPs determination in the three herbs. [Life Science Journal. 2007;4(1):40–42] (ISSN: 1097–8135).

Keywords: capillary gas chromatography; organochlorine pesticide; herbs

1 Introduction

Herbal medicines have been used in medical practice for thousands of years and recognized especially as a valuable and readily available resource for health care. A World Health Organization report indicated that about 70%–80% of the world populations rely on non-conventional medicine mainly of herbal sources in their primary health care. Traditional herbs and herbal products have been considered to be mild, non-toxic and even harmless because of their natural origin. Like other crops, medicinal plants are susceptible to insects and diseases both in the field and the storage, so pesticides are widely used for their protection. In fact, contamination of crude medicinal plants as well as their products has increasingly been reported^[1,2]. This has brought concerns and fears regarding practitioner's professionalism and quality, efficacy and safety of their treatment methods and products from herbal and natural sources available in market. Because of the high cost of pesticide-free cultivation, organic cultivation is only possible on a small scale and wild raw material is of insufficient quantity to meet the needs to the herbal drug market. The ever increasing consumption of medicinal plants necessitates large scale cultivation of medicinal plants which is not possible without use of pesticides. One of the character-

istics of herbal medicine preparation in traditional systems is that the herbal substrates are extracted with hot water during decoction process. Thus it would be toxicological interest to determine the actual amount of pesticides that is transferred from herbal substrates to infusion during its preparation, so that how much pesticide human intake may be measured. Many research workers have studied the pesticides residues in herbal material which are mainly based on surveying and monitoring the market samples. The objective of the present work is to investigate the transfer of pesticides from a range of herbal substrates, commonly used in traditional system of medicine, to their respective decoctions. This kind of data is useful as a pattern of reference in the management of pesticide residue problems and would help to formulate regulatory guidelines and recommendation for fixing of maximum residue limits on these products for quality assurance and control in herbal preparation. Attention is usually focused on contamination by organochlorine pesticides (OCPs) due to their toxicity and persistence in environment and contamination by common pesticides^[3,4]. There are extensively reported methods for monitoring pesticide residues in herb, food and feedstuff^[5–7]. They are based on either liquid-liquid extraction (LLE) or solid-phase extraction (SPE), followed by gas chromatography (GC) or HPLC separations employing wide range of detectors. For GC separations, electron capture detector (ECD) are popular for detection of OCPs residues. Although the use of organochlorine pesticides has been restricted or forbidden

*Corresponding author. Tel: 86-371-6776-2588; Email: dubin@zzu.edu.cn

by legislation, these compounds are still under investigation and they are included in the method adopted by the ChP-Chinese Pharmacopoeia. This paper describes an analytical method for the determination of organochlorine pesticide residues in three herbs. The extraction and clean-up procedures are carried out in a single step by concentrated H_2SO_4 . The pesticide compounds are quantitatively eluted with petroleumether and analysed by GC-ECD.

2 Materials and Methods

2.1 Reagents and apparatus

Selected pesticides and working solutions: The four stereoisomer of benzenehexachloride (α -BHC, β -BHC, γ -BHC, δ -BHC) 2,4-dichloronitrobenzene (internal standard) were obtained from the National Center of Standard Substance Research, with purity higher than 98.5%. Organic solvents are petroleum ether, standard stock solution (3000 $\mu g/L$) of each pesticide was prepared in petroleumether and the solutions required for preparing a standard curve (6, 18, 30, 60, 120, 180, 240 $\mu g/L$) and standard addition 1ml(180 $\mu g/L$) were prepared from the standard stock solution. All the solvents and chemicals used were of analytical grade and deionized water.

Apparatus: A varian 6890N gas-liquid chromatograph equipped with a 230 m \times 0.32 mm, i. d. glass column packed with SE-52, a constant current 63Ni electron capture detector. The operating conditions were as follows: Injection volume was 2 μl ; injector temperature, 200 °C; oven temperature, 160 °C; detector temperature 210 °C and the flow rate of the carrier gas (nitrogen) was maintained to 4 ml/min.

2.2 preparation of the samples

Dry herbal substrate in 60 °C for 4 hours, sieved and weighed 2 g sample was immersed in 10ml petroleum ether for 24 hours. The ultrasonic extract was filtered into a clean screwcap glass tube and then centrifuged at 100 rpm for 5 minutes. The supernatant was decanted into a 50 ml round-bottomed flask and then concentrated to about 1 ml at 40 °C using vacuum rotary evaporator. The solution was cleaned by H_2SO_4 . Additionally, the acid layer was discarded and ether layer was dehydrated by anhydrous sodium sulphate, transferred to 50 ml flask and concentrated to be nearly dry at 40 °C. Last the remnant was dissolved by petroleum ether to 10 ml measuring flask and added 1 ml internal standard solution.

2.3 Determination of response factors

The response factor of the standard pesticides relative to the internal standard, penta-chloronitrobenzene were carried out by injecting 2 μl into the GC-ECD system of a mixture consisted of the OCPs together with the I.S. at a concentration range of 6 – 300 $\mu g/L$. The

response factor was calculated based on the equation below:

$$\text{Response factor} = \frac{\text{Peak area of the pesticide standard}}{\text{Peak area of the internal standard}}$$

3 Results and Discussion

The gas chromatograph of a mixture of the benzenehexachloride standards plus the dichloronitrobenzene is shown in Figure 1. All the four enantiomeric forms are well resolved and eluted within a very reasonable time of about 10 minutes under the optimized GC conditions. Table 1 showed the retention times and the response factors for the OCPs and the linear regression equation of the calibration curve of each standard pesticide. Figure 2 showed samples and Table 2 gave results: the quantification were achieved in the three samples.

Table 1. Retention times, the linear regression equation and linearity range

BHC	Regression equation	r	Linearity range
α - BHC	$y = 0.0106x - 0.1034$	0.9963	6 ~ 300 $\mu g/L$
β - BHC	$y = 0.0032x - 0.0134$	0.9992	6 ~ 300 $\mu g/L$
γ - BHC	$y = 0.0100x - 0.0894$	0.9967	6 ~ 300 $\mu g/L$
δ - BHC	$y = 0.0087x - 0.0762$	0.9971	6 ~ 300 $\mu g/L$

Table 2. The detection results of the three samples

BHC	Gastrodia tuber	Fructus corni	Spica prunellae
α - BHC(ng/g)	40.31	44.04	not detected
β - BHC(ng/g)	27.88	32.04	not detected
γ - BHC(ng/g)	38.74	44.13	not detected
δ - BHC(ng/g)	40.49	42.31	not detected

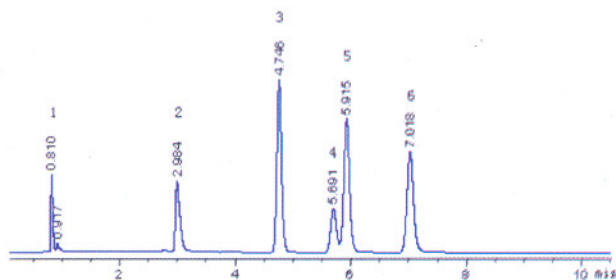


Figure 1. Gas chromatograph of OCP standards
1. solvent 2. internal standard dichloronitrobenzene 3. α -BHC 4. β -BHC 5. γ -BHC 6. δ -BHC

In order to evaluate the efficiency of the method, additional recovery analysis were carried out using petroleum ether. Table 3 showed the recovery and precision expressed as relative standarddeviation (RSD). Mean recoveries from samples fortified with α -BHC, β -BHC, γ -BHC, δ -BHC at levels from 6 to 300 $\mu g/L$, ranged from 77.13% to 102.33% with RSD values be-

tween 0.94% and 2.84%. These data have demonstrated the efficiency of the proposed method.

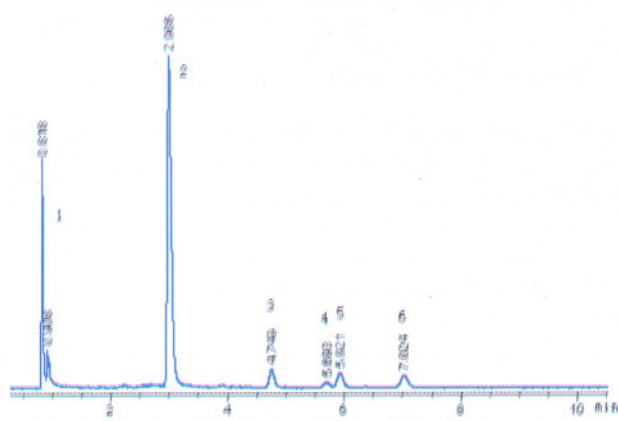


Figure 2. Gas chromatograph of the sample

1. solvent 2. internal standard dichloronitrobenzene 3. α -BHC
4. β -BHC 5. γ -BHC 6. δ -BHC

Table 3. Recovery and precision of the proposed method

Pesticides	Retention time (minute)	Mean recovery \pm RSD (range) (%)
α - BHC	4.75	91 \pm 8.2
β - BHC	5.69	91 \pm 10.8
γ - BHC	5.92	88 \pm 13.4
δ - BHC	7.02	92 \pm 7.2

4 Conclusion

The apparent current explosion of interest in commercial activity in the area of herbal products should be followed by accurate quality control. This could be as-

certained by imposing regulatory standards on these products that should be manufactured using good practices. The present study demonstrated transfer in decoctions of pesticides varied depending on their leaching potential. The actual amount of pesticides contributing to the dietary intake therefore may be quantified. This study showed an accurate and reliable method for OCPs determination in traditional Chinese medicines. It also showed that despite the numerous claims by both manufacturers and research groups on the usefulness of MAE for sample preparation. GC could be a more accurate alternative method for OCP determination in herbs.

References

1. Chan K. Some aspects of toxic contaminants in herbal medicines. *Chem* 2003; 52:1361 – 71.
2. Miraldi E, Giachetti D, Ferri S. Quality control of aromatic drugs reported in European Pharmacopoeia. II *Pharmacol* 2001(56), ; 365 – 71.
3. Tewary DK, Kumar V, Shanker A. Leaching of pesticides in herbal decoction. *Chemical Health & Safety* 2004; 3 (10): 259.
4. Sankararamakrishnan N, Sharma AK, Sanghi R. Organochlorine and organophosphorous pesticide residues in ground water and surface waters of Kanpur, Uttar Pradesh. *Environment International* 2005; 31(1):113 – 20.
5. Okolie NP, Osagie AU. Differential effects of chronic cyanide intoxication on heart, lung and pancreatic tissues. *Food and Chemical Toxicology* 2000; 38(6): 543 – 8.
6. Luciana P, Sannomiya M, Sader APO, et al. Extraction and clean-up procedure for analysis of organochlorine pesticide residues in ethoxylated lanolin. II *Farmaco* 2000, 55: 637 – 47.
7. Coler C, Manes J, Pico Y. Supercritical fluid extraction for pesticide multi-residue analysis in honey: determination by gas chromatography with electron-capture and mass spectrometry detection. *J Chromatogr A* 2004; 1048(2): 41 – 8.

Expression patterns and action analysis of genes associated with the responses to drugs, toxins, oxidation and unfolded proteins during rat liver regeneration[☆]

Hongpeng Han¹, Cunshuan Xu^{1,*}, Cuifang Chang¹, Gaiping Wang¹, Lijuan Su², Panfeng Liu², Xiaoguang Chen²

¹College of Life Science, Henan Normal University, Xinxiang, Henan 453007, China; ²Key Laboratory for Cell Differentiation Regulation, Xinxiang, Henan 453007, China

Received October 11, 2006

Abstract

Objective. The aim is to investigate the responses to drugs, toxins, oxidation and unfolded proteins after partial hepatectomy (PH) at transcriptional level. **Methods.** The genes associated with the responses to drugs, toxins, oxidation and unfolded proteins were obtained by collecting the data and thesis. Their expression changes in regenerating liver were checked by Rat Genome 230 2.0 Array. **Results.** It was found that 35, 14, 91 and 25 genes in sequence involved in the responses to drugs, toxins, oxidation, unfolded proteins were associated with liver regeneration (LR). The initial and total expressing gene numbers at four phases of LR, i.e., the initiation (0.5–4 hours after PH), the transition from G0 to G1 (4–6 hours after PH), the cell proliferation (6–66 hours after PH), the cell differentiation and structure-function reorganization (66–168 hours after PH) were 78, 21, 65, 2 and 78, 61, 137, 89, respectively, demonstrating the genes associated with LR were mainly triggered at the early phase, and worked at different phases. Based on their expression similarity, the genes were classified into 5 groups including only up, predominantly up, only down, predominantly down, and up/down regulation, involving in 55, 27, 40, 16 and 7 genes, respectively. The total times of their up and down-regulated expression were respectively 667 and 283, and the expression of the most genes was increased, whereas the minority decreased. According to the time relevance, they were classified into 13 groups, displaying that the cellular physiological and biochemical activities were staggered during LR. Their expression patterns were classified into 24 types, showing that the activities mentioned above were diverse and complicated during LR. **Conclusion.** The responses to drugs and oxidation were increased mainly in the early phase, prophase and late phases during LR, and the responses to toxins and unfolded proteins predominantly in the middle and late phases. 145 genes associated with LR played an important role. [Life Science Journal. 2007;4(1):43–51] (ISSN: 1097–8135).

Keywords: partial hepatectomy; Rat Genome 230 2.0 Array; responses to drugs, toxins, oxidation and unfolded proteins; genes; liver regeneration

1 Introduction

When organisms undergo distinct stimuli including physics^[1–5], chemistry^[5–9], biology^[10, 11], physiology^[12–19] and so on, the relevant stress protein (SP) genes are activated to protect organisms against these harmful stimuli. The stress response to one stimulus can usually increase cell tolerance to another stimulus. It implies stress proteins induced by different stimuli have functional cross^[20]. After partial hepatectomy (PH)^[21], the remnant hepatocytes were activated to proliferate to compensate the lost liver mass, which is called liver regeneration (LR)^[22, 23]. According to

the cellular physiological activities, the regeneration process is usually categorized into four stages including initiation phase (0.5–4 hours after PH), transition from G0 to G1 (4–6 hours after PH), cell proliferation (6–66 hours after PH), cell differentiation and reorganization of the structure-function (66–168 hours after PH)^[23]. According to time course, it was classified into four phases including forepart (0.5–4 hours after PH), prophase (6–12 hours after PH), metaphase (16–66 hours after PH), and anaphase (72–168 hours after PH)^[24]. In addition, PH, as an injurious stimulus, can induce many stress responses including the responses to drugs, toxins, oxidation and unfolded proteins. The above responses involved numerous genes and proteins, hence, it is almost impossible to clarify the action of genes associated with the above responses during LR at transcriptional level unless high-throughput gene expression arrays^[25, 26]. So, we used the Rat Genome 230 2.0 Array

[☆]Supported by the National Natural Science Foundation of China (No. 30270673).

*Corresponding author. Tel: 86-373-3326001; Fax: 86-373-3326524; Email:xucs@x263.net

containing 65 genes associated with drugs response, 23 genes to toxins, 179 genes to oxidation and 50 genes to unfolded proteins to detect gene expressions changes after PH^[27,28]. And 145 genes among them were found to be associated with LR^[29]. Moreover, their expression character, patterns and actions in regenerating liver were further analyzed.

2 Materials and Methods

2.1 Regenerating liver

Healthy Sprague-Dawley rats weighing 200 – 250 g were from the Animal Center of Henan Normal University. The rats were separated into two groups randomly, hepatectomized group and sham-operation (SO) group. Each group included 6 rats (male: female = 1:1). PH was performed according to Higgins and Anderson^[21], by which the left and middle lobes of liver were removed. Rats were killed by cervical vertebra dislocation at 0.5, 1, 2, 4, 6, 8, 12, 24, 36, 54, 66, 72, 120, 144 and 168 hours after PH and the regenerating livers were observed at corresponding time point. The livers were rinsed three times in PBS at 4 °C, and then 100 – 200 mg livers from middle parts of right lobe of each group (total 1 – 2 g livers, 0.1 – 0.2 g × 6 samples, per group) were gathered and mixed together, then stored at – 80 °C. SO group was the same as hepatectomized group except the liver lobes unremoved. The laws of animal protection of China were enforced strictly.

2.2 RNA isolation and purification

Total RNA was isolated from frozen livers according to the manual of Trizol kit (Invitrogen Corporation, Carlsbad, California, USA)^[30] and then purified base on the guide of RNeasy mini kit (Qiagen, Inc, Valencia, CA, USA)^[31]. Total RNA samples were checked to exhibit a 2:1 ratio of 28S rRNA to 18S rRNA intensities by agarose electrophoresis (180 V, 0.5 hour). Total RNA concentration and purity were estimated by optical density measurements at 260/280 nm^[32].

2.3 cDNA, cRNA synthesis and purification

As template, 1 – 8 µg total RNA was used for cDNA synthesis. cDNA purification was based on the way established by Affymetrix^[27]. cRNA labeled with biotin was synthesized using cDNA as the template, and cDNA and cRNA were purified according to the GeneChip Analysis^[27]. Measurement of cDNA, cRNA concentration and purity were the same as above.

2.4 cRNA fragmentation and microarray detection

15 µl (1 µg/µl) cRNA incubated with 5 × fragmentation buffer was digested into 35 – 200 bp fragments at 94 °C for 35 minutes. Rat Genome 230 2.0 microarray produced by Affymetrix was prehybridized, then the hybridization buffer was added at 45 °C, 60 rpm for 16 hours. The microarray was washed and stained by GeneChip fluidics station 450 (Affymetrix Inc, Santa Clara, CA, USA). The chips were scanned by GeneChip Scan 3000 (Affymetrix Inc, Santa Clara, CA, USA), and the signal values of gene ex-

pression were observed^[28].

2.5 Microarray data analysis

The normalized signal values, signal detections (P, A, M) and experiment/control (R_i) were obtained by quantifying and normalizing the signal values using GCOS (GeneChip operating software) 1.2^[28].

2.6 Normalization of the microarray data

To minimize error from the microarray analysis, each sample at each time point during LR was measured three times with Rat Genome 230 2.0 microarray. A total ratio was maximal (R^m) and the average of three housekeeping genes β-actin, hexokinase and glyceraldehyde-3-phosphate dehydrogenase approached 1.0 (R^h) was taken as a reference. The modified data were generated by applying a correction factor (R^m/R^h) multiplying the ratio of every gene in R^h at each time point. To remove spurious gene expression changes resulting from errors in the microarray analysis, the gene expression profiles at 0 – 4 hours, 6 – 12 hours and 12 – 24 hours after PH were reorganized by normalization analysis program (NAP) software according to the cell cycle progression of the regenerating hepatocytes. Data statistics and cluster analysis were done using GeneMath, GeneSpring, Microsoft Excel software^[28, 33, 34].

2.7 Identification of genes associated with LR

Firstly, the nomenclature of four physiological responses mentioned above was adopted from the GENEONTOLOGY database (www.geneontology.org) and input into the databases of NCBI (www.ncbi.nlm.nih.gov) and RGD (rgd.mcw.edu) to identify the rat, mouse and human genes associated with the responses to drugs, toxins, oxidation and unfolded proteins. In addition, according to maps of biological pathways embodied by GENMAPP (www.genmapp.org), KEGG (www.genome.jp/kegg/pathway.html#amino) and BIOCARTA (www.biocarta.com/genes/index.asp), the genes associated with the biological process were collated. The results of these analysis were codified, and compared with the results obtained from mouse and human searches to identify human and mouse genes which are different from those of rat. These genes (human and mouse genes differed from those of rat) were compared with the analysis output of the Rat Genome 230 2.0 Array. Those genes which showed more than twofold changes at expression level, observed as meaningful expression changes^[29], were referred to as rat homologous or rat specific genes associated with the responses to drugs, toxins, oxidation and unfolded proteins under evaluation. Genes, which displayed reproducible results with three independent analysis with the chip and which showed more than twofold changes at expression level in at least one time point in LR with significant difference ($0.01 \leq P < 0.05$) or extremely significant difference ($P \leq 0.01$) between PH and SO, were referred to as associated with LR.

3 Results

3.1 Expression changes of the genes associated with the responses to drugs, toxins, oxidation and unfolded proteins during LR

According to the data of NCBI, GENEMAP, KEGG, BIOCARTA and RGD, the responses to drugs, toxins, oxidation and unfolded proteins involved 74, 25, 195 and 58 genes respectively, in which 65, 23, 179 and 50 genes were contained in Rat Genome 230 2.0 Array separately. Among them, 35, 14, 91 and 25 genes displayed meaningful changes in expression at least at one time point after PH, showed significant or extremely significant differences in expression when comparing PH with SO, and were repeatable in three times of detection by Rat Genome 230 2.0 Array. The results

suggested that the genes were associated with LR. Up-regulation was 2–59.7 folds of control, and down-regulation 2–33.3 (Table 1). 55 genes were up-regulated, 40 genes down, 50 genes up/down during LR. The total up and down-regulated times were 667 and 283, respectively (Figure 1A). At the initiation stage (0.5–4 hours after PH), 52 genes were up-regulated, 26 genes down; at the transition phase from G0 to G1 (4–6 hours after PH), 42 genes revealed up-regulated, 19 genes down-regulated; at cell proliferation phase (6–66 hours after PH), 62 genes showed up-regulated, 41 genes down-regulated, 34 genes up/down-regulated; at cell differentiation and reorganization of the structure-function stage (66–168 hours after PH), 56 genes were up-regulated, 21 genes down-regulated, 12 genes up/down-regulated (Figure 1B).

Table 1. Expression abundance of 145 genes associated with responses to drugs, toxins, oxidation and unfolded proteins during rat LR

	Gene Accosiated Abbr. to others	Fold difference							
1 Drug									
Abca3	3	9.8	Ephx1	1.3	0.4, 2.8	Hnf4a	0.1, 4.5	*Tp53	2.9
Abcb1		4.6	Gata2	3	0.2, 7.0	Hspb1	4	Trpm2	0.4, 4.0
Abcb4		0.4	Gucy2c		0.4, 9.8	Htatip	0.4	Txnip	2.9
Abcc1	3	0.2	Mpst		0.1, 2.6	*Idh1	0.2, 2.4	Txnrd2	0.3
Abcc6		0.4	Pon1		0.4	*Ifng	6.5	Ucp3	0.5, 2.2
Abp1		2.6	3 Oxidation			Igf1r	0.4	Ugt1a7	2.1
Ahr		2.2	Aass		3.8	*Jak2	6.5	Vegfa	0.1, 4.5
Ahrr		0.1	Abca3	1	9.8	Jun	6.9	Xpa	0.2
Akr1c12		0.2, 2.22	Abcc1	1	0.2	Kdr	0.4, 2.4	Xrcc5	4.7
Akr1c6		0.03, 4.0	Ais2		0.5	Lpl	2.0	*Ptgs2	0.1, 2.1
Arnt	2	0.2, 3.0	Apoe		0.1	Mafk	0.3, 2.1	Gsta2	2
Arnt2	2	0.4, 6.8	Atm		0.3	Mapk1	2.7	4 Unfolded protein	
Blmh	2	3.7	Atox1		2.8	Mapk8	0.5, 19.7	Cebpb	3.1
Bphl	2	0.4	Bcl2		0.3	Matk	0.3, 4.9	Dnajb5	0.4
Cat	3	2.8	Bcl2a1		0.3, 5.3	*Mbl2	0.2	Dnajb9	0.3
Ces2	2	3.2	Blg1		2.7	*Mgst1	0.5	Dnajc3	0.4
Cyp2c		52.6	Blg3		5.3	Mmp9	0.5, 9.5	*Hspa1a	0.2
Cyp2d6		0.3	Ca3		14.0	Mra	1	Hspa1b	9.2
Drd1a		14.0	Casp8		10.6	Muc1	0.2, 6.8	Hspa2	11.0
Drd2		8.6	Cat	1	2.8	Nfkb1	0.4, 2.3	Hspa5	0.1, 5.7
Ebp		0.4	Cav		10.6	Nos3	0.3, 2.1	Hspa8	0.4, 9.8
Ephx1	2, 3	0.4, 2.8	Chek1		0.3, 5.3	Nox1	0.3, 8.6	Hspb1	3
Fpgs		0.5, 3.75	Creb1		0.5	Parg	4.8	Hspb2	4.7
Gabrg3		0.4	Crisp2		0.2	Pdim1	0.5, 3.2	Hspb3	0.5, 2.6
Gprk5		0.3, 9.1	*Crp		0.5	Plaur	13.9	Hspb7	0.2
Gsta5		5.6	Ctsb		3.6	Plcd1	0.2, 5.5	Hspb8	0.5, 6.8
Gstm2	3	4.5	Cycs		2.2	Ppp1r15b	0.1, 3.2	Hspca	2.0
Msra	3	0.5	Cyp1a1		59.7	Prdx3	0.5, 2.6	Hspe1	0.5, 2.8
Nat8		5.2	Ddit3		0.5, 2.7	Prdx5	0.5	Hyou1	0.4, 3.5
Oprs1		0.3	Dhcr24		0.1	Prdx6	2.3	*Lman1	0.3, 4.3
Pbp		3.7	Drd2		8.6	Prkaa2	0.2, 5.3	Npm1	0.4, 3.6
Slc18a1		0.4, 7.8	Dusp1		0.4, 6.0	Prkca	4.6	Osp94	0.5, 4.6
Sncs	3	0.2	Edn1		0.4, 2.6	*Prkcb1	8.2	Park2	2.9
Sult1a1		0.2, 2.2	*Egr1		18.6	Pten	0.5	Per1	2.4
2 Toxin									
Ace		0.5	Ephx1	1, 2	0.4, 2.8	Ptgs1	3.4	Serpinh1	2.1
Arnt	1	0.2, 3.0	Falz		0.1	Rps6ka5	5.6	*Tp53	2.9
Arnt2	1	0.4, 6.8	Fbp1		3.0	Sncs	1	Xbp1	0.4
As3mt		0.5	Foxm1		13.9	Sod2	5.6		
Blmh	1	3.7	Ggt1a1		4.0	Tap1	2.2		
Bphl	1	0.4	Gstm2	1	4.5	Tert	0.3, 5.3		
Ces2	1	3.2	H6pd		2.9	*Tgfb1	4.0		
			Hao1		0.5, 2.3	Tgfb1i1	0.5, 2.0		
			Hmox2		0.4	*Tnf	3.2		

* Reported genes associated with LR; Associated to others: involved in other responses

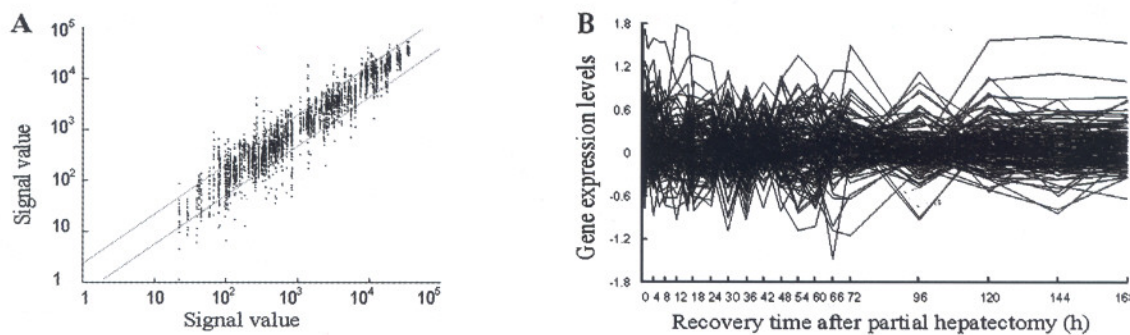


Figure 1. Expression frequency, abundance and changes of 145 genes associated with responses to drugs, toxins, oxidation and unfolded proteins during rat LR. Detection data of Rat Genome 230 2.0 Array were analyzed and graphed by Microsoft Excel. A. Gene expression frequency. The dots above bias represented the genes up-regulated more than twofold, and total times of up-regulation were 667; those under bias represented the genes down-regulated more than twofold, and down-regulation were 283 times; and the ones between biases represented the genes insignificantly changed. B. Gene expression abundance and changes. 105 genes were 2 – 59.7 folds up-regulated, and 90 genes 2 – 33.3 folds down-regulated.

3.2 Initiation expression time of the genes associated with the responses to drugs, toxins, oxidation and unfolded proteins during LR

At each time point of LR, the numbers of initial up, down and total up, down-regulated genes were in sequence: both 25 and 9 at 0.5 hour; 16, 6 and 38, 11 at 1 hour; 8, 1 and 36, 5 at 2 hours; 3, 10 and 36, 14 at 4 hours; 4, 4 and 33, 11 at 6 hours; 2, 2 and 32, 11 at 8 hours; 0, 4 and 24, 15 at 12 hours; 11, 7 and 36, 15 at 16 hours; 5, 7 and 36, 18 at 18 hours; 2, 4 and 34, 12 at 24 hours; 3, 2 and 22, 16 at 30 hours; 0, 3 and 30, 19 at 36 hours; 0, 1 and 29, 8 at 42 hours; 1,

1 and 37, 17 at 48 hours; 0, 2 and 29, 20 at 54 hours; 0, 0 and 30, 22 at 60 hours; 0, 0 and 30, 10 at 66 hours; 0, 0 and 31, 7 at 72 hours; 0, 0 and 21, 12 at 96 hours; 2, 0 and 32, 10 at 120 hours; 0, 0 and 24, 11 at 144 hours; 0, 0 and 22, 6 at 168 hours (Figure 2). Generally, gene expression changes occurred during the whole LR, and the up and down-regulation were respectively 667 and 283 times. The initially up-regulated genes were predominantly expressed in the forepart, and the down- in the prophase, pre-metaphase and mid-metaphase, whereas only few genes were initially up-expressed in the late metaphase and anaphase.

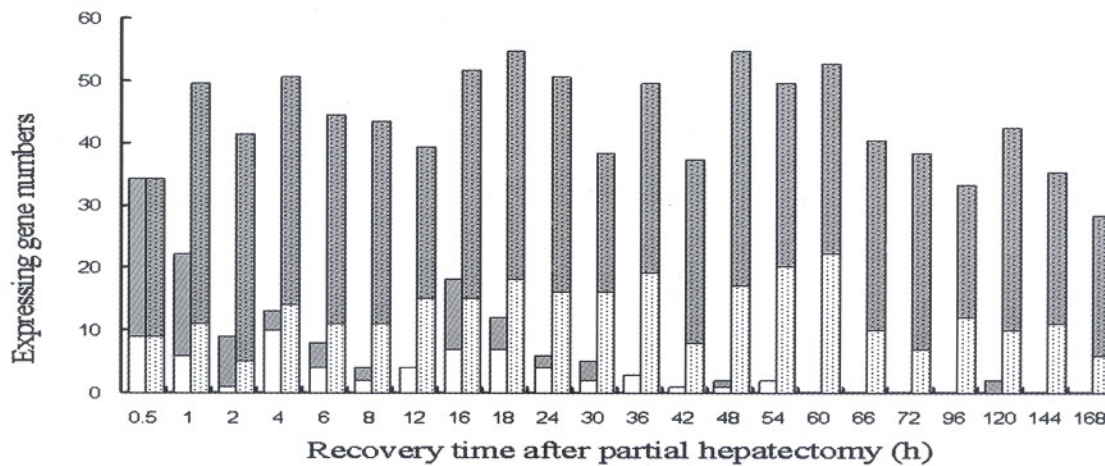


Figure 2. The initial and total expression profiles of 145 genes associated with responses to drugs, toxins, oxidation and unfolded proteins at each time point of LR. Grey bars: Up-regulated genes; White bars: Down-regulated genes. Blank bars represent initial expressing genes, in which up-regulation genes are predominant in the forepart, and the down- prophase, pre-metaphase and mid-metaphase, whereas almost none in the late metaphase and anaphase. Dotted bars represent the total expressing genes, in which some genes are up-regulation and others down-regulation during LR.

3.3 Expression similarity and time relevance of the genes associated with the responses to drugs, toxins, oxidation and unfolded proteins during LR

145 genes mentioned above during LR could be characterized based on their similarity in expression as following: only up, predominantly up, only down, predominantly down, and up/down-regulated, involving 55, 27, 40, 16 and 7 genes, respectively (Figure 3). 145 genes could also be classified based on time relevance into 13 groups including 0.5 and 144 hours, 1 and 2 hours, 4 and 6 hours, 8 and 12 hours, 16 hours, 18

hours, 24 and 30 hours, 36 and 48 hours, 42 and 54 hours, 60 and 66 hours, 72 and 96 hours, 120 hours, 168 hours, in which the up and down-regulated gene numbers were 49 and 20; 74 and 16; 69 and 25; 56 and 26; 36 and 15; 36 and 18; 56 and 32; 67 and 36; 58 and 38; 60 and 32; 52 and 19; 32 and 10; 22 and 6, respectively (Figure 3). The up-regulation genes were mainly associated with oxidative stress, drug metabolism and transport, folding and transport of peptide. The down-regulation genes were mostly those associated with anti-apoptosis and oxidative injury.

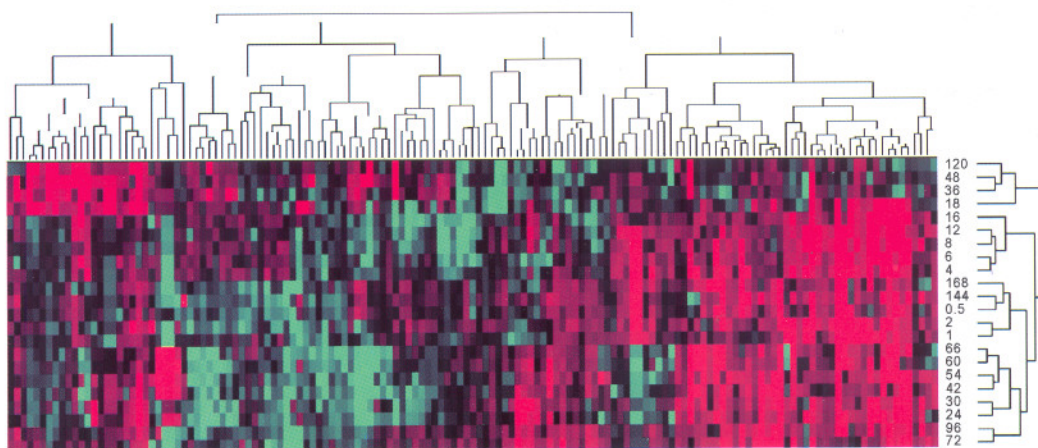


Figure 3. Expression similarity and time relevance cluster of 145 genes associated with responses to drugs, toxins, oxidation and unfolded proteins during LR. Detection data of Rat Genome 230 2.0 Array were analyzed by H-clustering. Red represents up-regulation genes mainly associated with oxidative stress, drug metabolism and transport, folding and transport of peptide; Green represents the down- ones mostly with anti-apoptosis and oxidative injury; Black indicates the genes with nonsense change in expression. The upper and right trees respectively show expression similarity and time series clusters, by which the above genes were classified into 5 and 13 groups separately.

3.4 Expression patterns of the genes associated with the responses to drugs, toxins, oxidation and unfolded proteins during LR

145 genes mentioned above during LR might be categorized into 24 clusters according to the changes in expression changes: (1) up-regulation at one time point, at 0.5, 6, 16, 30, 36, 48, 120 hours after PH (Figure 4A), involved in 9 genes; (2) up at two time points, at 16 and 42 hours, 16 and 96 hours, 30 and 42 hours (Figure 4B), in 4 genes; (3) up at three time points (Figure 4C), in 2 genes; (4) up at four time points (Figure 4C), in 3 genes; (5) up at one phase, 0.5–6 hours, 0.5–8 hours (Figure 4D), in 2 genes; (6) up at three phases (Figure 4D), in 2 genes; (7) up at one time point/one phase, at 8 and 1–4 hours, 120 and 1–24 hours, 120 and 6–8 hours (Figure 4D), in 3 genes; (8) up at two time points/one phase (Figure 4E), in 5 genes; (9) up at one time point/two phases (Figure 4F), in 5 genes; (10) up at two time points/two phases (Figure 4G), in 4 genes; (11) up at three time points/two phases (Figure 4H), in 4 genes; (12)

up at two time points/three phases (Figure 4I), in 6 genes; (13) at more time points or phases (Figure 4J), in 6 genes; (14) down at one time point, at 0.5, 4, 6, 12, 16, 24, 30, 36, 42, 54 hours (Figure 4K), in 11 genes; (15) down at two time points, at 1 and 66 hours, 1 and 168 hours, 2 and 12 hours, 12 and 36 hours, 16 and 30 hours, 24 and 54, 48 and 60 (Figure 4L), in 7 genes; (16) down at three time points (Figure 4M), in 2 genes; (17) down at four time points (Figure 4M), in 4 genes; (18) down at one phase, at 0.5–2 hours, 4–6 hours, 54–60 hours (Figure 4N), in 3 genes; (19) down at one time point/one phase, at 1 and 144–168 hours, 8 and 120–144 hours, 36 and 54–60 hours, 48 and 12–24 hours (Figure 4N), in 5 genes; (20) down at one time point/two phases (Figure 4O), in 2 genes; (21) down at more time points or phases (Figure 4P), in 6 genes; (22) first up and then down (Figure 4Q), in 12 genes; (23) first down and then up (Figure 4R), in 10 genes; (24) up/down mixed (Figure 4R), in 28 genes.

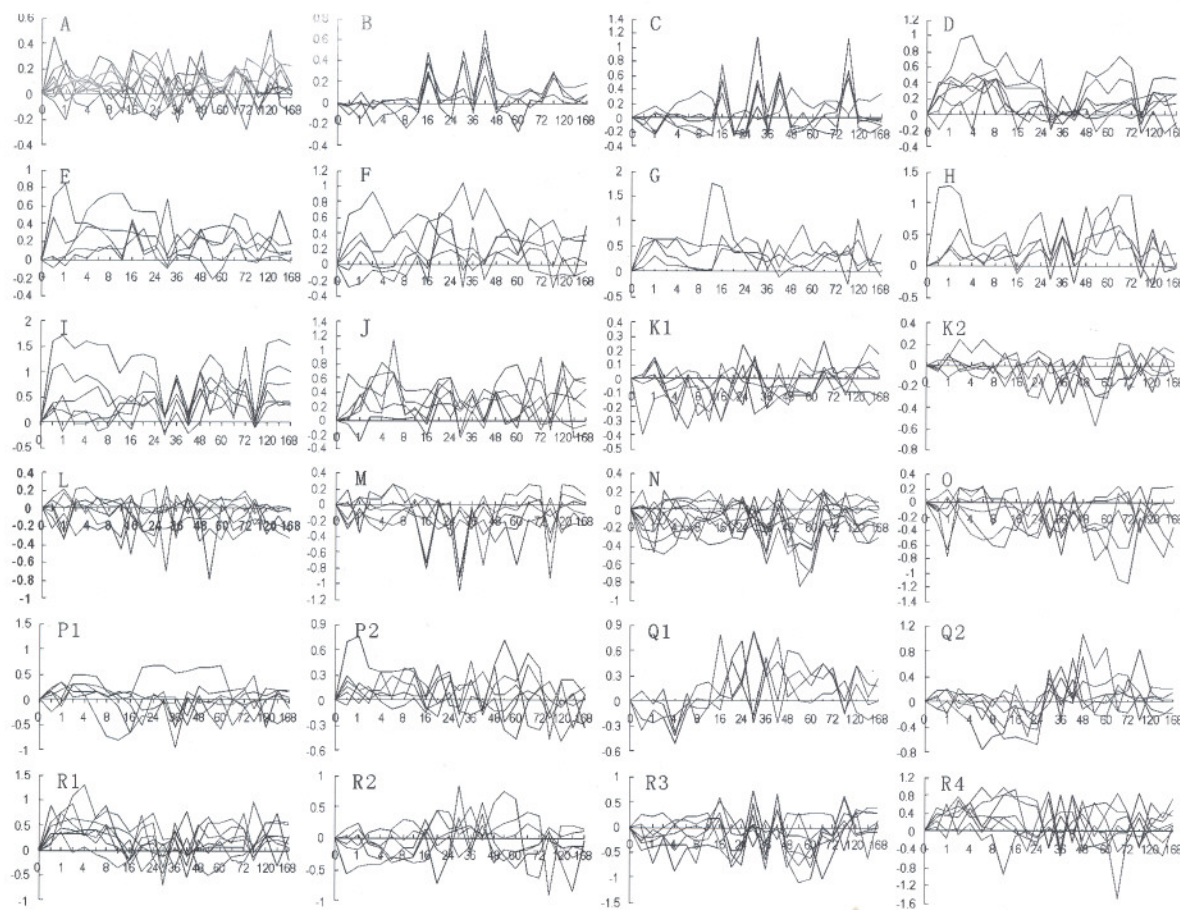


Figure 4. Twenty-four expression patterns of 145 genes associated with responses to drugs, toxins, oxidation and unfolded proteins during LR. Expression patterns were obtained by the analysis of detection data of Rat Genome 230 2.0 Array with Microsoft Excel. A – I: 55 up-regulated genes; J – O: 40 down-regulated genes; P – R: 50 up/down-regulated genes. X-axis represents recovery time after PH (h); Y-axis shows logarithm ratio of the signal values at each time point to control.

4 Discussion

Liver is an important organ metabolizing drugs and toxins^[35]. It can also respond to stress including oxidation and unfolded protein. In which, 15 kinds of proteins associated with drug metabolism, such as cytochrome P450 subfamily II C (CYP2C) etc., participate in transportation and catabolism of drugs^[36]. Dopamine receptor 1A, 2 (DRD1A, DRD2) are involved in drug addiction. Aryl hydrocarbon receptor repressor (AHRR) suppresses activation of aryl hydrocarbon receptor^[37]. Aryl hydrocarbon receptor nuclear translocator (ARNT) promotes secretion of trypsin^[38]. Aldo-ke-to reductase family 1 member C6 (AKR1C6) accelerates bile acid synthesis^[39]. Catalase (CAT) can protect cells against oxidation damage by decomposing H₂O₂^[40]. Follypolyglutamate synthase (FPGS) plays an important role in synthesis of nucleic acid^[41]. G protein-coupled receptor kinase 5 (GPRK5) can raise blood pressure^[42].

Phosphatidylethanolamine binding protein (PBP) is concerned with biomembrane formation^[43]. Amiloride-binding protein 1 (ABP1) can open Na⁺ channel of epithelia^[44]. Gamma-aminobutyric acid A receptor subunit gamma 3 (GABRG3) is associated with liver diseases depended on ethanol^[45]. N-acetyltransferase 8 (NAT8) debases cell conglutination^[46]. The meaningful expression changes of these genes showing the sameness or the similarity in some time points, then difference in other during LR perhaps co-regulate the response to drug. Especially, *cyp2c* displayed significant up-regulation during almost the LR, and had the highest abundance at 16 hours that was 9.1-fold of control. *drd1 a* was up at 16, 30, 42 and 96 hours post PH, and had peak expression showing 14-fold of control at 30 hours. It is speculated that the two play crucial roles in the drugs response.

Among proteins associated with response to toxin, uanylate cyclase 2c (GUCY2c) mediates acute secretory diarrhea induced by heat-stable enterotoxins^[47]. Arsenic

+ 3 oxidation state methyltransferase (AS3MT) prevents regenerating liver from toxicity of arsenic + 3 by catalyzing transfer of a methyl group to trivalent arsenicals^[48]. Mercaptopyruvate sulfurtransferase (MPST) plays a role in catabolism of cysteine and cyanide^[49]. Glutathione-S-transferase alpha type 2 (Gsta2) is concerned with detoxification by binding to hepatocyte nuclear factor 1 (HNF1)^[50]. Paraoxonase 1 (PON1) is involved in decomposition of lipid peroxides and organophosphorus compounds^[51]. UDP glycosyltransferase 1 family A7 (UGT1A7) is concerned with elimination of multifold toxin^[52]. Angiotensin I converting enzyme (ACE) protects tissues from chronic hypoxia to maintain the stabilization of cardiopulmonary function by converting angiotensin I into angiotensin II^[53]. The sameness or the similarity in some time points, then difference in others of meaningful expression changes of these genes during LR perhaps regulate the response to toxin in regenerating liver together. Remarkably, *gucy2c* was up during almost the whole LR, having a peak that was 9.8 folds of the control. *gsta2* was up at 30, 42 and 96 hours after PH, and reached a peak at 42 hours showing 7 times higher than control. It was presumed that the two play key roles in the response to toxin in regenerating liver.

Among proteins associated with response to oxidation, 18 kinds of proteins including cytochrome P450 subfamily 1 member A1 (CYP1A1) regulate oxidation reaction during LR and protect cells from oxidative damage^[54]. 3 kinds of proteins including lipoprotein lipase (LPL) participate in decomposing lipid through oxidation^[55]. Poly ADP-ribose glycohydrolase (PARG) resists inflammation^[56]. Adenosine monophosphate-activated protein kinase α 2 catalytic subunit (PRKA α 2) regulates the balance between energy supply and demand^[57]. Dual specificity phosphatase 1 (DUSP1) is relative to the release of endotoxin^[58]. The meaningful expression changes of these genes showing the sameness or the similarity in some time points, and difference in others during LR perhaps co-regulate the response to oxidation. Among them, *cyp1a1* was up during almost the whole LR, showing peak expression at 12 hours that was 59.7 folds of control, presuming that it plays a critical role in the oxidative stress.

Among the proteins associated with the response to unfolded protein, eleven kinds of proteins including 10 kDa heat shock protein 1 (HSPE1) play the role in the folding of proteins and the degradation of wrong folded proteins^[59]. 27 kDa heat shock protein 2 (HSPB2) restrains apoptosis by maintaining functions of mitochondrion^[60]. 27 kDa heat shock protein 3 (HSPB3) is involved in cells survival and differentiation^[61]. Hsp40 homolog subfamily C member 3 (DNAJC3) accelerates

the expression of p58 (a protein kinase) and depresses eukaryote translation initiation factor 2 (eIF2)^[62]. Hsp40 homolog subfamily B member 9 (DNAJB9) resists cell apoptosis^[63]. 70 kDa heat shock protein 1B (HSPA1B) can protect cell depending on CO and regulate immunoreaction^[64]. 70 kDa heat shock protein 2 (HSPA2) promotes the transition from G1 to S^[65]. 70 kDa heat shock protein 4-like (HSPA4L /OSP94) accelerates the secretion of CD1d and sends antigen to T cells^[66]. Nucleophosmin (NPM1) hastens the assembly of ribosome and maintains the manifold enzymatic activity in liver^[67]. That the meaningful expression changes of these genes are same or similar in some points, then different in others during LR perhaps presumably regulate the response to unfolded protein together. Among them, *hspa8* was up during almost the whole LR, and had a peak at 12 hours that was 9.8 folds of control. *hspa1b* showed up-regulation at multiple time points after PH, and had the highest abundance having 8.2-fold increase at 60 hours. *hspa2* was up-regulated at metaphase, anaphase, and reached a peak having a 10-fold increase at 30 hours. It was supposed that the three have key roles in the response to unfolded protein in regenerating liver.

In conclusion, the responses to drugs, toxins, oxidation and unfolded proteins were investigated using high-throughput gene expression profiles commencing from long time (0.5 hour – 7 days after PH) and multiple time points (total 23). It was primarily proved that the regenerating liver had an increase in the responses to drugs, toxins, oxidation and unfolded proteins, that Rat Genome 230 2.0 Array was a useful tool analyzing the above responses at transcriptional level. However, the processes, namely, DNA → mRNA → protein, were influenced by many factors including protein interaction. Therefore, later the above results will be further analyzed by the techniques, such as Northern blotting, protein chip, RNA interference, protein-interaction etc.

References

1. Evgen'ev MB, Garbuz DG, Zatsepina OG. Heat shock proteins: functions and role in adaptation to hyperthermia. Ontogenet 2005; 36 (4): 265 – 73.
2. Xu CS, Fracella F, Christiane RL, et al. Stress response of lysosomal, cysteine proteinases in rat C6 glioma cells. Comp Biochem Physiol B Biochem Mol Biol 1997; 117 (2): 169 – 78.
3. Dresios J, Aschrafi A, Owens GC, et al. Cold stress-induced protein Rbm3 binds 60S ribosomal subunits, alters microRNA levels, and enhances global protein synthesis. PNAS 2005; 102 (6): 1865 – 70.
4. Varela CA, Baez ME, Agosin E. Osmotic stress response: quantification of cell maintenance and metabolic fluxes in a Lysine-overproducing strain of corynebacterium glutamicum. Appl Environ Microbiol 2004; 70 (7): 4222 – 9.
5. Barbour E, Rawda N, Banat G, et al. Comparison of im-

- munosuppression in dry and lactating Awassi ewes due to water deprivation stress. *Vet Res Commun* 2005; 29 (1): 47–60.
6. Vitetta L, Anton B, Cortizo F, et al. Mind-body medicine: stress and its impact on overall health and longevity. *Ann N Y Acad Sci* 2005; 1057: 492–505.
 7. Huelmos RA, Garcia VMJ, Alegria EE, et al. Myocardial perfusion reserve studied by single-photon emission-computed tomography with thallium-201 and a drug stress test with adenosine triphosphate in patients with cardiovascular risk factors. *Rev Esp Cardiol* 1997; 50 (10): 696–708.
 8. Muto Y, Sato K. Pivotal role of actin in cell survival under oxidative stress in the zitter rat brain with genetic spongiform encephalopathy. *Brain Res Mol Brain Res* 2003; 111 (1–2): 111–22.
 9. Hohenblum H, Gasser B, Maurer M, et al. Effects of gene dosage, promoters, and substrates on unfolded protein stress of recombinant *Pichia pastoris*. *Biotechnol Bioeng* 2004; 85 (4): 367–75.
 10. Lucht JM, Mauch-Mani B, Steiner HY, et al. Pathogen stress increases somatic recombination frequency in *Arabidopsis*. *Nat Genet* 2002; 30 (3): 311–4.
 11. Estes DM, Turaga PS, Sievers KM, et al. Characterization of an unusual cell type ($CD4^+ CD3^-$) expanded by helminth infection and related to the parasite stress response. *J Immunol* 1993; 150 (5): 1846–56.
 12. Matsuzawa S, Suzuki T, Misawa M. Conditioned fear stress induces ethanol-associated place preference in rats. *Eur J Pharmacol* 1998; 341 (2–3): 127–30.
 13. Ono H, Ichiki T, Ohtsubo H, et al. Critical role of Mst1 in vascular remodeling after injury. *Arterioscler Thromb Vasc Biol* 2005; 25 (9): 1871–6.
 14. Oztas B, Akgul S, Arslan FB. Influence of surgical pain stress on the blood-brain barrier permeability in rats. *Life Sci* 2004; 74 (16): 1973–9.
 15. Liu LM, Dubick MA. Hemorrhagic shock-induced vascular hyporeactivity in the rat: relationship to gene expression of nitric oxide synthase, endothelin-1, and select cytokines in corresponding organs. *J Surg Res* 2005; 125 (2): 128–36.
 16. Hosford GE, Koyanagi KS, Leung WI, et al. Hyperoxia increases protein mass of 5-lipoxygenase and its activating protein, flap, and leukotriene B(4) output in newborn rat lungs. *Exp Lung Res* 2002; 28 (8): 671–84.
 17. Hasan SS, Chaturvedi PK. Response of whole body X-irradiation to inanition stress. *Strahlentherapie* 1983; 159 (6): 351–7.
 18. Spiler IJ, Molitch ME. Lack of modulation of pituitary hormone stress response by neural pathways involving opiate receptors. *J Clin Endocrinol Metab* 1980; 50 (3): 516–20.
 19. Spector MP. The starvation-stress response (SSR) of *Salmonella*. *Adv Microb Physiol* 1998; 40: 233–79.
 20. Riezman H. Why do cells require heat shock proteins to survive heat stress? *Cell Cycle* 2004; 3 (1): 61–3.
 21. Higgins GM, Anderson RM. Experimental pathology of the liver: restoration of the liver of the white rat following partial surgical removal. *Arch Pathol* 1931; 12: 186–202.
 22. Fausto N, Campbell JS, Riehle KJ. Liver regeneration. *Hepatology* 2006; 43 (2): S45–S53.
 23. Michalopoulos GK, De Frances M. Liver regeneration. *Adv Biochem Eng Biotechnol* 2005; 93: 101–34.
 24. Taub R. Liver regeneration: from myth to mechanism. *Nat Rev Mol Cell Biol* 2004; 5 (10): 836–47.
 25. Xu CS, Chang CF, Yuan JY, et al. Expressed genes in regenerating rat liver after partial hepatectomy. *World J Gastroenterol* 2005; 11 (19): 2932–40.
 26. Dransfeld O, Gehrmann T, Keo hrer K, et al. Oligonucleotide microarray analysis of differential transporter regulation in the regenerating rat liver. *Liver International* 2005; 25 (6): 1243–58.
 27. Li L, Roden J, Shapiro BE, et al. Reproducibility, fidelity, and discriminant validity of mRNA amplification for microarray analysis from primary hematopoietic ells. *J Mol Diagn* 2005; 7 (1): 48–56.
 28. Hood L, Leroy Hood expounds the principles, practice and future of systems biology. *Drug Discov Today* 2003; 8 (10): 436–8.
 29. Yue H, Eastman PS, Wang BB, et al. An evaluation of the performance of cDNA microarrays for detecting changes in global mRNA expression. *Nucleic Acids Res* 2001; 29 (8): E41.
 30. Knapp JH, Geahr MA, Forman MS, et al. Comparison of automated and manual nucleic acid extraction methods for detection of enterovirus RNA. *J Clin Microbiol* 2003; 41 (8): 3532–6.
 31. Nuyts S, Van Mellaert L, Lambin P, et al. Efficient isolation of total RNA from *Clostridium* without DNA contamination. *J Microbiol Methods* 2001; 44 (3): 235–8.
 32. Arkin A, Ross J, McAdams HH. Stochastic kinetic analysis of developmental pathway bifurcation in phage lambda-infected *Escherichia coli* cells. *Genetics* 1998; 149 (4): 1633–48.
 33. Eisen MB, Spellman PT, Brown PO, et al. Cluster analysis and display of genome-wide expression patterns. *Proc Natl Acad Sci* 1998; 95 (25): 14863–8.
 34. Werner T. Cluster analysis and promoter modelling as bioinformatics tools for the identification of target genes from expression array data. *Pharmacogenomics* 2001; 2 (1): 25–36.
 35. Elkayam T, Amitay-Shaprut S, Dvir-Ginzberg M, et al. Enhancing the drug metabolism activities of C3A-a human hepatocyte cell line-by tissue engineering within alginate scaffolds. *Tissue Eng* 2006; 12 (5): 1357–68.
 36. Hosagrahara VP, Rettie AE, Hassett C, et al. Functional analysis of human microsomal epoxide hydrolase genetic variants. *Chem Biol Interact* 2004; 150 (2): 149–59.
 37. Tsuchiya Y, Nakajima M, Itoh S, et al. Expression of aryl hydrocarbon receptor repressor in normal human tissues and inducibility by polycyclic aromatic hydrocarbons in human tumor-derived cell lines. *Toxicological Sciences* 2003; 72 (2): 253–9.
 38. Levisetti MG, Polonsky KS. Diabetic pancreatic beta cells ARNT all they should be. *Cell Metab* 2005; 2 (2): 78–80.
 39. Carninci P, Kasukawa T, Katayama S, et al. The Transcriptional landscape of the mammalian genome. *Science* 2005; 309 (5740): 1559–63.
 40. Muramatsu S, Suga Y, Mizuno Y, et al. Differentiation-specific localization of catalase and hydrogen peroxide, and their alterations in rat skin exposed to ultraviolet B rays. *J Dermatol Sci* 2005; 37 (3): 151–8.
 41. Howard KM, Muga SJ, Zhang L, et al. Characterization of the rat cytoplasmic Cl-tetrahydrofolate synthase gene and analysis of its expression in liver regeneration and fetal development. *Gene* 2003; 319: 85–97.
 42. Reyes-Salcido V, Villalobos-Molina R. Evidence that dl-propranolol increases thymidine kinase activity, cell mitosis, and beta-adrenoceptors during rat liver regeneration. *Arch Med Res* 2003; 34 (4): 273–5.

43. Vance JE. Molecular and cell biology of phosphatidylserine and phosphatidylethanolamine metabolism. *Prog Nucleic Acid Res Mol Biol* 2003; 75: 69–111.
44. Lingueglia E, Renard S, Voilley N, et al. Molecular cloning and functional expression of different molecular forms of rat amiloride-binding proteins. *Eur J Biochem* 1993; 216 (2): 679–87.
45. Dick DM, Edenberg HJ, Xuei X, et al. Association of GABRG3 with alcohol dependence. *Alcohol Clin Exp Res* 2004; 28 (1): 4–9.
46. Popuseva AE, Luchinskaya NN, Ludwig AV, et al. Overexpression of camello, a member of a novel protein family, reduces blastomere adhesion and inhibits gastrulation in *Xenopus laevis*. *Dev Biol* 2001; 234 (2): 483–96.
47. Schulz S, Lopez MJ, Kuhn M, et al. Disruption of the guanylyl cyclase-C gene leads to a paradoxical phenotype of viable but heat-stable enterotoxin-resistant mice. *J Clin Invest* 1997; 100 (6): 1590–5.
48. Lin S, Shi Q, Nix FB, et al. A novel S-adenosyl-L-methionine: arsenic (III) methyltransferase from rat liver cytosol. *J Biol Chem* 2002; 277 (13): 10795–803.
49. Billaut-Laden I, Rat E, Allorge D, et al. Evidence for a functional genetic polymorphism of the human mercaptopyruvate sulfurtransferase (MPST), a cyanide detoxification enzyme. *Toxicol Lett* 2006; 165 (2): 101–11.
50. Voss SH, Whalen R, Boyer TD. Mechanism of negative regulation of rat glutathione S-transferase A2 by the cytokine interleukin 6. *Biochem J* 2002; 365 (Pt 1): 229–37.
51. Trudel K, Sinnett D, James RW, et al. Iron-ascorbic acid-induced oxidant stress and its quenching by paraoxonase 1 in HDL and the liver: comparison between humans and rats. *J Cell Biochem* 2005; 96 (2): 404–11.
52. Grove AD, Kessler FK, Metz RP, et al. Identification of a rat olitipraz-inducible UDP-glucuronosyltransferase (UGT1A7) with activity towards benzo(a)pyrene-7,8-dihydrodiol. *J Biol Chem* 1997; 272 (3): 1621–7.
53. Lam SY, Fung ML, Leung PS. Regulation of the angiotensin-converting enzyme activity by a time-course hypoxia in the carotid body. *J Appl Physiol* 2004; 96 (2): 809–13.
54. Moore SD, Helmle KE, Prat LM, et al. Tissue localization of the copper chaperone ATOX1 and its potential role in disease. *Mamm Genome* 2002; 13 (10): 563–8.
55. Kratky D, Zimmermann R, Wagner EM, et al. Endothelial lipase provides an alternative pathway for FFA uptake in lipoprotein lipase-deficient mouse adipose tissue. *J Clin Invest* 2005; 115 (1): 161–7.
56. Cuzzocrea S, Di Paola R, Mazzon E, et al. PARG activity mediates intestinal injury induced by splanchnic artery occlusion and reperfusion. *FASEB J* 2005; 19 (6): 558–66.
57. Pallottini V, Montanari L, Cavallini G, et al. Mechanisms underlying the impaired regulation of 3-hydroxy-3-methylglutaryl coenzyme A reductase in aged rat liver. *Mech Ageing Dev* 2004; 125 (9): 633–9.
58. Hamer M, Mages J, Dietrich H, et al. Dual specificity phosphatase 1 (DUSP1) regulates a subset of LPS-induced genes and protects mice from lethal endotoxin shock. *J Exp Med* 2006; 203 (1): 15–20.
59. Shan YX, Liu TJ, Su HF, et al. Hsp10 and Hsp60 modulate Bcl-2 family and mitochondria apoptosis signaling induced by doxorubicin in cardiac muscle cells. *J Mol Cell Cardiol* 2003; 35 (9): 1135–43.
60. Kadono T, Zhang XQ, Srinivasan S, et al. CRYAB and HSPB2 deficiency increases myocyte mitochondrial permeability transition and mitochondrial calcium uptake. *J Mol Cell Cardiol* 2006; 40 (6): 783–9.
61. Sugiyama Y, Suzuki A, Kishikawa M, et al. Muscle develops a specific form of small heat shock protein complex composed of MKBP/HSPB2 and HSPB3 during myogenic differentiation. *J Biol Chem* 2000; 275 (2): 1095–104.
62. Yan W, Frank CL, Korth MJ, et al. Control of PERK eIF2alpha kinase activity by the endoplasmic reticulum stress-induced molecular chaperone P58IPK. *Proc Natl Acad Sci USA* 2002; 99 (25): 15920–5.
63. Berger BJ, Muller TS, Buschmann IR, et al. High levels of the molecular chaperone Mdg1/ERdj4 reflect the activation state of endothelial cells. *Exp Cell Res* 2003; 290 (1): 82–92.
64. Schroder O, Schulte KM, Ostermann P, et al. Heat shock protein 70 genotypes HSPA1B and HSPA1L influence cytokine concentrations and interfere with outcome after major injury. *Crit Care Med* 2003; 31 (1): 73–9.
65. Rohde M, Daugaard M, Jensen MH, et al. Members of the heat-shock protein 70 family promote cancer cell growth by distinct mechanisms. *Genes Dev* 2005; 19 (5): 570–82.
66. Colgan SP, Pitman RS, Nagaishi T, et al. Intestinal heat shock protein 110 regulates expression of CD1d on intestinal epithelial cells. *J Clin Invest* 2003; 112 (5): 745–54.
67. Szebeni A, Olson MO. Nucleolar protein B23 has molecular chaperone activities. *Protein Sci* 1999; 8 (4): 905–12.

Expression patterns and action analysis of genes associated with the responses to physical stimuli during rat liver regeneration[☆]

Panfeng Liu¹, Lifeng Zhao¹, Weimin Zhang¹, Xiaoguang Chen¹, Cunshuan Xu^{2,*}

¹Key Laboratory for Cell Differentiation Regulation, Xinxiang, Henan 453007, China; ²College of Life Science, Henan Normal University, Xinxiang, Henan 453007, China

Received October 11, 2006

Abstract

Objective. This project is to study the responses to physical stimuli in regenerating liver at transcriptional level. **Methods.** The genes associated with the responses to physical stimuli were obtained by collecting the data of databases and referring to thesis, and the gene expression changes during LR were checked by the Rat Genome 230 2.0 Array. **Results.** It was found that 120 genes were associated with liver regeneration. The initial and total expressing gene numbers occurring in initiation phase of liver regeneration (0.5–4 hours after PH), G0/G1 transition (4–6 hours after PH), cell proliferation (6–66 hours after PH), cell differentiation and structure-function reconstruction (66–168 hours after PH) were 52, 11, 66, 2 and 52, 37, 115, 78, respectively, illustrating that the associated genes were mainly triggered in the early phase of LR, and worked at different phases. According to their expression similarity, these genes were classified into 5 groups: only up-, predominantly up-, only down-, predominantly down-, up- and down-regulation, involving in 41, 20, 33, 19 and 7 genes, respectively, and the total times of their up- and down-regulation expression were 431 and 296, respectively, demonstrating that the expression of the major genes were increased, and that of the minutes ority decreased. According to time relevance, they were classified into 15 groups, showing that the cellular physiological and biochemical activities were staggered during liver regeneration. According to gene expression patterns, they were classified into 31 types, displaying that the cellular physiological and biochemical activities were diverse and intricate during liver regeneration. **Conclusion.** The responses to physical stimuli including visible light, ultraviolet, X-ray, sonic wave, osmotic pressure and proton gradient are enhanced mainly in the forepart and prophase of liver regeneration, in which 120 genes associated with liver regeneration play important roles. [Life Science Journal. 2007;4(1):52–60] (ISSN: 1097–8135).

Keywords: partial hepatectomy; Rat Genome 230 2.0 Array; responses to physical stimuli; genes; liver regeneration

1 Introduction

When organism is stimulated by various physical factors, such as squeezing, press, sonic wave, radiation, osmotic pressure, potential difference and so on, the cells can transmit these extracellular stimuli into intracellular signal by ligand-receptor binding or special channel in the cell membrane^[1, 2], and trigger the responses to the stimuli in organism and cells^[3, 4]. Usually, these responses contain three phases^[1–9]: perception of stimuli, signal transduction and reaction. In brief, the sonic wave, osmotic pressure and electrochemical proton gradient are converted by mechanosensitive ion channels into electric or chemical signal^[8, 9], then stimulate many of physiological and biochemical changes including cell proliferation, the regeneration of damaged

tissue, gene mutation, cell transformation and so on^[10–12]. And the stimuli, such as visible light, ultraviolet (UV) and X-ray are mainly converted into electric or chemical signal by ligand-receptor binding^[8] or rhodopsin-mediated phototransduction, then regulate the above activities^[13].

Partial hepatectomy (PH)^[14], a violent physical stimuli resulting in tissue injury, can cause the responses to physical stimuli and induce liver regeneration (LR)^[15, 16]. Generally, based on the physiological activities of cell, the regeneration process is classified into 4 phases: the initiation (0.5–4 hours after PH), the transition from G0 to G1 (4–6 hours after PH), the cell proliferation (6–66 hours after PH), the cell differentiation and structure-function reorganization (66–168 hours after PH)^[16]. According to time course, it is divided into 4 phases including forepart (0.5–4 hours after PH), prophase (6–12 hours after PH), metaphase (16–66 hours after PH), and anaphase (66–168 hours after PH)^[17], which are regulated by

[☆]Supported by the National Natural Science Foundation of China (No. 30270673).

*Corresponding author. Tel: 86-373-3326001; Fax: 86-373-3326524; Email:xucs@x263.net

many factors including the physical factors^[18]. Previously, the relationship between the response to chemical stimuli and the LR had been studied^[19]. In order to study the response to physical stimuli during LR at transcriptional level^[20, 21], the expression changes of genes in regenerating liver after PH were detected by Rat Genome 230 2.0 Array^[22] containing 227 physical stimuli-associated genes, and it was identified that 120 genes were associated with LR^[23]. And expression changes, patterns and action of them were primarily analyzed.

2 Materials and Methods

2.1 Regenerating liver preparation

Healthy Sprague-Dawley rats weighing 200–250 g were obtained from the Animal Center of Henan Normal University (Xinxiang, China). The rats were separated into two groups at random and each group included 6 rats (male:female=1:1). PH was performed according to Higgins and Anderson^[14], the left and middle lobes of liver were removed. Rats were killed by cervical vertebra dislocation at 0.5, 1, 2, 4, 6, 8, 12, 24, 36, 54, 66, 72, 120, 144 and 168 hours after PH and the regenerating liver tissues were observed at corresponding time point. The livers were rinsed three times in PBS at 4 °C, then 100–200 mg livers from middle parts of right lobe, and six samples of each group were gathered and mixed together to 1–2 g (0.1–0.2 g × 6) total liver tissue, then stored at –80 °C. The sham-operation (SO) group was the same as PH ones except the liver lobes unremoved. The laws of animal protection of China were enforced strictly.

2.2 RNA isolation and purification

Total RNA was isolated from frozen liver tissue according to the manual of Trizol kit (Invitrogen Corporation, Carlsbad, California, USA)^[24] and then purified base on the guide of RNeasy mini kit (Qiagen, Inc, Valencia, CA, USA)^[25]. Total RNA samples were checked to exhibit a 2:1 ratio of 28S to 18S rRNA intensities by agarose electrophoresis (180 V, 0.5 hour). Total RNA concentration and purity were estimated by optical density measurements at 260/280 nm^[26].

2.3 cDNA, cRNA synthesis and purification

As template, 1–8 µg total RNA was used for cDNA synthesis. cDNA purification was proceeded based on the way established by Affymetrix^[27]. cRNA labeled with biotin was synthesized using cDNA as the template and then purified^[27]. Measurement of cDNA, cRNA concentration and purity were the same as above.

2.4 cRNA fragmentation and microarray detection

15 µl (1 µg/µl) cRNA incubated with 5 × fragmentation buffer was digested into 35–200 bp fragments at 94 °C for 35 minutes. Rat Genome 230 2.0 Array produced by Affymetrix was prehybridized, then

the hybridization buffer was added at 45 °C, 60 rpm for 16 hours. The microarray was washed and stained by GeneChip fluidics station 450 (Affymetrix Inc., Santa Clara, CA, USA). The chips were scanned by GeneChip Scan 3000 (Affymetrix Inc., Santa Clara, CA, USA), and the signal values of gene expression were observed^[22].

2.5 Microarray data analysis

The normalized signal values, signal detections (P, A, M) and experiment/control (R_i) were obtained by quantifying and normalizing the signal values using GCOS (GeneChip operating software) 1.2^[22].

2.6 Normalization of the microarray data

To minimize error from the microarray analysis, each analysis was performed three times. Results with a total ratio were maximal (R^m) and that whose average of three housekeeping genes β-actin, hexokinase and glyceraldehyde-3-phosphate dehydrogenase approached 1.0 (R^h) were taken as a reference. The modified data were generated by applying a correction factor (R^m/R^h) multiplying the ratio of every gene in R^h at each time point. To remove spurious gene expression changes resulting from errors in the microarray analysis, the gene expression profiles at 0–4 hours, 6–12 hours and 12–24 hours after PH were reorganized by normalization analysis program (NAP) software according to the cell cycle progression of the regenerating hepatocytes. Data statistics and cluster analysis were done using GeneMath, GeneSpring, Microsoft Excel software^[22, 28, 29].

2.7 Identification of genes associated with LR

Firstly, the nomenclature of six kinds of physical stimuli mentioned above were adopted from the GENEONTOLOGY database (www.geneontology.org), and input into the databases at NCBI (www.ncbi.nlm.nih.gov) and RGD (rgd.mcw.edu) to identify the rat, mouse and human genes associated with the responses to physical stimuli. According to maps of biological pathways embodied by GENMAPP (www.genmapp.org), KEGG (www.genome.jp/kegg/pathway.html) and BIOCARTA (www.biocarta.com/genes/index.asp), the genes associated with the biological process were collated. The results of this analysis were codified and compared with the results obtained for human and mouse searches in order to identify human and mouse genes which are different from those of rat. Comparing these genes with the analysis output of the Rat Genome 230 2.0 Array, those genes which showed more than twofold change in expression level, observed as meaningful expression changes^[23], were referred to as rat homologous or rat specific genes associated with the responses to physical stimuli under evaluation. Genes, which displayed reproducible results with three independent analysis with the chip and which showed more than twofold change in expression level in at least one time point during LR with significant difference ($0.01 \leq P < 0.05$) or extremely significant difference ($P \leq 0.01$) be-

tween PH and SO, were referred to as associated with LR.

3 Results

3.1 Expression changes of the genes associated with the responses to physical stimuli during LR

According to the data of databases at NCBI, GENMAPP, KEGG, BIOCARTA and RGD, 316 genes were associated with blood coagulation. In which, 226 genes were contained in the Rat Genome 230 2.0 Array. Among them, the expression of 120 genes displayed meaningful changes at least at one time point after PH, showed significant or extremely significant differences in expression when comparing PH with SO, and displayed reproducible results with three detections with Rat Genome 230 2.0 Array, suggesting that the genes were associated with LR. Range of up-regulation

was 2–60 times higher than control, and down-regulation was 2–16 (Table 1). The analysis indicated that 41 genes were up-regulated, 33 genes down-, and 46 genes up/down- during LR. The total up- and down-regulated times were 431 and 296, respectively (Figure 1A). According to the gene expression changes during liver regeneration, at the initiation phase (0.5–4 hours after PH), 33 genes displayed up-regulation, 18 genes down, and 2 genes up/down; at the transition phase from G0 to G1 (4–6 hours after PH), 28 genes up, and 11 genes down; at the cell proliferation phase (6–66 hours after PH), 49 genes up, 39 genes down, and 28 genes up/down; at cell differentiation and structure-function reorganization phase (66–168 hours after PH), 37 genes up, and 31 genes down, and 12 genes up/down (Figure 1B).

Table 1. Expression abundance of 120 response to physical stimuli-associated genes during rat LR

Gene Abbr.	associated to	Fold difference									
Adcyap1r1	1	0.4, 2.3	Kit	1, 2, 3	0.4	Vax2	1, 2, 3	0.3	Pres	4	0.1, 2.2
Bhlhb2	1	4.1	Lum	1, 2, 3	0.1, 10.3	Cd151	1, 2, 3, 4	0.2, 4.3	Ptpn11	4	0.5
Bhlhb3	1	0.1, 2.5	Mapk12	1, 2, 3	0.2, 2.4	Eml2	1, 2, 3, 4	3.7	Rad54l	4	0.3, 2.3
Gng8	1	0.1	Merk	1, 2, 3	0.4	Fech	2	2.2	Rpgr	4	0.1, 2.8
Rho	1	0.2, 2.0	Myc	1, 2, 3	19.7	Fen1	2	0.2, 2.7	Slc19a2	4	0.2, 2.5
Rhob	1	8.1	Myoc	1, 2, 3	0.5	Hmgn1	2	3	Snai2	4	0.1, 3.2
Zcwcc2	1	4.6	Nnmt	1, 2, 3	0.3, 9.4	Msh6	2	2.7	Sox21	4	0.5, 12.1
*Abcc6	1, 2, 3	0.4	Nphp1	1, 2, 3	0.5, 2	Rev1l	2	2.2	Thrb	4	0.2
Adra1b	1, 2, 3	0.4	Oat	1, 2, 3	5.2	Tp53	2, 3	2.9	Timm8a	4	3.3
Aipl1	1, 2, 3	0.1, 2.0	Opn1sw	1, 2, 3	0.4, 5.3	Atp6V1b1	4	4	Timm8b	4	0.4, 2.4
App	1, 2, 3	6.4	Opn4	1, 2, 3	0.2, 2.5	Cdkn2d	4	3.3	Timm9	4	0.3, 2.7
Arr3	1, 2, 3	7	Pax6	1, 2, 3	0.1, 2.1	Chrna9	4	0.1	Tnfrsf11a	4	8.6
Bcl2L1	1, 2, 3	0.4, 2.1	Pdc	1, 2, 3	0.4, 17.1	Cldn14	4	0.3	Tub	4	0.4, 2.1
Cds1	1, 2, 3	0.3	Pde6g	1, 2, 3	0.2	Cntn5	4	0.4, 7.0	Ush2a	4	0.3, 4.9
Chm	1, 2, 3	0.1	Pitpn	1, 2, 3	3.4	Coch	4	0.2, 2.3	Vit	4	0.3
Clns1a	1, 2, 3	4.8	Ppm1d	1, 2, 3	6.8	Col11a1	4	0.3, 3.1	Wfs1	4	0.2
Col18a1	1, 2, 3	3.1	Ppt	1, 2, 3	0.5	Col1a2	4	3	Accn1	4, 5, 6	0.3, 10.1
Crybb1	1, 2, 3	3.2	Prom1	1, 2, 3	0.4	Col2a1	4	0.3, 3.8	Accn3	4, 5, 6	4.0, 5
Crybb3	1, 2, 3	0.2	Rax	1, 2, 3	4.8	Diap1	4	0.4	Ccl7	4, 5, 6	22.6
Crygd	1, 2, 3	8	Rcvrn	1, 2, 3	21.1	Dspp	4	3.4	Dnah1	4, 5, 6	0.1
Cyp1b1	1, 2, 3	3.5	Rgr	1, 2, 3	6.1	Ercc5	4	2.4	Elv1	4, 5, 6	0.3, 3.9
Fbn1	1, 2, 3	2.8	Rp1H	1, 2, 3	0.2, 59.7	Gata3	4	0.4	Gfi1	4, 5, 6	0.2, 2.4
Fyn	1, 2, 3	0.4	Slc24a1	1, 2, 3	0.4, 3.24	Jag2	4	0.2	Itgb2	4, 5, 6	0.5
Gnat1	1, 2, 3	18.5	Slc24a2	1, 2, 3	0.2	Kcne1	4	0.5, 9.8	Mpz	4, 5, 6	8.0, 4
Gngt2	1, 2, 3	2.8	Sord	1, 2, 3	3.3	Kcne1l	4	0.2	Nos3	4, 5, 6	0.3, 2.1
Grk1	1, 2, 3	5.2	Syngap1	1, 2, 3	0.4, 2.1	Mgp	4	2.3	Prx1l	4, 5, 6	0.1, 2.5
Grm8	1, 2, 3	0.4	*Timp3	1, 2, 3	0.5	Mtap1a	4	0.5	Prx	4, 5, 6	2.1
Guca1a	1, 2, 3	0.4, 5	Trpc3	1, 2, 3	0.3, 2.6	Nog	4	0.3, 3.3	Ptk2	4, 5, 6	8.9
Gucy2d	1, 2, 3	0.4, 5.3	Tulp1	1, 2, 3	0.4, 2.9	Phyh	4	2.3	Slc14a2	5	0.4
Impg1	1, 2, 3	0.4, 4.0	Unc119	1, 2, 3	0.3	Pmp22	4	2.2	Trpv1	5, 6	0.3

*Reported genes associated with LR; 1. Response to visible light; 2. Response to UV; 3. Response to X-ray; 4. Response to sonic wave; 5. Response to osmotic pressure; 6. Response to the electrochemical proton gradient.

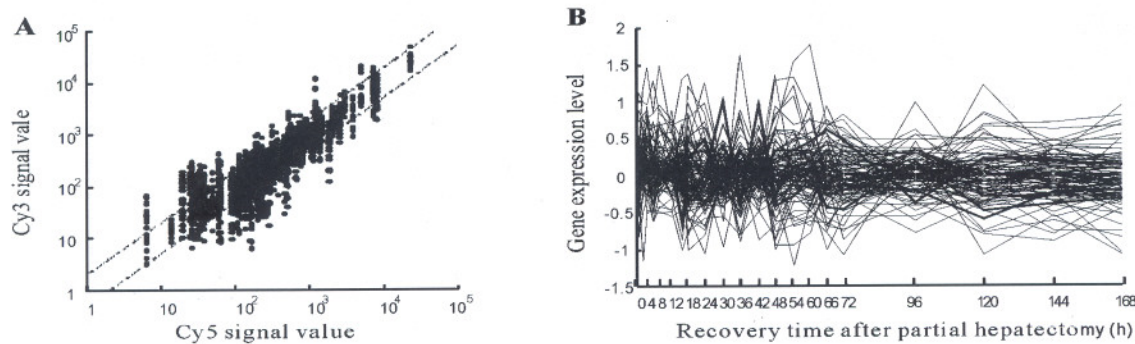


Figure 1. Expression frequency, abundance and changes of 120 physical stimuli-associated genes during rat LR. Detection data of Rat Genome 230 2.0 Array were analyzed and graphed by Microsoft Excel. A. Gene expression frequency. The dots above bias represent the genes up-regulated more than two folds, and total times of up-regulation were 431; those under bias down-regulated more than two folds, and that of down-regulation were 296; and the ones between biases no-sense alterative; B. Gene expression abundance and changes, in which 87 genes were 2.0–60 folds up-regulated, and 79 genes 2–16 folds down-.

3.2 Initiation expression time of the genes associated with the responses to physical stimuli during LR

At each time point of liver regeneration, the numbers of initial up-, down-regulated and total up-, down-regulated genes were in sequence: both 10 and 6 at 0.5 hour; 10, 11 and 17, 14 at 1 hours; 9, 1 and 23, 3 at 2 hours; 4, 1 and 23, 4 at 4 hours; 3, 3 and 16, 9 at 6 hours; 1, 0 and 20, 5 at 8 hours; 2, 1 and 22, 7 at 12 hours; 7, 5 and 18, 11 at 16 hours; 9, 12 and 23, 25 at 18 hours; 3, 3 and 25, 28 at 24 hours; 5, 3 and 16, 12 at 30 hours; 1, 1 and 16, 14 at 36 hours; 2, 2 and 20, 10 at 42 hours; 0, 1 and 24, 22 at 48 hours; 1, 0

and 27, 10 at 54 hours; 1, 0 and 25, 16 at 60 hours; 0, 0 and 26, 15 at 66 hours; 0, 0 and 19, 19 at 72 hours; 1, 0 and 21, 11 at 96 hours; 0, 1 and 15, 20 at 120 hours; 0, 0 and 13, 17 at 144 hours; 0, 0 and 12, 18 at 168 hours (Figure 2). Generally, gene expression changes occurred during the whole liver regeneration, and the up- and down-regulation times were 431 and 296, respectively. The initially up-regulated genes were predominantly expressed in the forepart, and the number of the initially up- and down- genes were similar in the prophase and metaphase, while few genes were initially expressed in the anaphase.

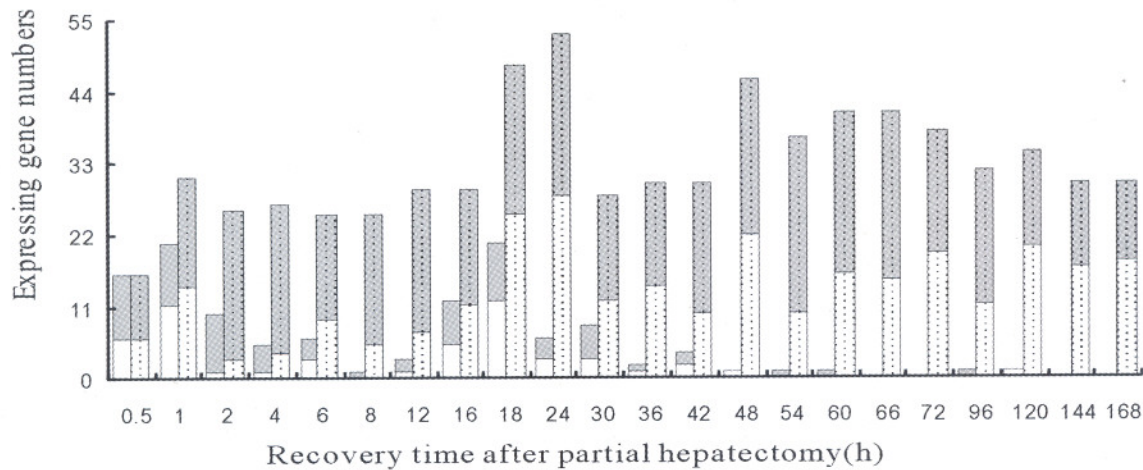


Figure 2. The initial and total expression profiles of 120 physical stimuli-associated genes at each time point of LR. Grey bars: Up-regulated gene; White bars: Down-regulated. Blank bars represent initial expressing genes, in which up-regulation genes are predominant in the forepart, and the up- and down- are similar in the prophase and metaphase, and very few in the anaphase. Dotted bars represent the total expressing genes, in which some genes are up-regulation, and the others down- during LR.

3.3 Expression similarity and time relevance of the genes associated with the responses to physical stimuli during LR

120 genes mentioned above could be characterized

based on their similarity in expression as following: only up-, predominantly up-, only down-, predominantly down-, up/down-regulated, involved in 41, 20, 33, 19 and 7 genes, respectively (Figure 3). According to time

relevance, they were classified into 15 groups, including 0.5 and 1 hour, 2 hours, 4 and 8 hours, 6 hours, 12 hours, 16 hours, 18 hours, 24 and 48 hours, 30 and 42 hours, 36 hours, 54 and 60 hours, 66 and 72 hours, 96 hours, 120 hours, 144 and 168 hours, and the up- and down-regulated times were 37 and 20, 23 and 3, 43 and 9, 16 and 9, 22 and 7, 18 and 11, 23 and 25, 49 and

50, 36 and 22, 16 and 14, 52 and 26, 45 and 34, 21 and 11, 15 and 20, 25 and 35, respectively (Figure 3). The up-regulation expression genes were chiefly associated with the responses to visible light and sonic wave, and the down- mostly with conduction of the physical stimuli.

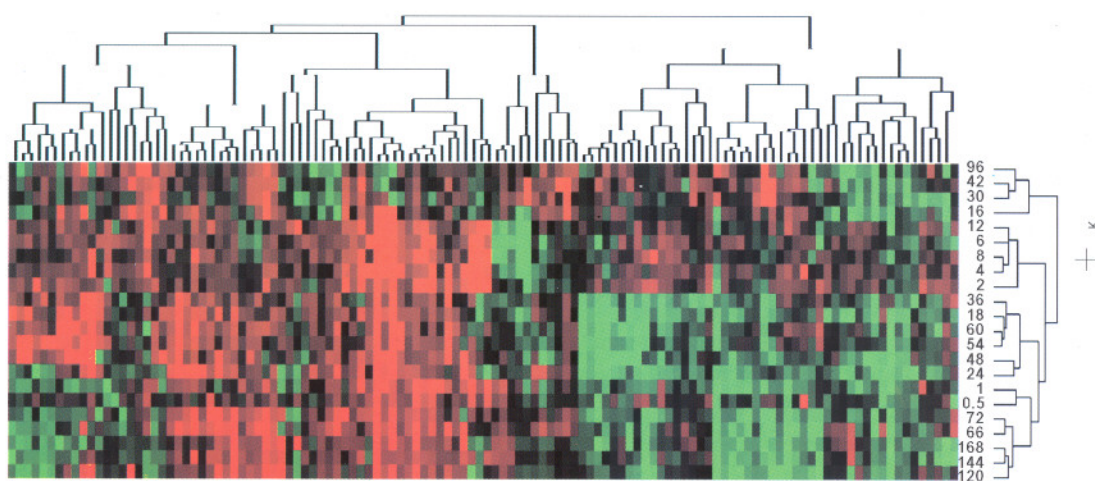


Figure 3. Expression similarity and time relevance clusters of 120 physical stimuli-associated genes during LR. Detection data of Rat Genome 230 2.0 Array were analyzed by H-clustering. Red represents up-regulation genes chiefly associated with promoting blood coagulation; Green represents down-regulation ones mainly associated with inhibiting blood coagulation; Black: No-sense in expression change. The upper and right trees respectively show function and time series clusters, by which the above genes were classified into 5 and 15 groups separately.

3.4 Expression patterns of the genes associated with the responses to physical stimuli during LR

120 genes mentioned above were categorized into 31 patterns, according to the changes in their expression. (1) up-regulation at one time point, i.e. 1, 12, 24, 30, 42, 60, 96 hours after PH (Figure 4A), 8 genes involved; (2) up at two time points, i.e. 0.5 and 4 hours (Figure 4B), 1 gene involved; (3) up at three time points (Figure 4B), 2 genes involved; (4) up at multiple time points (Figure 4B), 1 gene involved; (5) up at one phase, i.e. 0.5–12 hours or 6–12 hours (Figure 4C), 2 genes involved; (6) up at two phases, i.e. 30–42 and 60–96 hours (Figure 4C), 1 gene involved; (7) up at multiple time phases (Figure 4C), 1 gene involved; (8) up at one time point/phase, i.e. 24 and 66–72 hours, 66 and 18–24 hours, 18 and 48–60 hours (Figure 4D), 3 genes involved; (9) up at one time point/two phases (Figure 4D), 4 genes involved; (10) up at one time point/three phases (Figure 4E), 5 genes involved; (11) up at one time point/multiple phases (Figure 4E), 1 gene involved; (12) up at two time points/one phase (Figure 4F), 3 genes involved; (13) up at two time points/phases (Figure 4F), 1 gene

involved; (14) up at three time points/one phase (Figure 4F), 1 gene involved; (15) up at three time points/two phases (Figure 4G), 3 genes involved; (16) up at multiple time points/phases (Figure 4G), 4 genes involved; (17) down at one time point, i.e. 6, 16, 18, 30, 36, 42, 48 hours (Figure 4H1-H2), 10 genes involved; (18) down at two time points, i.e. 24 and 36 hours (Figure 4I), 1 gene involved; (19) down at three time points (Figure 4I), 2 genes involved; (20) down at multiple time points (Figure 4I), 2 genes involved; (21) down at one phase, i.e. 4–18 hours, 6–12 hours, 18–24 hours, 24–30 hours (Figure 4J), 4 gene involved; (22) down at two phases, i.e. 16–48 and 60–120 hours, 18–24 and 48–60 hours (Figure 4J), 2 genes involved; (23) down at one time point/phase, i.e. 48 and 18–24 hours (Figure 4K), 2 genes involved; (24) down at one time point/two phases (Figure 4K), 3 genes involved; (25) down at two time points/one phase (Figure 4L), 3 genes involved; (26) down at two time points/phases (Figure 4L), 2 genes involved; (27) down at three time points/one phase (Figure 4L), 1 gene involved; (28) down at three time points/two phases (Figure 4L), 1 gene involved; (29)

predominantly up (Figure 4M1 – 4M3), 20 genes involved; (30) predominantly down (Figure 4N1 –

4N3), 19 genes involved; (31) similarly up/down (Figure 4O), 7 genes involved.

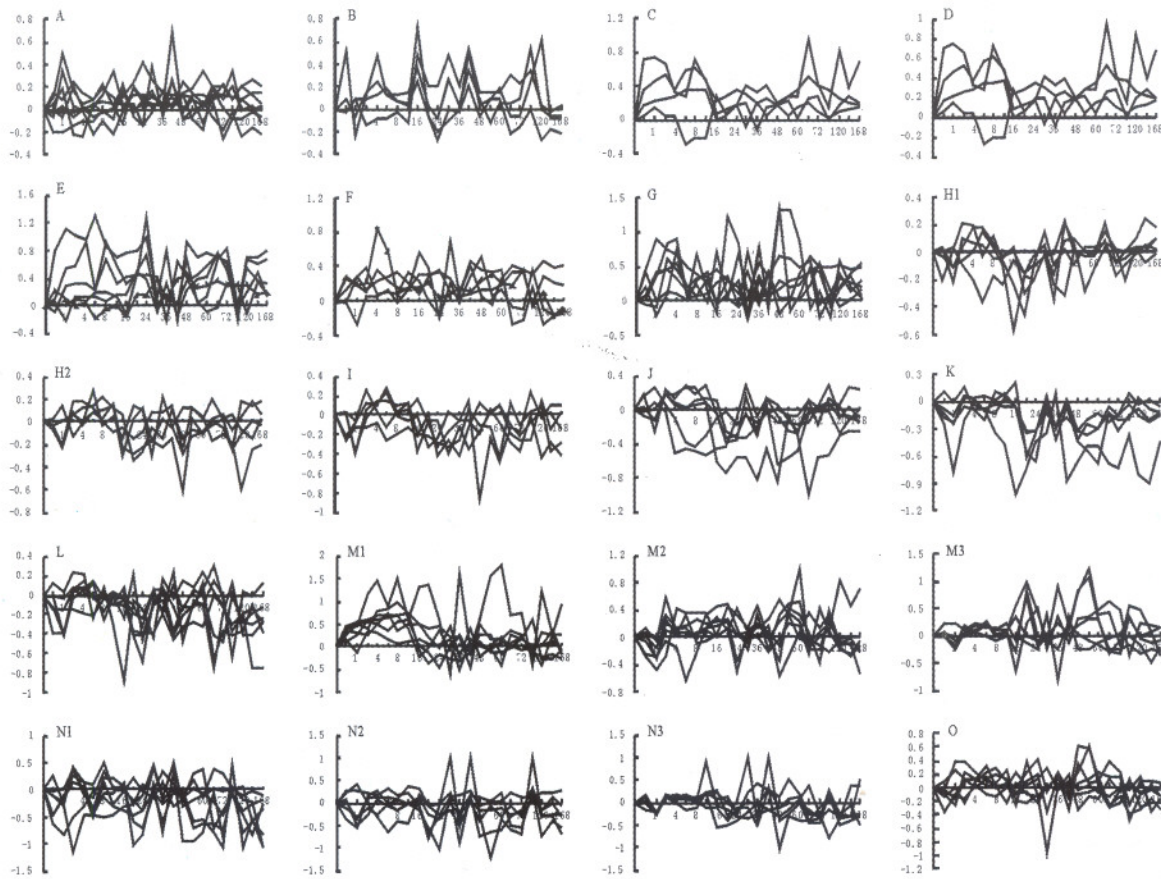


Figure 4. Thirty-one expression patterns of 120 physical stimuli-associated genes during LR. Expression patterns were obtained by the analysis of detection data of Rat Genome 230 2.0 Array with Microsoft Excel. A – G. 27 up-regulated genes; H – L. 22 down-regulated genes; M – O. 21 up/down-regulated genes. X-axis represents recovery time after PH; Y-axis shows logarithm ratio of the signal values of genes at each time point to control.

4 Discussion

Organisms can respond to all kinds of environmental stimuli including physical stimuli in instinct, which is closely linked with organisms' survival^[19]. The proteins associated with the response to visible light are stated as follows. Nine proteins including guanine nucleotide binding protein (G protein) γ transducing activity polypeptide 2 (GNGT2) are associated with visual signal transduction by G-protein coupled receptor protein signaling pathway^[30]. Eight proteins including retinitis pigmentosa 1 homolog (RP1H) accelerate the rhodopsin-mediated phototransduction by conducting signal cascade^[31]. Six proteins including myelocytomatosis viral oncogene homolog (MYC) have an anti-radiation effect by accelerating the cell's stress response to radiation^[32]. Twelve proteins including ornithine

aminotransferase (OAT) promote the signal conduction of retinitis and maintain normal visual perception, and the mutation of the corresponding genes can cause retinitis pigmentosa and other eye diseases^[33]. Opsin 1 short-wave-sensitive (OPN1SW), an component of rhodopsin, is involved in transduction of the visual signal^[34]. Solute carrier family 24 member 1 (SLC24A1) can transmit the visual signal by transporting sodium, kalium, calcium ion^[35]. Guanylate cyclase activator 1a (GUCA1A) relates to the rods-mediated conduction of the visual signal^[36]. Rhodopsin (RHO) is response for perception of light stimuli^[37]. Basic helix-loop-helix domain containing class B2 (BHLHB2) adjusts photoperiod by light perception^[38]. Crystallin γ D (CRYGD) is related to the formation of lens^[39]. Transient receptor potential cation channel subfamily C member 3 (TRPC3) can convert light stimuli into electric sig-

nal^[40]. Arrestin 3 retinal (ARR3) may bind to phosphorylated receptors to deactivate the phototransduction cascade^[41]. ATP-binding cassette sub-family C member 6 (ABCC6), coupling with ATPase, accelerates the conduction of the visual signal^[42]. Tissue inhibitor of metalloproteinase 3 (TIMP3) may play a role in light signal-transduction by receptor tyrosine protein kinase-mediated signal transduction pathway^[43]. The meaningful expression profiles of genes mentioned above are same or similar at some points while different at others, indicating that they may co-regulate the responses to physical stimuli. Among them, *abcc6* was down-regulated 2.3 times at 6 hours during LR, which is generally consistent with Dransfelds' result^[20]. *tmp3* was down-regulated 2.1 times at 18–24 hours, which wasn't consistent with Dransfelds', and it needed to be further analyzed by Northern blotting^[20]. *gnat1* was up-regulated at 1–4, 8–24, 48–72 and 144 hours, and reached a peak at 24 hours that is 18.5 times higher than the control. *rpl1h* was up at 0.5–24, 36, 48–72, 120 and 168 hours, having a peak at 60 hours that is 59.7 times higher than the control. *crygd* was up at 1–4, 18, 36–66, 120 and 168 hours, and reached a peak at 4 hours that is 8 fold of control. It is presumed that they play a key role in the response to visual light during LR.

The proteins associated with the responses to UV and X-ray are stated as follows. Five proteins including ferrochelatase (FECH), which can prevent and repair DNA damage caused by UV, may take a role in antiradiation^[44]. Tumor protein p53 (TP53) prevents the DNA damage resulting from UV and X-ray irradiation by base-excision repair^[45]. The meaningful expression profiles of genes mentioned above are same or similar at some points while different at others, indicating that they may co-regulate the responses to UV and X-ray. Among them, the highest expression abundance of *fech* at 1 hour after PH was 2.7 folds of control. *tp53* was up-regulated at 18–24, 48–60 and 96 hours, and reached a peak at 24 hours that was 2.9 times higher than the control. It is presumed that they are of importance in the response to visual light stimuli during liver regeneration.

The proteins associated with the response to sonic wave are stated as following. Seven proteins including neuronal amiloride-sensitive cation channel 1 (ACCN1), serving as ion channel, transmit the signal of sound, light and other stimuli^[46]. Five proteins including noggin (NOG) can perceive sonic wave, and their mutation can cause hearing loss etc^[47]. Three proteins including procollagen type XI α 1 (COL11A1) are the components of system of sound transduction^[49]. Translocase of inner mitochondrial membrane 8 homolog a (TIMM8A) en-

codes a small protein known as deafness/dystonia peptide involved in perception of sound stimulus^[50]. Tumor necrosis factor receptor superfamily member 11a (TNFRSF11A) promotes the transduction of sound stimulus^[51]. Ets variant gene 1 (ETV1) is involved in the response to mechanical stimulus^[52]. The meaningful expression profiles of genes mentioned above are same or similar at some points while different at others, indicating that they may co-regulate the response to sonic wave. Among them, *accn1* was up-regulated at 30 and 42 hours after PH, having the highest abundance of 10.1 folds at 30 hours. *tnfrsf11a* was up at multiple phases, reaching a peak at 8 hours that is 8.2 times higher than the control. *etv1* was up at 0.5–12 and 144 hours, and reached a peak at 12 hours that is 4-fold of control. It is supposed that they play crucial roles in the response to visual light stimuli during liver regeneration.

The proteins associated with the responses to osmotic pressure and electrochemical proton gradient are stated as follows. Solute carrier family 14 member 2 (SLC14A2) regulates the osmotic pressure of cell by transporting urea^[53]. *slc14a2* was down-regulated at the metaphase during liver regeneration. Transient receptor potential cation channel subfamily V member 1 (TRPV1), a cation channel, participates in the stress responses to osmotic pressure and the electrochemical proton gradient^[54], and it was down only at one time point (120 hours after PH) after PH. It is speculated that the capacity of anti-osmotic pressure and the response to electrochemical proton gradient decrease in the anaphase of liver regeneration.

In conclusion, based on the experimental methods of longer time and multiple time points being adopted, the expression changes of the genes associated with the response to six kinds of physical stimuli during liver regeneration were investigated by high-throughput gene expression analysis. It was primarily proved that the regenerating liver response to physical stimuli was different in different phase; that Rat Genome 230 2.0 Array was a useful tool analyzing the above responses at transcriptional level. Whereas these processes DNA → mRNA → protein were influenced by many factors including proteins interaction. Therefore, the above results need to be further analyzed by the techniques, such as Northern blotting, protein chip, RNA interference, protein-interaction etc.

References

- Castanho MA, Fernandes MX. Lipid membrane-induced optimization for ligand-receptor docking: recent tools and insights for the "membrane catalysis" model. Eur Biophys J 2006; 35 (2): 92–103.
- Sukharev S, Corey DP. Mechanosensitive channels: multiplicity of families and gating paradigms. Sci STKE 2004; 2004

- (219): re 4.
3. Martinac B. Mechanosensitive ion channels: molecules of mechanotransduction. *J Cell Sci* 2004; 117 (Pt 12): 2449–60.
 4. Blount P. Molecular mechanisms of mechanosensation: big lessons from small cells. *Neuron* 2003; 37 (5): 731–4.
 5. Garcia-Anoveros J, Corey DP. The molecules of mechanosensation. *Annu Rev Neurosci* 1997; 20: 567–94.
 6. Zou Y, Hu Y, Metzler B, et al. Signal transduction in arteriosclerosis: mechanical stress-activated MAP kinases in vascular smooth muscle cells (review). *Int J Mol Med* 1998; 1 (5): 827–34.
 7. Karin M. Signal transduction from the cell surface to the nucleus through the phosphorylation of transcription factors. *Curr Opin Cell Biol* 1994; 6 (3): 415–24.
 8. Kung C. A possible unifying principle for mechanosensation. *Nature* 2005; 436 (7051): 647–54.
 9. O’Neil RG, Heller S. The mechanosensitive nature of TRPV channels. *Pflugers Arch* 2005; 451 (1): 193–203.
 10. Hiragami F, Kano Y. Formation of hydroxyapatite-mediated three-dimensional structures by mouse fibroblasts in response to physical stimulation. *Tissue Eng* 2003; 9 (2): 357–64.
 11. Halliday GM. Inflammation, gene mutation and photoimmunosuppression in response to UVR-induced oxidative damage contributes to photocarcinogenesis. *Mutat Res* 2005; 571 (1–2): 107–20.
 12. Rugo RE, Secretan MB, Schiestl RH. X radiation causes a persistent induction of reactive oxygen species and a delayed reinduction of TP53 in normal human diploid fibroblasts. *Radiat Res* 2002; 158 (2): 210–9.
 13. Brainard GC, Rollag MD, Hanifin JP. Photic regulation of melatonin in humans: ocular and neural signal transduction. *J Biol Rhythms* 1997; 12 (6): 537–46.
 14. Higgins GM, Anderson RM. Experimental pathology of the liver: restoration of the liver of the white rat following partial surgical removal. *Arch Pathol* 1931; 12: 186–202.
 15. Fausto N, Campbell JS, Riehle KJ. Liver regeneration. *Hepatology* 2006; 43 (2): S45–S53.
 16. Michalopoulos GK, DeFrances M. Liver regeneration. *Adv Biochem Eng Biotechnol* 2005; 93: 101–34.
 17. Taub R. Liver regeneration: from myth to mechanism. *Nat Rev Mol Cell Biol* 2004; 5 (10): 836–47.
 18. Sato Y, Tsukada K, Hatakeyama K. Role of shear stress and immune responses in liver regeneration after a partial hepatectomy. *Surg Today* 1999; 29 (1): 1–9.
 19. Qin SW, Zhao LF, Chen XG, et al. Expression patterns and action analysis of the genes associated with the responses to chemical stimuli during rat liver regeneration (III): To chemokines, nutrients, inorganic and organic substances. *World J Gastroenterol* 2006; 12(45): 7285–91.
 20. Dransfeld O, Gehrmann T, Kohrer K, et al. Oligonucleotide microarray analysis of differential transporter regulation in the regenerating rat liver. *Liver International* 2005; 25 (6): 1243–58.
 21. Xu CS, Chang CF, Yuan JY, et al. Expressed genes in regenerating rat liver after partial hepatectomy. *World J Gastroenterol* 2005; 11 (19): 2932–40.
 22. Hood L. Leroy Hood expounds the principles, practice and future of systems biology. *Drug Discov Today* 2003; 8 (10): 436–8.
 23. Yue H, Eastman PS, Wang BB, et al. An evaluation of the performance of cDNA microarrays for detecting changes in global mRNA expression. *Nucleic Acids Res* 2001; 29 (8): E41.
 24. Knupp JH, Geahr MA, Forman MS, et al. Comparison of automated and manual nucleic acid extraction methods for detection of enterovirus RNA. *J Clin Microbiol* 2003; 41 (8): 3532–6.
 25. Kuyls S, Van Mellaert L, Lambin P, et al. Efficient isolation of total RNA from Clostridium without DNA contamination. *J Microbiol Methods* 2001; 44 (3): 235–8.
 26. Arkin A, Ross J, McAdams HH. Stochastic kinetic analysis of developmental pathway bifurcation in phage lambda-infected *Escherichia coli* cells. *Genetics* 1998; 149 (4): 1633–48.
 27. Li L, Roden J, Shapiro BE, et al. Reproducibility, fidelity, and discriminant validity of mRNA amplification for microarray analysis from primary hematopoietic cells. *J Mol Diagn* 2005; 7 (1): 48–56.
 28. Eisen MB, Spellman PT, Brown PO, et al. Cluster analysis and display of genome-wide expression patterns. *Proc Natl Acad Sci* 1998; 95 (25): 14863–8.
 29. Werner T. Cluster analysis and promoter modelling as bioinformatics tools for the identification of target genes from expression array data. *Pharmacogenomics* 2001; 2 (1): 25–36.
 30. Ong OC, Hu K, Rong H, et al. Gene structure and chromosome localization of the G gamma c subunit of human cone G-protein (GNGT2). *Genomics* 1997; 44 (1): 101–9.
 31. Zimmermann K, Ritter E, Bartl FJ, et al. Interaction with transducin depletes metarhodopsin III: a regulated retinal storage in visual signal transduction. *J Biol Chem* 2004; 279 (46): 48112–9.
 32. Maclean KH, Keller UB, Rodriguez-Galindo C, et al. c-Myc augments gamma irradiation-induced apoptosis by suppressing Bcl-XL. *Mol Cell Biol* 2003; 23 (20): 7256–70.
 33. Inana G, Chambers C, Hotta Y, et al. Point mutation affecting processing of the ornithine aminotransferase precursor protein in gyrate atrophy. *J Biol Chem* 1989; 264 (29): 17432–6.
 34. Vihtelic TS, Doro CJ, Hyde DR. Cloning and characterization of six zebrafish photoreceptor opsin cDNAs and immunolocalization of their corresponding proteins. *Vis Neurosci* 1999; 16 (3): 571–85.
 35. Sharon D, Yamamoto H, McGee TL, et al. Mutated alleles of the rod and cone Na-Ca-K-exchanger genes in patients with retinal diseases. *Invest Ophthalmol Vis Sci* 2002; 43 (6): 1971–9.
 36. Makino CL, Dodd RL, Chen J, et al. Recoverin regulates light-dependent phosphodiesterase activity in retinal rods. *J Gen Physiol* 2004; 123 (6): 729–41.
 37. Terada N, Ohno N, Ohguro H, et al. Immunohistochemical detection of phosphorylated rhodopsin in light-exposed retina of living mouse with in vivo cryotechnique. *J Histochem Cytochem* 2006; 54 (4): 479–86.
 38. Honma S, Kawamoto T, Takagi Y, et al. Dec1 and Dec2 are regulators of the mammalian molecular clock. *Nature* 2002; 419 (6909): 841–4.
 39. Shentu X, Yao K, Xu W, et al. Special fasciculiform cataract caused by a mutation in the gamma D-crystallin gene. *Mol Vis* 2004; 10: 233–9.
 40. Xu XZ, Li HS, Guggino WB, et al. Coassembly of TRP and TRPL produces a distinct store-operated conductance. *Cell* 1997; 89 (7): 1155–64.
 41. Craft CM, Whitmore DH, Wiechmann AF. Cone arrestin identified by targeting expression of a functional family. *J Biol Chem* 1994; 269 (6): 4613–9.
 42. Gorgels TG, Hu X, Scheffer GL, et al. Disruption of Abcc6

- in the mouse: novel insight in the pathogenesis of pseudoxanthoma elasticum. *Hum Mol Genet* 2005; 14 (13): 1763–73.
43. Beckers J, Herrmann F, Rieger S, *et al.* Identification and validation of novel ERBB2 (HER2, NEU) targets including genes involved in angiogenesis. *Int J Cancer* 2005; 114 (4): 590–7.
44. Magness ST, Maeda N, Brenner DA. An exon 10 deletion in the mouse ferrochelatase gene has a dominant-negative effect and causes mild protoporphiria. *Blood* 2002; 100 (4): 1470–7.
45. Shibue T, Takeda K, Oda E, *et al.* Integral role of Noxa in p53-mediated apoptotic response. *Genes Dev* 2003; 17 (18): 2233–8.
46. Peng BG, Ahmad S, Chen S, *et al.* Acid-sensing ion channel 2 contributes a major component to acid-evoked excitatory responses in spiral ganglion neurons and plays a role in noise susceptibility of mice. *J Neurosci* 2004; 24 (45): 10167–75.
47. Xiao S, Yu C, Chou X, *et al.* Dentinogenesis imperfecta 1 with or without progressive hearing loss is associated with distinct mutations in DSPP. *Nat Genet* 2001; 27 (2): 201–4.
48. Bachiller D, Klingensmith J, Kemp C, *et al.* The organizer factors Chordin and Noggin are required for mouse forebrain development. *Nature* 2000; 403 (6770): 658–61.
49. Richards AJ, Yates JR, Williams R, *et al.* A family with Stickler syndrome type 2 has a mutation in the COL11A1 gene resulting in the substitution of glycine 97 by valine in alpha 1 (XI) collagen. *Hum Mol Genet* 1996; 5 (9): 1339–43.
50. Jin H, Kendall E, Freeman TC, *et al.* The human family of Deafness/Dystonia peptide (DDP) related mitochondrial import proteins. *Genomics* 1999; 61 (3): 259–67.
51. Anderson DM, Maraskovsky E, Billingsley WL, *et al.* A homologue of the TNF receptor and its ligand enhance T-cell growth and dendritic-cell function. *Nature* 1997; 390 (6656): 175–9.
52. Arber S, Ladle DR, Lin JH, *et al.* ETS gene Er81 controls the formation of functional connections between group Ia sensory afferents and motor neurons. *Cell* 2000; 101 (5): 485–98.
53. Nakayama Y, Naruse M, Karakashian A, *et al.* Cloning of the rat Slc14a2 gene and genomic organization of the UT-A urea transporter. *Biochim Biophys Acta* 2001; 1518 (1–2): 19–26.
54. Caterina MJ, Leffler A, Malmberg AB, *et al.* Impaired nociception and pain sensation in mice lacking the capsaicin receptor. *Science* 2000; 288 (5464): 306–13.

Expression patterns and action analysis of genes associated with the responses to fear, wound and pain during rat liver regeneration[☆]

Hongpeng Han¹, Cuifang Chang¹, Gaiping Wang¹, Lijuan Su², Panfeng Liu², Xiaoguang Chen², Cunshuan Xu^{1,*}

¹College of Life Science, Henan Normal University, Xinxiang, Henan 453007, China; ²Key Laboratory for Cell Differentiation Regulation, Xinxiang, Henan 453007, China

Received October 11, 2006

Abstract

Objective. The aim of this investigation was to study the responses to fear, wound and pain after partial hepatectomy (PH) at transcriptional level. **Methods.** The genes associated with the responses to fear, wound and pain were obtained by collecting the data of databases and referring to thesis. Their expression changes during liver regeneration (LR) were checked by Rat Genome 230 2.0 Array. **Results.** It was found that the mRNA level of 22, 117 and 14 genes involved in the responses to fear, wound and pain respectively were significantly changed during LR. The initial and total expressed gene numbers at the four phases of LR, i.e. the initiation (0.5–4 hours after PH), the transition from G0 to G1 (4–6 hours after PH), the cell proliferation (6–66 hours after PH), the cell differentiation and structure-function reorganization (66–168 hours after PH) were 70, 15, 65, 6 and 70, 51, 133, 99, respectively, demonstrating the associated genes were mainly triggered at the early phase, and worked at different phases. Based on their expression similarity, the genes were classified into 5 groups: only up-, predominantly up-, only down-, predominantly down-, up- and down-regulation, involving in 55, 19, 44, 18 and 5 genes, respectively, and the total times of their up- and down-regulation expression were 600 and 343 respectively, demonstrating that the expression of most genes was increased, whereas the few was declined. Time relevance and expression patterns of the genes were respectively sorted into 13 and 25 groups, displaying that the cellular physiological and biochemical activities were staggered, diverse and complex during LR. **Conclusion.** The responses to fear and pain were increased mainly in the early phase and prophase during LR, and wound in the early phase, prophase and later phase, and 141 genes associated with LR play an important role in these responses. [Life Science Journal. 2007;4(1):61–70] (ISSN: 1097–8135).

Keywords: partial hepatectomy; Rat Genome 230 2.0 Array; responses to fear, wound and pain; genes; liver regeneration

1 Introduction

When prokaryote and eukaryote undergo distinct stimuli such as heat^[1,2], cold^[3], change of osmotic pressure^[4], water deprivation^[5], drug^[6], toxicant^[7], oxidation^[8], unfolded protein^[9], pathogen infection^[10, 11], fear^[12], wound^[13], pain^[14], hypoxia^[15], ischemia^[16], nutritional deficiency^[17], hormonoprivileged^[18], starvation^[19] and so on, the relevant stress protein (SP) genes are activated to protect organisms against these harmful stimuli. Highly conservative SPs in structure and function (e.g. heat shock protein 70 family) can be nearly induced by all stimuli although other SPs generated by different stress responses are diverse.

Moreover, phenomenon that the stress response activated by one stimulus can increase cellular tolerance to another stimulus implies functional cross of SPs induced by different stimuli^[20].

Rat liver has strong capacity for regeneration^[21, 22]. The remnant hepatocytes compensate the lost liver tissue by proliferating after partial hepatectomy (PH)^[23], which is called liver regeneration (LR)^[24]. According to the cellular physiological activities, the regeneration process is usually categorized into four stages: initiation phase (0.5–4 hours after PH), transition from G0 to G1 (4–6 hours after PH), cell proliferation (6–66 hours after PH), cell differentiation and reorganization of the structure-function (66–168 hours after PH)^[24]. According to time course, it is classified into four phases including forepart (0.5–4 hours after PH), prophase (6–12 hours after PH), metaphase (16–66 hours after PH), and anaphase (72–168 hours after PH)^[22]. In addition, as a harmful stimulus, PH can in-

[☆]Supported by the National Natural Science Foundation of China (No. 30270673).

*Corresponding author. Tel: 86-373-3326001; Fax: 86-373-3326524; Email: xucs@x263.net

duce the responses to fear, wound and pain that involve more than 300 genes. Moreover, there exist gene-gene interactions. It is almost impossible to clarify the action of genes associated with the responses to fear, wound and pain during LR at transcriptional level unless high-throughput gene expression arrays are used^[24-26]. So, we used the Rat Genome 230 2.0 Array containing 38 genes involved in fear response, 217 genes in wound and 26 genes in pain to detect the gene expression changes after PH. 141 genes were found to be associated with LR. Meanwhile, their expression character, patterns and actions in regenerating liver were further analyzed.

2 Materials and Methods

2.1 Regenerating liver preparation

Healthy Sprague-Dawley rats weighing 200–250 g were obtained from the Animal Center of Henan Normal University. The rats were separated into two groups at random and each group included 6 rats (male: female=1:1). Partial hepatectomy (PH) was performed according to Higgins and Anderson^[21], the left and middle lobes of liver were removed. Rats were killed by cervical vertebra dislocation at 0.5, 1, 2, 4, 6, 8, 12, 24, 36, 54, 66, 72, 120, 144 and 168 hours after PH and the regenerating livers were observed at corresponding time point. The livers were rinsed three times in PBS at 4 °C. Then 100–200 mg of liver tissues from the middle regions of the right lobe (0.1–0.2 g × 6 samples, per group) were gathered and stored at –80 °C. The sham-operation (SO) group was the same as PH ones except the liver lobes unremoved. The laws of animal protection of China were enforced strictly.

2.2 RNA isolation and purification

Total RNA was isolated from frozen livers according to the manual of Trizol kit (Invitrogen Corporation, Carlsbad, California, USA)^[30] and then purified base on the guide of RNeasy mini kit (Qiagen, Inc, Valencia, CA, USA)^[31]. Total RNA samples were checked to exhibit a 2:1 ratio of 28S rRNA to 18S rRNA intensities by agarose electrophoresis (180 V, 0.5 hour). Total RNA concentration and purity were estimated by optical density measurements at 260/280 nm^[32].

2.3 cDNA, cRNA synthesis and purification

As template, 1–8 µg total RNA was used for cDNA synthesis. cDNA purification was proceeded based on the way established by Affymetrix^[27]. cRNA labeled with biotin was synthesized using cDNA as the template, and cDNA and cRNA were purified followed by the GeneChip analysis purification procedure^[27]. Measurement of cDNA, cRNA concentration and purity were the same as above.

2.4 cRNA fragmentation and microarray detection

15 µl (1 µg/µl) cRNA incubated with 5 × fragmentation buffer was digested into 35–200 bp frag-

ments at 94 °C for 35 minutes. Rat Genome 230 2.0 microarray produced by Affymetrix was prehybridized, then the hybridization buffer was added at 45 °C, 60 rpm for 16 hours. The microarray was washed and stained by GeneChip fluidics station 450 (Affymetrix Inc., USA). The chips were scanned by GeneChip Scan 3000 (Affymetrix Inc., USA), and the signal values of gene expression were observed^[28].

2.5 Microarray data analysis

The normalized signal values, signal detections (P, A, M) and experiment/control (R_i) were obtained by quantifying and normalizing the signal values using GCOS (GeneChip operating software) 1.2^[28].

2.6 Normalization of the microarray data

To minimize error, each sample at each time point during LR was analyzed three times by Rat Genome 230 2.0 microarray. Results with a total ratio were maximal (R^m) and the average of three housekeeping genes (β-actin, hexokinase and glyceraldehyde-3-phosphate dehydrogenase) approached 1.0 (R^h) was taken as a reference. The modified data were generated by applying a correction factor (R^m/R^h) multiplying the ratio of every gene in R^h at each time point. To remove spurious gene expression changes resulting from errors in the microarray analysis, the gene expression profiles at 0–4 hours, 6–12 hours and 12–24 hours after PH were reorganized by normalization analysis program (NAP) software according to the cell cycle progression of the regenerating hepatocytes. Data statistics and cluster analysis were done using GeneMath, GeneSpring, Microsoft Excel software^[28, 33, 34].

2.7 Identification of genes associated with LR

Firstly, the nomenclature of the above three physiological responses obtained from the GENEONTOLOGY database (www.geneontology.org) was input into the databases at NCBI (www.ncbi.nlm.nih.gov) and RGD (rgd.mcw.edu) to identify the rat, mouse and human genes associated with the physiological responses. And the genes associated with the above responses were collated according to maps of biological pathways embodied by GENMAPP (www.genmapp.org), KEGG (www.genome.jp/keg/pathway.html#amino) and BIOCARTA (www.biocarta.com/genes/index.asp). Secondly, the results of these analysis were codified, and then compared with the results from mouse and human searches to identify human and mouse genes which are different from those of rat. These genes (human and mouse genes differed from those of rat) were compared with the analysis output of the Rat Genome 230 2.0 Array. Those genes which showed more than twofold changes in expression level, observed as meaningful expression changes^[35], were referred to as rat homologous or rat specific genes associated with the responses to fear, wound and pain under evaluation. Genes, which displayed reproducible results with three independent analysis with the chip and which showed

more than twofold change in expression level in at least one time point during LR with significant difference ($0.01 \leq P < 0.05$) or extremely significant difference ($P \leq 0.01$) between PH and SO, were referred to as associated with LR.

3 Results

3.1 Expression changes of the genes associated with the responses to fear, wound and pain during LR

According to the NCBI, GENMAPP, KEGG, BIOMARTA and RGD databases, the responses to fear, wound and pain involved in 40, 251 and 26 genes respectively, with separately 38, 217 and 26 genes contained in Rat Genome 230 2.0 Array. Among them, 22, 117 and 14 genes displayed meaningful changes in expression at least at one time point after PH, showed significant or extremely significant differences in expression when PH was compared with SO, and were repeatable in three Rat Genome 230 2.0 Array. The results

suggested that the genes were associated with LR. Abundance change in up-regulation ranged from 2 to 128 folds of control, and down-regulation from 2 to 10 (Table 1). The analysis indicated that 55 genes were up-regulated, 44 genes down-, 42 genes up/down- during LR. Total up- and down-regulated frequencies were 600 and 343, respectively (Figure 1A). At the initiation stage of LR (0.5–4 hours after PH), 42 genes displayed up-regulation, 26 genes down-regulation, 2 genes up/down- regulation; at the transition phase from G0 to G1 (4–6 hours after PH), 36 genes revealed up-regulation, 14 genes down- regulation, 1 gene up/down-regulation; at cell proliferation phase (6–66 hours after PH), 60 genes showed up-regulation, 43 genes down-regulation, 30 genes up/down-regulation; at cell differentiation and reorganization of the structure-function stage (66–168 hours after PH), 52 genes were up-regulated, 33 genes down-regulated, 14 genes up/down-regulated (Figure 1B).

Table 1. Expression abundance of 141 genes associated with the responses to fear, wound and pain during rat LR

Gene Abbr.	Accosiated to others difference	Fold	Gene Abbr.	Accosiated to others difference	Fold	Gene Abbr.	Accosiated to others difference	Fold	Gene Abbr.	Accosiated to others difference	Fold
1 Fear											
Alo2		0.5	*Ccl2		128.0	Irf1		0.3	Scn3a		0.5, 2.8
Bdnf	3	0.4, 2.6	*Ccl20		8.0	Itgb3		0.2	Scube1		3.2
Camkk2		0.5, 7.6	Ccl4		0.2, 3.0	Kirc2		0.4, 2.3	Sele		12.9
Cnr1		0.1	Ccr1		0.4, 27.9	*Kng1		2.1	Serpina5		0.1, 7.8
Creb1	3	0.5	*Cd36		0.1	Ltb4r		0.5, 8.7	*Serpind1		0.1
Drd2	3	8.6	Cd3d		0.4, 4.0	*Lyz		0.4, 3.7	Serpine1		16.7
*Egr1	2, 3	18.6	Ckif1		8.3	Mbp		0.4	Sod2		5.6
Fmr1		0.4, 2.5	Coch		0.2, 2.3	Mcpt6		0.2	*Spn		0.2, 4.0
*Fos	3	28.4	Copeb		10.6	Mif		3.2	Tac1	3	0.2
Gap43	2	0.3	*Cramp		0.4, 2.8	Msn		5.0	Tap1		2.2
Grik2		0.4, 2.4	Crcp		0.3	Mug1		0.1, 3.5	*Tcrb		0.2
Mapk1	3	2.7	*Csf2		0.3	Nfkbia	1	0.4, 2.3	Tcrg		0.3
Neurod2		3.2	Ctgf		13.9	Ninj1		5.3	Tff1		0.1
Nfkbia	2	0.4, 2.3	Ctsb		3.6	Ninj2		2.6	Tff3		0.3
Nr3c1		4.7	Ctse		0.4	Ocil		0.1, 9.1	Tfp1		4.4
Rein		0.3	Cybb		2.5	Oldrl1		0.3, 6.5	Tbhd		9.6
Sgk		6.5	Cysltr1		0.1, 2.1	P2ry12		0.1	Tm4sf11		0.4, 4.3
Siat8b		0.1	Dad1		0.2, 2.5	P2y12		0.2	Tm4sf3		3.6
Slc6a4		0.0	Ddt		4.4	Pap		66.2	*Tm4sf4		2.0
Sncs		0.2	Edg3		4.0	Pawr		0.3	*Tnf	3	3.2
Stmn1	0.2, 15.9	*Egr1	1, 3	18.6	Pecam1		3.5	Tnfrsf4		0.3, 2.3	
Vdac3		6.0	F10		0.5	Plat		0.4, 4.9	Umod		0.4, 3.0
2 Wound											
*A2m	0.4, 46.2	*F2rl2		0.2	Pip		0.1	3 Pain			
Abhd2	0.4	F5		0.5	*Piscr1		7.5	Bdnf	1	0.4, 2.6	
Adam15	14.0	Gap43	1	0.3	*Ppbp		0.1, 2.1	Creb1	1	0.5	
Ager	0.4	Gdnf		0.4	Prdx5		0.5	Cyp19a1		0.2, 6.5	
Alox5	0.2, 2.5	Gfap		0.3, 2.6	Prkca		4.6	Drd2	1	8.6	
Alox5ap	4.9	Ggtla1		4.0	Proc		0.3	Edn1		0.4, 2.6	
Anxa2	4.5	Hdac7a		0.5, 4.3	Procr		6.5	*Egr1	1, 2	18.6	
Art2b	0.3	Hnf4a		0.1, 4.5	Pros1		2.1	*Fos	1	28.4	
Atrn	4.4	Hoxb13		0.5, 3.5	Prrx2		3.6	Gja4		3.8	
B4galnt1	3.1	Hrh1		0.5, 9.9	Ptafr		7.1	Il1b		0.4	
Bcl10	2.3	*Ifng		6.5	Ptger3		0.2	Mapk1	1	2.7	
C1qr1	5.5	Ighe		0.2, 2.5	*Ptprc		0.1, 3.0	Ptg2		0.1, 2.1	
C3	0.2	*Il1r1		0.5	Rab27a		3.4	Tac1	2	0.2	
*C5r1	0.4, 2.6	Il2ra		0.3, 4.3	S100a8		6.5	*Tnf	2	3.2	
Ccl17	0.1	Il4		0.1, 2.6	S100a9		4.9	Trpv1		0.3	

*Reported genes associated with LR; Associated to others: involved in other responses

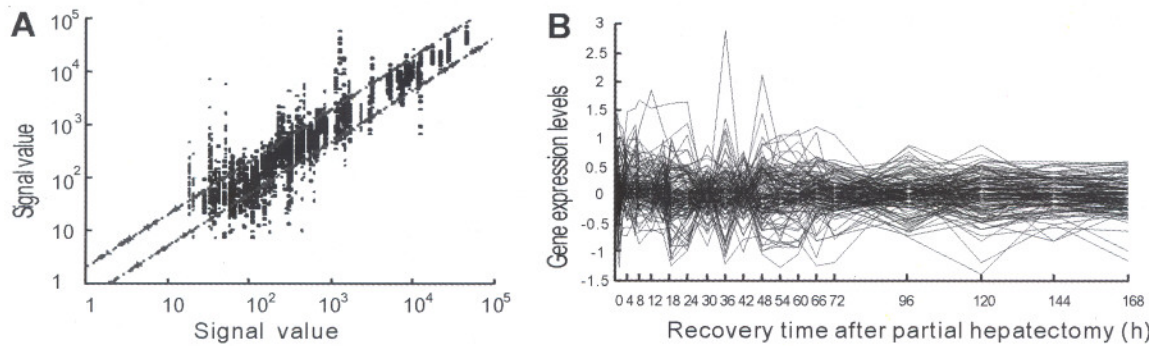


Figure 1. Expression frequency, abundance and changes of 141 genes associated with the responses to fear, wound and pain during rat LR. Detection data of Rat Genome 230 2.0 Array were analyzed and graphed by Microsoft Excel. A. Gene expression frequency. The dots above bias represent the genes up-regulated more than two folds, and total times of up-regulation were 600; those under bias down-regulated more than two folds, and that of down-regulation were 343; and the ones between biases no-sense alterative; B. Gene expression abundance and changes. 97 genes were 2–128 folds up-regulated, and 86 genes 2–10 folds down-regulated.

3.2 Initiation expression time of the genes associated with the responses to fear, wound and pain during LR

At each time point of LR, the numbers of initial up, down and total up, down-regulated genes were in sequence: both 17 and 7 at 0.5 hour; 10, 14 and 26, 19 at 1 hour; 9, 2 and 30, 6 at 2 hours; 6, 5 and 34, 9 at 4 hours; 3, 1 and 30, 11 at 6 hours; 0, 0 and 30, 7 at 8 hours; 2, 3 and 31, 11 at 12 hours; 11, 8 and 37, 14 at 16 hours; 8, 12 and 32, 27 at 18 hours; 1, 2 and 31, 22 at 24 hours; 2, 3 and 19, 16 at 30 hours; 0, 2 and 30, 21 at 36 hours; 0, 2 and 19, 12 at 42 hours; 2, 2 and 42, 29 at 48 hours; 1, 0 and 27, 21 at 54

hours; 0, 0 and 27, 16 at 60 hours; 0, 0 and 24, 16 at 66 hours; 0, 0 and 20, 11 at 72 hours; 2, 1 and 23, 18 at 96 hours; 1, 2 and 31, 23 at 120 hours; 0, 0 and 22, 12 at 144 hours; 0, 0 and 18, 15 at 168 hours (Figure 2). On the whole, gene expression changes span the whole LR, with 600 times in up-regulation and 343 times in down-regulation, respectively. The initially up-regulated genes were predominant in the forepart and prophase, and the down-regulated in the metaphase, whereas there was almost no initial expression in the anaphase.

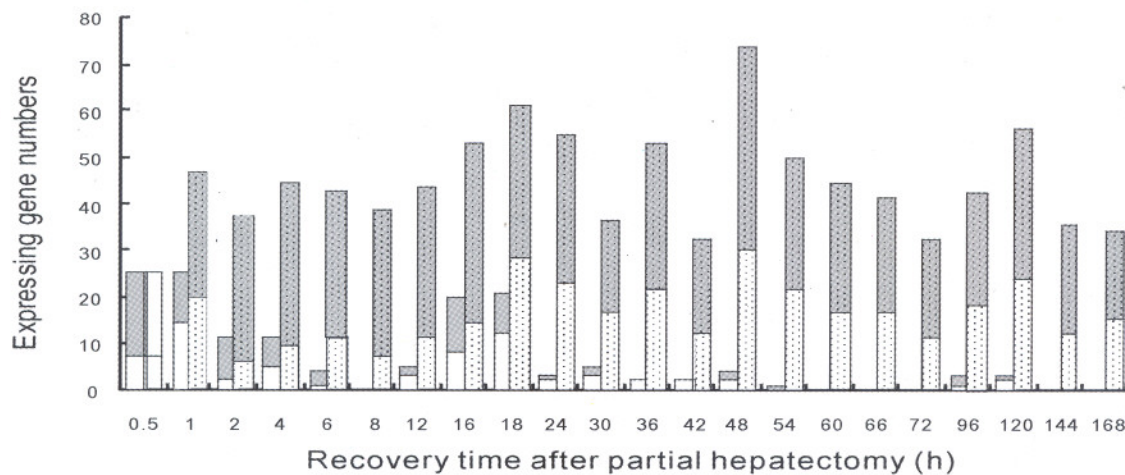


Figure 2. The initial and total expression profiles of 141 genes associated with the responses to fear, wound and pain at each time point of LR. Grey bars: Up-regulated genes; White bars: Down-regulated genes. Blank bars indicate initially expressed genes, in which up-regulation genes are predominant in the forepart and prophase, and the down-regulation in the metaphase, whereas very few in the anaphase. Dotted bars indicate the totally expressed genes, in which some genes are up regulation and others down during LR.

3.3 Expression similarity and time relevance of the genes associated with the responses to fear, wound and pain during LR

141 genes mentioned above during LR could be

characterized based on their similarity in expression as following: only up-, predominantly up-, only down-, predominantly down-, and up-/down-regulated, involved in 55, 19, 44, 18 and 5 genes, respectively

(Figure 3). 141 genes could also be classified based on time relevance into 13 groups including 0.5 and 168h, 1 and 2 hours, 4 hours, 6 and 8 hours, 12 and 16 hours, 18 and 120 hours, 24 and 30 hours, 36 and 48 hours, 42 hours, 54 hours, 60 and 66 hours, 72 and 96 hours, 144 hours, in which the up- and down-regulated gene numbers were 35 and 22; 56 and 25; 34 and 9; 64 and 20; 68 and 25; 62 and 45; 49 and 37; 72 and 50; 19

and 12; 27 and 21; 44 and 27; 45 and 30; 22 and 12, respectively (Figure 3). The up-regulation genes were mainly associated with inflammation response, structure-function reconstruction of nervous tissue, oxidation resisting, revascularization and anti-coagulation. The down genes were mostly with immune response and pro-coagulation.

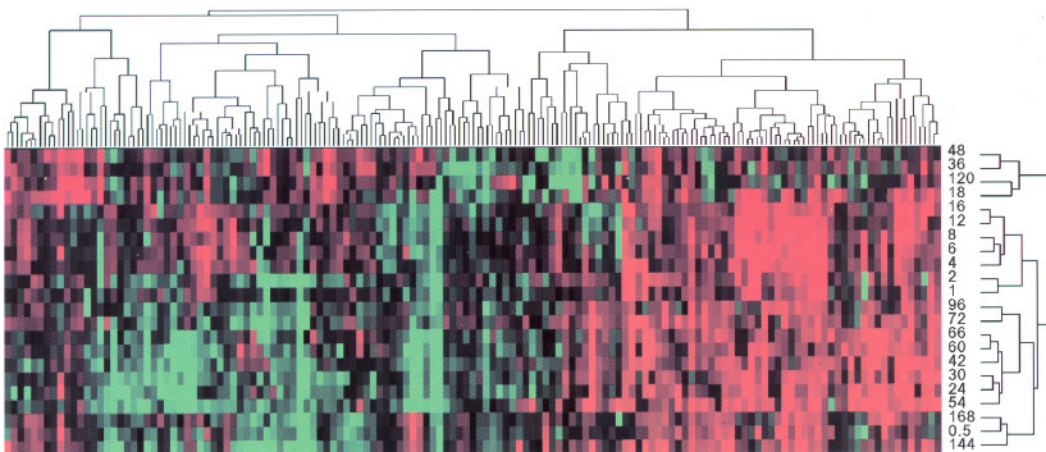


Figure 3. Expression similarity and time relevance cluster of 141 genes associated with the responses to fear, wound and pain during LR. Detection data of Rat Genome 230 2.0 Array were analyzed by H-clustering. Red represents up-regulation genes mainly associated with inflammation response, structure-function reconstruction of nervous tissue, oxidation resisting, revascularization and anti-coagulation; Green represents the down ones mostly associated with alcohol degradation; Black: No-sense change in expression. The upper and right trees respectively show expression similarity and time series clusters, by which the above genes were classified into 5 and 13 groups separately.

3.4 Expression patterns of the genes associated with the responses to fear, wound and pain during LR

Above 141 genes during LR might be categorized according to the expression changes into 25 patterns: (1) up-regulation at one time point, at 6, 16, 30, 48, 54, 66, 96, 120 hours after PH (Figure 4A), 10 genes involved; (2) up at two time points, at 16 and 42 hours, 16 and 96 hours, 48 and 120 hours (Figure 4B), 3 genes involved; (3) up at three time points (Figure 4B), 3 genes involved; (4) up at four time points (Figure 4C), 5 genes involved; (5) up at one phase, at 1–48 hours, 18–24 hours (Figure 4D), 2 genes involved; (6) up at two time points/one phase (Figure 4D), 4 genes involved; (7) up at three time points/one phase (Figure 4E), 3 genes involved; (8) up at one time point/two phases (Figure 4E), 3 genes involved; (9) up at two time points/two phases (Figure 4F), 4 genes involved; (10) up at three time points/two phases (Figure 4G), 5 genes involved; (11) up at two time points/three phases (Figure 4H), 5 genes involved; (12) up at one time point/four phases (Figure 4H), 3 genes involved; (13) at more time points/phases (Figure 4I), 5

genes involved; (14) down at one time point, at 6, 16, 24, 36, 42, 48, 96, 120 hours (Figure 4J), 10 genes involved; (15) down at two time points, at 0.5 and 18 hours, 6 and 12 hours, 16 and 30 hours, 18 and 48 hours, 18 and 54 hours, 24 and 54 hours, 30 and 42 hours, 30 and 48 hours, 30 and 96 hours, 36 and 48 hours, 48 and 60 hours (Figure 4K), 11 genes involved; (16) down at three time points (Figure 4L), 2 genes involved; (17) down at four time points (Figure 4L), 4 genes involved; (18) down at one phase, at 6–12 hours, 120–168 hours (Figure 4M), 2 genes involved; (19) down at one time point/one phase, at 1 and 120–144 hours, 36 and 12–24 hours, 48 and 18–24 hours, 120 and 18–24 hours (Figure 4M), 4 genes involved; (20) down at one time point/two phases (Figure 4N), 2 genes involved; (21) down at two time points/two phases (Figure 4N), 2 genes involved; (22) down at more time points or phases (Figure 4O), 7 genes involved; (23) first up and then down (Figure 4P), 9 genes involved; (24) first down and then up (Figure 4Q), 6 genes involved; (25) up/down mixed (Figure 4R), 27 genes involved.

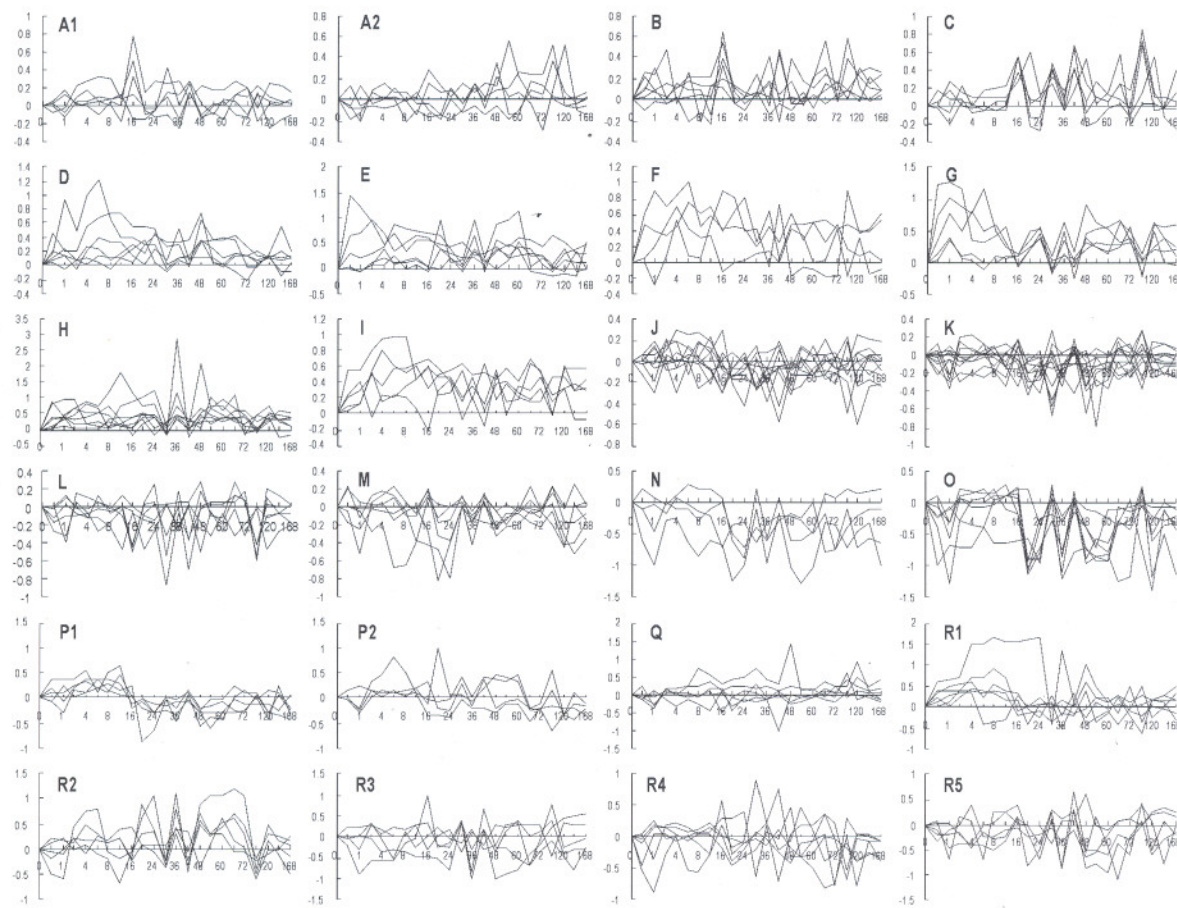


Figure 4. Twenty-five expression patterns of 141 genes associated with the responses to fear, wound and pain during LR. Expression patterns were obtained by the analysis of detection data of Rat Genome 230 2.0 Array with Microsoft Excel. A – I. 55 up-regulated genes; J – O. 44 down-regulated genes; P – R. 42 up/down-regulated genes. X-axis represents recovery time after PH (h); Y-axis shows logarithm ratio of the signal values of genes at each time point to control.

4 Discussion

PH serves as an inducement to physiological responses, such as fear, wound and pain and so on, which result from direct or indirect interaction between various proteins. Among the proteins associated with fear response, five kinds of proteins including calcium/calmodulin-dependent protein kinase kinase 2 (CAMKK2) are associated with emotion, memory and fear^[36]. Six kinds of proteins including dopamine receptor 2 (DRD2) are related to regulation of neurotransmission and anxiety^[37]. Four kinds of proteins including early growth response 1(EGR1) regulate apoptosis^[38]. Four kinds of proteins including cannabinoid receptor 1 (CNR1) participate in neuron activation and nerve regeneration, and prevent the neurodegenerative process from occurring^[39]. The meaningful expression changes of these genes are same or similar at some time points, then different at other points during LR, speculating that they

co-regulate the response to fear. Among them, *egr1* was up-regulated during almost the whole LR, especially significantly in the forepart, and reached a peak at 1 hour that is 18.6 folds of control, which was consistent with the results reported by Mueller *et al*^[40]. *camkk2* was up at 18 – 24, 36 and 48 hours after PH, and reached a peak at 18 hours that was 7.6 folds of control. *drd2* was mainly up at 0.5 – 18 and 48 – 60 hours, and reached a peak at 2 hours that was 8.6 folds of control. It is assumed that the genes mentioned above play important roles in fear response during LR.

Among the proteins associated with response to wound, six kinds of proteins including thrombomodulin (THBD) restrain coagulation^[41]. Five proteins including coagulation factor 5 (F5) are concerned with coagulation^[42]. Seven proteins including selectin E (SELE) accelerate inflammation^[43]. Fourteen proteins including alpha-2-macroglobulin (a2M) are concerned with inflammation^[44]. Four proteins including pancreatitis-associated protein (PAP) suppress inflammation^[45]. Fif-

teen proteins including leukotriene B4 receptor (LTB4R) regulate immunoreactions to protect cells against damnification^[46]. Gamma-glutamyltransferase-like activity 1 (GGTLA1) and peroxiredoxin 5 (PRDX5) can protect cells from oxidation damage^[47]. Nine proteins including core promoter element binding protein (COPEB) hasten cell growth and proliferation^[48]. Three kinds of proteins including serine or cysteine peptidase inhibitor clade E member 1 (SERPINE1) suppress cell proliferation^[49]. Eight proteins including glial cell line derived neurotrophic factor (GDNF) can protect nerve^[50]. Four proteins including nerve injury-induced protein 1 (NINJ1) can facilitate nerve regeneration^[51]. Four proteins including a disintegrin and metalloproteinase domain 15 (ADAM15) play a role in angiogenesis^[52]. Defender against cell death 1 (DADI1) and interleukin 4 (IL-4) prevent cells from apoptosis^[53]. Four proteins including early growth response 1 (EGR1) can induce and accelerate cell apoptosis^[13]. Lymphocyte antigen 68 (C1QR1) can promote cell-cell interaction and prevent cells impaired by pathogen or harmful cell fragment^[54]. Coagulation factor C homolog (COCH) induces cells aggregation and mucopolysaccharide deposition^[55]. Transmembrane 4 superfamily member 11 (TM4SF11) relates to formation of myelin sheath^[56]. Fatty acid binding protein 5 (FABP5) concerns lipid metabolism^[57]. Hepatocyte nuclear factor 4 alpha (HNF4a) is involved in embryonal liver development and regulation of gene expression in adult liver^[58]. Annexin A2 (ANXA2) is associated with movement of endocytic vesicles^[59]. Histamine receptor H 1 (HRH1) stimulates nitric oxide synthesis to facilitate vasodilatation^[60]. Moesin (MSN) is associated with lipopolysaccharide-mediated secretion of tumor necrosis factor^[61]. Cathepsin E (CTSE) restrains communion of substance between cytoplasm and lysosome^[62]. Superoxide dismutase 2 (SOD2) is involved in elimination of free radicals and degradation of matrix^[63]. Cytochrome b-245 beta polypeptide (CYBB) can induce reactive oxygen species produced by endothelial cells^[64]. Trefoil factor 1 (TFF1) can hasten mucosal regeneration^[65]. Overexpression of trefoil factor 3 (TFF3) can result in hepatoma^[66]. Glial fibrillary acidic protein (GFAP) can accelerate astrocyte producing laminin^[67]. Complement component 3 (C3) accelerates formation of fatty liver^[68]. Tissue plasminogen activator (PLAT) is associated with toxicosis of neural excitability^[69]. Homeo box B13 (HOXB13) promotes cell differentiation and repair of injury^[70]. The sameness or similarity in some time points, then dissimilarity in others of meaningful expression changes of these genes during LR perhaps regulate the response to wound together.

Notably, *thbd* showed up-regulation during almost the whole LR, and had the highest abundance of 9.6 times higher than control at 6 hours, which was generally in line with the result reported by Takatori *et al*^[71]. *pap* was up-regulated at multiple phages after PH, especially significantly at the middle phase, and had the highest abundance of 68.6-fold at 12 hours, which was on the whole agree with the result reported by Simon *et al*^[72]. *serpine1* was up at 1–48 hours after PH, and reach a peak with 16.7 folds of control at 66 hours, which was in conformity with the result reported by Mueller *et al*^[40]. *sele* and *c1qr1* were up at multiple time points and multiple phages respectively, and showed the highest abundances of 13 folds at 66 hours and 5.5 folds at 8 hours in sequence. *a2m* was up significantly at metaphase, and had the highest abundance at 8 hours that was 46.2 folds of control. *ltb4r* was up at 0.5–14 hours post PH, and had the highest abundance at 8 hours that was 8.7 folds of control. *copeb* showed up-regulation during the whole LR, and had the highest abundance at 6 hours that was 10.6 folds of control. *ninj1* was up-regulated at 15, 30, 42 and 96 hours after PH, and reached a peak at 96 hours, that was 5.3 folds than control. *adam15* was mainly up in the metaphase, and had the highest abundance at 60 hours that was 14 folds of control. It is speculated that the genes mentioned above play crucial roles in the response to wound during LR.

Among the proteins associated with response to pain, FBJ murine osteosarcoma viral oncogene homolog (FOS) is response for the activation of neuron^[73]. Tachykinin 1 (TAC1) has a role of acesodyne by repressing excitatory synaptic transmission^[74]. Transient receptor potential cation channel subfamily V member 1 (TRPV1) can assuage pain and counteract inflammation^[75]. Prostaglandin-endoperoxide synthase 2 (PTGS2), associating with neuron damage related to epilepsy, prevents toxic shock occurring^[76]. Endothelin 1 (EDN1) and gap junction membrane channel protein alpha 4 (GJa4) are involved in conduction of impulses^[15]. The sameness or similarity in some time points, then dissimilarity in others of meaningful expression changes of these genes during LR perhaps co-regulate the response to pain. Among them, *fos* was up at 0.5–30 and 42–48 hours post PH, especially significantly in the early phase, and had the highest abundance at 0.5 hour that was 28.4 folds of control, which was basically consistent with the result reported by Coni *et al*^[77]. It is supposed that it play a key role in the response to pain.

In summary, commencing from long times (0.5 hour–7 days after PH) and multiple time points (total 23), high-throughput gene expression analysis was used to investigate the expression changes of the genes associ-

ated with the responses to fear, wound and pain. It was primarily proved that PH can cause various physiological responses including responses to fear, wound and pain etc; that Rat Genome 230 2.0 Array was a useful tool analyzing the above responses at transcriptional level. Whereas, these processes DNA → mRNA → protein were influenced by many factors including interaction between proteins. Therefore, the expression changes and actions of genes in regenerating liver need to be further analyzed with the techniques, such as Northern blotting, protein chip, RNA interference, protein-interaction etc.

References

1. Evgen'ev MB, Garbus DG, Zatsepina OG. Heat shock proteins: functions and role in adaptation to hyperthermia. *Ontogeny* 2005; 336 (4): 265–73.
2. Xu CS, Fracella F, Christiane RL, et al. Stress response of lysosomal, cysteine proteinases in rat C6 glioma cells. Comparative. *Biochemistry & Molecular Biology* 1997; 117 (2): 169–78.
3. Dresios J, Aschrafi A, Owens GC, et al. Cold stress-induced protein Rbm3 binds 60S ribosomal subunits, alters microRNA levels, and enhances global protein synthesis. *PNAS* 2005; 102 (6): 1865–70.
4. Varela CA, Baez ME, Agosin E. Osmotic stress response: quantification of cell maintenance and metabolic fluxes in a Lysine-overproducing strain of corynebacterium glutamicum. *Applied and Environmental Microbiology* 2004; 70 (7): 4222–9.
5. Barbour E, Rawda N, Banat G, et al. Comparison of immunosuppression in dry and lactating Awassi ewes due to water deprivation stress. *Veterinary Research Communications* 2005; 29 (1): 47–60.
6. Vitetta L, Anton B, Cortizo F, et al. Mind-body medicine: stress and its impact on overall health and longevity. *Ann NY Acad Sci* 2005; 1057: 492–505.
7. Huelmos RA, Garcia VMJ, Alegria EE, et al. Myocardial perfusion reserve studied by single-photon emission-computed tomography with thallium-201 and a drug stress test with adenosine triphosphate in patients with cardiovascular risk factors. *Rev Esp Cardiol* 1997; 50 (10): 696–708.
8. Muto Y, Sato K. Pivotal role of actin in cell survival under oxidative stress in the zitter rat brain with genetic spongiform encephalopathy. *Brain Research Molecular Brain Research* 2003; 111 (1–2): 111–22.
9. Hohenblum H, Gasser B, Maurer M, et al. Effects of gene dosage, promoters, and substrates on unfolded protein stress of recombinant *Pichia pastoris*. *Biotechnology and Bioengineering* 2004; 85 (4): 367–75.
10. Lucht JM, Mauch-Mani B, Steiner HY, et al. Pathogen stress increases somatic recombination frequency in *Arabidopsis*. *Nature Genetics* 2002; 30 (3): 311–4.
11. Estes DM, Turaga PS, Sievers KM, et al. Characterization of an unusual cell type ($CD4^+ CD3^-$) expanded by helminth infection and related to the parasite stress response. *Journal of Immunology* 1993; 150 (5): 1846–56.
12. Matsuzawa S, Suzuki T, Misawa M. Conditioned fear stress induces ethanol-associated place preference in rats. *European Journal of Pharmacology* 1998; 341 (2–3): 127–30.
13. Ono H, Ichiki T, Ohtsubo H, et al. Critical role of Mst1 in vascular remodeling after injury. *Arterioscler Thromb Vasc Biol* 2005; 25 (9): 1871–6.
14. Oztas B, Akgul S, Arslan FB. Influence of surgical pain stress on the blood-brain barrier permeability in rats. *Basic Life Sciences* 2004; 74 (16): 1973–9.
15. Liu LM, Dubick MA. Hemorrhagic shock-induced vascular hyporeactivity in the rat: relationship to gene expression of nitric oxide synthase, endothelin-1, and select cytokines in corresponding organs. *J Surg Res* 2005; 125 (2): 128–36.
16. Hosford GE, Koyanagi KS, Leung WI, et al. Hyperoxia increases protein mass of 5-lipoxygenase and its activating protein, flap, and leukotriene B(4) output in newborn rat lungs. *Exp Lung Res* 2002; 28 (8): 671–84.
17. Hasan SS, Chaturvedi PK. Response of whole body X-irradiation to inanition stress. *Strahlentherapie* 1983; 159 (6): 351–7.
18. Spiler IJ, Molitch ME. Lack of modulation of pituitary hormone stress response by neural pathways involving opiate receptors. *J Clin Endocrinol Metab* 1980; 50 (3): 516–20.
19. Spector MP. The starvation-stress response (SSR) of *Salmonella*. *Adv Microb Physiol* 1998; 50 (3): 516–20.
20. Riezman H. Why do cells require heat shock proteins to survive heat stress? *Cell Cycle* 2004; 3 (1): 61–3.
21. Fausto N, Campbell JS, Riehle KJ. Liver regeneration. *Hepatology* 2006; 43 (2): S45–S53.
22. Michalopoulos GK, DeFrances M. Liver regeneration. *Adv Biochem Eng Biotechnol* 2005; 93: 101–34.
23. Okochi O, Kaneko T, Sugimoto H, et al. ICG pulse spectrophotometry for perioperative liver function in hepatectomy. *J Surg Res* 2002; 103 (1): 109–13.
24. Xu CS, Chang CF, Yuan JY, et al. Expressed genes in regenerating rat liver after partial hepatectomy. *World J Gastroenterol* 2005; 11 (19): 2932–40.
25. Calvano SE, Xiao W, Richards DR, et al. A network-based analysis of systemic inflammation in humans. *Nature* 2005; 437 (7061): 1032–7.
26. Dransfeld O, Gehrmann T, Köhrer K, et al. Oligonucleotide microarray analysis of differential transporter regulation in the regenerating rat liver. *Liver International* 2005; 25 (6): 1243–58.
27. Higgins GM, Anderson RM. Experimental pathology of the liver: restoration of the liver of the white rat following partial surgical removal. *Arch Pathol* 1931; 12: 186–202.
28. Knupp JH, Gear MA, Forman MS, et al. Comparison of automated and manual nucleic acid extraction methods for detection of enterovirus RNA. *J Clin Microbiol* 2003; 41 (8): 3532–6.
29. Nuysts S, Van Mellaert L, Lambin P, et al. Efficient isolation of total RNA from *Clostridium* without DNA contamination. *J Microbiol Methods* 2001; 44 (3): 235–8.
30. Arkin A, Ross J, McAdams HH. Stochastic kinetic analysis of developmental pathway bifurcation in phage lambda-infected *Escherichia coli* cells. *Genetics* 1998; 149 (4): 1633–48.
31. Li L, Roden J, Shapiro BE, et al. Reproducibility, fidelity, and discriminant validity of mRNA amplification for microarray analysis from primary hematopoietic cells. *J Mol Diagn* 2005; 7 (1): 48–56.
32. Hood L. Leroy Hood expounds the principles, practice and future of systems biology. *Drug Discov Today* 2003; 8 (10): 436–8.
33. Eisen MB, Spellman PT, Brown PO, et al. Cluster analysis

- and display of genome-wide expression patterns. *Proc Natl Acad Sci* 1998; 95 (25): 14863–8.
34. Werner T. Cluster analysis and promoter modelling as bioinformatics tools for the identification of target genes from expression array data. *Pharmacogenomics* 2001; 2 (1): 25–36.
 35. Yue H, Eastman PS, Wang BB, et al. An evaluation of the performance of cDNA microarrays for detecting changes in global mRNA expression. *Nucleic Acids Res* 2001; 29 (8): E41.
 36. Ko S, Zhao MG, Toyoda H, et al. Altered behavioral responses to noxious stimuli and fear in glutamate receptor 5 (GluR5)- or GluR6-deficient mice. *J Neurosci* 2005; 25 (4): 977–84.
 37. Montagna P, Cevoli S, Marzocchi N, et al. The genetics of chronic headaches. *Neurol Sci* 2003; 2: S51–6.
 38. Kar S, Wang M, Rosi KS, et al. Inhibition of rat liver regeneration after partial hepatectomy and induction of ERK phosphorylation by Cpd 5, a K vitamin-based anticancer compound. *Carcinogenesis* 2004; 25 (12): 2345–51.
 39. Ramirez BG, Blazquez C, Gomez del Pulgar T, et al. Prevention of Alzheimer's disease pathology by cannabinoids: neuroprotection mediated by blockade of microglial activation. *J Neurosci* 2005; 25 (8): 1904–13.
 40. Mueller L, Broering DC, Meyer J, et al. The induction of the immediate-early-genes Egr-1, PAI-1 and PRL-1 during liver regeneration in surgical models is related to increased portal flow. *J Hepatol* 2002; 37 (5): 606–12.
 41. Coni P, Simbula G, de Prati AC, et al. Differences in the steady-state levels of c-fos, c-jun and c-myc messenger RNA during mitogen-induced liver growth and compensatory regeneration. *Hepatology* 1993; 17 (6): 1109–16.
 42. Wang J, Yao A, Wang JY, et al. cDNA cloning and sequencing, gene expression, and immunolocalization of thrombomodulin in the Sprague-Dawley rat. *DNA Res* 1999; 6 (1): 57–62.
 43. Liu N, Makino T, Nogaki F, et al. Coagulation in the mesangial area promotes ECM accumulation through factor V expression in MsPGN in rats. *Am J Physiol Renal Physiol* 2004; 287 (4): F612–20.
 44. Fontenot JD, Rasmussen JP, Gavin MA, et al. A function for interleukin 2 in Foxp3-expressing regulatory T cells. *Nat Immunol* 2005; 6 (11): 1142–51.
 45. Garcia GE, Xia Y, Ku G, et al. IL-18 translational inhibition restricts IFN-gamma expression in crescentic glomerulonephritis. *Kidney Int* 2003; 64 (1): 160–9.
 46. Anders HJ, Ninichuk V, Schlondorff D. Progression of kidney disease: blocking leukocyte recruitment with chemokine receptor CCR1 antagonists. *Kidney Int* 2006; 69 (1): 29–32.
 47. Diskin T, Tal-Or P, Erlich S, et al. Closed head injury induces upregulation of Beclin 1 at the cortical site of injury. *J Neurotrauma* 2005; 22 (7): 750–62.
 48. Potdar PD, Andrews KL, Nettesheim P, et al. Expression and regulation of gamma-glutamyl transpeptidase-related enzyme in tracheal cells. *Am J Physiol* 1997; 273 (5 Pt 1): L1082–9.
 49. Zeng ZJ, Yang LY, Ding X, et al. Expressions of cysteine-rich61, connective tissue growth factor and Nov genes in hepatocellular carcinoma and their clinical significance. *World J Gastroenterol* 2004; 10 (23): 3414–8.
 50. Wang H, Vohra BP, Zhang Y, et al. Transcriptional profiling after bile duct ligation identifies PAI-1 as a contributor to cholestatic injury in mice. *Hepatology* 2005; 42 (5): 1099–108.
 51. Kholodilov N, Yarygina O, Oo TF, et al. Regulation of the development of mesencephalic dopaminergic systems by the selective expression of glial cell line-derived neurotrophic factor in their targets. *J Neurosci* 2004; 24 (12): 3136–46.
 52. Toyama T, Sasaki Y, Horimoto M, et al. Ninjurin1 increases p21 expression and induces cellular senescence in human hepatoma cells. *J Hepatol* 2004; 41 (4): 637–43.
 53. Yang RB, Ng CK, Wasserman SM, et al. Identification of a novel family of cell-surface proteins expressed in human vascular endothelium. *J Biol Chem* 2002; 277 (48): 46364–73.
 54. Yamada T, Takatsu Y, Kasumi M, et al. A homolog of the defender against apoptotic death gene (DADI) in senescent gladiolus petals is down-regulated prior to the onset of programmed cell death. *J Plant Physiol* 2004; 161 (11): 1281–3.
 55. Dean YD, McGreal EP, Akatsu H, et al. Molecular and cellular properties of the rat AA4 antigen, a C-type lectin-like receptor with structural homology to thrombospondin. *J Biol Chem* 2000; 275 (44): 34382–92.
 56. Bhattacharya SK, Rockwood EJ, Smith SD, et al. Proteomics reveal Cochlin deposits associated with glaucomatous trabecular meshwork. *J Biol Chem* 2005; 280 (7): 6080–4.
 57. Gillen C, Gleichmann M, Greiner-Petter R, et al. Full-length cloning, expression and cellular localization of rat plasmolipin mRNA, a proteolipid of PNS and CNS. *Eur J Neurosci* 1996; 8 (2): 405–14.
 58. Alshuraifa HN, Stenton GR, Wallace JL, et al. A protease activated receptor-2 (PAR-2) activating peptide, tc-LIGRLO-NH₂, induces protease release from mast cells: role in TNF degradation. *BMC Pharmacol* 2004; 4: 12.
 59. Xu CS, Zhao LF, Yang KJ, et al. The origin and the function of liver stem cell. *Acta Biologiae Experimentalis Sinica* 2004; 37 (1): 72–7.
 60. Hayes MJ, Merrifield CJ, Shao D, et al. Annexin 2 binding to phosphatidylinositol 4,5-bisphosphate on endocytic vesicles is regulated by the stress response pathway. *J Biol Chem* 2004; 279 (14): 14157–64.
 61. Yang QZ, Hatton GI. Histamine H1-receptor modulation of inter-neuronal coupling among vasopressinergic neurons depends on nitric oxide synthase activation. *Brain Res* 2002; 955 (1–2): 115–22.
 62. Iontcheva I, Amar S, Zawawi KH, et al. Role for Moesin in lipopolysaccharide-stimulated signal transduction. *Infection and Immunity* 2004; 72 (4): 2312–20.
 63. Shibata M, Sakai H, Sakai E, et al. Disruption of structural and functional integrity of alpha 2-macroglobulin by cathepsin E. *Eur J Biochem* 2003; 270 (6): 1189–98.
 64. Kitamura N, Tohyama H, Nishihira J, et al. Stress deprivation enhances manganese superoxide dismutase expression in the rat patellar tendon. *Int J Mol Med* 2004; 14 (4): 537–43.
 65. Banisadr G, Fontanges P, Haour F, et al. Neuroanatomical distribution of CXCR4 in adult rat brain and its localization in cholinergic and dopaminergic neurons. *Eur J Neurosci* 2002; 16 (9): 1661–71.
 66. Hoffmann W. Trefoil factors TFF (trefoil factor family) peptide-triggered signals promoting mucosal restitution. *Cell Mol Life Sci* 2005; 62 (24): 2932–8.
 67. Okada H, Kimura MT, Tan D, et al. Frequent trefoil factor 3 (TFF3) overexpression and promoter hypomethylation in mouse and human hepatocellular carcinomas. *Int J Oncol* 2005; 26 (2): 369–77.

68. Rozovsky I, Wei M, Stone DJ, *et al.* Estradiol (E2) enhances neurite outgrowth by repressing glial fibrillary acidic protein expression and reorganizing laminin. *Endocrinology* 2002; 143 (2): 636–46.
69. Bykov I, Junnikkala S, Pekna M, *et al.* Complement C3 contributes to ethanol-induced liver steatosis in mice. *Ann Med* 2006; 38 (4): 280–6.
70. Lochner JE, Honigman LS, Grant WF, *et al.* Activity-dependent release of tissue plasminogen activator from the dendritic spines of hippocampal neurons revealed by live-cell imaging. *J Neurobiol* 2006; 66 (6): 564–77.
71. Mack JA, Li L, Sato N, *et al.* Hoxb13 up-regulates transglutaminase activity and drives terminal differentiation in an epidermal organotypic model. *J Biol Chem* 2005; 280 (33): 29904–11.
72. Takatori M, Iwabuchi S, Ro S, *et al.* Increased serum levels and sinusoidal expression of thrombomodulin in acute liver damage. *Thromb Res* 1999; 93 (3): 113–20.
73. Simon MT, Pauloin A, Normand G, *et al.* HIP/PAP stimulates liver regeneration after partial hepatectomy and combines mitogenic and anti-apoptotic functions through the PKA signaling pathway. *FASEB J* 2003; 17 (11): 1441–50.
74. Kombian SB, Ananthalakshmi KV, Parvathy SS, *et al.* Substance P depresses excitatory synaptic transmission in the nucleus accumbens through dopaminergic and purinergic mechanisms. *J Neurophysiol* 2003; 89 (2): 728–37.
75. Hutter MM, Wick EC, Day AL, *et al.* Transient receptor potential vanilloid (TRPV-1) promotes neurogenic inflammation in the pancreas via activation of the neurokinin-1 receptor (NK-1R). *Pancreas* 2005; 30 (3): 260–5.
76. Kawaguchi K, Hickey RW, Rose ME, *et al.* Cyclooxygenase-2 expression is induced in rat brain after kainate-induced seizures and promotes neuronal death in CA3 hippocampus. *Brain Res* 2005; 1050 (1–2): 130–7.
77. Przybyla-Zawislak BD, Kim CS, Ali SF, *et al.* The differential JunB responses to inhibition of succinate dehydrogenase in rat hippocampus and liver. *Neurosci Lett* 2005; 381 (3): 354–7.

Conditional genetic analysis on quantitative trait loci for yield and its components in rice[☆]

Gangqiang Cao^{1,*}, Jun Zhu²

¹Department of Bioengineering, Zhengzhou University, Zhengzhou, Henan 450052, China; ²Department of Agronomy, Zhejiang University, Hangzhou, Zhejiang 310029, China

Received April 7, 2006

Abstract

Conditional mapping method was used to analyze QTLs for rice yield and its components: number of productive panicles, number of full-filled grains, and kilo-grain weight. By unconditional mapping, some pleiotropic or closely linked QTLs were detected; by conditional mapping, QTL number of yield decreased greatly after excluding the effect from full grain, which indicated that full grain gave the most contribution to yield. The phenomenon was discussed that small number of QTLs for yield seems not to fit too much the very complex trait that is generally believed controlled by many genes. [Life Science Journal. 2007;4(1):71–76] (ISSN: 1097–8135).

Keywords: quantitative trait locus; conditional genetics; rice yield; yield components

1 Introduction

Yield is a very important trait in rice breeding, and as a complex quantitative trait can be dissected into a number of causal components such as number of productive panicles per plant, number of full-filled grains per panicle and kilo-grain weight. A number of studies have been made to locate QTLs for yield and its components^[1–3]. However, in these studies, the contribution of each component to yield has not been analyzed in detail. Conditional QTL mapping approach provides a useful tool for understanding contributions of the causal components in multi-component traits. Therefore, the present studies used the unconditional and conditional QTL mapping for yield and its components to reveal the contribution of each component to yield.

2 Materials and Methods

2.1 Materials

A population of 123 double haploid (DH) lines derived from a cross between an irrigated *indica* variety IR64 and an upland *japonica* variety Azucena^[4] were used in the experiments. The genetic map of this population containing 175 markers distributed among 12 chromosomes covering 2005 cm with an average distance of 11.5 cm between markers^[5] was used for QTL mapping.

2.2 Field experiment

The 123 DH lines and their parents, IR64 and Azucena, were grown in a randomized complete design with two replications at Hainan in 1995 and Hangzhou of China in 1996, 1998. Hainan and Hangzhou show great difference in climate, soil conditions, day length, and even rice growing seasons. The experiment was conducted from early December 1995 to late April 1996 at Hainan where rice can grow well all year round. At Hangzhou, experiments were carried out from late May to early November in 1996, and middle May to middle October in 1998. In all environments, the germinated seeds were sown in a seedling bed and the seedlings were transplanted to a paddy field 30 days later, with a single plant per hill spaced at 15×20 cm. Each plot included four lines with eight plants per line. At the maturity stage, 6 central plants of each plot were measured.

2.3 Phenotypic measurement

Observations were taken on the six central plants of each plot at Hainan in 1995 and Hangzhou in 1996 and 1998 for the productive panicle number per plant (panicle number, PN), full grain number per panicle (full grain, FG), and the weight of 1000 grains (kilo-grain weight, KW). The yield per plant (YD) was calculated as the formula of $YD = PN \times FG \times KW / 1000$.

2.4 Phenotypic and genotypic correlations

Phenotypic and genotypic correlation coefficients among different traits were calculated using MINQUE (1)^[6].

2.5 QTL analysis for yield and yield components

With the unconditional and conditional QTL mapping procedures^[7], QTLs with additive and additive × additive epistatic effects as well as their environmental

[☆]Supported by the National Natural Science Foundation of China (No. 39893350).

*Corresponding author. Email: caogq@zzu.edu.cn

interaction effects in DH population could be searched for multi-component quantitative traits such as yield and its components. The conditional genetic effects of the yield given its component will indicate the net effects of gene expression excluding those of the given component, revealing the contribution of the left components on the formation of yield. The conditional phenotypic value was obtained by the mixed model approaches for conditional genetics of quantitative traits^[8]. The likelihood ratio value of 11.5, which is equal to a LOD score of 2.5^[9], was used as a threshold for detection of QTL or epistasis.

3 Results and Analysis

3.1 Phenotypic variation

Table 1. Phenotypic values of yield and yield components for the DH population and its parents under three environments

Trait	Env.	Parents		DH population					
		IR64	Azucena	Mean	Max	Min	Stdev	Skew	Kurt
Panicle number	1	6.1	3.5	6.7	11.6	3.8	1.5	0.5	0.1
	2	13.4	10.1	8.9	15.3	4.5	2.4	0.6	-0.1
	3	9.0	4.9	7.5	12.2	3.0	2.1	0.35	-0.52
Full grain	1	46.8	66.5	37.0	106.7	0.7	18.1	0.5	1.1
	2	35.7	78.8	94.1	182.1	20.3	32.0	0.1	-0.4
	3	60.9	95.5	69.2	127.3	15.3	25.7	0.11	-0.43
Kilo-grain weight	1	27.1	29.0	27.0	40.3	19.3	4.2	0.4	-0.1
	2	25.6	24.9	25.4	33.8	17.8	2.9	0.2	0.2
	3	25.6	28.2	23.0	30.8	16.0	3.4	0.23	-0.44
Yield	1	7.7	6.7	7.0	20.7	1.1	3.3	0.77	1.71
	2	12.2	19.8	19.3	34.3	6.1	6.4	0.30	-0.49
	3	14.0	13.2	11.9	23.0	1.7	4.4	0.16	-0.02

Env. 1, 2, 3 represent Hainan in 1995, Hangzhou in 1996 and 1998.

3.2 Correlations between yield and each of its components

Significant positive correlations were discovered between yield with each of its components while the components showed negative correlations between each other

The phenotypic values of the parents and the DH population for yield and its components were presented in Table 1. The parent IR64 was observed to be inferior to Azucena for full grain number per panicle under three environments, for kilo-grain weight at Hainan 1995 and Hangzhou 1998, and for calculated yield at Hangzhou 1996, but superior to Azucena for yield and its components at other situations. The data presented in Table 1 also indicated transgressive variation in the DH population for yield and its components in three environments with skew and kurt values being less than 1.0 except a few cases suggesting that the data were like normal distribution and suitable for QTL analysis.

(Table 2). Because of significant correlations between yield with its components, the unconditional and conditional QTL mapping could be used to fully dissect the contributions of yield components to yield.

Table 2. Genotypic correlations (upper triangle) and phenotypic correlations (lower triangle) among yield and yield components

	Panicle number	Full grain	Kilo-grain weight	Yield
Panicle number		-0.06*	-0.16**	0.14**
Full grain	-0.02		-0.08*	0.53**
Kilo-grain weight	-0.12**	-0.04		0.07*
Yield	0.19**	0.50**	0.08*	

* and ** represent significance level of $P = 0.01$ and 0.005 , respectively.

3.3 Unconditional QTLs and their effects for yield components and yield

All of the QTLs with additive effects and/or additive \times additive epistasis effects and their putative posi-

tions in the genome detected by unconditional mapping for yield components and yield were presented in Table 3. QTL for each trait was named as abbreviation of the trait name with the number of chromosome on which the

QTL was located. If there were more than one QTL in a chromosome, the serial number was added after chromosomal number separated by a hyphen. The positions of these QTLs were indicated by the marker interval bracketing the concerned QTL with the estimated distance in Morgan (M) from the left marker. There were totally 11, 9, 17 and 10 QTLs for panicle number, full grain, kilo-grain weight and yield, respectively.

In Table 4, the estimated unconditional additive effects and the additive \times additive epistatic effects at significance level of 0.01 or 0.005 under three environments for each trait were presented. Among the total QTLs with additive and additive \times additive epistasis effects for yield components and yield, 9, 6, 11 and 8 QTLs were found with additive main effect (*a*) and/or additive \times environment interaction effect (*ae*) for each trait, respectively. QTLs within a same marker interval

between yield and each of its components were found, such as Yd1-2 and Pn1, Yd1-1 and Kw1-1, Yd2 and Fg2-2. These three pairs of QTLs had also similar directions of effects. A QTL Fg4 for full grain was found with relatively large *a* and *ae* effects within marker interval RG163-RZ590, also closely linked with QTL Pn4 for panicle number and QTL Yd4 for yield. There were 8, 7, 11 and 5 digenic epistatic interactions with epistatic main effects and/or epistasis by environment interaction effects were detected to be associated with the yield components and yield, respectively (Table 4). There were 1, 3, 8 and 2 interactions included the loci without detectable QTL additive effects for each trait, respectively. Unlike the situation of additive QTLs, no similar epistatic interactions between yield and each of its components were found.

Table 3. QTLs with additive effect and/or additive \times additive epistatic effect for yield and yield components

Panicle number			Full grain			Kilo-grain weight			Yield		
QTL	Marker interval	Distance(M)	QTL	Marker interval	Distance(M)	QTL	Marker interval	Distance(M)	QTL	Marker interval	Distance(M)
Pn1	RZ730-RZ801	0.12	Fg1	<i>RG345-RG381</i>	0	Kw1-1	RGS32-W1	0.14	Yd1-1	RG532-W1	0
Pn2-1	RG544-RG171	0.04	Fg2-1	RG437-RG544	0.08	Kw1-2	RZ801-RGS10	0.02	Yd1-2	RZ730-RZ801	0.22
Pn2-2	RZ213-RZ123	0	Fg2-2	RZ123-RG520	0.12	Kw2-1	<i>Pal1-RZ58</i>	0	Yd2	RZ123-RG520	0
Pn3	Pgi_1-CDO87	0.06	Fg3	RZ284-RZ394	0.06	Kw2-2	RG256-RZ213	0.1	Yd3	<i>RZ574-RZ284</i>	0.1
Pn4	RZ675-RG163	0.16	Fg4	RG163-RZ590	0.02	Kw3-1	<i>RG104-RG348</i>	0.06	Yd4	RZ590-RG214	0.02
Pn6	RG162-RG172	0	Fg6	<i>RG162-RG172</i>	0.02	Kw3-2	RZ337A-RZ448	0.06	Yd6	RZ398-RG213	0
Pn7	PGMS007-CDO59	0.16	Fg8	<i>TGMS102-A10K250</i>	0.02	Kw4	RZ262-RG190	0.08	Yd8	<i>RZ66-AC5</i>	0
Pn8-1	RG20-A5J560	0.1	Fg9	RZ12-RG667	0.06	Kw5-1	RG229-RG13	0.16	Yd10	RZ625-CDO93	0
Pn8-2	<i>RZ66-AC5</i>	0.24	Fg12	RG463-RG901	0.02	Kw5-2	<i>RZ70-RZ225</i>	0	Yd11-1	Adh1-RG1094	0.06
Pn9	CDO590-C711	0				Kw6	RG172-CDO544	0.06	Yd11-2	Npb44-RG247	0
Pn10	CDO93-CDO98	0				Kw7	<i>RZ337B-CDO497</i>	0.12			
						Kw8	RG418B-Amp-2	0			
						Kw9-1	<i>C711-GI03</i>	0.12			
						Kw9-2	RZ228-RZ12	0			
						Kw10	RG134-RZ500	0.02			
						Kw11	<i>RG247-RG103</i>	0.24			
						Kw12	RG958-RG181	0.3			

The QTLs with both additive and epistatic effects were presented in regular form while the QTLs involved in epistasis but without additive effects were presented in bold italic letters, and the QTLs with only additive effects but no epistatic effects were notified with underling lines.

3.4 QTLs and their effects for yield conditional on each of its components

All of the QTLs with additive effects and/or additive \times additive epistasis effects and their putative positions in the genome for yield conditional on each of its components were presented in Table 5. There were totally 13, 5 and 12 QTLs for yield conditional on panicle number, full grain and kilo-grain weight, respectively.

The estimated conditional additive effects and the additive \times additive epistatic effects at significance level of 0.01 or 0.005 under three environments were presented in the Table 6. The conditional QTL effects of the yield given the observed phenotype of yield component indicated the net effects of gene expression from the other components that was independent to the causal effects from the given component. When yield was conditional on panicle number, 10 QTLs with conditional ad-

ditive main effects and/or conditional additive \times environment interaction effects were detected. The number of QTLs was more than that of unconditional yield. This might indicate that after excluding the negative interference of panicle number, the other two left components might give larger contribution to yield. When yield was conditional on full grain, three QTLs with conditional additive main effects and/or conditional additive \times environment interaction effects were detected. This might indicate that after excluding the effect on yield from full grain, the other two left components gave little contribution to yield. This was consistent with that the full grain had the larger genotypic correlation of 0.53 with yield than those of 0.14 and 0.07 that the panicle number and kilo-grain weight had. When yield was conditional on kilo-grain weight, seven QTLs with conditional additive main effects and/or conditional additive

\times environment interaction effects were detected. This might indicate that after excluding the effect on yield from kilo-grain weight, the other two components gave nearly the same contribution to yield with that in the

situation of including the effect from kilo-grain weight, which meant that kilo-grain weight was not considerably important for the formation of yield in this study.

Table 4. Unconditional QTL effects for yield per plant and its components

Trait	QTL	Additive effect			Additive \times additive epistatic effect					
		<i>a</i>	<i>ae</i> ₁	<i>ae</i> ₂	<i>ae</i> ₃	<i>QTLi</i>	<i>QTLj</i>	<i>aa</i>	<i>aae</i> ₁	<i>aae</i> ₂
PN	Pn1	0.37**	-0.39**		0.48*	Pn1	Pn3	0.30*		
	Pn2-1	0.54**	0.45**	-1.42**	0.97**	Pn1	Pn7	0.37*		
	<u>Pn2-2</u>	-0.57**				Pn1	Pn8-1		-0.32**	-1.34**
	Pn3	0.48*		0.70*		Pn2-1	Pn3			-0.26*
	Pn4	0.91**	0.46**	1.14**	-1.60**	Pn3	Pn4	-0.42*	-0.36**	-0.89**
	Pn6	-1.86**		-0.67**	0.60**	Pn3	Pn9		0.17**	-0.16**
	Pn7				-0.20**	Pn6	Pn8-1			-1.53**
	Pn8-1	-2.55**	0.56**	1.90**	-2.45**	<u>Pn8-2</u>	<u>Pn10</u>			-0.56*
	Pn9			-0.26**	0.26**					
FG	Fg2-1		3.47**	9.86**	-13.33**	Fg1	Fg9		3.79*	-6.24**
	Fg2-2		-1.40**		1.59**	Fg2-1	Fg8	7.91*		
	Fg3		-0.97*	7.15**	-6.18**	Fg2-2	Fg4	3.67*		4.80*
	Fg4	-9.70**	8.23**	-6.88**		Fg3	Fg4		-1.62**	1.60**
	Fg9	4.12*	5.52**	3.34**	-8.87**	Fg3	Fg9	-6.05**	-9.99**	5.98**
	Fg12	-3.46*			-1.42**	Fg4	Fg6	3.90*	4.14*	
						Fg9	Fg12		-4.33*	4.61*
KW	Kw1-1		-0.70*		0.62**	Kw1-1	Kw2-1	0.54*		
	Kw1-2	-0.80**		-0.71*	0.61*	Kw1-2	Kw3-1		-0.41**	-2.14**
	Kw2-2		-0.18**			Kw1-2	Kw6	0.62**	2.34**	-2.00**
	Kw3-2	-0.57*	-0.91**		0.78**	Kw1-2	Kw8	0.47*		-0.34**
	Kw4	0.76*				Kw2-1	Kw3-1	0.51*		-0.39*
	Kw5-1			-1.81*	1.11*	Kw3-2	Kw5-2		-0.37**	0.35**
	Kw6		1.56**	-0.32**	-1.25**	Kw4	Kw12		-0.85*	
	Kw8		0.35**		-0.35**	Kw5-1	Kw11	1.24**		-0.74*
	Kw9-2	-0.46**			-0.69**	Kw6	Kw9-1	0.29**		-0.36**
	Kw10	0.80**		0.32**	-0.40**	Kw7	Kw8	0.72*		
	Kw12		0.85*			Kw9-2	Kw11		-1.45**	1.24**
YD	Yd1-1	-1.47**	-2.62**	1.10**	1.52**	Yd1-1	Yd8		0.88**	-2.77**
	Yd1-2	1.24**	-1.84**	2.29**		Yd1-2	Yd6		-0.25**	0.41*
	<u>Yd2</u>			-0.64**	0.45**	Yd3	Yd10	1.08*		
	Yd4	-1.42**	1.54**	-1.60**		Yd4	Yd11-1		0.27**	-0.71**
	Yd6	1.06**	1.03**	-2.81**	1.78**	Yd11-1	Yd11-2	-1.48*		0.44*
	Yd10	1.09*								
	Yd11-1	2.01**								
	Yd11-2	-1.56*								

a, *aa*, *ae*₁, *ae*₂, *ae*₃, *aae*₁, *aae*₂, *aae*₃ represent additive main effect, epistatic main effect and additive \times environment interaction effect, epistasis \times environment interaction effect at Hainan in 1995, at Hangzhou in 1996 and 1998, respectively. * and ** represent the significance level of $P=0.01$ and 0.005 , respectively. The forms of bold italic letter and the underling lines have the same meaning with those in Table 3.

In the three conditional analysis cases, common QTLs between unconditional yield and yield conditional on each of its components were identified. They were Yd1-2 and Yd|Kw1-2, Yd6 and Yd|Fg6, Yd11 and Yd|Pn11. Between yield conditional on panicle number and yield conditional on kilo-grain weight, a common QTL Yd|Pn4 or Yd|Kw4 was identified. This QTL

had effect on yield after excluding the causal effects from panicle number and kilo-grain weight, but missed after excluding the effects from full grain, so this QTL might be through affection on full grain to improve the yield. In fact, this QTL was really identified for full grain by unconditional mapping, and a closely linked QTL Yd4 was identified for final yield.

There were 7, 2 and 9 digenic epistatic interactions with epistatic main effects and/or epistasis by environment interaction effects were detected to be associated with the yield conditional on panicle number, full grain and kilo-grain weight, respectively (Table 6). While no similar epistatic interaction was identified among yield and yield conditional on its components, a pair of inter-

action Fg4 and Fg6 for full grain by unconditional mapping were found similar with the interaction Yd | Pn4 and Yd | Pn6-2 for yield conditional on panicle number, in which Fg4 and Yd | Pn4 were pleiotropic or closely linked genes, thus resulting the association of the two pairs of interactions between full grain and the formation of yield.

Table 5. Loci with QTL additive effect and/or with additive \times additive epistatic effect for yield conditional on each of its components

YD PN			YD FG			YD KW		
QTL	Marker interval	Distance (M)	QTL	Marker interval	Distance (M)	QTL	Marker interval	Distance (M)
Yd Pn1-1	W1-RG173	0	Yd Fg3	Pgi-1-CDO87	0.12	Yd Kw1-1	U10-RG532	0.04
Yd Pn1-2	RZ730-RZ801	0.2	Yd Fg4	RZ675-RG163	0.08	Yd Kw1-2	RZ730-RZ801	0.22
Yd Pn2	RG654-RG256	0	Yd Fg5	RZ70-RZ225	0	Yd Kw3-1	RG348-RZ329	0.12
Yd Pn3	RG348-RZ329	0.06	Yd Fg6	RZ398-RG213	0.02	Yd Kw3-2	Pgi-1-CDO87	0
Yd Pn4	RG163-RZ590	0.02	Yd Fg8	A5J560-A3E396	0.06	Yd Kw4	RG163-RZ590	0
Yd Pn5	RZ67-RZ70	0.08				Yd Kw5	RZ556-RG403	0.16
Yd Pn6-1	Est-2-RZ144	0				Yd Kw7	CDO59-RG711	0
Yd Pn6-2	RG172-CDO544	0.04				Yd Kw8-1	RZ143-RG20	0
Yd Pn8	RGI-Amy3DE	0.1				Yd Kw8-2	AG8_Aro-RZ617	0.02
Yd Pn10	RG134-RZ500	0				Yd Kw10	G1084-RG257	0
Yd Pn11	Adh1-RG1054	0.06				Yd Kw11	RG103-RG1109	0.08
Yd Pn12-1	AF6-RG457	0.08				Yd Kw12	RG463-RG901	0
Yd Pn12-2	RG958-RG181	0						

The forms of bold italic letter and the underling lines have the same meaning with those in Table 3.

Table 6. QTL effect (g) for yield per plant conditional on each of its components

Trait	QTL	Additive effect				Additive \times Additive epistatic effect			
		a	ae ₁	ae ₂	ae ₃	QTL <i>i</i>	QTL <i>j</i>	aa	aae
YD PN									
Yd Pn1-1		-0.22 **	2.08 **	-1.86 **		Yd Pn1-1		0.54 *	
Yd Pn2	-0.97 *					Yd Pn1-2	Yd Pn4	-0.36 *	0.53 **
Yd Pn4	-1.31 **	1.72 **	-1.40 **			Yd Pn2	Yd Pn5	-2.07 **	-1.55 **
Yd Pn5	1.61 **	-1.61 **	2.96 **	-1.34 **		Yd Pn3	Yd Pn8	-1.41 **	0.74 *
Yd Pn6-1		1.91 **	-2.15 **	0.24 *		Yd Pn4	Yd Pn6-2		-1.15 *
Yd Pn6-2		-0.69 **	0.61 *			Yd Pn5	Yd Pn11		-0.39 *
Yd Pn10		-0.62 **	0.94 *			Yd Pn12-1	Yd Pn12-2	-0.97 **	
Yd Pn11	0.87 *								
Yd Pn12-1			2.41 **	-1.36 **					
Yd Pn12-2	0.90 *								
YD FG									
Yd Fg3	1.17 **	0.14 **	-0.71 **	0.57 **		Yd Fg4	Yd Fg5	-0.96 **	0.77 *
Yd Fg6	-2.02 **					Yd Fg6	Yd Fg8	2.23 **	-1.32 **
Yd Fg8				0.95 *					1.69 **
YD KW									
Yd Kw1-1	-0.82 **					Yd Kw1-1	Yd Kw12	-0.80 *	
Yd Kw1-2	1.32 **					Yd Kw1-2	Yd Kw8-1		1.40 *
Yd Kw3-1	-0.77 **	0.90 *	-1.52 **			Yd Kw1-2	Yd Kw8-2		
Yd Kw4	-1.64 **	1.73 **	-3.34 **			Yd Kw3-1	Yd Kw4	0.34 *	-0.43 **
Yd Kw8-2		-2.25 **		2.43 **		Yd Kw3-2	Yd Kw4	0.48 **	
Yd Kw10	0.46 *					Yd Kw4	Yd Kw7	-1.35 **	1.18 *
Yd Kw11			-0.51 **			Yd Kw4	Yd Kw12		
						Yd Kw5	Yd Kw8-2	0.66 **	-0.44 **
						Yd Kw8-2	Yd Kw11		-1.40 *

a, ae₁, ae₂, ae₃, aa, aae₁, aae₂, aae₃, * and ** have the same meaning with those in Table 4. The forms of bold italic letter and the underling lines have the same meaning with those in Table 3.

4 Discussion

Conditional mapping technique permits detection of the net QTL effect of the integrated trait excluding the causal genetic effects of the given component. The unique feature of the conditional mapping approach is that it exploits the variability of integrated trait conditioned on variability of the given component to detect QTLs. In contrast, unconditional mapping for the final integrated trait allows identification of the QTLs based on the integrated effect of all its components. The variation in the population caused by such integrated effects can be made leveled by the opposite effects of the components in the formation of the final trait so that some QTLs will be made undetectable or biased by unconditional mapping.

In this study, conditional mapping helped to identify more QTLs for yield conditional on its components than those detected only for final yield. Other studies^[10,11] also indicated that a relative small number of QTLs for final yield seemed not fitting too much the complex trait that was generally believed controlled by many genes. The conditional mapping might give an explanation for this phenomenon and the components contribute to the final yield oppositely, so that many genes would not be detected.

Practically, the formation of yield is a very complex biological pathway and genetic dissection of yield seems considerably difficult. Previous studies using molecular markers have indicated some putative QTLs controlling yield and its components. However, in these studies the phenotypic values of the final trait were used for QTL mapping. With the conditional approach, not only we mapped QTLs for yield but also we investigated the net effects on yield from its components. It was also found that when compared to other components, full grain

gave the highest contribution in this study. So genetic investigation on full grain might be also useful in capture genes for final yield.

References

1. Cao LY, Zhan XD, Zhuang JY, Zheng KL, Cheng SH. QTL mapping and epistasis analysis for yield components in a RIL population of rice (*Oryza sativa* L. subsp. *indica*). *Scientia Agricultura Sinica* 2003; 36(11): 1241–7.
2. Xiao J, Li J, Yuan LP, Tanksley SD. Identification of QTLs affecting traits of agronomic importance in recombinant inbred population derived from a subspecific rice cross. *Theor Appl Genet* 1995; 92: 230–44.
3. Zhuang JY, Lin HX, Lu J, Qian HR, Hittalmani S, Huang N, Zheng K L. Analysis of QTL environment interaction for yield components and plant height in rice. *Theor Appl Genet* 1997; 95: 799–808.
4. Guideroni E, Galinato E, Luisro J, Vergara G. Anther culture of tropical japonica/ indica hybrids of rice (*Oryza sativa* L.). *Euphytica* 1992; 62: 219–24.
5. Huang N, Parco A, Mew T, Magpantay G, McCouch S, Guideroni E, Xu J, Subudhi P, Angeles, ER, Khush GS. RFLP mapping of isozymes, RAPD and QTL for grain shape, brown plant hopper resistance in a doubled haploid rice population. *Mol breed* 1997; 3: 105–13.
6. Zhu J. Mixed model approaches for estimating genetic variances and covariances. *J Biomath* 1992; 7: 1–11.
7. Zhu J. Mixed model approaches of mapping genes for complex quantitative traits. *J Zhejiang Univ (Natural Sci)* 1999; 33 (3): 327–35.
8. Zhu J. Analysis of conditional genetic effects and variance components in developmental genetics. *Genetics* 1995; 141: 1633–9.
9. Zeng ZB, Weir BS. Statistical methods for mapping quantitative trait loci. *Acta Agronomica Sinica* 1996; 22: 535–49.
10. Veldboom LR, Lee M. Genetic mapping of quantitative trait loci in maize in stress and non-stress environments: I. Grain yield and yield components. *Crop Sci* 1996; 36: 1310–9.
11. Xiao, J, Grandillo S, Ahn SN, McCouch SR, Tanksley SD, Li J, Yuan LP. Genes from wild rice improve yield. *Nature* 1996; 384: 223–4.

Application of a transformation method via the pollen-tube pathway in agriculture molecular breeding[☆]

Xiaoming Song, Yunhong Gu*, Guangyong Qin

Henan Key Laboratory of Ion Beam Bioengineering, Zhengzhou University, Zhengzhou, Henan 450052, China

Received November 20, 2006

Abstract

The transformation method via pollen-tube pathway has great function in agriculture molecular breeding. This article is to introduce the mechanism, molecular evidence, technique details and the latest achievement applying this method. And we compare the advantages and shortages of this method with other transformation pathways. [Life Science Journal. 2007;4(1):77–79] (ISSN: 1097–8135).

Keywords: pollen-tube pathway; molecular breeding

1 Foundation and Its Theoretical Evidence of the Transformation Method via the Pollen-tube Pathway

According to Chinese scientist Zhou's hypothesis in 1979, the normal distant hybridization existed the hybridization of DNA segment^[1], and a new plant transformation method was put forward, it was called the pollen-tube pathway transformation technique. And heterologous DNA was introduced into cotton successfully in 1983, the new anti-wilt cotton cultivars was obtained^[2]. The technique invented by Chinese scientists was paid attention to broadly.

After angiosperms' blooming, pollen bourgeoned on the stigma and the pollen tube grew. Before pollen tube entered the ovule, nucelli and embryo sac were closing entity culture. In process of pollen tube extending, some cells of nucelli began degenerate and became pollen tube pathway through which pollen tube could enter embryo sac by nucelli. The pathway was larger than pollen tube, and then between pollen tube formation and closing, heterologous DNA could enter embryo sac and integrate into the zygote cell and the forepart embryo cells.

2 The Molecular Evidence of the Pollen-tube Pathway Transformation Technique

The mechanism of the pollen tube pathway transformation was confirmed by isotope tracer method. Gong^[3] labeled cotton total DNA using ³H, and injected the labeled DNA into cotton ovary at 24 hours after the self pollination. After 30 minutes, ³H-DNA was found

in some embryos. Between 2–4 hours ³H-DNA was found in more than 80% of embryos. Except the pathway from micropyle to embryo, there was no isotope trace autoradiography spot in other part of nucelli and pollen tube which entered the embryo. In addition, it was observed that micropyle was close state before pollen tube arrived, and when pollen tube arrived at ovule, micropyle opened. Experiments confirmed that the nucelli pathway of pollen tube after self pollination was the only pathway that heterologous DNA entered the embryo from micropyle.

Huang^[4] transferred GFP gene into cotton and obtained transformed young embryo plants through measurement of fluorescence microscope and handled ultraviolet purple and molecular hybridization. The results provided dependable cell and molecular biology proofs for the possibility of pollen-tube transformation technique.

In a report^[5], the gramineous expression vectors pGU4AGBar and pGBI4AGBar were used, respectively. The s gna gene, a synthetical agglutinin gene of Galanthus nivivis, had been transferred into the winter wheat varieties Xinong 2208 and Xinong 132 by pollen-tube pathway. The PCR and Southern blotting analysis showed that 20 transgenic plants with s gna gene were obtained. Western blotting analysis revealed that the target protein was expressed in the transgenic plants. The transformation frequency was 0.28%–0.84%.

The cryIa gene, a synthetical insecticidal crystal protein gene of *Bacillus thuringiensis*, was transferred into the wheat varieties Xinong 2208 and Xinong 132 using the gramineous expression vector pGU4ABBar by pollen-tube pathway. By PCR and Southern blotting analysis 27 transgenic plants with cryIa gene were obtained. Western blotting analysis showed that the protein was expressed in the transgenic plants. The transformation frequency was about 1.13%–1.21%^[6].

[☆]Supported by the National Natural Science Foundation of China (No. 10505018).

*Corresponding author. Tel: 86-371-6776-7728; Email: guyunhong@zzu.edu.cn

Wang^[7] transformed *bar* gene into indica cultivars E32 and obtained transformed plants which had resistance to herbicide basta. The result confirmed *bar* gene had integrated and expressed in transformed plants.

15 seeds of D0 were obtained by pollen-tube pathway transformation method, using plasmid pBI121 with *NPTII* gene and *GUS* gene as donor, and using rice breed of Teqing NO. 2 as transgenic acceptor^[8]. 1500 seeds of D1 were obtained by breeding D0 seeds. 18 green seedling were obtained when the seeds haired in the Kana water. Distill the DNA of the green seedling, using the probe with the *NPTII* gene segment, the southern result reported heterologous DNA had integrated into the rice genome.

The leaf senescence inhibition gene *P_{SAG12}-IPT* was used to improve wheat varieties that had disadvantage of leaf presenility^[9]. With wheat cultivar Xinong 1376 as material, 5 transgenic plants were obtained through pollen tube pathway mediated transformation. By means of PCR amplification, GUS histochemical analysis, Dot and Southern blot hybridization, the target gene with specific promoter was demonstrated to integrate into the wheat genome already. The *P_{SAG12}-IPT* gene could inherit steadily in the most transgenic plants. The leaf cytokinin, chlorophyll, senescence development and agronomical character of transgenic plants were discussed. The results indicated that *P_{SAG12}-IPT* gene might specifically express in the senescent leaf of some transgenic plants, and the leaf senescence was obviously delayed.

Chalcone synthase-A (CHSA) was a key enzyme in the biosynthesis of all classes of flavonoids, and alteration of its expression might affect the colour of flowers. CHSA gene was cloned from flowers petals of *petunia* (*Petunia hybrida*) just coming into bloom, and was inserted into expression vector – pBI121 and pWM101, which contains CaMV 35S promoter in a sense-orientation^[10]. First transferred *Cyclamen persicum* via pollen-tube pathway of germ line transformation. More than 4400 seeds were gotten. Among them the transgenic plants had altered the flower colour. Yellow or light yellow spots took on the edge of some petals in 8 plants with white flowers, even the whole petal turned yellow. Half petal of a few turned peach(Er qiao) among 3 plants with white flowers, even the whole flower turned peach. PCR assay of the transgenic Cyclamen plant is positive.

The above molecular biology evidence found the theoretical basis for application of pollen-tube pathway transformation in genetic breeding.

3 Optimization of Pollen-tube Pathway Technique

When heterologous DNA was sent into ovary in certain time after pollination, the heterologous DNA

could enter into embryo sac by itself. Recombinant plasmid with target gene or donor total DNA that the target gene wasn't separated, could use the technique to transform. The technique operation was simple, but some condition need explore and optimize, for example weather term while transformation, different flower structure, pollination time, the density of DNA and teach melting agent.

Maize and cotton had the bigger flower structure than others', and could adopt the ovary injection. But small flower botany such as rice adopted instilling method. Both right method and transformation time were needed to notice. Cotton pollen tube arrived at ovary 8 hours after blooming^[11]. While 20 hours, the pollen-tube pathway became. While 20–24 hours, bolt structure became from neck outer edge to ovary, and affected the DNA enter ovary. While 1–3 hours after rice self pollination, 1/3 hull could be removed, and distilled the heterologous DNA^[12]. Also some people thought that 2–3 hours after rice self pollination was fitter. While 0.5–3 hours after wheat blooming, feather-like neck could be cut and distilled DNA solution immediately^[13]. Because 50 hours was needed to complete the fertilization process, the fitter transformation time should be chosen at 10–20 hours after blooming^[14]. The soybean was cleistogamy pollination crop. While 6 hours after self pollination fertilization started. So 6 hours after self pollination was a right time to distill DNA solution. The best period of pollen-tube pathway transformation technique was 6–20 hours after pollination^[15]. Anyway, it was necessary to choose the right time to transformation, and couldn't cut neck too early and led to fertilize disfully and the fruit fall.

The density of the target DNA was also a very important parameter in transformation. The most suitable density of different crop was different, for example the wheat use 100–300 µg/ml, also use 700 µg/ml and obtained better transformation result; soybean was 300–500 µg/ml; the rice was 100 µg/ml, cucumber was 1000 µg/ml. the certain DNA pure degree was necessary, OD260/OD280 > 1.8 and OD260/OD230 > 2 could meet the request.

4 The Advantages and Shortages of Pollen-tube Pathway Transformation Technique

The operation of pollen-tube pathway transformation technique was done at receptor plant, and didn't touch with the receptor cell directly. It had no dependence to species and cultivars. Theoretically, it could apply in any flower botany. Recombinant plasmid with target gene or donor total DNA that the target gene wasn't separated, could be used in this technique. And it wasn't necessary to know the genetic back of the donor and the acceptor plant. It wasn't restricted by

genotype.

It needn't the tissue culture process, and overcame the technique obstacle of transformation receptor regeneration. Seeds could be obtained directly, reduced the variety possibility in process of vitro transformation, especially for the plant that it was difficulty to regenerate in *vitro* culture; it had the great application value in heterologous DNA transformation.

It could be operated in field experiment environment. Transformation frequency was higher, but need to be aimed at the flower structure, blooming behaviour, fertilization process, temperature and humidity while transformation. The stability time of transformation offspring was shorter than traditional breeding process. For example, cotton and rice need 3–4 generation to obtain stability variety using the technique. The shortcoming of the technique was that it could be used only in blooming botany, and that it could be operated only in flowers period. If using total DNA to transformation, some unwanted gene DNA segment would be transformed. And it was reported the transformation offspring would bring variety.

References

- Zhou GY, Gong ZZ, Wang ZF. The molecular basis of remote hybridization: an evidence of the hypothesis that DNA segments of distantly related plants may be hybridized. *Acta Genetica Sinica* 1979; 6(4): 405–13.
- Zhou GY, Zeng Y, Huang J, et al. Introduction of exogenous DNA into cotton embryos. *Methods in Enzymology* 1983; 101: 433–48.
- Gong ZZ, Shen WF, Zhou GY, et al. Technique of transformation exogenous DNA into plant after pollination-DNA fragments were transferred into embryos via pollen tube. *Science in China (B)* 1988; 6: 611–4.
- Huang GC, Dong YM, Sun JS. Transformation exogenous DNA via pollen tube pathway with GFP gene. *Chinese Science Bulletin* 1998; 43(23): 2531–3.
- Hou WS, Guo SD, Lu M. Development of transgenic wheat with Galanthus nivalis Agglutinin gene(s *gna*) via the pollen-tube pathway. *Chinese Bulletin of Botany* 2003; 20(2): 198–204.
- Hou WS, Guo SD, Lu M. Development of transgenic wheat with a synthetical insecticidal crystal protein gene via pollen-tube pathway. *Acta Agronomica Sinica* 2003; 29(6): 806–9.
- Wang CL, Zhao L, Zong SY, et al. Inheritance of herbicide resistance in offsprings of bar transgenic rice (*Oryzopsis tival*.) obtained by pollen tube pathway method. *Acta Agronomica Sinica* 2004; 30(4): 403–5.
- Chen CH, Wang ZJ, Sun L, et al. Research of transformation exogenous DNA into rice via pollen tube pathway. *Guang Dong Agriculture Science* 1998; 4: 2–3.
- Xi YJ, Lin YJ, Zhang QF, et al. Studies on introduction of leaf senescence-inhibition gene PSAG12-IPT into common wheat through pollen-tube pathway. *Acta Agronomica Sinica* 2004; 30(6): 608–12.
- Zhao WL, Jiang SP, Fu XS, et al. Introduction of chalcone synthase-A (CHSA) gene into cyclamen per-sicum via pollen-tube pathway. *Molecular Plant Breeding* 2005; 3(4): 531–6.
- Huang JQ, Qian SY, Liu GL, et al. Variations in the characters of upland cotton (*Gossypium hirsutum*) induced by exotic DNA of sea-island cotton (*Gossypium barbadense*). *Acta Genetica Sinica* 1981; 8(1): 56–62.
- Duan XL, Chen SB. Variation of the characters in rice (*Oryza sativa*) induced by foreign DNA uptake. *Scientia Agricultura Sinica* 1985; 3: 6–10.
- Yan XF, Liu YX, Hu XY. Preliminary report on the effects of exogenous DNA treatment on seeds and seedling and florals of wheat and induced variation. *Acta Agriculturae Universitatis Henanensis* 1991; 25(4): 359–65.
- Chen HY, Zhang JH, Zhuang TM, et al. Developing new germplasms of *Lycopersicon esculentum* for salt tolerance by pollen tube method. *Acta Bot Boreal-Occident Sin* 2004; 24 (1): 12–6.
- Wu JJ, Xu PF, Zhang SZ. Several problems in soybean breeding transformation exogenous DNA via pollen tube pathway. *Soybean Bulletin* 2005; 4: 6.

Monitoring phytoplankton diversity in the hill stream Chandrabbaga of Garhwal Himalaya

Archana Sharma¹, Ramesh C. Sharma^{1,*}, Ashish Anthwal^{1,2}

¹Department of Environmental Sciences, H. N. B Garhwal University, P. Box-67, Srinagar Garhwal 246174, Uttarakhand, India;

²G. B. Pant Institute of Himalayan Environment and Development, Garhwal Unit, P. Box-92, Srinagar Garhwal 246174, Uttarakhand, India

Received October 4, 2006

Abstract

Phytoplanktonic diversity and abundance of hill stream Chandrabhaga have been monitored for the present study from October 2000 to September 2001. A total of 31 genera of phytoplankton belonging to the families Bacillariophyceae, Chlorophyceae and Cyanophyceae were identified. These comprised of diatoms (95%), green algae (2.8%), blue green algae (1.6%) and miscellaneous (0.8%). The diversity of phytoplankton was found to be maximum during winter and minimum in monsoon. The study revealed that water current, water temperature and turbidity influenced the diversity of phytoplankton. [Life Science Journal. 2007;4(1):80 – 84] (ISSN: 1097 – 8135).

Keywords: phytoplankton; algae; hill stream; Chandrabhaga; Himalaya

1 Introduction

The ultimate aim of ecology is to study the interaction of organisms with their environment and the other organisms living in it (Wilson, 1992; Krebs, 2001). Riverine ecosystems are the integral and important component of freshwater ecosystems. However, the mountain fluvial ecosystem is unique as well as distinct in all aspects. The Chandrabhaga is a typical perennial hill stream and is one of the many tributaries of upper Ganges. The entire stretch of the stream has rich riparian vegetation for providing conducive environment for the growth of aquatic organisms. Many studies in the headwater streams have shown that the freshwater contain representatives of benthic flora and fauna, washed up from the streambed. Continuous downstream movement of clear water with much dissolved and suspended matter characterize these streams. The limnological parameter of freshwater bodies is of great significance, as these play a vital role in restricting the distribution of any species within a certain range of ecosystem habitat. High mountain lakes have attracted the interest of limnologists for a long time, mainly because of their extreme climatic and physicochemical conditions. Despite the large amount of literature available on the spatial and temporal variations in phytoplankton in lakes, little information is available on their distribution in hill stream.

The phytoplankton of high altitude cold water are most distinct than those of any other type of aquatic habitat and include a large percentage of species which are restricted to this particular habitat. These provide the main food item of fishes directly or indirectly and can be used as indicator of the trophic phase of water body. Phytoplankton abundance is controlled by several physicochemical factors of water. The dominant genera in algal groupings change not only spatially but seasonally as physical, chemical and biological conditions change in water body. A general pattern of seasonal succession of phytoplankton has been correlated with environmental factors of many lakes. According to Crayton and Sommerfield (1979), phytoplankton abundance and species richness appeared to be influenced by high turbidity, water velocity, fluctuating water level and age of water.

Many species of river phytoplankton reproduce prolifically in rivers and achieve biomass levels of 250 μg chlorophyll (Friedrich and Viehweg, 1984; Gliwicz *et al*, 1985; Reynolds, 1988, 1994; Reynolds *et al*, 1994). Diatoms usually dominate in the plankton of rivers and streams, particularly in winter. Perenniation of phytoplankton in rivers arises from surviving periphytic and benthic populations (Reynolds and Descy, 1996). The present investigation was aimed at determining quantitative composition of phytoplankton in the hill stream Chandrabhaga.

2 Investigated Area

The Chandrabhaga catchment is one of the micro-

*Corresponding author. Tel: 91-1370-267740; Fax: 91-1370-267740; Email: drrameshcsarma@yahoo.com

watersheds of the river Alknanda in the Pauri Garhwal district of Uttarakhand. Chandrabhaga stream originates from the Chandrabadni area (2,278 m above m. s. l.) and make confluence with the river Alknanda at Bagwan (500 m above m. s. l.). The study area is located between latitude $30^{\circ} 13' 15'' - 30^{\circ} 18' 20''$ N and longitude $78^{\circ} 36' 20'' - 78^{\circ} 40' 18''$ E.

Three sampling sites, one each in all the three zones (upper, middle and lower) of the hill stream Chandrabhaga were selected. The first sampling site (S_1) was selected at Pataun (940 m above m. s. l.). This site was a riffle zone and downstream to the source of the stream. The substrata of this site constituted mostly of cobbles and pebbles and only few big boulders were found in the area. The second site (S_2) was selected at Bhatgaon (720 m above m. s. l.) in the middle stretch of stream. This site was the pool section of the river. The substrata at this site were constituted of pebbles with sand and clay. The third sampling site (S_3) was selected at Bagwan (500 m above m. s. l.) just before the confluence with the river Chandrabhaga. This site was a riffle zone with sparsity vegetation. The general vegetation of the study area shows the dry climate of the region. The Chandrabhaga stream is the fourth order stream and has two third order streams except few first order streams having their discharge through perennial springs which is used by the local inhabitants.

3 Materials and Methods

Monthly sampling was conducted during the period of October 1999 – September 2000 from all the three sampling sites for recording physicochemical variables and phytoplankton density. The water (100 litres) was sieved through number 20 plankton net, concentrated into a 60 ml vial and preserved in 5% formaldehyde. 60 ml of samples were concentrated to 20 ml by centrifugation. A Hensen-Stempel pipette was used to take 1 ml aliquots into four Sedgewick Rafter counting chambers. Each cell was then examined under microscope for identification and counting. The phytoplankton identification was done following Welch and Ward and Whipple.

Water temperature was recorded with a centigrade ($0 - 110^{\circ}\text{C}$) thermometer. The mean velocity was measured using electromagnetic current meter (Model-PVM-2A). pH was determined by pH meter on the spot and in the laboratory by control dynamics pH meter (Model-APX15/C), while turbidity was measured with the help of Metzer digital turbidity meter. The physicochemical parameters were monitored following Apha.

4 Results

4.1 Aquatic environment

Monthly variations in physicochemical attributes

have been presented in Table 1. The air temperature was found to be maximum in the month of September (25.3 ± 2.30) and minimum (16.5 ± 2.2) in January. Maximum water temperature was recorded in June (27 ± 1) and minimum (14.1 ± 2.02) in the month of January. Water current remained high throughout the year but it attained the peak value (2.77 ± 1.77) during monsoon months (July-August) due to frequent flash floods.

Dissolved oxygen was found maximum during the winter months. Turbidity, free carbon dioxide, nitrates, total dissolved solids and phosphates showed a decreasing trend from October to January and then started increasing up to August. Nitrate concentration (0.07 ± 0.002) and phosphate concentration (1 ± 0.01) were recorded high in winter months. Sodium and potassium contents in the hill stream Chandrabhaga showed an irregular trend in their concentrations.

4.2 Taxonomic diversity

A total of 31 genera of phytoplankton belonging to the families Bacillariophyceae (18 genera), Chlorophyceae (8 genera) and Cyanophyceae (5 genera) were recorded during the period of investigation (Table 2). The largest and most diverse group was the Bacillariophyceae (diatoms) which contributed 95.9% of the total phytoplankton. *Achnanthes*, *Cymbella*, *Navicula*, *Amphora*, *Nitzschia* and *Fragilaria* was the dominant genera among diatoms and was present throughout the year. While other diatoms like *Cocconeis*, *Diatoma*, *Gomphonema* and *Synedra* started appearing from autumn to winter and were absent in monsoon. Few genera like *Frustulia*, *Gyrosigma*, *Stauroneis* and *Tabellaria* occurred irregularly.

Green algae (Chlorophyceae) contributed 2.65% of the total phytoplankton. The important genera of green algae recorded were *Spirogyra*, *Ulothrix*, *Zygema*, *Cladophora*, *Closterium*, *Cosmarium* and *Gonatozygon* and blue green algae (Cyanophyceae) by *Anabaena*, *Nostoc*, *Oscillatoria*, *Polycystic* and *Rivularia* were less in abundance during monsoon due to increased turbulence which consequently leads to detachment of algal filaments from the substratum. Similar observations were made by Sehgal (1992) in river Beas, Dobriyal and Singh (1988) in river Mandakini, Kala and Sharma (2001) in river Alknanda.

Seasonal density of phytoplankton dwelling in the hill stream Chandrabhaga are presented in Table 3. In the hill stream river Chandrabhaga maximum phytoplankton density was observed in winter (1,009 units/l) when turbidity (14.6 ± 13.3 NTU) and water velocity (0.67 ± 0.53 m/s) were low. The minimum mean value of phytoplankton (75.88 units/l) was recorded during monsoon month which may be due to high turbidity (93.3 ± 35.11 NTU) and high water velocity (2.77 ± 1.77 m/s).

Winter maxima of phytoplankton have also been recorded by Chakraborty *et al* (1959) and Pahwa and Mehrotra (1966) in river Jamuna and Ganga. Kohler

(1993) on river spree has indicated that in majority of rivers diatoms dominated among the algal communities.

Table 1. Physicochemical characteristics of the aquatic environment of the river Chandrabhaga during the period of October 2000 – September 2001

	Oct	Nov	Dec	Jan	Feb	Mar	Apr	May	Jun	Jul	Aug	Sep
Air temperature (°C)	23. 3 ± 2.3	20. 6 ± 2.08	16. 6 ± 1.15	16. 5 ± 2.2	17. 1 ± 1.6	20. 1 ± 0.76	25 ± 1.73	30. 3 ± 2.08	31. 5 ± 2.12	27. 6 ± 1.52	24. 3 ± 1.52	25. 3 ± 2.30
Water temperature (°C)	20. 5 ± 0.5	18. 8 ± 0.76	14. 6 ± 1.15	14. 1 ± 2.02	14. 6 ± 2.11	17 ± 1	21. 3 ± 2.08	24. 6 ± 1.15	27 ± 1	24. 3 ± 0.57	22. 3 ± 0.57	21. 6 ± 0.57
Water current (m/s)	1. 3 ± 0.97	0. 99 ± 0.89	0. 67 ± 0.53	0. 74 ± 0.38	0. 71 ± 0.27	0. 88 ± 0.42	1. 04 ± 0.66	1. 48 ± 0.82	1. 99 ± 1.19	2. 39 ± 1.38	2. 77 ± 1.77	1. 9 ± 1.4
Hydro median Depth (m)	0. 71 ± 0.58	0. 73 ± 0.67	0. 69 ± 0.66	0. 62 ± 0.7	0. 54 ± 0.62	0. 55 ± 0.72	0. 65 ± 0.94	0. 59 ± 0.85	0. 79 ± 1.16	1. 15 ± 1.21	1. 14 ± 1.16	0. 75 ± 0.59
Transparency (m)	0. 42 ± 0.11	0. 43 ± 0.25	0. 32 ± 0.11	0. 28 ± 0.12	0. 28 ± 0.18	0. 32 ± 0.32	0. 39 ± 0.48	0. 39 ± 0.5	0. 34 ± 0.38	0. 47 ± 0.18	0. 32 ± 0.17	0. 37 ± 0.16
Turbidity (NTU)	36 ± 32.18	53. 3 ± 51.3	14. 6 ± 13.3	18. 6 ± 3.21	33. 3 ± 7.57	28. 3 ± 19.5	44. 3 ± 14.3	30. 3 ± 35.2	22. 3 ± 9.29	50. 6 ± 10.06	93. 3 ± 35.11	58 ± 28.47
pH	7. 9 ± 0.1	8 ± 0.17	8 ± 0.1	8. 1 ± 0.26	8. 06 ± 0.15	8. 01 ± 0.1	8. 13 ± 0.12	7. 73 ± 0.2	8. 13 ± 0.05	8. 06 ± 0.28	7. 87 ± 0.12	7. 93 ± 0.15
Alkalinity (mg/l)	155 ± 13.2	159 ± 1	160 ± 0	156. 6 ± 2.88	153. 3 ± 2.88	151. 6 ± 5.77	181. 6 ± 7.63	202. 3 ± 11.01	217. 6 ± 7.5	221. 6 ± 17.5	178. 3 ± 16.07	165 ± 5
TDS (mg/l)	112. 3 ± 15.69	126. 6 ± 47.25	109. 3 ± 31	121. 2 ± 52.78	106 ± 29.44	144. 6 ± 48.01	126. 6 ± 15.27	144 ± 34.17	149. 3 ± 26.85	155. 6 ± 27.6	171 ± 35.67	113. 3 ± 13.3
D.O. (mg/l)	12. 3 ± 2.02	13. 6 ± 1.65	14. 5 ± 1.1	14. 6 ± 1.2	13. 6 ± 1.04	12. 43 ± 1.2	13. 13 ± 0.8	12. 5 ± 1.5	11. 16 ± 0.28	11. 06 ± 0.92	10. 93 ± 1.2	12. 16 ± 1.25
Free CO ₂ (mg/l)	0. 2 ± 0.13	0. 23 ± 0.05	0. 23 ± 0.02	0. 24 ± 0.04	0. 4 ± 0.1	0. 22 ± 0.14	0. 11 ± 0.14	0. 21 ± 0.18	0. 16 ± 0.14	0. 18 ± 0.16	0. 27 ± 0.02	0. 18 ± 0.05
Nitrates (mg/l)	0. 05 ± 0.005	0. 06 ± 0.005	0. 07 ± 0.002	0. 06 ± 0.02	0. 05 ± 0.004	0. 03 ± 0.005	0. 02 ± 0.002	0. 03 ± 0.006	0. 06 ± 0.007	0. 06 ± 0.003	0. 04 ± 0.007	0. 03 ± 0.005
Phosphates (mg/l)	0. 07 ± 0.008	0. 07 ± 0.003	0. 08 ± 0.003	1 ± 0.01	0. 08 ± 0.002	0. 08 ± 0.002	0. 11 ± 0.005	0. 09 ± 0.002	0. 11 ± 0.01	0. 2 ± 0.01	0. 17 ± 0.007	0. 12 ± 0.01
Sodium (mg/l)	5. 26 ± 1.05	4. 36 ± 0.5	2. 86 ± 0.8	1. 73 ± 1.5	6. 6 ± 3.9	9. 3 ± 0.9	9 ± 0.51	8. 06 ± 0.57	8. 06 ± 0.57	7. 4 ± 0	5. 2 ± 0.45	3. 86 ± 0.28
Potassium (mg/l)	1. 33 ± 0.22	1. 16 ± 1.02	1. 38 ± 0.56	1. 36 ± 0.75	1. 71 ± 0.27	1. 07 ± 0.93	1. 12 ± 1	1. 18 ± 0.99	0. 49 ± 0.78	0. 88 ± 0.77	1. 24 ± 0.41	0. 91 ± 0.95

5 Discussion

In the fluvial ecosystem of Chandrabhaga, several factors were known to influence the distribution of aquatic floral diversity. In the hill streams water temperature, flow and substrate composition may be considered as the major factor controlling the phytoplankton communities (Wetzel, 1983). Factors controlling phytoplankton growth includes light, temperature, water current, substrate, water chemistry and invertebrate grazing, all these factors have potential effects on periphytic populations (Whitton, 1975; Hynes, 1971; Biggs, 1996). Phytoplanktons are sensitive to velocity and turbulence of flow in the streams, thus inhibiting the development of new plankton and suppress any ex-

isting organisms discharged from associated lentic waters. Thus agitated water of rithron in the Chandrabhaga support little plankton at S₁ and S₃ while maximum density is recorded at S₂ the pool section of the stream. Welcomme (1985) also gave similar observations.

According to Hynes water movement, turbidity, temperature and nutrients are the main environmental factors which control the abundance of plankton. Turbidity has a negative impact on the growth of plankton in the river Chandrabhaga. Similar observations have been recorded by Hynes (1971) in Volga River. Ellis states that erosive silt in the rivers acts as an opaque screen to all wavelengths of light not allowing the phytoplankton to carry out photosynthesis. Chandler (1937) and Cushing (1965) report that mechanical destruction

of plankton occurs by the grinding action of water heavily laden with silt. Chankraborty *et al* (1959) reported low densities in fast flow areas and high densities in slow flow areas. Turbidity and water current are the detrimental factor which limits the plankton growth during monsoon. Increased density in winter is due to high transparency and high dissolved oxygen. Thus, there is a combined effect of all the physicochemical factors on the density of phytoplankton in river Chandrabhaga.

The freshwater must be recognized as the blood of society (Wetzel, 2000), despite the extensive discussion and evolution of human needs for water of reasonable quality, it is essential to know how aquatic ecosystem function in order to manage them successfully. Management of stream must be determined in consideration of its significance for conservation on the basis of which management priorities and objectives need to be clearly spelt out.

Table 2. Diversity and seasonal abundance of phytoplankton dwelling the river Chandrabhaga

Taxon	Winter	Summer	Monsoon	Autumn
Bacillariophyceae				
<i>Achnanthes affinis</i>	+++	++	+	+
<i>A. bisoletiana</i>	++	+	-	+
<i>A. brevipes</i>	+		-	-
<i>A. clevei</i>	++	++	+	-
<i>A. exilis</i>	+	+	+	-
<i>A. fragilareoides</i>	+++	++	++	+
<i>A. lanceolata</i>	+	+	-	-
<i>A. lanceolata f. capitata</i>	+	+	-	-
<i>A. lanceolata var elliptica</i>	+	+	+	-
<i>A. lanceolata var rostrata</i>	+	++	-	-
<i>A. ovalis</i>	+	+	-	-
<i>Calonies bacillum</i>	++	-	-	+
<i>C. silicula</i>	+	-	-	+
<i>C. beccariana</i>	++	-	-	-
<i>Ceratoneis arcus</i>	++	+	-	-
<i>Coccneis placentula</i>	++	++	-	-
<i>C. pediculus</i>	+	-	-	+
<i>Cyclotella glomerata</i>	+	-	-	-
<i>Cymatopleura spp</i>	+	+	-	-
<i>Cymbella affinis</i>	+++	+	+	-
<i>C. lacustris</i>	+	-	-	-
<i>C. parva</i>	++	+	-	-
<i>C. turgida</i>	+	+	+	+
<i>Diatoma anceps</i>	+++	++	-	+
<i>D. vulgare</i>	++	+	-	-
<i>Eunotia arcus</i>	++	+	+	-
<i>E. pectinalis</i>	+	-	+	+
<i>Frazilaria capucina</i>	+++	+	++	-
<i>F. intermedia</i>	+++	-	+	-
<i>F. lapponica</i>	+++	-	-	-
<i>F. pinnata</i>	+++	-	++	-
<i>Gomphonema gracile</i>	+	-	+	+
<i>G. longiceps</i>	+++	-	+	+
<i>G. subtile</i>	+	+	+	-
<i>Hantzschia spp</i>	+++	++	-	-
<i>Meridion circulare</i>	++	-	-	-
<i>Navicula bacillum</i>	++	-	+	-
<i>N. radiosa</i>	+++	+	-	-
<i>N. rostellata</i>	+	+	-	+
<i>Nitzschia amphibia</i>	+++	+	-	-
<i>N. capitella</i>	++	-	-	-
<i>N. denticulata</i>	++	+	-	-
<i>N. dissipata</i>	+	++	-	+
<i>N. hantzschiana</i>	++	-	-	+
<i>N. hybrida</i>	+	+	+	-
<i>N. linearis</i>	++	+	-	-
<i>Synedra acus</i>	++	+++	-	-
<i>S. rumpens</i>	++	-	-	-
<i>S. ulna</i>	++	++	-	+
Chlorophyceae				
<i>Cladophora glomerata</i>	++	++	-	-
<i>Closterium spp</i>	+	++	+	+
<i>Cosmarium spp</i>	++	++	+	++
<i>Hydrodictyon</i>	+	++	+	+
<i>Microspora</i>	++	+	-	-
<i>Protococcus</i>	+	+	-	-
<i>Spirogyra</i>	++	++	+	+
<i>Gonatozygon</i>	++	+	-	-
<i>Stegeclonium staganatila</i>	++	+	+	++
<i>Tetraspora</i>	++	-	-	-
<i>Ulothrix zonata</i>	++	++	-	-
<i>Zygema</i>	+++	-	-	-
Cyanophyceae				
<i>Anabaena spp</i>	-	+	+	+
<i>Nostoc spp</i>	+	++	+	-
<i>Oscillatoria spp</i>	++	++	-	+
<i>Polycystis spp</i>	+	+	-	-
<i>Rivularia spp</i>	-	++	+	-

+++ : Abundant; ++ : Common; + : Rare; - : Absent

Table 3. Seasonal density of phytoplankton at S₁, S₂ and S₃ of river Chandrabhaga recorded during October 2000 to September 2001

Sites	Phytoplankton	Oct 2000 – Sept 2001			
		Winter	Summer	Monsoon	Autumn
S ₁	Bacillariophyceae	1795	1213	85	203
	Chlorophyceae	37	36	45	5
	Cyanophyceae	7	3	19	2
		613 ± 1023.75	417.33 ± 689.26	49.66 ± 33.24	70 ± 115.19
S ₂	Bacillariophyceae	4830	2988	318	608
	Chlorophyceae	103	103	28	9
	Cyanophyceae	42	13	32	1
		1658.33 ± 2746.91	1034.66 ± 1692.23	126 ± 166.28	206 ± 348.16
S ₃	Bacillariophyceae	2230	1761	110	309
	Chlorophyceae	33	45	30	11
	Cyanophyceae	10	6	16	3
		757.66 ± 1275.13	604 ± 1002.18	52 ± 50.71	107.66 ± 174.40
Mean ± SD		1009.66 ± 566.39	685.33 ± 316.59	75.88 ± 43.41	127.88 ± 70.21

References

- Biggs BJF. Patterns in benthic algae of streams. In Algal Ecology: Freshwater Benthic Ecosystems (eds. Stevenson RJ, Bothwell ML, Lowe RL), Academic Press, New York 1996; 256 – 96.
- Chakraborty RD, Roy P, Singh SB. A quantitative study of plankton and the physicochemical conditions of the river Yamuna at Allahabad in 1954 – 55. Indian J Fish 1959; 61: 186 – 208.
- Chandler OC. Fate of typical lake Plankton in streams. Ecol Monogr 1937; 7: 445 – 75.
- Crayton WM, Sommerfield MR. Composition and abundance of phytoplankton in tributaries of the lower Colorado river, Grand Canyon region. Hydrobiologia 1979; 66: 81 – 93.
- Cushing EC. Plankton and water chemistry in the Montreal River lake stream, Saskatchewan. Ecolog 1965; 45: 306 – 13.
- Dobriyal AK, Singh HR. Ecological basis for ichthyofaunal variations in two hill streams of Garhwal Himalaya. Ibid 1988; 3: 30 – 4.
- Friedrich G, Viehweg M. Recent developments of the phytoplankton and its activity in the lower Rhine. Verh Internat Verein Limnol 1984; 22: 2029 – 35
- Gliwicz ZM, Dawidowicz P, Pijanowska J. Structure of phytoplankton in rivers and in lakes of north eastern Poland. Ekol Polska 1985; 33: 537 – 46.
- Hynes HBN. The Ecology of Running Waters. Liverpool University Press, Liverpool 1971; 1 – 555.
- Kala R, Sharma C. Seasonal abundance of phytoplankton in the lotic ecosystem of Alaknanda, Garhwal Himalaya. J Natural and Physical Sciences 2001; 15(1 – 2): 71 – 80.
- Kohler J. Growth, production and losses of phytoplankton in the lowland river Spree 1-Population dynamics. J Plankton Res 1993; 15: 335 – 49.
- Krebs CJ. Ecology. 5th ed, Addison-Wesley, San Francisco 2001; 695.
- Pahwa DV, Mehrotra SN. Observations in the abundance of plankton in relation to certain hydrobiological conditions of river Ganges. Proc Natl Acad Sci 1966; 36(2): 157 – 89.
- Reynolds CS. Potamoplankton: Paradigms, paradoxes and prognoses. In F. E. Round (ed) Algae and the Aquatic Environment. Biopress Ltd Bristol 1988; 285 – 311.
- Reynolds CS. The long, the short and the stalled: On the attributes of phytoplankton selected by physical mixing in lakes and rivers. Hydrobiologia 1999; 289: 9 – 21.
- Reynolds CS, Descy JP. The production, biomass and structure of phytoplankton in large rivers. Arch Hydrobiol Suppl 1996; 113: 161 – 87.
- Reynolds CS, Descy JP, Podisak J. Are phytoplankton dynamics in rivers so different from those in shallow lakes? Hydrobiologia 1994; 289: 1 – 7.
- Sehgal KL. Review and status of coldwater fisheries research in India. NRC-CWF, Spl Publ 1992; 3: 60.
- Ward HB, Whipple GC. Freshwater Biology. 2nd ed, John Wiley and Sons, New York 1992; 1248.
- Wash DC: APHA. Standard methods for the examination of water and wastewater. American Public Health Association. 17th ed, New York, USA 1989.
- Welch PC. Limnology. Mc Graw Hill Book Corn Inc, London 1952.
- Welcomme RL. River Fisheries. FAO Fisheries Technical Paper 1985; 262: 330.
- Wetzel RG. Limnology. Saunders Publishers, Philadelphia 1983; 1 – 650.
- Whitton BA. River Ecology. University of California Press, Berkeley 1975; 215.
- Wilson EO. The Diversity of Life. Penguin Books, London 1992; 406.

Extraction method of soil microbial DNA for molecular ecology research

Jinyong Huang^{1,*}, Wei Zhou¹, Linhai Chen²

¹Department of Bioengineering, Zhengzhou University, Zhengzhou, Henan 450001, China; ²Henan Key Laboratory of Ion Beam Bioengineering, Zhengzhou University, Zhengzhou, Henan 450001, China

Received October 14, 2006

Abstract

The effective of three soil DNA extraction methods which based on different lytic principles for isolation of the total farmland microbial DNA were compared and comprehensive evaluated for the yields and purity. The results show that the chemical-enzymatic-mechanical method got the highest total DNA yield, but with the highest humic acid contamination which will strongly restrain the following PCR and DGGE analysis. The chemical-enzymatic method obtained the best DNA with the highest molecular weight and purity and was more propitious to molecular ecology study. [Life Science Journal. 2007;4(1):85–88] (ISSN: 1097–8135).

Keywords: molecular ecology; soil microbial DNA; extraction method

1 Introduction

Soil is the most important habitat for microbes. Any change of the environment can influence the composition of the microbial community, and a certain environment has its unique microbial composition. So the diversity of the microbial community in soil is an important issue in modern soil microbiology^[1]. Routine methods for detection of bacteria in soil usually use methods which are based on the culture method, by which only 0.1% – 3% of the total bacterial population can grow under laboratory condition with artificial media^[2]. So the result can't truly reflect the original community composition of the soil. In order to solve this problem, many molecular strategies were introduced to the soil ecology study^[3]. Molecular methods which analyse DNA directly extracted from the soil samples can study microbial diversity in soil samples without cultivation^[4,5]. Now the soil DNA analysis has replaced the soil bacterial culture to evaluate the microbial diversity in the ecology study^[6]. The molecular techniques based on total community DNA extracted from soil have been widely applied^[7]. These include community DNA hybridization^[8], single-strand-conformation polymorphism (SSCP) analysis of PCR products of 16S rDNA^[9], denaturing gradient gel electrophoresis (DGGE) and temperature gradient gel electrophoresis (TGGE)^[7], and so on. However, extraction of DNA is not simple, as the soil contains a number of compounds such as humic acids,

phenolic compound and heavy metal^[10]. So the critical step is separation of DNA from humic substance since these are acid macromolecules. That will interfere with the following PCR amplify and other molecular analysis^[4]. Thus, the application of a proper DNA extraction protocol is critical^[10]. As PCR is critical for the following molecular analysis, it's important to identify the DNA function by PCR analysis.

In this study, we compared three DNA isolation methods which stand for three different techniques based on their lytic principle. They are the typical delegate of chemical-enzymatic method, chemical-mechanical method and chemical-enzymatic-mechanical method. The three way of soil DNA extraction will be valued with same samples. Attention was paid to the efficiency, the quality (the fragment size) and the yield of the different extraction method, and the DNA function will be compared by PCR with 2 primers.

2 Materials and Methods

2.1 Soil sample

The soil was sampled under the ground at the deep of 0 – 10 cm and 20 – 30 cm respectively on the farmland, located at Gouzhao of Zhengzhou, China, which was rotated maize and wheat for more than 10 years. The samples were stored at –20 °C during the experiment period.

2.2 DNA isolation

Three DNA extraction methods were applied in parallel, 5 g sample was used for each method. The key differences of the three methods were listed in Table 1.

Method 1 was the chemical-enzymatic method, in

*Corresponding author. Email: jinyhuang@zzu.edu.cn

which the nucleic acids were extracted by the modified protocol^[11]: 5 g of soil samples, 13.5 ml of DNA extraction buffer (100 mM Tris pH 8.0; 100 mM sodium EDTA, pH 8.0; 100 mM sodium phosphate, pH 8.0; 1.5 M NaCl; 1% CTAB) and 100 μ l Proteinase K (10 mg/ml) in a oakridge tube. Those were mixed with by horizontal shaking with 225 rpm at 37 °C for 30 minutes to get the sample mixture. Add 1.5 ml of 20% SDS to the sample mixture and to be incubated for 2 hours at 65 °C water bath with gentle inversion each 15—20 minutes. To be extracted by the centrifuge with 6000 rpm for 10 minutes at room temperature and transfer the supernatant to a 50 ml centrifuge tube. Continue to be extracted two times by adding 4.5 ml of the extraction buffer and 0.5 ml of 20% SDS with 10 seconds. Vortex, incubating at 65 °C for 10 minutes and centrifuge too. Transfer and combine the three times extraction supernatant to a 50 ml centrifuge tube.

Method 2 was the chemical-mechanical method which was derived from Kuske's^[12] method. 10 ml of TENS buffer (50 mM Tris, pH 8.0; 20 mM disodium EDTA; 100 mM NaCl; 1% sodium dodecyl sulfate) was added to 5 g soil samples, then to be mixed thoroughly by vortex and to be incubated in a 70 °C water bath for 1 hour. The samples were mixed well at 15-minute intervals during the incubation, and then were centrifuged at 6000 rpm for 10 minutes, and the supernatant was collected. The soil pellet were washed with 5 ml of TEN buffer (TENS buffer without sodium dodecyl sulfate) and centrifuged again. Drop the supernatant and then the soil pellet was re-suspended in 7.5 ml of TEN buffers and exposed to three sets of thermal shocks by immersion of the tubes at -20 °C for 10 minutes. Followed by rapid thawing in a 65 °C water bath. After centrifugation at 6000 rpm, the supernatants were collected.

Method 3 was the chemical-enzymatic-mechanical method invented by Tsai^[13]. 5 g soil samples were mixed with 10 ml of 120 mM sodium phosphate buffer (pH 8.0) by shaking at 150 rpm for 15 minutes. The slurry was palletized by centrifugation at 6000 rpm for 10 minutes. The pellet was washed again with phosphate buffer, re-suspended in 10 ml of lyses solution I (0.15 M NaCl; 0.1 M disodium EDTA, pH 8.0) containing 15 mg of lysozyme/ml, and incubated in a 37 °C water bath for 2 hours with agitation at 20 to 30 minutes intervals, and then 10 ml of lyses solution II (0.1 M NaCl; 0.5 M Tris-HCl, pH 8.0; 10% sodium dodecyl sulfate) was added. Three cycles of freezing in -20 °C and thawing in a 65 °C water bath were conducted to release DNA from the microbial cells in the soil, and then centrifuged at 6000 rpm for 15 minutes to get the supernatants.

Each supernatant which got from the different

methods was mixed with an equal volume of chloroformisoamyl alcohol (24:1, vol/vol). The aqueous phase was recovered by centrifugation and precipitated with 0.6 volume of isopropanol at room temperature for 1 hour. The pellet of crude nucleic acids was obtained by centrifugation at 12000 rpm for 20 minutes at room temperature, washed with cold 70% ethanol, and re-suspended in sterile deionized water, and to give a final volume of 500 μ l.

Table 1. Treatments for soil sample lyses in different methods

Method	Lyses treatment		
	Mechanical	Chemical	Enzymatic
1	SDS CTAB	Proteinase K	
2	SDS		Freezing and thawing
3	SDS	Lysozyme	Freezing and thawing

The DNA quality and quantity were compared and estimated by agarose gel electrophoresis and spectrophotometry.

Samples of extracted DNA were analyzed in 0.8% agarose gel containing 1 μ g of ethidium bromide per ml. To determine the quality of extracted DNA, the concentration of DNA in the crude extraction was determined spectrophotometrically at 260 nm. Spectrophotometric A260/A280 and A260/A230 ratios were determined to evaluate levels of protein and humic acid impurities, respectively^[11].

2.3 PCR analysis

The DNA was purified with the TaKaRa agarose gel purification kit. And then we used two different universal primers to amplify the 16s rDNA and the V3 fragments. F338gc and R518 were used to amplify the V3 fragments sized about 260 bp^[7], BR8 and BL1541 were used to amplify the 16s rDNA fragments sized about 1500 bp^[13], and the PCR reaction system and cycling condition have been described previously^[7,11]. The PCR products were analysed by electrophoresis in 1.5% agarose gels and ethidium bormide staining.

3 Results

Figure 1 showed that the quality of the DNA extracted from the two soil samples with the different method have notable difference. DNA isolated from method 1 yielded fragments of larger molecular size than the other method. From the electrophoresis result in the agarose gel we can see that, the amounts of DNA extracted from the two samples differed greatly. With the first method we got high molecular weight and few small DNA fragment. The fragment is larger than 20 bp. The DNA got by the other two methods was not very good, as the fragments of the DNA are not identical and yield

broad spectra. And the second method is better than the third one, because it yield lighter broad spectra and higher molecular size. We can also learn that each method has a good reproducibility.

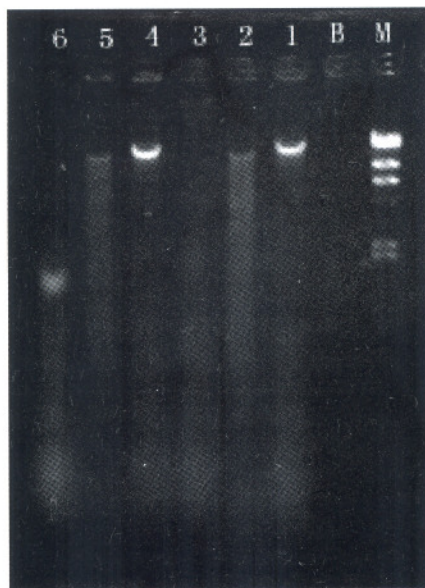


Figure 1. DNA extracted with different method. M: Marker digested by λ -Hind III; B: Blank; Lane 1 and Lane 4: DNA extracted by method 1; Lane 2 and Lane 5: DNA extracted by method 2; Lane 3 and lane 6: DNA extracted by method 3.

The effect of three different methods on DNA yield and purity is apparent in the Table 2. It shows that the quality and purity of the DNA got from three different methods are discrepant. The absorbency under 260 nm stands for the concentration of the DNA, and the absorbency under 280 nm and 230 nm show us the content of the protein and humic substance. The purity of DNA was assessed spectrophotometrically by calculating A260/A230 and A260/A280 ratios for humic acid contamination and protein impurities respectively. Though the quality of the DNA yield from the first method is lower than the other two methods, the purity is higher. So the first method which is based on chemical-enzymatic method is reproducible and has high efficiency.

Table 2. The OD of the DNA extracted by different methods

Method	Deep (cm)	OD				
		230 nm	260 nm	280 nm	A260/ A280	A260/ A230
1	0—10	0.319	0.267	0.230	1.161	0.837
	10—20	0.267	0.240	0.189	1.270	0.899
2	0—10	0.464	0.361	0.312	1.157	0.780
	10—20	0.340	0.239	0.209	1.144	0.703
3	0—10	0.842	0.339	0.409	0.829	0.403
	10—20	0.653	0.410	0.380	1.079	0.628

DNA isolated using different methods were amplified with universal bacterial primers in PCR reactions, and the result was shown in Figure 2 and Figure 3. PCR amplification of the 16S rDNA and the V3 fragments were successful by method 1 and method 2, but failed to get any PCR fragment by method 3. And the quality and yield of the product got by method 1 are best. This result also indicated that the chemical-enzymatic method is more suitable for the microbial molecular ecology research.



Figure 2. Agarose gel electroctiophoresis of 16s rDNA amplified by different DNA. M: DL2000; B: Blank; Lane 1 and Lane 2: DNA extracted by method 1; Lane 3 and Lane 4: DNA extracted by method 2; Lane5 and Lane 6: DNA extracted by method 3.

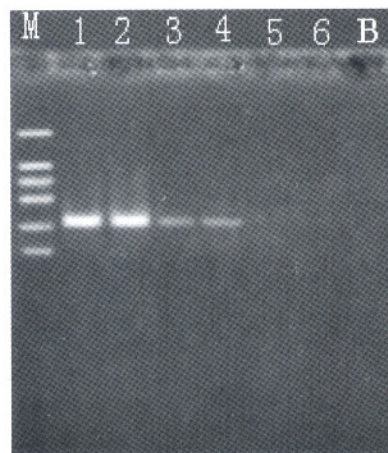


Figure 3. Agarose gel electroctiophoresis of the V3 fragments amplified by different DNA. M: DL2000; B: Blank; Lane 1 and Lane 2: DNA extracted by method 1; Lane 3 and Lane 4: DNA extracted by method 2; Lane5 and Lane 6: DNA extracted by method 3.

4 Discussion

A large number of methods have been published for the extraction of total microbial community DNA from

soils^[4,11,12,13]. We can classified them into three kinds of method by their lytic principles: chemical-enzymatic, chemical-mechanical and chemical-enzymatic-mechanical method. Our result shows that with the chemical-enzymatic method, we can get the best DNA with high molecular weight and purity. The help of enzyme and the chemical substance such as SDS and CTAB can make the cell lyses more efficiency. But with the freezing and thawing method, when the cell was destroyed, the DNA fragments were also broken. So the DNA got with the other two methods is smeared. So the DNA extracted with the enzyme and chemistry substance is more efficient. It's more suitable for the further molecular analysis.

References

1. Wang YS, Wen CY, Chiu TH, Yen JH. Effect of fungicide iprodione on soil bacterial community. *Ectotoxicology and Environmental Safety* 2004; 59: 127 – 32.
2. Amann RI, Ludwig W, Schleifer KH. Phylogenetic identification and in situ detection of individual microbial cells without cultivation. *FEMS Microbiology Reviews* 1995; 59: 143 – 69.
3. Schloter L, Lebuhn M, Heulin T, Hartmann A. Ecology and evolution of bacterial microdiversity. *FEMS Microbiology Reviews* 2000; 24: 647 – 60.
4. Niemi RM, Heiskanen I, Wallenius K, Lindström K. Extraction and purification of DNA in rhizosphere soil sample for PCR-DGGE analysis of bacterial consortia. *Journal of Microbiological Methods* 2001; 45: 155 – 6.
5. Ranjard L, Poly F, Nazaret S. Monitoring complex bacterial communities using culture-independent molecular technique: application to soil environment. *Research in Microbiology* 2000; 151: 167 – 77.
6. Head IM, Saunders JR, Pickup RW. Microbial evolution, diversity, and ecology: a decade of ribosomal RNA analysis of uncultivated microorganisms. *Microbial Ecology* 1998; 35: 1 – 21.
7. Muyzer G, Smalla K. Application of denaturing gradient gel electrophoresis (DGGE) and temperature gradient gel electrophoresis (TGGE) in microbial ecology. *Antonie van Leeuwenhoek* 1998; 73: 127 – 41.
8. Griffiths BS, Ritz K, Ebbelwhite N, Dobson G. Soil microbial community structure: effects of substrate loading rates. *Soil Biology & Biochemistry* 1999; 31: 145 – 53.
9. Lee DH, Zo YG, Kim SJ. Nonradioactive method to study genetic profiles of natural bacterial communities by PCR-single-strand-conformation polymorphism. *Apple and Environment Microbiology* 1996; 62: 3112 – 20.
10. De Lipthy JR, Enzinger C, Johansen K, Aamand J, Sørensen SJ. Impact of DNA extraction method on bacterial community composition measured by denaturing gradient gel electrophoresis. *Soil Biology & Biochemistry* 2004; 36: 1607 – 43.
11. Zhou JZ, Mary AB, James MT. DNA recovery from soils of diverse composition. *Apple and Environment Microbiology* 1996; 62: 316 – 22.
12. Kuse CR, Barns SM, Busch JD. Diverse uncultivated bacterial groups from soils of the arid southwestern United States that are present in many geographic regions. *Apple and Environment Microbiology* 1997; 63: 3614 – 5.
13. Tsai YL, Olson BH. Rapid method for direct extraction of DNA from soil and sediments. *Apple and Environment Microbiology* 1991; 57: 1070 – 4.

Kinetics of methylene blue biosorption by phoenix tree's leaves powder

Weihua Zou¹, Lu Zhu², Shujian Cheng², Runping Han^{2,*}

¹College of Chemical Engineering, Zhengzhou University, Zhengzhou, Henan 450001, China; ²Department of Chemistry, Zhengzhou University, Zhengzhou, Henan 450001, China

Received November 23, 2006

Abstract

The effect of contact time and the determination of the kinetic parameters of biosorption of methylene blue (MB) from aqueous solution onto phoenix tree's leaves powder are important in understanding the biosorption mechanism. The effect of contact time on biosorption quantity was studied at different initial concentration of 30, 70 and 130 mg/l (295 K), and at different temperatures of 295, 309 and 333 K (initial concentration of 130 mg/l), respectively. The pseudo-first-order model and pseudo-second-order model were adopted to fit the experimental data using non-linear regressive analysis and both can describe the adsorptive process. But the pseudo-second-order model was the better choice to express the biosorption behavior according to higher determined coefficient ($R^2 > 0.99$) and the small difference (less than 1 mg/l) between the calculated equilibrium quantity and the experimental equilibrium quantity, suggesting that the biosorption mechanism be a chemisorption process. The intraparticle diffusion model was also used to express the adsorption process at three steps. The activation energy of biosorption (E_a) was determined 15.5 kJ/mol based on the pseudo-second-order rate constants. The lower value of E_a shows that MB biosorption process by leaves powder may be an activated chemical adsorption. The results show that the process of biosorption MB is endothermic process and rise in temperature favors the biosorption. [Life Science Journal. 2007;4(1):89–93] (ISSN: 1097–8135).

Keywords: phoenix tree's leaves powder; biosorption; methylene blue; kinetic; non-linear regressive analysis

1 Introduction

Many industries use dyes to color their products and also consume substantial volumes of water. The presence of small amounts of dyes in water is highly visible and undesirable^[1]. Due to increasingly stringent restrictions on pollutant content of industrial effluents, it is necessary to remove dyes from wastewater before it is discharged into environment.

Adsorption techniques are proved to be an effective and attractive process for removal of non-biodegradable pollutants (including dyes) from wastewater^[2,3]. Activated carbon is commonly used as adsorbent to remove dyes from wastewater due to its excellent adsorption ability. But the high cost limited its widespread use. Many low-cost adsorbents, including natural materials, biosorbents, and waste materials from industry and agriculture, have been proposed by some workers^[4–7].

In China many cities have planted phoenix tree's in main roads, parks and schools. So a lot of phoenix tree's leaves fallen in autumn and often are collected as

waste by cleaners. Like other plant materials, the phoenix tree's leaves contain abundant floristic fiber, protein and some functional groups such as carboxyl, hydroxyl and amidogen etc, which make biosorption processes possible^[8]. Thus the research is needed to develop an alternative technology for utilizing these leaves. Several researchers reported plant-leaf used to adsorb heavy metals from solution^[9–11], but no research was reported about the kinetic of dye biosorption onto fallen leaves.

Methylene blue (MB) is selected as a model compound in order to evaluate the capacity of adsorbents for the removal of MB from aqueous solutions. The researchers had proved several low-cost biomaterials such as giant duckweed, sawdust, and rice husk and cereal chaff could be used for the removal of MB from solutions^[12–15]. The equilibrium and isotherms of MB adsorption by phoenix tree's leaves has been studied, but the kinetic behavior has not been studied^[16]. The aim of this work was to study the kinetic of the utilization of phoenix tree's leaves powder to adsorb MB from aqueous solutions. The kinetic parameters, such as the rate constant of pseudo-first-order adsorption (k_1), the rate constant of pseudo-second-order adsorption (k_2), the

*Corresponding author. Tel: 86-371-6776-3707; Fax: 86-371-6776-7220; Email: rphan67@zzu.edu.cn

constants of intraparticle diffusion model and the apparent activation energy (E_a), were calculated to determine rate constants and adsorption mechanism.

1.1 Kinetic models of adsorption

The models of adsorption kinetics are correlated with the solution uptake rate, hence these models are important in water treatment process design. In order to elucidate the adsorption mechanism and potential rate controlling step, three kinetic models including the pseudo-first-order, the pseudo-second-order and intraparticle diffusion models are tested to fit experimental data obtained from batch MB adsorption experiments^[17-18].

1.1.1 Pseudo-first-order rate equation of Lagergren

The pseudo-first-order equation of Lagergren is generally expresses as follows:

$$\frac{dq_t}{dt} = k_1(q_e - q_t) \quad (1)$$

where q_e and q_t are the amount of MB adsorbed per unit weight of biosorbent at equilibrium and at any time t , respectively (mg/g) and k_1 is the rate constant of pseudo-first-order adsorption (g/mg·min). After integration and applying boundary conditions, for $t=0$, $q=0$, the form of Eq. (1) becomes Eq. (2):

$$q_t = q_e(1 - e^{-k_1 t}) \quad (2)$$

1.1.2 Pseudo-second-order rate equation

The pseudo-second-order equation based on adsorption equilibrium capacity can be expressed as:

$$\frac{dq_t}{dt} = k_2(q_e - q_t)^2 \quad (3)$$

where k_2 is the rate constant of pseudo-second-order adsorption (g/mg·min)

Integrating this equation for boundary conditions for $t=0$, $q=0$ gives

$$q_t = \frac{k_2 q_e^2 t}{1 + k_2 q_e t} \quad (4)$$

1.1.3 Intraparticle diffusion model

The intraparticle diffusion model is

$$q_t = k_i t^{1/2} + C \quad (5)$$

where k_i is the intraparticle diffusion rate constant (g/mg·1/2min), C is the intercept.

The value of q_e , k_1 , k_2 , k_i and C , can be determined using non-linear regressive analysis by least square sum of difference between calculated values and experimental values through the relation of $q_t \sim t$ shown in Eq. (2), (4), (5), respectively.

1.2 Determination of activation energy

The activation energy for MB adsorption was calculated by the Arrhenius equation^[18,19,20]:

$$k = k_0 e^{-\frac{E_a}{RT}} \quad (6)$$

where k_0 is the temperature independent factor in g/mg·min, E_a is the apparent activation energy of the reaction of adsorption in J/mol, R is the gas constant,

8.314 J/mol·K and T is the adsorption absolute temperature, K. The linear form is:

$$\ln k = -\frac{E_a}{RT} + \ln k_0 \quad (7)$$

When $\ln k$ is plotted versus $1/T$, a straight line with slope $-E_a/R$ is obtained.

2 Materials and Methods

2.1 Materials

The phoenix tree's leaves powder was obtained from Zhengzhou city in autumn. The collected materials were washed with distilled water for several times to remove the dirt particles. The washed leaf was dried in an oven at 373 K for 24 hours, then ground and screened through a set of sieves to get different geometrical sizes 40–60 mesh. This produced a uniform material for the complete set of biosorption tests which was stored in an air-tight plastic container for all investigations. The results of element analysis about leaf are 45.8% for carbon, 5.4% for hydrogen, 36.4% for oxygen, 1.0% for nitrogen, 0.1% for sulfur.

The stock solutions of MB were prepared in distilled water. All working solutions were prepared by diluting the stock solution with distilled water to the needed concentration. Both leaf and MB solution were placed in a 50 ml conical flask for adsorptive experiment. Fresh dilutions were used for each biosorption study.

2.2 Methods

The phoenix tree's leaves of 0.02 g were added to each 10 ml volume of MB solution (the pH of initial solution is near 7.5). The initial concentrations of MB solution tested were 30, 70 and 130 mg/l, and the experiments were carried out at 295 K in a constant temperature shaker bath (100 rpm). The samples were then collected at different time intervals and were centrifuged. Then the samples were analyzed using a UV spectrophotometer (Shimadzu Brand UV-3000) to monitor the absorbance changes at a wavelength of maximum absorbance (668 nm).

Batch biosorption tests were also done at different contacting time at the initial concentration of MB 130 mg/l and the temperatures were controlled with a water bath at 309 K and 323 K, respectively.

The data obtained in batch mode studies was used to calculate the MB biosorption quantity at given time. It was calculated by using the following expression:

$$q_t = \frac{V(c_0 - c_t)}{m} \quad (8)$$

Where q_t is the MB biosorption quantity at the given time in mg/g, V is the sample volume, c_0 is the initial MB concentration, c_t is the MB concentration at related given time, and m is the dry weight of the biomass.

3 Results and Discussion

3.1 Effect of contact time on biosorption quantity

Figure 1 showed the effect of contact time on biosorption quantity per gram leaves powder (q_t) at different conditions.

As shown in Figure 1, a third-stage kinetic behavior is evident: a rapid initial biosorption followed by a slower biosorption rate, then the biosorption is near equilibrium with longer period of much slower uptake. The values of q_t increased quickly at initial stage of biosorption. The time to reach step of slower biosorption is significantly different at various initial concentration. The time is long with initial concentration increasing.

Also from Figure 1, the bigger capacity of MB biosorption was observed in the higher temperature. It was due to the increasing tendency of MB ions to adsorb from the solution to the interface with increasing temperature. The increase of the values of q_t at the same given time with increased temperature indicated that the biosorption of MB ions onto leaf was endothermic in nature.

3.2 Analysis kinetic constants

Linear regressive analysis method is simple and convenient, so it is often used to obtain the isotherm and kinetic constants according to the experimental data^[21-25]. But different forms of the equation affected R^2 values more significantly during the linear analysis. The non-linear analysis may be a method of avoiding such errors^[26]. In this paper, a non-linear Chi-square of determination test was used. According to Eq. (2), (4) and (5), the constant of pseudo-first-order and pseudo-second-order models were listed in Table 1 using non-linear regressive analysis. The fitted curves of first and second kinetic model were shown in Figure 1 and Figure 2, respectively.

The equilibrium adsorption quantity became larger with an increase of initial MB concentration. However, both values of k_1 and k_2 decreased for the increase of the initial concentration. And all values of k_1 and $q_{e(\text{theo-1})}$, k_2 and $q_{e(\text{theo-2})}$ increased with the temperature increasing.

From Table 1, the theoretical $q_{e(\text{theo-2})}$ obtained from pseudo-second-order model agreed more perfectly with the experimental $q_{e(\text{exp})}$ values than those from pseudo-first-order model. Furthermore, the determined coefficients (R^2) of second order model were larger than those of first order model, respectively. These showed that the pseudo-second-order biosorption mechanism appear to produce a better model for adsorption in MB/leaf systems at the experimental conditions. So the process could be best described by the second-order equation. The overall rate of MB biosorption process appeared to

be controlled by the chemical process. This suggested that the rate-limiting step may be the chemical adsorption^[23] and the pseudo-second-order kinetic model can be applied to predict the amount of dye uptake at different contact time intervals and at equilibrium.

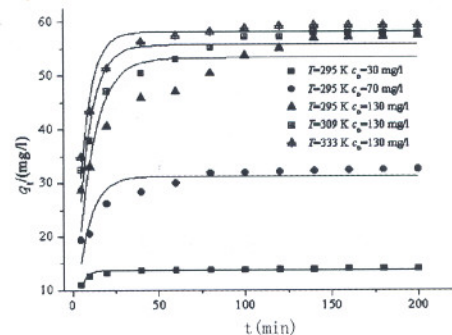


Figure 1. The fitted curves of pseudo-first-order kinetic model and the experimental points at different conditions.

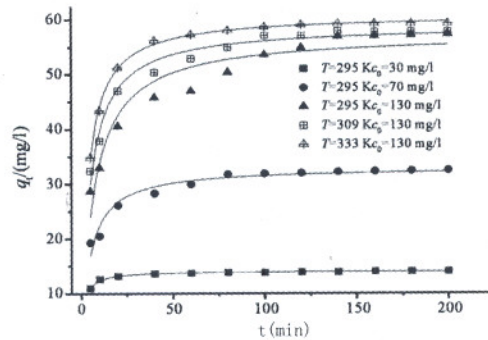


Figure 2. The fitted curves of pseudo-second-order kinetic model and the experimental points at different conditions.

The pseudo-second (or first)-order kinetic model cannot give a definite mechanism of biosorption. So the intraparticle diffusion model is considered as a rate-limiting step^[18,27]. The dye was adsorbed by the exterior surface of the leaf particle at the beginning of biosorption, and the biosorption rate was very fast. As the biosorption of the exterior surface was near saturation, the MB molecular entered into the leaf particle by the pore within the particle and was adsorbed by the interior surface. When the molecular dye diffused in the pore of the particle, the diffusion resistance increased and the diffusion rate decreased^[28,29]. As MB concentration in the solution decreased, the diffusion rate became lower and lower and the diffusion processes reached the final equilibrium stage. Figure 3 was the plot of $q_t \sim 1/t$ with three-step stage at different experimental conditions.

Table 2 listed the parameters of non-linear regressive analysis according to three adsorptive steps. The values of k_{i1} , k_{i2} and k_{i3} increased with initial MB con-

centration rise. The driving force of diffusion was important during biosorption processes. The increases of MB concentration results in increase of the driving force, which will increase the diffusion rate of the molecular dye in pore^[28,29]. The values of k_{i1} increased with temperature rise, but the values of k_{i2} and k_{i3} are

opposite with temperature rise.

As the constants of C in Table 2 is not zero, the fitted curves did not pass through the origin, so the biosorption process may be of a complex nature consisting of both surface adsorption and intraparticle diffusion^[14,28,29].

Table 1. Kinetic parameters for the biosorption of MB onto fallen phoenix leaves powder at various initial MB concentration and temperature using non-linear regressive analysis

Kinetic model	295 K 30 mg/l	295 K 70 mg/l	295 K 130 mg/l	309 K 130 mg/l	323 K 130 mg/l
Pseudo-first-order equation					
k_1 (g/mg·min)	0.304 ± 0.019	0.131 ± 0.019	0.101 ± 0.018	0.130 ± 0.016	0.153 ± 0.02
$q_e(\text{theo-1})$ (mg/g)	13.76 ± 0.09	31.24 ± 0.72	53.23 ± 1.65	55.64 ± 1.12	58.13 ± 0.70
$q_e(\text{exp})$ (mg/g)	14.0	33.2	57.8	58.5	60.0
R^2	0.900	0.806	0.776	0.856	0.932
Pseudo-second-order equation					
k_2 (g/mg·min)	0.0534 ± 0.00185	0.00643 ± 0.00077	0.00250 ± 0.00040	0.00360 ± 0.00030	0.00432 ± 0.00009
$q_e(\text{theo-2})$ (mg/g)	14.06 ± 0.29	32.98 ± 0.47	57.35 ± 1.28	58.85 ± 0.59	60.84 ± 0.14
$q_e(\text{exp})$ (mg/g)	14.0	33.2	57.8	58.5	60.0
R^2	0.992	0.950	0.927	0.976	0.998

Table 2. Estimated parameters of intraparticle diffusion model at various stages using non-linear regressive analysis

	295 K, 30 mg/l	295 K, 70 mg/l	295 K, 130 mg/l	309 K, 130 mg/l	323 K, 130 mg/l
Step-1					
k_{i1} (g/mg·1/2min)	0.949 ± 0.352	3.12 ± 0.82	4.26 ± 0.48	6.56 ± 0.28	7.29 ± 0.90
C_1	9.14 ± 1.20	11.70 ± 2.82	19.79 ± 2.09	17.52 ± 0.96	19.18 ± 3.08
R^2	0.879	0.934	0.975	0.998	0.985
Step-2					
k_{i2} (g/mg·1/2min)	0.0582 ± 0.0118	1.33 ± 0.13	2.40 ± 0.17	1.81 ± 0.04	0.682 ± 0.033
C_2	13.24 ± 0.10	19.80 ± 1.02	28.79 ± 1.73	38.89 ± 0.1	51.95 ± 0.27
R^2	0.924	0.990	0.985	0.999	0.995
Step-3					
k_{i3} (g/mg·1/2min)	0.0380 ± 0.0122	0.151 ± 0.012	0.202 ± 0.035	0.180 ± 0.059	0.0518 ± 0.0280
C_3	13.48 ± 0.15	30.37 ± 0.15	54.47 ± 0.48	55.37 ± 0.35	58.61 ± 0.35
R^2	0.764	0.982	0.970	0.753	0.632

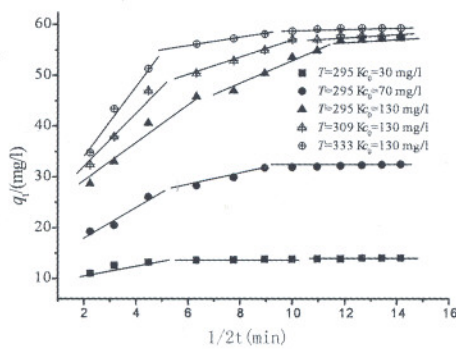


Figure 3. Plots of q_t and $1/2t$ with three-step stage at different conditions.

3.3 The apparent activation energy of the biosorption of MB on leaf

The magnitude of activation energy may give an idea about the type of adsorption. There are two main

types of adsorption: physical and chemical. Chemical adsorption is specific and involves forces much stronger than physical adsorption. There are two kinds of chemical adsorption including activated and nonactivated ones. Activated chemical adsorption means that the rate varies with temperature according to finite activation energy (8.4 – 83.7 kJ/mol) in the Arrhenius equation. In nonactivated chemical adsorption, the activation energy is near zero^[22]. The values of rate constant from the pseudo-second-order can be used to calculate the activation energy of adsorptive process. The energy of activation (E_a) was determined from the slope of the Arrhenius plot of $\ln k_2$ versus $1/T$ (figure not shown) according to Eq. (7) and was found to be 15.5 kJ/mol. These values are of the same magnitude as the activation energy of activated chemical adsorption. The positive values of E_a suggest that rise in temperature favors the biosorption and the process is an endothermic in nature.

4 Conclusion

The following conclusions can be drawn:

(1) The phoenix tree's leaves powder was found to have a much higher biosorption capacity for removing MB.

(2) The capacity of MB biosorption on leaf powder increased with an increasing of temperature.

(3) The biosorption kinetics study of MB are good in accordance with the pseudo-first-order model and pseudo-second-order model using non-linear analysis and later is better to express the biosorption process. The intraparticle diffusion model also can express the adsorption at different stage. The biosorption process may be of a complex nature.

(4) The process of MB adsorbed onto leaf may be controlled by chemical adsorption. But they have the lower activated energy, the adsorption may be controlled by an activated chemical adsorption.

References

- Crini G. Non-conventional low-cost adsorbents for dye removal: a review. *Bioresource Technology* 2006; 97: 1061 – 85.
- Robinson T, McMullan G, Marchant R, Nigam P. Remediation of dyes in textile effluent: a critical review on current treatment technologies with a proposed alternative. *Bioresource Technology* 2001; 77: 247 – 55.
- Aksu Z. Application of biosorption for the removal of organic pollutants: a review. *Process Biochemistry* 2005; 40: 997 – 1026.
- Namasivayam C, Sumithra S. Removal of direct red 12B and methylene blue from water by adsorption onto Fe(III)/Cr(III) hydroxide, an industrial solid waste. *Journal of Environmental Management* 2005; 74: 207 – 15.
- Annadurai G, Juang RS, Lee DJ. Use of cellulose based wastes for adsorption of dyes from aqueous solutions. *Journal of Hazardous Materials* 2002; B92: 263 – 74.
- Ghosh D, Bhattacharyya KG. Adsorption of methylene blue on kaolinite. *Applied Clay Science* 2002; 20: 295 – 300.
- Robinson T, Chandran B, Nigam P. Removal of dyes from a synthetic textile dye effluent by biosorption on apple pomace and wheat straw. *Water Research* 2002; 36: 2824 – 30.
- Yang GY, Zhang JH, Zou WH, Han RP. Comparison of infrared spectra of native phoenix tree's leaf before and after adsorbed copper cation. *Chinese Journal of Spectroscopy Laboratory* 2006; 23: 390 – 2.
- Ahlawalia SS, Goyal D. Removal of heavy metals by waste tea leaves from aqueous solution. *Engineering and Life Science* 2005; 5: 158 – 62.
- Zhang HY, Ji LT, Wang NY, Shen NH. Preliminary research on adsorption of heavy metals by fallen leaves litter of Chinese parasol tree. *Fine Chemicals* 2002; 19: 80 – 2.
- Zaqqut FR. Kinetic removal of lead from water by decaying *Tamix* leaves. *Journal of Environmental and Engineering Science* 2005; 4: 299 – 305.
- Waranusantigul P, Pokethitiyook P, Kruatrachue M, Upatham ES. Kinetics of basic dye (methylene blue) biosorption by giant duckweed (*Spirodela polyrrhiza*). *Environmental Pollution* 2003; 125: 385 – 92.
- Garg VK, Amita M, Kumar R, Gupta R. Basic dye (methylene blue) removal from simulated wastewater by adsorption using Indian Rosewood sawdust: a timber industry waste. *Dyes and Pigments* 2004; 63: 243 – 50.
- Vadivelan V, Vasanth Kumar K. Equilibrium, kinetics, mechanism, and process design for the sorption of methylene blue onto rice husk. *Journal of Colloid and Interface Science* 2005; 286: 90 – 100.
- Han RP, Wang YF, Han P, Shi J, Yang J, Lu YS. Removal of methylene blue from aqueous solution by chaff in batch mode. *Journal of Hazardous Materials* 2006; B137: 550 – 7.
- Han RP, Zou WH, Yu WH, Cheng SJ, Wang YF, Shi J. Biosorption of methylene blue from aqueous solution by fallen phoenix tree's leaves. *Journal of Hazardous Materials* 2007; 141: 156 – 62.
- Lagergren S. Zur theorie der sogenannten adsorption gelöster stoffe. *Kungliga Svenska Vetenskapsakademiens. Handlingar* 1898; 24: 1 – 39.
- Ho YS, McKay G. Kinetic models for the sorption of dye from aqueous solution by wood. *Process Safety and Environmental Protection* 1998; 76: 183 – 91.
- Namasivayam C, Ranganathan K. Waste Fe(III)/Cr(III) hydroxide as adsorbent for the removal of Cr(VI) from aqueous solution and chromium plating industry wastewater. *Environmental pollution* 1993; 82: 255 – 61.
- Zou WH, Han RP, Chen ZZ, Zhang JH, Shi J. Kinetic study of adsorption of Cu(II) and Pb(II) from aqueous solutions using manganese oxide coated zeolite in batch mode. *Colloids and Surfaces A: Physicochemistry and Engineering Aspects* 2006; 279: 238 – 46.
- Han RP, Zhang JH, Zhu L, Zou WH, Shi J. Determination of the equilibrium, kinetic and thermodynamic parameters of the batch biosorption of copper (II) ions onto Chaff. *Life Science Journal* 2006; 3: 81 – 8.
- Aksu Z. Determination of the equilibrium, kinetic and thermodynamic parameters of the batch biosorption of lead (II) ions onto *Chlorella vulgaris*. *Process Biochemistry* 2002; 38: 89 – 99.
- Han RP, Zhang JH, Zou WH, Shi J, Liu HM. Equilibrium biosorption isotherm for lead ion on chaff. *Journal of Hazardous Materials* 2005; B125: 266 – 71.
- Öztürk A, Artan T, Ayar A. Biosorption of nickel (II) and copper (II) ions from aqueous solution by *Streptomyces coelicolor A3(2)*. *Colloids and Surfaces B: Biointerfaces* 2004; 34: 105 – 11.
- Taty-Costodes VC, Fauduet H, Porte C, Delacroix A. Removal of Cd(II) and Pb(II) ions from aqueous solutions by adsorption onto saw-dust of *Pinus sylvestris*. *Journal of Hazardous Materials* 2003; B105: 121 – 42.
- Ho YS. Selection of optimum sorption isotherm. *Carbon* 2004; 42: 2115 – 6.
- Basibuyuk M, Forster CF. An examination of the adsorption characteristics of a basic dye (Maxilon Red BL-N) on to live activated sludge system. *Process Biochemistry* 2003; 38: 1311 – 6.
- Gryglewicz G, Lorenc-Grabowska E. Adsorption of lignite-derived humic acids on coal-based mesoporous activated carbons. *Journal of Colloid and Interface Science* 2005; 284: 416 – 23.
- Sun QY, Yang LZ. The adsorption of basic dyes from aqueous solution on modified peat-resin particle. *Water Research* 2003; 37: 1535 – 44.

Author Index

Authors	Authors	Authors			
Anthwal Ashish	80-84	Li Qi	17-20	Wang Lidong	1-5, 21-23
Cao Gangqiang	71-76	Li Xinchao	40-42	Wang Zhiju	13-16
Chai Yurong	6-12	Liu Baichi	1-5, 21-23	Wei Jinxing	17-20
Chang Cuifang	43-51, 61-70	Liu Bin	21-23	Wu Aiqun	1-5, 21-23
Chen Kuisheng	24-28	Liu Hong	40-42	Xin Wenjun	32-36
Chen Linhai	85-88	Liu Panfeng	43-51, 52-60, 61-70	Xing Guolan	1-5, 21-23
Chen Xiaoguang	43-51, 52-60, 61-70	Liu Shanting	29-31	Xu Cunshuan	43-51, 52-60, 61-70
Cheng Shujian	89-93	Liu Xianguo	32-36	Xu Jitian	32-36
Dong Ziming	13-16, 37-39	Lou Weihua	29-31	Xue Lexun	6-12
Du Bin	40-42	Meng Zhaozhong	29-31	Zhang Hongxin	24-28
Fan Zongmin	21-23	Pan Weidong	6-12	Zhang Lan	24-28
Feng Changwei	21-23	Qiao Baoping	17-20	Zhang Mei	1-5, 21-23
Feng Xiaoshan	1-5, 21-23	Qin Guangyong	77-79	Zhang Qian	37-39
Gao Dongling	24-28	Qin Yupei	1-5	Zhang Weimin	52-60
Gao Shanshan	21-23	Sang Jianzhong	29-31	Zhang Weixing	17-20
Gu Yunhong	77-79	Sharma Archana	80-84	Zhang Yanrui	21-23
Han Hongpeng	43-51, 61-70	Sharma Ramesh C.	80-84	Zhang Yunhan	24-28
Han Runping	89-93	Song Xiaoming	77-79	Zhao Guoqiang	13-16
He Fucheng	24-28	Song Xin	21-23	Zhao Lifeng	52-60
He Xin	21-23	Su Lijuan	43-51, 61-70	Zhao Ming	29-31
Huang Jinyong	85-88	Sun Yun	6-12	Zhao Wenchao	13-16
Jia Yanlong	6-12	Timofeyev Valeriy	37-39	Zhou Wei	85-88
Jiao Xinying	21-23	Tu Huiyin	32-36	Zhu Jun	71-76
Li Jilin	21-23	Wang Gaiping	43-51, 61-70	Zhu Lu	89-93
Li Min	13-16	Wang Jiaxiang	17-20	Zou Weihua	89-93

Subject Index

Keywords	Keywords	Keywords
5-fluorouracil	17 herbs	40 phytoplankton
algae	80 high-incidence area	21 pollen-tube pathway
atrioventricular node	37 hill stream	80 precancerous lesion
automatic activity	37 Himalaya	80 protein profile
bcl-2	29 immunohistochemistry	29 quantitative trait locus
biomarker	1 interferon	17 RACE
biosorption	89 kinetic	89 Rat Genome 230 2.0 Array
Ca ²⁺ -activated K ⁺ channel	37 laryngeal squamous cell carcinoma	29 rbcL
capillary gas chromatography	40 liver regeneration	43, 52, 61 renal clear cell carcinoma
carcinogenesis	1 lung adenocarcinoma	13 responses to drugs, toxins,
Chandrabhaga	80 lymphatic metastasis	24 oxidation and unfolded proteins
conditional genetics	71 methylene blue	89 responses to fear, wound and pain
conduction	37 mitogen-activated protein kinase	32 responses to physical stimuli
degenerate primer	6 molecular breeding	77 rice yield
<i>Dunalieilla salina</i>	6 molecular ecology	85 Rubisco
EC9706 cells	24 multidrug resistance	13 SB203580
esophageal carcinoma	1 neuropathic pain	32 soil microbial DNA
esophageal neoplasm	21 non-linear regressive analysis	89 thymidine phosphorylase
esophageal squamous cell carcinoma	24 organochlorine pesticide	40 VEGF-C
esophagus	21 p38	32 ventral rhizotomy
extraction method	85 p53	29 yield components
gastric cardia	21 paclitaxel	13 Z-line
gene knockout	37 partial hepatectomy	89
genes	43, 52, 61 phoenix tree's leaves powder	

Instructions to Authors

1. General Information

(1) **Goals:** As an international journal published both in print and on internet, *Life Science Journal* is dedicated to the dissemination of fundamental knowledge in all areas of life science. The main purpose of *Life Science Journal* is to enhance our knowledge spreading in the world under the free publication principle. It publishes full-length papers (original contributions), reviews, rapid communications, and any debates and opinions in all the fields of life science.

(2) **Categories of publication:** Research articles, reviews, objective descriptions, research reports, opinions/debates, news, letters to editor, meeting report. (3) **Cover feature:** The covers of *Life Science Journal* feature illustrations the Editor-in-Chief selects from the articles scheduled for publication in that issue. Authors whose articles are chosen for a cover feature will be asked to provide a high-quality version of the selected illustration as well as a brief legend (four to five sentences) describing the significance of the image. In light of the rapid production schedule for journal covers, authors are expected to provide the requested material within 3 days.

(4) **Publication costs:** US \$ 30 per printed page of an article to defray costs of the publication will be paid by the authors when it is accepted. Extra expense for color reproduction of figures will be paid by authors (estimate of cost will be provided by the publisher for the author's approval). For the starting, publication fee will be waived for the current issues and they will be supported by Zhengzhou University.

(5) **Journal copies to authors:** Two hard copies of the journal will be provided free of charge for each author.

(6) **Additional copies bought by authors:** Additional hard copies could be purchased with the price of US \$ 4/issue (mailing and handling cost included).

(7) **Distributions:** Web version of the journal is freely opened to the world without payment or registration. The journal will be distributed to the selected libraries and institutions for free. US \$ 5/issue hard copy is charged for the subscription of other readers.

(8) **Advertisements:** The price will be calculated as US \$ 400/page, i. e. US \$ 200/a half page, US \$ 100/a quarter page, etc. Any size of the advertisement is welcome.

2. Manuscripts Submission

(1) **Submission methods:** Electronic submission through email is encouraged and hard copies plus an IBM formatted computer diskette would also be accepted.

(2) **Software:** The Microsoft Word file will be preferred.

(3) **Font:** Normal, Times New Roman, 10 pt, single space.

(4) **Indent:** Type 4 spaces in the beginning of each new paragraph.

(5) **Manuscript:** Do not use "Footnote" or "Header and Footer".

(6) **Title:** Use Title Case in the title and subtitles, e. g. "Debt and Agency Costs".

(7) **Figures and tables:** Use full word of figure and table, e. g. "Figure 1. Annual income of different groups", **Table 1.** Annual increase of investment".

(8) **References:** Number the references in the order of their first mention in the text. References should include all the authors' last names and initials, title, journal, year, volume, issue, and pages etc.

Reference examples :

Journal article: Hacker J, Hentschel U, Dobrindt U. Prokaryotic chromosomes and disease. *Science* 2003;301(34):790–3.

Book: Berkowitz BA, Katzung BG. Basic and clinical evaluation of new drugs. In: Katzung BG, ed. *Basic and Clinical Pharmacology*. Appleton & Lange Publisher. Norwalk, Connecticut, USA. 1995;60–9.

(9) **Submission address:** America: lifesciencej@gmail.com, Marsland Press, P. O. Box 21126, Lansing, Michigan 48909, USA.

China: lifesciencej@zzu.edu.cn, Zhengzhou University, 100 Science Road, Zhengzhou, Henan 450001, China.

(10) **Reviewers:** Authors are encouraged to recommend 2–8 competent reviewers with their names and email addresses.

3. Manuscript Preparation

Each manuscript is suggested to include the following components but authors can do their own ways:

(1) Title. Including each author's full name; institution(s) with which each author is affiliated, with city, state/province, zip code, and country.

(2) Abstract. Including Background, Materials and Methods, Results, and Discussion.

(3) Keywords.

(4) Abbreviations. All abbreviations needed are listed here, so that they could be used directly in the article.

(5) Introduction.

(6) Materials and Methods.

(7) Results.

(8) Discussion.

(9) Acknowledgments.

(10) Correspondence. Correspondence author's full name, institution, city, state/province, zip code, country, telephone number, facsimile number (if available), and email address are listed here.

(11) References.

4. Copyright and Permissions

All rights reserved. No part of this publication may be reproduced, stored in a retrieval system in any form or by any means for commercial use, without permission in writing from the copying holder.

Life Science Journal

Acta Zhengzhou University Overseas Edition

Volume 4 Number 1, March 2007

Published by:

Zhengzhou University
Marsland Press

Sponsor:

North American Branch of Zhengzhou University Alumni

Zhengzhou University
100 Science Road
Zhengzhou, Henan 450001, China
Telephone: 86-371-6778-1272
Email: lifesciencej@zju.edu.cn
Website: <http://life.zju.edu.cn>

Marsland Press
P.O. Box 21126
Lansing, Michigan 48909, USA
Telephone: 517-349-2362
Email: lifesciencej@gmail.com
Website: <http://www.sciencepub.org>

ISSN 1097-8135



9 771097 813088